5-2015

Computational Prediction and Rational Design of Novel Clusters, Nanoparticles, and Solid State Materials

Alexander S. Ivanov
Utah State University

COMPUTATIONAL PREDICTION AND RATIONAL DESIGN OF NOVEL CLUSTERS, NANOPARTICLES, AND SOLID STATE MATERIALS

by

Alexander S. Ivanov

A dissertation submitted in partial fulfillment
of the requirements for the degree

of

DOCTOR OF PHILOSOPHY

in

Chemistry

Approved:

_____	_____
Dr. Alexander I. Boldyrev Major Professor	Dr. Steve Scheiner Committee Member
_____	_____
Dr. Stephen Bialkowski Committee Member	Dr. David Farrelly Committee Member
_____	_____
Dr. T. C. Shen Committee Member	Dr. Mark R. McLellan Vice President for Research and Dean of the School of Graduate Studies

UTAH STATE UNIVERSITY
Logan, Utah

2015

ABSTRACT

Computational Prediction and Rational Design of Novel Clusters, Nanoparticles, and Solid State Materials

by

Alexander S. Ivanov, Doctor of Philosophy

Utah State University, 2015

Major Professor: Dr. Alexander I. Boldyrev
Department: Chemistry and Biochemistry

The creation of new materials is absolutely essential for developing new technologies. However, experimental efforts toward the material discovery are usually based on trial-and-error approach and thus require a huge amount of time and money. Alternatively, computational predictions can now provide a more systematic, rapid, inexpensive, and reliable method for the design of novel materials with properties suitable for new technologies. This dissertation describes the technique of theoretical predictions and presents the results on the successfully predicted and already produced (in some cases) unusual molecules, clusters, nanoparticles, and solids. The major part of scientific efforts in this dissertation was devoted to rationalizing of size- and composition-dependent properties of the materials based on understanding of their

electronic structure and chemical bonding. It was shown that understanding relations between bonding and geometric structure, bonding and stability, and bonding and reactivity is an important step toward rational design of new, yet unknown materials with unusual properties. Our findings led to the discovery of the first simplest inorganic double helix structures, which can be used in the design of novel molecular devices. A significant part of this work also deals with the pseudo Jahn-Teller effect, which potentially can be a powerful tool for rationalizing and predicting molecular and solid state structures, their deformations, transformations, and properties. Therefore, the works on the pseudo Jahn-Teller effect presented in this dissertation can be considered the steps toward further generalization and elevation of the pseudo Jahn-Teller effect to a higher level of understanding of the origin of molecular and solid state properties.

(388 pages)

PUBLIC ABSTRACT

Computational Prediction and Rational Design of Novel Clusters, Nanoparticles, and Solid State Materials

by

Alexander S. Ivanov, Doctor of Philosophy

Utah State University, 2015

Major Professor: Dr. Alexander I. Boldyrev
Department: Chemistry and Biochemistry

The prediction of structure at the atomic level is one of the most fundamental challenges in materials science. Indeed, the structure is arguably the most important piece of information about a material, as it determines pretty much all properties of a material. Knowing the structure, one can analyze a large number of properties of a material, even before it is synthesized – the crucial importance of structure prediction for computational molecular design. This dissertation describes the technique of reliable theoretical predictions and presents the results on the successfully predicted unusual clusters, nanoparticles and solid state materials. The major part of this work also demonstrates how understanding of the electronic structure and chemical bonding in studied systems could aid in the rational design of novel materials with tailored properties.

ACKNOWLEDGMENTS

First and foremost, I would like to express my very great appreciation to my advisor, Prof. Alexander I. Boldyrev. Dr. Boldyrev's passion for science, productivity, and his involvement in scientific debates with Nobel Prize laureates makes him a great scientist and a true leader. Whenever I meet students from other universities, I always recall the words from the book by F. Scott Fitzgerald: "just remember that all the people in this world haven't had the advantages that you've had" and realize again what an outstanding mentor Dr. Boldyrev is.

I cannot express enough thanks to the members of my supervisory committee for their continued support and encouragement: Prof. Stephen Bialkowski, Prof. David Farrelly, Prof. T. C. Shen, and Prof. Steve Scheiner. I offer my sincere appreciation for the learning opportunities provided by my committee.

I have been extremely fortunate to have been able to collaborate with many great scientists: Prof. Lai-Sheng Wang (Brown University, USA), Prof. G. Frenking (Philipp University of Marburg, Germany), Prof. C. J. Pickard (University College London, UK), and Prof. T. Sato (Kyoto University, Japan), as well as their group members. My completion of the research projects presented in this dissertation could not have been accomplished without their indispensable contribution.

I take this opportunity to express gratitude to all of the Department of Chemistry and Biochemistry faculty members for their help and support, especially: Dr. Alvan C. Hengge and his wife, Maribeth Evensen-Hengge.

I would also like to thank the Boldyrev group alumni and current members for their help, openness for questions and fruitful discussions.

Most importantly, I would like to thank my parents and my younger sister for their constant love and support, and for their faith in me.

Finally, to my caring, loving, and supportive wife, Svetlana: my deepest gratitude. Her support and help was in the end what made this dissertation possible. I also thank my wife for encouraging me in all of my pursuits and inspiring me to follow my dreams.

During my four years at Utah State University, I have been supported by the National Science Foundation (grants CHE-1057746 and CHE-1361413 to Prof. Alexander I. Boldyrev) and Teaching Assistantships (Department of Chemistry and Biochemistry, Utah State University). Computer, storage and other resources from the Division of Research Computing in the Office of Research and Graduate Studies at Utah State University and the Center for High Performance Computing at the University of Utah are gratefully acknowledged.

Alexander S. Ivanov

CONTENTS

Page

ABSTRACT iii

PUBLIC ABSTRACT v

ACKNOWLEDGMENTS vi

LIST OF TABLES xiv

LIST OF FIGURES xvi

CHAPTER

1. INTRODUCTION 1

1-1. Ionic, atomic, and molecular clusters 1

1-1.1. Boron-carbon mixed clusters 4
1-1.2. Tantalum doped boron clusters 5
1-1.3. Development of program for calculating the intensity of spectral lines in vibrationally resolved photoelectron spectrum 6
1-1.4. Li_3N_3 cluster: all-nitrogen analogue of ozone molecule 6
1-1.5. Microsolvation study of dichloride Cl^-–Cl^- anion pair 7

1-2. Inorganic double helix structures 7

1-2.1. Double helix Li_nP_n (n = 5–9) clusters, infinite LiP chains, and LiP solids 8
1-2.2. Circular double helix species 8

1-3. Deciphering chemical bonding in hypervalent iodine compounds and porphyrinoids 9

1-3.1. Description of aromaticity and chemical bonding in porphyrinoids 10
1-3.2. Description of chemical bonding in hypervalent iodine compounds 11

1-4. Restoring planarity of molecular structures 11

1-4.1. Suppression of the pseudo Jahn-Teller effect in $Si_{6-n}C_nH_6$ (n = 0–6) series 12
1-4.2. Suppression of the pseudo Jahn-Teller effect in middle E_6 (E = P, As, Sb) rings of triple-decker sandwich complexes 13
1-4.3. Pseudo Jahn-Teller origin of distortions in 2D triazine-based graphitic carbon nitride sheets 13
References 14

2. MOLECULAR WHEEL TO MONOCYCLIC RING TRANSITION IN BORON–CARBON MIXED CLUSTERS $C_2B_6^-$ AND $C_3B_5^-$ 23

Abstract 23
2-1. Experimental section 32
2-2. Theoretical section 33
Notes and references 33

3. ON THE WAY TO THE HIGHEST COORDINATION NUMBER IN THE PLANAR METAL-CENTRED AROMATIC $Ta©B_{10}^-$ CLUSTER: EVOLUTION OF THE STRUCTURES OF TaB_n^- (n = 3 – 8) 44

Abstract 44
3-1. Introduction 45

3-2. Experimental and computational methods 48

3-2.1. Photoelectron spectroscopy method 48
3-2.2. Global optimization method 49

3-3. Experimental results 50

3-4. Theoretical results 52

3-4.1. TaB_3^- 52
3-4.2. TaB_4^- 53
3-4.3. TaB_5^- 53
3-4.4. TaB_6^- 53
3-4.5. TaB_7^- 54
3-4.6. TaB_8^- 54

3-5. Interpretation of the photoelectron spectra 55

3-5.1. TaB_3^- 55
3-5.2. TaB_4^- 56

3-5.3. TaB_5^- 57
3-5.4. TaB_6^- 57
3-5.5. TaB_7^- 58
3-5.6. TaB_8^- 59

3-6. Structural evolution and chemical bonding in TaB_n^- 60

3-6.1. TaB_n^- (n = 3–5): nucleation of B around Ta 61
3-6.2. TaB_6^- and TaB_7^-: structural excursions 62
3-6.3. TaB_8^-: on the way to $Ta©B_{10}^-$ 63

3-7. Conclusions 64
References 65

4. ASSESSING INTENSITIES OF SPECTRAL LINES IN VIBRATIONALLY RESOLVED PHOTOELECTRON SPECTRA 91

Abstract 91
References 95

5. ALL-NITROGEN ANALOGUE OF OZONE: Li_3N_3 SPECIES 99

Abstract 99
5-1. Introduction 99
5-2. Results and discussion 102
5-3. Conclusions 106
5-4. Computational and theoretical methods 107
References 108

6. STABILIZATION OF $Cl^- – Cl^-$ ANION PAIR IN THE GAS PHASE: AB INITIO MICROSOLVATION STUDY 117

Abstract 117
6-1. Introduction 117
6-2. Computational and theoretical methods 120
6-3. Results and discussion 123

6-3.1. $[Cl_2(H_2O)_2]^{2-}$ clusters 125
6-3.2. $[Cl_2(H_2O)_3]^{2-}$ clusters 126
6-3.3. $[Cl_2(H_2O)_4]^{2-}$ clusters 126
6-3.4. $Cl_2(H_2O)_5]^{2-}$ clusters 127
6-3.5. $[Cl_2(H_2O)_6]^{2-}$ clusters 127
6-3.6. $[Cl_2(H_2O)_7]^{2-}$, $[Cl_2(H_2O)_8]^{2-}$ clusters 128

6-3.7. $[Cl_2(H_2O)_9]^{2-}$, $[Cl_2(H_2O)_{10}]^{2-}$ clusters 129
6-4. Conclusions 134
References 135

7. INORGANIC DOUBLE HELIX STRUCTURES OF UNUSUALLY SIMPLE Li-P SPECIES 154

Abstract 154
7-1. Introduction 154
7-2. Results and discussion 156
7-3. Conclusions 160
7-4. Computational and theoretical methods 160
References 161

8. INORGANIC DOUBLE-HELIX NANOTOROID OF SIMPLE LITHIUM-PHOSPHORUS SPECIES 178

Abstract 178
8-1. Introduction 178
8-2. Results and discussion 181
8-3. Conclusions 186
8-4. Computational and theoretical methods 187
References 188

9. DECIPHERING AROMATICITY IN PORPHYRINOIDS VIA ADAPTIVE NATURAL DENSITY PARTITIONING 197

Abstract 197
9-1. Introduction 197
9-2. Results and discussion 200
9-3. Experimental section 205
9-4. Conclusions 206
Notes and references 207

10. THE I=X (X = O, N, C) DOUBLE BOND IN HYPERVALENT IODINE COMPOUNDS: IS IT REAL? 217

Abstract 217
10-1. Introduction 217
10-2. Results and discussion 218
10-3. Conclusions 223
10-4. Computational and theoretical methods 223

References 224

11. $Si_{6-n}C_nH_6$ (n = 0–6) SERIES: WHEN DO SILABENZENES BECOME PLANAR AND GLOBAL MINIMA? 235

Abstract 235
11-1. Introduction 235
11-2. Computational and theoretical methods 237
11-3. Results and discussion 239

11-3.1. Si_6H_6 Isomers 239
11-3.2. Si_5CH_6 Isomers 241
11-3.3. $Si_4C_2H_6$ Isomers 243
11-3.4. $Si_3C_3H_6$ Isomers 244
11-3.5. $Si_2C_4H_6$ Isomers 245
11-3.6. SiC_5H_6 Isomers 246
11-3.7. C_6H_6 Isomers 247
11-3.8. Chemical Bonding Pictures Revealed by the AdNDP 247

11-4. Conclusions 249
References 250

12. ON THE SUPPRESSION MECHANISM OF THE PSEUDO-JAHN−TELLER EFFECT IN MIDDLE E_6 (E = P, As, Sb) RINGS OF TRIPLE-DECKER SANDWICH COMPLEXES 267

Abstract 267
12-1. Introduction 267
12-2. Theoretical section 269
12-3. Results and discussion 271
12-4. Conclusions 274
References 275

13. PSEUDO JAHN-TELLER ORIGIN OF BUCKLING DISTORTIONS IN TWO-DIMENSIONAL TRIAZINE-BASED GRAPHITIC CARBON NITRIDE (g-C_3N_4) SHEETS 282

Abstract 282
13-1. Introduction 282
13-2. Methods and computational details 284
13-3. Results and discussion 288
13-4. Triazine-based graphitic carbon nitride clusters 290

13-5. Chemical bonding 292
13-6. Suppression of the PJT effect 293
13-7. Conclusions 297
References 297

14. SUMMARY 311

APPENDIX 320

CURRICULUM VITAE 356

LIST OF TABLES

Table Page

2-1 Comparison of the experimental VDEs with calculated values for the structure I.1. C_{2v} ($^2A_1$) and I.2. C_s ($^2A'$) of the $C_2B_6^-$ cluster. All energies are in eV 37

2-2 Comparison of the experimental VDEs with calculated values for the structure II.1. C_{2v} ($^1A_1$) of the $C_3B_5^-$ cluster. All energies are in eV 38

3-1 Experimental vertical detachment energies (VDEs) compared with calculated VDEs for the global minimum structure I.1 (C_{2v}, $^4B_1$) of TaB_3^-. All energies are in eV 70

3-2 Experimentally VDEs compared with calculated VDEs for the II.1 (C_{2v}, $^1A_1$) global minimum and the II.2 (C_s, $^3A''$) low-lying isomer of TaB_4^-. All energies are in eV 71

3-3 Experimental VDEs compared with calculated VDEs for the III.1 (C_{2v}, $^2A_1$) global minimum and C_1 low-lying isomer of TaB_5^-. All energies are in eV 72

3-4 Experimental VDEs compared with calculated VDEs for the IV.1 (C_{2v}, $^3A_2$) global minimum, and IV.2 (C_{2v}, $^1A_1$) and IV.3 (C_{2v}, $^1A_1$) low-lying isomers of TaB_6^-. All energies are in eV 73

3-5 Experimental VDEs compared with calculated VDEs for the V.1 (C_s, $^2A'$) global minimum of TaB_7^-. All energies are in eV 74

3-6 Experimental VDEs compared with calculated VDEs for the VI.1 (C_s, $^3A''$) global minimum and the VI.2 (C_{4v}, $^1A_1$) low-lying isomer of TaB_8^-. All energies are in eV 75

3-7 Calculated VDEs for the I.2 (C_{2v}, $^2A_2$), and I.3 (C_{2v}, $^4A_2$) low-lying isomers of TaB_3^-. All energies are in eV 76

6-1 Calculated Stabilization Energies of $Cl^-(H_2O)_n$ Clusters (kcal/mol) at Different Levels of Theory 144

6-2 Calculated Stabilization Energies of $[Cl_2(H_2O)_n]^{2-}$ (n = 2-10) Clusters (kcal/mol) at Different Levels of Theory 145

6-3 Calculated Dissociation Energies for Different Dissociation Channels $Cl^-(H_2O)_nCl^- \rightarrow Cl^-(H_2O)_m + Cl^-(H_2O)_k$, where m + k = n (kcal/mol).....146

6-4 Calculated Adiabatic (ADE) and Vertical (VDE) Electron Binding Energies for $[Cl_2(H_2O)_n]^{2-}$ (n = 2-10) in eV 147

6-5 Atomic Charges |e| on Ions Calculated with Natural Population Analysis (NPA) 148

8-1 Structural parameters of Li_7P_7 (C_1, ^1A), Li_8P_8 (C_1, ^1A), Li_9P_9 (C_1, ^1A) double helices, and $Li_{90}P_{90}$ (C_2, ^1A) circular double helix at different levels of theory. Distances between corresponding atoms are given in Å.....192

13-1 The calculated orbital energy gap, orbital vibronic coupling constants (OVCCs) of the e" mode, and OVCC over orbital energy gap between occupied valence orbital *i* and unoccupied orbital *j*. Only the orbital pairs with large vibronic coupling constants are tabulated.....306

13-2 The energy difference (ΔE) between planar and corrugated structures, HOMO-LUMO gaps, largest frequency of buckling, and root-mean square displacement of atomic coordinates (R), necessary to achieve a planar configuration. All the values are given at M05-2X/6-31+G(d,p), B3PW91/6-31+G(d,p) (in brackets), and TD-B3PW91/6-31+G(d,p) (in curly brackets).....307

LIST OF FIGURES

Figure Page

2-1 Photoelectron spectra of $C_2B_6^-$ at a) 266 nm (4.661 eV) and b) 193 nm (6.424 eV). The inset shows a partial PES at 355 nm (3.455 eV). The short vertical lines represent the TD-B3LYP values of VDE for structure I.1(bottom) and I.2 (top) 39

2-2 Photoelectron spectra of $C_3B_5^-$ at (a) 266 nm (4.661 eV) and (b) 193 nm (6.424 eV) 40

2-3 Representative optimized isomers of the $C_2B_6^-$ cluster, their point group symmetries, spectroscopic states and relative energies. The ZPE corrected energies are given at the RCCSD(T)/6-311+G(2df)//B3LYP/6-311+G*, B3LYP/6-311+G* (in square brackets), and B3LYP/3-21G (in curly brackets) levels of theory 41

2-4 Adiabatic Detachment Energies (ADE) of the $C_2B_6^-$ and $C_3B_5^-$ clusters....41

2-5 Optimized isomers of the $C_3B_5^-$ cluster, their point group symmetries, spectroscopic states and relative energies. The ZPE corrected energies are given at the RCCSD(T)/6-311+G(2df)//B3LYP/6-311+G*, B3LYP/6-311+G* (in square brackets), and B3LYP/3-21G (in curly brackets) levels of theory 42

2-6 Wheel-type to monocyclic ring structural transition in the series of the $C_xB_{8-x}^-$ (x=1-3) clusters. Relative energies are given at RCCSD(T)/6-311+G(2df)//B3LYP/6-311+G* 42

2-7 The chemical bonding patterns revealed by the AdNDP analysis for the $C_2B_6^{2-}$ cluster at the optimized geometries of the global minimum wheel-type structure I.1 (**A**) and lowest ring isomer I.6 (**B**) of the $C_2B_6^-$ cluster. The extra electron was added in order to avoid complications of the chemical bonding picture caused by spin polarization in the open-shell $C_2B_6^-$ cluster. The 2c-2e C-B and B-B bonds of both isomers are superimposed on a single molecular framework 43

2-8 The chemical bonding patterns revealed by the AdNDP analysis for the global minimum ring isomer II.1 (**A**) and the lowest wheel-type isomer II.5 (**B**) of the $C_3B_5^-$ cluster. The 2c-2e C-B and B-B bonds of both isomers are superimposed on a single molecular framework 43

3-1 Photoelectron Spectra of TaB_n^- (n = 3–8) at 193 nm (left) and 266 nm (right) 77

3-2 The global minimum structures and low-lying isomers of (a) TaB_3^-, (b) TaB_4^-, (c) TaB_5^-, and (d) TaB_6^-, optimized at the PBE0/Ta/Stuttgart/B/aug-cc-pVTZ level. Also given are the point group symmetries, spectroscopic states, and relative energies at the CCSD(T)/Ta/Stuttgart/B/aug-cc-pVTZ level with ZPE corrections at the PBE0/Ta/Stuttgart/B/aug-cc-pVTZ level. Bond lengths for the global minimum structures are given in Å 78

3-3 The global minimum structures of (a) TaB_7^-, (b) TaB_8^-, (c) TaB_9^-, and (d) TaB_{10}^-, optimized at PBE0/Ta/Stuttgart/B/aug-cc-pVTZ level. Bond lengths in Å, point group symmetries, and spectroscopic states are also shown. The structures of TaB_9^- and TaB_{10}^-, which were reported previously,[35, 38] are given for comparison 78

3-4 Results of AdNDP analyses for the global minimum structures of TaB_3^- (I.1), TaB_4^- (II.1), and TaB_5^- (III.1) 79

3-5 Results of AdNDP analyses for the global minimum structures of TaB_6^- (IV.1) and TaB_7^- (V.1) 80

3-6 Results of AdNDP analyses for the C_{8v} and C_s TaB_8^- 81

3-7 Photoelectron Spectra of TaB_3^- at (a) 532 nm, (b) 355 nm, (c) 266 nm, and (d) 193 nm. 82

3-8 Photoelectron Spectra of TaB_4^- at (a) 355 nm, (b) 266 nm, and (c) 193 nm 83

3-9 Photoelectron Spectra of TaB_5^- at (a) 355 nm, (b) 266 nm, and (c) 193 nm 84

3-10 Low-lying structures of TaB_3^-, their point group symmetries, spectroscopic states and ZPE corrected relative energies. The energies are given at: CCSD(T)/Ta/Stuttgart/B/aug-cc-pVTZ (top), CCSD(T)/Ta/Stuttgart/B/aug-cc-pVQZ (in brackets), PBE0/Ta/Stuttgart/B/aug-cc-pVTZ (square brackets), all at PBE0/Ta/Stuttgart/B/aug-cc-pVTZ optimized geometries 85

3-11 Low-lying structures of TaB_4^-, their point group symmetries, spectroscopic states and ZPE corrected relative energies. The energies are given at: CCSD(T)/Ta/Stuttgart/B/aug-cc-pVTZ (top), CCSD(T)/Ta/Stuttgart/B/aug-cc-pVQZ (in brackets),

PBE0/Ta/Stuttgart/B/aug-cc-pVTZ (square brackets), all at PBE0/Ta/Stuttgart/B/aug-cc-pVTZ optimized geometries 86

3-12 Low-lying structures of TaB_5^-, their point group symmetries, spectroscopic states and ZPE corrected relative energies. The energies are given at: CCSD(T)/Ta/Stuttgart/B/aug-cc-pVTZ (top), CCSD(T)/Ta/Stuttgart/B/aug-cc-pVQZ (in brackets), PBE0/Ta/Stuttgart/B/aug-cc-pVTZ (square brackets), all at PBE0/Ta/Stuttgart/B/aug-cc-pVTZ optimized geometries 87

3-13 Low-lying structures of TaB_6^-, their point group symmetries, spectroscopic states and ZPE corrected relative energies. The energies are given at: CCSD(T)/Ta/Stuttgart/B/aug-cc-pVTZ (top), PBE0/Ta/Stuttgart/B/aug-cc-pVTZ (square brackets), all at PBE0/Ta/Stuttgart/B/aug-cc-pVTZ optimized geometries 88

3-14 Low-lying structures of TaB_7^-, their point group symmetries, spectroscopic states and ZPE corrected relative energies. The energies are given at: CCSD(T)/Ta/Stuttgart/B/aug-cc-pVTZ (top), PBE0/Ta/Stuttgart/B/aug-cc-pVTZ (square brackets), all at PBE0/Ta/Stuttgart/B/aug-cc-pVTZ optimized geometries 89

3-15 Low-lying structures of TaB_8^-, their point group symmetries, spectroscopic states and ZPE corrected relative energies. The energies are given at: CCSD(T)/Ta/Stuttgart/B/aug-cc-pVTZ (top), PBE0/Ta/Stuttgart/B/aug-cc-pVTZ (square brackets), all at PBE0/Ta/Stuttgart/B/aug-cc-pVTZ optimized geometries 90

4-1 (a) Experimental photoelectron spectrum of B_3^- at 355 nm from reference 9, (b) simulated photoelectron spectrum of B_3^- 97

4-2 (a) Experimental photoelectron spectrum of B_5^- at 355 nm from reference 10, (b) simulated photoelectron spectrum of B_5^- 97

4-3 Simulated photoelectron spectrum of the second lowest isomer of B_5^- 98

5-1 Representative optimized isomers of Li_3N_3 species, their point group symmetries, spectroscopic states, and zero-point energy (ZPE) corrected energies. The relative energies are given at: CCSD(T)/6-311++G**//CCSD(T)/6-311++G** (bold) and CCSD(T)/aug-cc-pvTZ//B3LYP/aug-cc-pvTZ (in brackets). Here and

elsewhere the red and blue spheres represent lithium and nitrogen atoms, respectively 112

5-2 The transition state barriers diagram, showing large energy separation between isomers I.2 and I.4. The energies of the barriers are given at the CCSD(T)/aug-cc-pvTZ//B3LYP/aug-cc-pvTZ level of theory.....112

5-3 Simulated vibrational spectrum of the ozone-like (C_{2v}) cluster at the CCSD(T)/6-311++G** level of theory. Corresponding wavenumbers are presented for the most intense transitions.....113

5-4 Chemical bonding pattern of a) Li_3N_3 and b) O_3 structures revealed by the AdNDP analysis. ON stands for occupation number.....113

5-5 Lowest-lying structures of Li_3N_3, their point group symmetries, spectroscopic states and ZPE corrected relative energies. The energies are given at: CCSD(T)/aug-cc-pvTZ (bold) and B3LYP/aug-cc-pvTZ (in brackets) levels of theory, all at B3LYP/aug-cc-pvTZ optimized geometries. Here the red and yellow spheres represent lithium and nitrogen atoms, respectively 114

5-6 Computed UV-visible absorption spectrum for C_{2v} Li_3N_3 ozone-like cluster at the B3LYP/aug-cc-pvTZ level of theory.....115

5-7 Chemical bonding pattern of Li_3N_3 structure I.3 revealed by the AdNDP analysis and structural parameters of I.3 at CCSD(T)/6-311++G**. Significantly lower occupation numbers (ON) have been obtained for the first N-N π bond due to the close location of lithium atoms that make this pi bond delocalized over the lithium atoms 116

6-1 Representative optimized structures of A) $[Cl_2(H_2O)_2]^{2-}$, B) $[Cl_2(H_2O)_3]^{2-}$, and C) $[Cl_2(H_2O)_4]^{2-}$, their point group symmetries, spectroscopic states and ZPE (M06-2X/aug-cc-pvTZ) corrected relative energies. The energies are given at: CCSD(T)/aug-cc-pvDZ (bold), M06-2X/aug-cc-pvTZ (in brackets), M06-2X/aug-cc-pvDZ (square brackets). Here and elsewhere hydrogen bonds between adjacent water molecules are marked with tiny blue lines 149

6-2 Representative optimized structures of D) $[Cl_2(H_2O)_5]^{2-}$ and E) $[Cl_2(H_2O)_6]^{2-}$, their point group symmetries, spectroscopic states and ZPE (M06-2X/aug-cc-pvTZ) corrected relative energies. The energies are given

at: CCSD(T)/aug-cc-pvDZ (bold), M06-2X/aug-cc-pvTZ (in brackets), M06-2X/aug-cc-pvDZ (in square brackets).....150

6-3 Representative optimized structures of F) $[Cl_2(H_2O)_7]^{2-}$ and G) $[Cl_2(H_2O)_8]^{2-}$, their point group symmetries, spectroscopic states and ZPE corrected relative energies. The energies are given at: M06-2X/aug-cc-pvTZ (bold), M06-2X/aug-cc-pvDZ (in brackets).....151

6-4 Representative optimized structures of H) $[Cl_2(H_2O)_9]^{2-}$ and I) $[Cl_2(H_2O)_{10}]^{2-}$, their point group symmetries, spectroscopic states and ZPE corrected relative energies. The energies are given at: M06-2X/aug-cc-pvTZ (bold), M06-2X/aug-cc-pvDZ (in brackets).....152

6-5 Optimized (M06-2X/aug-cc-pvDZ) structures of $[Cl_2(H_2O)_{36}]^{2-}$ (left) and $[Cl_2(H_2O)_{40}]^{2-}$ (right) clusters, their point group symmetries and spectroscopic states.....153

7-1 Optimized structures of Li_5P_5, Li_6P_6, Li_7P_7, Li_8P_8 and Li_9P_9 helices. a) Li_5P_5 (C_1, ^1A), b) Li_6P_6 (C_1, ^1A), c) Li_7P_7 (C_1, ^1A), (d) Li_8P_8 (C_1, ^1A), e) Li_9P_9 (C_1, ^1A).....164

7-2 Representative optimized structures of Li_7P_7, their point group symmetries, spectroscopic states, and zero-point energy (ZPE) corrected (B3LYP/6-311+G*) relative energies at the CCSD(T)/CBS//B3LYP/6-311+G* level of theory 164

7-3 Three periodic repetitionsof the LiP infinite double-helix chain geometry optimized at the DFT-PBE level of theory.....165

7-4 A 2X2 supercell containing a *P*21/*c* symmetric Li_1P_1 bulk phase comprising of packed double helices.....165

7-5 Lowest-lying structures of Li_5P_5, their point group symmetries, spectroscopic states and ZPE corrected relative energies. The energies are given at: CCSD(T)/CBS (bold), CCSD(T)/cc-pvTZ (in brackets), CCSD(T)/cc-pvDZ (square brackets), and B3LYP/6-311+G* (curly brackets) levels of theory, all at B3LYP/6-311+G* optimized geometries.....166

7-6 Lowest-lying structures of Li_6P_6, their point group symmetries, spectroscopic states and ZPE corrected relative energies. The energies are given at: CCSD(T)/CBS (bold), CCSD(T)/cc-pvTZ (in brackets),

CCSD(T)/cc-pvDZ (square brackets), and B3LYP/6-311+G* (curly brackets) levels of theory, all at B3LYP/6-311+G* optimized geometries.....167

7-7 Lowest-lying structures of Li_7P_7, their point group symmetries, spectroscopic states and ZPE corrected relative energies. The energies are given at: CCSD(T)/CBS (bold), CCSD(T)/cc-pvTZ (in brackets), CCSD(T)/cc-pvDZ (square brackets), and B3LYP/6-311+G* (curly brackets) levels of theory, all at B3LYP/6-311+G* optimized geometries.....168

7-8 Global minimum exo and edo isomers of S_7 and helical isomer S_7, their point group symmetries, spectroscopic states and ZPE corrected relative energies. The energies are given at B3LYP/6-311+G* level of theory, all at B3LYP/6-311+G* optimized geometries.....169

7-9 Lowest-lying structures of Li_8P_8, their point group symmetries, spectroscopic states and ZPE corrected relative energies. The energies are given at the B3LYP/6-311+G* level of theory, all at B3LYP/6-311+G* optimized geometries.....170

7-10 Lowest-lying structures of Li_9P_9, their point group symmetries, spectroscopic states and ZPE corrected relative energies. The energies are given at the B3LYP/6-311+G* level of theory, all at B3LYP/6-311+G* optimized geometries.....171

7-11 The results of NBO analysis for L_5P_5 double helix structure (here and elsewhere P is green, Li is violet).....172

7-12 The results of NBO analysis for L_6P_6 double helix structure.....173

7-13 The results of NBO analysis for L_7P_7 double helix structure.....174

7-14 The results of NBO analysis for L_8P_8 double helix structure.....175

7-15 The results of NBO analysis for L_9P_9 double helix structure.....176

7-16 Phonon dispersion of the infinite chain using the local-density approximation and norm-conserving pseudopotentials with a basis set containing plane-waves with energies up to 500 eV. The structure is stable to distortions hence a local minimum. There is a vibrational mode with small negative frequency (~ -6 cm^{-1}) at the Gamma point, which is a torsional mode associated with the orientation of the chain within the finite supercell.....177

8-1 Optimized (BP86/6-31G(d)) $Li_{90}P_{90}$ (C_2, ^1A) double-helical toroid structure with internal diameter of 25.6 Å and its side view showing helical arrangement of lithium and phosphorus atoms. Colour scheme: green, phosphorus; red, lithium 193

8-2 Simulated vibrational spectrum of $Li_{90}P_{90}$ cluster at the BP86/6-31G(d) level of theory 193

8-3 Cohesive energy per formula unit as a function of the number of units (n) in the Li_nP_n double helices. The blue rhombi correspond to straight double-helical clusters, whereas the green circle corresponds to the double-helical ring. The blue horizontal line corresponds to the cohesive energy of the infinite double-helical chain.....194

8-4 Chemical bonding pattern of $Li_{90}P_{90}$ shown by the AdNDP analysis. ON stands for occupation number 194

8-5 Optimized (BP86/STO-3G) $Li_{90}P_{90}$ (C_6, ^1A) double helical toroid structure with internal diameter of 22.2 Å 195

8-6 Optimized (B3LYP/6-31G(d)) $Li_{90}P_{90}$ (C_2, ^1A) double helical toroid structure with internal diameter of 25.4 Å 195

8-7 Lone pairs (s- and p-type) of S_7 (left) and Li_7P_7 (right) clusters showing the difference in the size of the corresponding orbitals 196

9-1 AdNDP π bonding pattern for [18]annulene. The corresponding point group symmetry and spectroscopic state are given in parenthesis. I), II) possible bond structures proposed for [18]annulene; III) symbolic representation of [18]annulene according to AdNDP. Here and elsewhere three center – two electron (3c-2e) bonds and delocalized bonding in the AdNDP symbolic representation are depicted with bend lines and circles, respectively 212

9-2 AdNDP π bonding pattern for dideazaporphyrin. The corresponding point group symmetry and spectroscopic state are given in parenthesis. I) possible resonance structure proposed for dideazaporphyrin; II) symbolic representation of dideazaporphyrin according to AdNDP 213

9-3 AdNDP π bonding pattern for porphyrin. The corresponding point group symmetry and spectroscopic state are given in parenthesis. I), II), III) representative porphyrin structures illustrating three different models for

porphyrinoid aromaticity, where I) shows the 18-π-electron delocalization, II) - the 22-π-electron delocalization, and III) - the three local 6-π-electron delocalizations recovered by AdNDP 214

9-4 AdNDP π bonding pattern and symbolic representation of antiaromatic dihydrodideazaporphyrin. The corresponding point group symmetry and spectroscopic state are given in parenthesis.....215

9-5 AdNDP π bonding pattern for C_2 symmetric bond-alternate [18]annulene. The corresponding point group symmetry and spectroscopic state are given in parenthesis.....216

10-1 Common representation of hypervalent iodine compounds with I=X (X= O, N, C) double bonds (structures **1**-**5**) adopted in research literature and the polymeric structure of iodosylbenzene **6** 230

10-2 I) General representation of the IO4- structure; II) Symbolic representation of IO4- according to AdNDP; III) AdNDP bonding pattern of IO4-. The corresponding point group symmetry and spectroscopic state of IO4- are given in parenthesis. ON stands for the occupation number here and elsewhere.....230

10-3 I) General representation of the PhIO structure; II) Symbolic representation of PhIO according to AdNDP. III) AdNDP bonding pattern for PhIO). The corresponding point group symmetry and spectroscopic state of PhIO are given in parenthesis.....231

10-4 I) General representation of the $PhINSO_2Ar$ structure; II) Symbolic representation of $PhINSO_2Ar$ according to AdNDP; III) AdNDP bonding pattern of the $PhINSO_2Ph$ molecule on the I-N, S-N, and I-C fragments 232

10-5 I) General representation of the $PhIC(CO_2Me)_2$ structure; II) Symbolic representation of $PhIC(CO_2Me)_2$ according to AdNDP; III) AdNDP bonding pattern of the $PhIC(CO_2Me)_2$ molecule on the I-C, C-C fragments 232

10-6 Complete AdNDP analysis of chemical bonding in PhIO molecule. ON stands for the occupation number here and elsewhere.....233

10-7 Complete AdNDP analysis of chemical bonding in $PhIO_2$ molecule 233

10-8 Complete AdNDP analysis of chemical bonding in $PhIO_3$ molecule 234

11-1 Selected lowest-energy structures of Si_6H_6, their point group symmetries, spectroscopic states and ZPE (B3LYP/6-311++G**) corrected relative energies (CCSD(T)/CBS//B3LYP/6-311++G**). The structures are labeled in accordance with Figure 11-5 257

11-2 Representative optimized isomers of each species in the $Si_{6-n}C_nH_6$ (n = 0–6) series, their point group symmetries, spectroscopic states and ZPE (B3LYP/6-311++G**) corrected relative energies (CCSD(T)/CBS//B3LYP/6-311++G**). Here and elsewhere the yellow, violet and blue spheres represent carbon, silicon and hydrogen atoms, respectively 258

11-3 Two representations of chemical bonding patterns of the I.1 global minimum structure revealed by the AdNDP 259

11-4 Chemical bonding patterns of the II.1, II.1, IV.1, V.1 and VI.1 global minimum structures revealed by the AdNDP 260

11-5 Lowest-lying structures of Si_6H_6, their point group symmetries, spectroscopic states and ZPE corrected relative energies. The energies are given at: CCSD(T)/CBS (bold), CCSD(T)/cc-pvTZ (in brackets), CCSD(T)/cc-pvDZ (square brackets), and B3LYP/6-311++G** (curly brackets), all at B3LYP/6-311+G* optimized geometries 261

11-6 Lowest-lying structures of Si_5CH_6, their point group symmetries, spectroscopic states and ZPE corrected relative energies. The energies are given at: CCSD(T)/CBS (bold), CCSD(T)/cc-pvTZ (in brackets), CCSD(T)/cc-pvDZ (square brackets), and B3LYP/6-311++G** (curly brackets), all at B3LYP/6-311++G** optimized geometries 262

11-7 Lowest-lying structures of $Si_4C_2H_6$, their point group symmetries, spectroscopic states and ZPE corrected relative energies. The energies are given at: CCSD(T)/CBS (bold), CCSD(T)/cc-pvTZ (in brackets), CCSD(T)/cc-pvDZ (square brackets), and B3LYP/6-311++G** (curly brackets), all at B3LYP/6-311++G** optimized geometries 263

11-8 Lowest-lying structures of $Si_3C_3H_6$, their point group symmetries, spectroscopic states and ZPE corrected relative energies. The energies are given at: CCSD(T)/CBS (bold), CCSD(T)/cc-pvTZ (in brackets), CCSD(T)/cc-pvDZ (square brackets), and B3LYP/6-311++G** (curly brackets), all at B3LYP/6-311++G** optimized geometries 264

11-9 Lowest-lying structures of $Si_2C_4H_6$, their point group symmetries, spectroscopic states and ZPE corrected relative energies. The energies are given at: CCSD(T)/CBS (bold), CCSD(T)/cc-pvTZ (in brackets), CCSD(T)/cc-pvDZ (square brackets), and B3LYP/6-311++G** (curly brackets), all at B3LYP/6-311++G** optimized geometries 265

11-10 Lowest-lying structures of SiC_5H_6, their point group symmetries, spectroscopic states and ZPE corrected relative energies. The energies are given at: CCSD(T)/CBS (bold), CCSD(T)/cc-pvTZ (in brackets), CCSD(T)/cc-pvDZ (square brackets), and B3LYP/6-311++G** (curly brackets), all at B3LYP/6-311++G** optimized geometries 266

12-1 Selected lowest-energy structures of P_6, their point group symmetries, spectroscopic states and ZPE (B3LYP/6-311+G*) corrected relative energies (CCSD(T)/CBS//B3LYP/6-311+G*) 279

12-2 Interaction of the pairs of occupied and unoccupied molecular orbitals of the D_{6h} ($^1A_{1g}$) structure of P_6 responsible for the PJT effect: interactions cause distortion toward the D_2 (^1A) structure upon following the doubly degenerate $\omega_{1,2}(e_{2u})$ imaginary frequency mode 279

12-3 Optimized structures, point group symmetry, spectroscopic states and bond lengths of the middle-deck fragments in the triple-decker sandwich complexes 280

12-4 One-to-one correspondence of unoccupied canonical molecular orbitals of P_6 (D_{6h}, $^1A_{1g}$) to those of $CpMoP_6MoCp$ (C_i, ^1A_g), where occupation in the latter results in the suppression of the PJT effect.....280

12-5 The chemical bonding picture of the $CpMoP_6MoCp$ triple-decker sandwich complex a) obtained by the AdNDP method: b), c) σ-bonds recovered on the $C_5H_5^-$ units; d) σ-bonds recovered on the P_6 unit; e) direct Mo-Mo σ-bond; f), g) π-bonds recovered on the $C_5H_5^-$ units; h) π-bonds recovered on the MoP_6Mo fragment; i) δ-bonds recovered on the MoP_6Mo fragment 281

13-1 (a) Vibrational vector for the PJT e_g'' mode of planar T3G cluster, (b) 55th MO, (c) next LUMO (74th), (d) overlap between MO(55) and MO(74), (e) potential derivative for the PJT e_g'' mode, and (f) orbital vibronic

coupling density (OVCD). The isovalues are 3 x 10^{-2} a.u. for (b) and (c), 1 x 10^{-3} a.u. for (d), 1 x 10^{-2} a.u. for (e), and 1 x 10^{-5} a.u. for (f).....308

13-2 Structures of graphitic triazine-based clusters, their point group symmetries, and spectroscopic states. Here and elsewhere the gray, blue, and white spheres represent carbon, nitrogen, and hydrogen atoms, respectively 308

13-3 (a) Structure and SSAdNDP chemical bonding pattern for *TGCN* sheet, (b) structure and AdNDP chemical bonding pattern for T3G cluster model. ON stands for occupation numbers. The isovalues are 8 x 10^{-3} a.u.....309

13-4 (a) Top and side views of optimized T3G ⋯ $2Be^{2+}$ complex, (b) top and side views of optimized Be^{2+} decorated *TGCN* sheet, (c) its band structure.....310

13-5 (a) 67^{th} MO, (b) next LUMO (76^{th}), (c) overlap between MO(67) and MO(76), (d) potential derivative for the e_g'' mode, and (e) orbital vibronic coupling density (OVCD). The isovalues are 3 x 10^{-2} a.u. for (a) and (b), 1 x 10^{-3} a.u. for (c), 1 x 10^{-2} a.u. for (d), and 1 x 10^{-5} a.u. for (e) 310

CHAPTER 1

INTRODUCTION

1-1. Ionic, atomic, and molecular clusters

The word *cluster* was first introduced by F. A. Cotton in 1960 to name the compounds with direct metal – metal bonds.[1] However, this definition has gradually changed to describe other substances containing nonmetal – metal and nonmetal – nonmetal bonds. Nowadays, *cluster* is a group of atoms bound together by inter-atomic forces and represents an intermediate form of matter[2] that bridges the gap between gas phase, where condensation starts to occur, and solutions or solids.[3] In fact there is no qualitative difference between small atomic clusters and molecules, but as the number of atoms in the system increases, atomic clusters start showing the specific properties making them unique physical objects, which are distinct from both isolated molecules and bulk materials. There are various types of atomic clusters: metal clusters,[4,5] fullerenes,[6] van der Waals clusters,[7] mixed clusters,[8] and they can exist in different geometries: spheres, triangles, rings, linear chains, spirals, etc. However, one can distinguish between different types of clusters by determining the nature of the chemical bonds, dictating spatial organization within the clusters. Therefore new theoretical approaches, including the development of new chemical bonding models, efficient ways of exploring complex potential energy surfaces, and new-generation force fields are very essential for cluster science, which can be viewed as the foundation of the increasingly important field of nanotechnology.

Clusters can serve as building blocks of many solid-state materials[9-11] or they can be synthesized by introducing appropriate stabilizing ligands including halides, carbon monoxide, alkenes, and hydrides.[12,13] Biological iron-sulfur clusters represent a group of chemically versatile inorganic structures that are attached to many proteins.[14] These clusters are deeply involved in the functions of the proteins and they are required to support life on earth. In spite of the diversity of stable clusters in solutions and crystalline phases, "bare" clusters are thermodynamically metastable species at ambient conditions, and thus can not be isolated. For instance, the second most stable (after N_2) homonuclear diatomic molecule in the second period, C_2, is not kinetically persistent and cannot fill any bottle at 1 atm and 293 K, because it tends to quickly polymerize.[15] But such "bare" metastable molecules and clusters can still be produced and studied in a molecular beam or under matrix isolation conditions. Using these specific experimental techniques, 13 excited electronic states of C_2 were successfully studied.[16]

One of the most powerful techniques developed for cluster studies in the gas phase is anion photoelectron spectroscopy.[17,18] Cluster anions, produced by the laser vaporization, are mass-selected, and the electron is photodetached to form the neutral cluster. The energy of the departing electron is energy analyzed to generate the electronic spectrum of the cluster. Because the cluster can be left vibrationally or electronically excited, the spectrum can contain vibrational progression, as well as some features that indicate electronically excited states.[19] Though anion photoelectron spectroscopy is not a structural method of analysis, the geometric structure of the observed cluster or molecule can be established by the comparison of experimental vertical electron detachment energies (VDEs) determined from the spectra with theoretically calculated VDEs.[20-22] It

should be noted that the newly produced cluster usually corresponds to the global minimum structure found theoretically because the experimental conditions of thermodynamic equilibrium allow detecting only the global minimum structure or isomers that are very close in energy to their ground state. In order to successfully find the global minimum structure, one needs to address two issues. First, it is quite important to sample a large region of configuration space to find the most stable geometric structures of chemical species for a given stoichiometry. Second, one needs to use accurate enough theoretical methods, which could guarantee that the predicted global minimum structure is indeed the true global minimum on the potential energy surface.[23] Therefore, if one wants to make a reliable prediction of a novel non-conventional cluster, and then get an experimental verification of this prediction using anion photoelectron spectroscopy, it is important to prove that the species of interest represents the global minimum structure. Such a joint experimental and theoretical approach has been confirmed very efficient in the development of cluster science and the exploration of new, yet unknown clusters and molecules in the gas phase.[2,21]

Some of the cluster related projects (Chapters 2–4) included in this dissertation were done in collaboration with photoelectron spectroscopy experimentalists: the group of Prof. Lai-Sheng Wang at Brown University. All the clusters discussed in Chapters 2–4 were produced and their photoelectron spectra were recorded using a magnetic-bottle photoelectron spectroscopy apparatus equipped with a laser vaporization cluster source.[24] Theoretically, for a given stoichiometry, global minimum and low-lying isomers (usually within ~30 kcal/mol) were established using the Coalescence Kick program[25,26] and subsequent high-level *ab initio* calculations. Also, theoretically calculated VDEs for the

lowest energy structures were compared with the experimentally observed peaks in photoelectron spectrum to make a conclusion about the validity of theoretical results on the predicted global minimum structure. Additionally, the intensities of peaks in the vibrational progression (Chapter 4) were simulated using the program for Franck-Condon analysis of spectral lines in photoelectron spectrum. Finally, in order to gain additional insight into the clusters' stability, geometries, and electronic properties, we performed chemical bonding analyses using the Adaptive Natural Density Partitioning (AdNDP) method[27,28] developed in the group of Prof. Boldyrev.

1-1.1. Boron-carbon mixed clusters

Boron clusters have been extensively characterized using photoelectron spectroscopy and *ab initio* theoretical calculations, which have identified the planar or quasi-planar geometric structures of small boron clusters.[12,29-32] However, in spite of the fact that boron and carbon are neighbors in the Periodic Table, the shapes of small carbon clusters are significantly different from those of boron. It has been shown that small anionic and neutral carbon clusters prefer to form linear structures.[33-36] Therefore, it would be interesting to investigate mixed carbon-boron clusters, because one can expect that doping pure boron clusters with carbon atoms may eventually lead to the structural transition of planar species into linear ones. Previous theoretical studies on mixed carbon-boron clusters reported the species with quite unusual chemical bonding motifs containing pentacoordinate,[37] hexacoordinate,[38,39] heptacoordinate,[39] and octacoordinate[40] planar carbon. However, recent experimental and high-level *ab initio* studies demonstrated that the carbon atom would rather occupy the peripheral position in the

mixed carbon-boron clusters;[41,42] and a logical planar-to-linear structural transition has been discovered in the $C_xB_{5-x}^-$ (x = 1–5) series.[43,44]

Chapter 2 reports a new type of structural transition in the series of $C_xB_{8-x}^-$ (x = 1–8) mixed clusters upon increase of the carbon concentration from x = 2 to x = 3. This transition is surprising since a wheel-to-ring instead of planar-to-linear transition was observed and confirmed by means of anion photoelectron spectroscopy and quantum-chemical calculations.

1-1.2. Tantalum doped boron clusters

Due to its electron-deficient character and tendency for deltahedral bond formation, boron can be successfully used for designing ring systems containing one or more hypercoordinate elements. A lot of boron rings enclosing planar hypercoordinate main group elements have been theoretically predicted.[45-48] However, none of them has experimentally been confirmed, except planar highly-symmetric B_8^{2-} [49] and B_9^- [50] clusters with hepta- and octacoordinate boron atoms in the central positions, respectively. A number of works were devoted to the exploration of the viability of boron wheels containing transition metals.[51-54] In 2011 the first experimental detection of boron rings in the gas phase with a central transition metal atom was reported.[55,56] The obtained clusters ($Co©B_8^-$, $Ru©B_9^-$, $Rh©B_9^-$, and $Ir©B_9^-$, where the © sign is used to designate the central position of the doped atom in monocyclic structures of $M©B_n^-$ type planar clusters) are remarkable in chemistry because of their perfectly planar structures with coordination numbers of 8 and 9. One year later, the highest coordination number (10) known so far for planar clusters was reported.[57] It was shown that $Ta©B_{10}^-$ and $Nb©B_{10}^-$ species possess perfectly D_{10h} symmetric structures.

Chapter 3 of this dissertation deals with a systematic study of small tantalum doped boron clusters TaB_n^- (n = 3–8) to trace the growth of these species leading to the formation of the planar metal-centered aromatic borometallic cluster $Ta©B_{10}^-$ with the highest coordination number for a metal atom in a planar geometry. The chapter also provides a detailed interpretation of photoelectron spectra, chemical bonding, and structural characteristics of the global minima found for different stoichiometric compositions of TaB_n^- (n = 3–8) clusters.

1-1.3. Development of program for calculating the intensity of spectral lines in vibrationally resolved photoelectron spectrum

Experimental photoelectron spectra of produced anion clusters are often complex and contain vibrational progression. Since there are many structural isomers for a particular stoichiometric composition, it is difficult to identify which anion structure is being photodetached and to elucidate the nature of the electronic or vibrational features in the photoelectron spectrum. Thus, theoretical calculations are important to aid in the spectral assignments. Chapter 4 describes the program capable of assessing intensities in the vibrational progression of photoelectron spectra and presents the results of the theoretical simulations for B_3^- and B_5^- clusters.

1-1.4. Li_3N_3 cluster: all-nitrogen analogue of ozone molecule

Nitrogen molecule possesses a strong triple bond, causing difficulty to convert N_2 into different compounds. However, despite the complicated synthesis of polynitrogen substances, they are of great interest as promising candidates for high-energy-density materials (HEDMs),[58] because of the ability to release large amounts of useful energy.

Chapter 5 provides a theoretical prediction of a new ozone-like polynitrogen molecule Li_3N_3 with an unusual N_3^{3-} molecular motif, which represents a viable species and thus might be synthesized.

1-1.5. Microsolvation study of dichloride Cl^-–Cl^- anion pair

Molecular clusters are aggregates of two to tens of molecules which are held together by intermolecular forces rather than covalent or ionic chemical bonds. These molecular clusters can be produced in the gas phase by expanding a high pressure reaction mixture containing the components of interest (solute and solvent molecules) into vacuum, and their photoelectron spectra can be recorded. The study of the molecular clusters enables consideration of certain aspects of solvation mechanism in exquisite detail as they represent good molecular models for understanding complicated processes of solvation in the bulk.

There are a lot of experimental and theoretical works on halide–water clusters, where most of these studies are devoted to hydrated monochloride anions.[59-61] However, studies on like-charged ion dihalide hydrates are rare and only recently became an attractive area of research. Chapter 6 describes a systematic study of microsolvation of dichloride anion pair by water molecules. The main objective of this work is to find theoretically the number of waters that would be sufficient to make like-charged Cl^-–Cl^- pair stable and accessible for the experimental photoelectron spectroscopy investigations.

1-2. Inorganic double helix structures

A helix is a geometric motif which can be present in both natural and synthetic structures. The most famous helical configuration is probably the structure of

deoxyribonucleic acid (DNA) in which the two helical strands are connected by hydrogen bonds between the corresponding bases.[62] Therefore, the double helix structure is essential for life, because it enables to store and transmit the important genetic information. In nature, there are also many other examples of molecular architectures with a helical spatial arrangement of molecular fragments.[63-65] However, inorganic single helices and double helices are less commonly observed species, which usually represent very complex compounds involving multiple building units.[66] Chapters 7 and 8 report the first evidence of the existence of simplest inorganic double helix structures composed of only two types of elements – phosphorus and lithium. The possibility of the experimental realization of extended LiP nanocoils, circular LiP "donut" shaped nanoparticles and periodic crystal structures is also discussed in these chapters.

1-2.1. Double helix Li_nP_n (n = 5–9) clusters, infinite LiP chains, and LiP solids

Chapter 7 is devoted to the theoretical prediction of chiral inorganic double helix structures (clusters Li_5P_5, Li_6P_6, Li_7P_7, Li_8P_8, Li_9P_9; infinite LiP chain, and two bulk phases of LiP of different symmetry) at the atomic level. The viability of lithium-phosphorus (LiP) double helices is confirmed by extensive *ab initio* quantum-chemical calculations. If synthesized, the LiP helical structures might be very useful for designing novel molecular devices such as sensors with the helical structures acting like springs whose contracting motion affects many important electrical properties.

1-2.2. Circular double helix species

Lithium doped phosphorus clusters are valence isoelectronic to sulfur clusters. It is well known that chains of sulfur atoms are able to form stable ring structures with the

largest experimentally identified circular sulfur cluster containing up to 18 atoms.[67] Logically, a few interesting questions arise concerning inorganic Li_nP_n double helix motif: is it possible to design a circular inorganic double helix consisting of Li and P atoms? And if yes, would it be stable? Chapter 8 answers these questions by providing a solid theoretical confirmation on the existence of the peculiar $Li_{90}P_{90}$ nanotoroid, which represents a new chemical bonding motif in inorganic chemistry.

1-3. Deciphering chemical bonding in hypervalent iodine compounds and porphyrinoids

Advancement of understanding relations between bonding and structure, bonding and stability, and bonding and reactivity is an important step towards rational design of new materials and catalysts. Therefore, developing and testing the new bonding models is of great importance in chemistry. A robust chemical bonding model allows researchers to rationalize structure, stability, and reactivity of a variety of chemical species, and can be used for rational design of new compounds and materials with useful properties.

Modern *ab initio* techniques allow one to calculate many molecular properties with almost experimental accuracy. However, polyatomic wavefunctions obtained in such calculations are highly complex and they are composed of molecular orbitals delocalized over the entire molecule. Natural Bond Orbital (NBO)[68] analysis is a backbone tool in dissecting a polyatomic wavefunction into two-centered two-electron bonds (2c-2e) and lone pairs providing a bridge between quantum chemical description of molecules with completely delocalized molecular orbitals and classical chemical language of Lewis theory.[69] However, NBO and other theoretical tools are not capable of

dissecting completely delocalized wave function into areas of partial delocalization over molecular fragments including 3, 4, 5 and larger number of atoms. The Adaptive Natural Density Partitioning (AdNDP)[27,28] method developed in the Prof. Boldyrev group represents chemical bonding as a set of localized (lone pairs and 2c-2e bonds) and delocalized multi-center bonds, which are associated with the concepts of aromaticity and antiaromaticity.[70] Chapters 9 and 10 show that our AdNDP analysis of chemical bonding is not limited to exotic clusters only, but can be successfully used to describe factors that govern structure, stability, and reactivity of porphyrinoids and sophisticated hypervalent iodine reagents, which are widely used in organic synthesis.

1-3.1. Description of aromaticity and chemical bonding in porphyrinoids

Porphyrinoids are macrocyclic compounds that have received much attention because of their unique structures and a wide spectrum of very useful physicochemical and biological properties.[71] However, despite the successful syntheses of various porphyrinoids and their analogues, there is no generally accepted description of aromaticity in such complicated macrocyclic systems. The concept of aromaticity has played an important role in the design and experimental realization of novel porphyrinoid compounds since the early 1930s.[72] Thus, the correct description of aromaticity and chemical bonding is vital for predicting new members of the porphyrin family. Chapter 9 explains bonding features and aromaticity of annulene, dideazaporphyrin, porphyrin, and dihydrodideazaporphyrin molecules.

1-3.2. Description of chemical bonding in hypervalent iodine compounds

Hypervalent iodine reagents are useful synthetic tools in organic chemistry because of their low toxicity, ready availability, and ease of handling.[73] However, despite extensive practical interest in these compounds, a small number of theoretical studies on structure, chemical bonding, and reactivity of these polyvalent iodine compounds have been reported. In particular, the question concerning the nature of I–X (X = O, N, C) bonds has not been thoroughly addressed. In the majority of textbooks and scientific papers they are drawn with double bonds between iodine and oxygen, nitrogen or carbon.[73-76] Chapter 10 analyzes I–X (X = O, N, C) bonds in the related hypervalent iodine compounds based on the AdNDP approach and suggests that the bonds within these compounds are of dative character, as opposed to the widely used double bond notation.

1-4. Restoring planarity of molecular structures

Two-dimensional (2D) materials and high-symmetry planar molecules have attracted considerable attention owing not only their unique electronic structures, but useful properties.[77] Thus, molecular and crystal symmetries exert great impact on physical and chemical properties of species. There are a lot of experimental and theoretical studies aimed at the production or prediction of novel planar and quasi-planar structures. However, these studies usually do not reveal directly the origin of the species' geometric configuration. Therefore, one cannot expand the results obtained for a specific system to other systems without unified theory capable of explaining structural transformations of the studied systems. According to Bersuker et al.[78] the best approach

to investigate molecular geometries should be based on how electrons control molecular configurations. Based on first principles it was proved that the pseudo Jahn-Teller (PJT) effect is the only source of instability and distortions of high-symmetry configurations of polyatomic systems.[78-80] Therefore, understanding of the PJT effect can be a powerful tool for rationalizing and predicting molecular and solid state structures, their deformations, transformations, and properties. So, the goal of the remaining part of this dissertation is to further generalize and elevate the PJT effect to a higher level of understanding of the origin of molecular and solid state properties. Chapters 11, 12, and 13 report that the PJT effect is responsible for the distortions in hexasilabenzene Si_6H_6 and hexaphosphabenzene P_6 molecules as well as in the recently synthesized 2D triazine-based graphitic carbon nitride (g-C_3N_4) sheets.[81] Newly discovered techniques of quenching the PJT effect and flattening the corresponding structures are also discussed in these chapters.

1-4.1. Suppression of the pseudo Jahn-Teller effect in $Si_{6-n}C_nH_6$ (n = 0–6) series

The aromatic benzene molecule is by far the lowest-energy structure of C_6H_6 stoichiometric composition, with benzvalene and prismane being more than 70 kcal/mol energetically less stable.[82] However, hydrocarbon analogs of Si_6H_6 are not the most stable isomers on the potential energy surface, because silicon hydrides usually tend to form electron-poor bonds with considerably weak π–π interactions.[83-86] All-silicon analog of benzene, the D_{6h} symmetric hexasilabenzene structure, is not even a local minimum, but a first-order saddle point.[87] The main objective of Chapter 11 is to trace the effect of isolobal substitution (Si–H groups by C–H groups) on structural transitions of global minimum species (from three-dimensional to two-dimensional) and on the quenching of

the PJT effect, which is the main source of the distortions in the cyclic isomers along $Si_{6-n}C_nH_6$ (n = 0–6) series.

1-4.2. Suppression of the pseudo Jahn-Teller effect in middle E_6 (E = P, As, Sb) rings of triple-decker sandwich complexes

Cyclo-P_6 hexaphosphabenzene, being a valence isoelectronic analog of benzene, doesn't adopt a planar hexagonal structure. It was shown that the planar P_6 structure is unstable towards out-of-plane distortions due to the pseudo Jahn-Teller effect.[88] However, Scherer et al.[89] successfully synthesized and characterized the $\{(\eta^5\text{-}Me_5C_5)Mo\}_2(\mu,\eta^6\text{-}P_6)$ triple-decker sandwich complex containing a planar P_6 ring with almost equal P–P bonds. Thus, aromatic and planar P_6 molecule can exist. Chapter 12 elucidates the mechanism of the PJT effect suppression in cyclic P_6, As_6, and Sb_6 molecules that become planar under complexation.

1-4.3. Pseudo Jahn-Teller origin of distortions in 2D triazine-based graphitic carbon nitride sheets

Since the preparation of single, free-standing 2D sheets of graphite, graphene[90] has been suggested by researchers as the most promising candidate material for post-silicon electronics. However, it is missing the typical electronic band gap that would make it a semiconductor. Recently, triazine-based graphitic carbon nitride (TGCN) was synthesized.[81] It represents a layered material that is similar to graphene, but which exhibits semiconducting properties. Thus, TGCN is of immense interest for future microelectronic devices. However, the material is at an early stage of development and electronic structure as well as electronic properties of TGCN have not been thoroughly

investigated. In particular, the source of instability of planar layers of TGCN towards puckering distortions has not been fully elucidated and understood. Chapter 13 investigates the distortions in the graphitic carbon nitride layers by considering the origin of the pseudo Jahn-Teller effect in this material. The knowledge of the mechanism of the PJT is important, since it allows for manipulation of this effect by means of external perturbations. So, the possible ways of obtaining completely planar TGCN sheet are also elaborated in this chapter.

References

(1) Mingos, D. M. P.; Wales, D. J. *Introduction to Cluster Chemistry*; N.J.: Prentice Hall, Englewood Cliffs, 1990.

(2) Castleman, A. W.; Jena, P. *Proc. Natl. Acad. Sci.* **2006**, *103*, 10552–10553.

(3) Alonso, J. A. *Structure and Properties of Atomic Nanoclusters*; Imperial College Press: London, 2012.

(4) Moskovits, M. *Annu. Rev. Phys. Chem.* **1991**, *42*, 465–499.

(5) Braunstein, P.; Oro, L. A.; Raithby, P. R. *Metal Clusters in Chemistry*; Wiley-VCH: New York, 1999.

(6) Kroto, H. W.; Heath, J. R.; Obrien, S. C.; Curl, R. F.; Smalley, R. E. *Nature* **1985**, *318*, 162–163.

(7) Chalasinski, G.; Szczesniak, M. M. *Chem. Rev*. **1994**, *94*, 1723–1765.

(8) Geoffroy, G. L. *Acc. Chem. Res*. **1980**, *13*, 469–476.

(9) Todorov, I.; Sevov, S. C. *Inorg. Chem*. **2004**, *43*, 6490–6494.

(10) Fokwa, B. P. T.; Hermus, M. *Angew. Chem. Int. Ed*. **2012**, *51*, 1702–1705.

(11) Long, J. R.; McCarty, L. S.; Holm, R. H. *J. Am. Chem. Soc*. **1996**, *118*, 4603–4616.

(12) Alexandrova, A. N.; Boldyrev, A. I.; Zhai, H. J.; Wang, L.-S. *Coord. Chem. Rev*. **2006**, *250*, 2811–2866.

(13) Seyferth, D. *Adv. Organomet. Chem*. **1976**, *14*, 97–144.

(14) Johnson, M. K. *Curr. Opin. Chem. Biol*. **1998**, *2*, 173–181.

(15) Hoffmann, R.; Schleyer, P. v. R.; Schaefer III, H. F. *Angew. Chem. Int. Ed*. **2008**, *47*, 7164–7167.

(16) Clementi, E. *Astrophys. J*. **1961**, *133*, 303–308.

(17) Leopold, D. G.; Ho, J.; Lineberger, W. C. *J. Chem. Phys*. **1987**, *86*, 1715–1726.

(18) Coe, J. V.; Snodgrass, J. T.; Friedhoff, C. B.; McHugh, K. M.; Bowen, K. H. *J. Chem. Phys*. **1985**, *83*, 3169–3179.

(19) Castleman, A. W.; Keesee, R. G. *Chem. Rev*. **1986**, *86*, 589–618.

(20) Boldyrev, A. I.; Wang, L.-S. *J. Phys. Chem. A* **2001**, *105*, 10759–10775.

(21) Boldyrev, A. I.; Wang, L.-S. *Chem. Rev*. **2005**, *105*, 3716–3757.

(22) Zubarev, D. Yu.; Averkiev, B. B.; Zhai, H.-J.; Wang, L.-S.; Boldyrev, A. I. *Phys. Chem. Chem. Phys*. **2008**, *10*, 257–267.

(23) Ivanov, A. S.; Boldyrev, A. I. *Phys. Chem. Chem. Phys*. **2012**, *14*, 15943–15952.

(24) Wang, L.-S.; Cheng, H.-S.; Fan, J. *J. Chem. Phys*. **1995**, *102*, 9480–9493.

(25) Averkiev, B. B. Geometry and Electronic Structure of Doped Clusters via the Coalescence Kick Method. PhD Dissertation, Utah State University, Logan, UT, 2009.

(26) Sergeeva, A. P.; Averkiev, B. B.; Zhai, H.-J.; Boldyrev, A. I.; Wang, L.-S. *J. Chem. Phys*. **2011**, *134*, 224304–224311.

(27) Zubarev, D. Yu. Analysis of Chemical Bonding in Clusters by Means of the Adaptive Natural Density Partitioning. PhD Dissertation, Utah State University, Logan, UT, 2008.

(28) Zubarev, D. Y.; Boldyrev, A. I. *Phys. Chem. Chem. Phys*. **2008**, *10*, 5207–5217.

(29) Zhai, H.-J.; Alexandrova, A. N.; Birch, K. A.; Boldyrev, A. I.; Wang, L.-S. *Angew. Chem. Int. Ed*. **2003**, *42*, 6004–6008.

(30) Alexandrova, A. N.; Zhai, H.-J.; Wang, L.-S.; Boldyrev, A. I. *Inorg. Chem*. **2004**, *43*, 3552–3554.

(31) Li, Q. S.; Zhao, Y.; Xu, W.; Li, N. *Int. J. Quantum Chem*. **2005**, *101*, 219–229.

(32) Sergeeva, A. P.; Popov, I. A.; Piazza, Z. A.; Li, W.-L.; Romanescu, C.; Wang, L.-S.; Boldyrev, A. I. *Acc. Chem. Res*. **2014**, *47*, 1349–1358.

(33) Van Orden, A.; Saykally, R. *J. Chem. Rev*. **1998**, *98*, 2313–2358.

(34) Watts, J. D.; Cernusak, I.; Bartlett, R. J. *Chem. Phys. Lett*. **1991**, *178*, 259–265.

(35) Yang, S.; Taylor, K. J.; Craycraft, M. J.; Conceicao, J.; Pettiette, C. L.; Cheshnovsky, O.; Smalley, R. E. *Chem. Phys. Lett*. **1988**, *144*, 431–436.

(36) v. Helden, G.; Kemper, P. R.; Gotts, N. G.; Bowers, M. T. *Science* **1993**, *259*, 1300–1302.

(37) Wang, Z.-X.; Schleyer, P. v. R. *Science* **2001**, *292*, 2465–2469.

(38) Exner, K.; Schleyer, P. v. R. *Science* **2000**, *290*, 1937–1940.

(39) Islas, R.; Heine, T.; Ito, K.; Schleyer, P. v. R.; Merino, G. *J. Am. Chem. Soc.* **2007**, *129*, 14767–14774.

(40) Minyaev, R. M.; Gribanova, T. N.; Starikov, A. G.; Minkin, V. I. *Mendeleev Commun*. **2001**, *11*, 213–214.

(41) Wang, L.-M.; Huang, W.; Averkiev, B. B.; Boldyrev, A. I.; Wang, L.-S. *Angew. Chem. Int. Ed*. **2007**, *46*, 4550–4553.

(42) Averkiev, B. B.; Wang, L.-M.; Huang, W.; Wang, L.-S.; Boldyrev, A. I. *Phys. Chem. Chem. Phys*. **2009**, *11*, 9840–9849.

(43) Averkiev, B. B.; Zubarev, D. Yu.; Wang, L.-M.; Huang, W.; Wang, L.-S.; Boldyrev, A. I. *J. Am. Chem. Soc.* **2008**, *130*, 9248–9250.

(44) Wang, L.-M.; Averkiev, B. B.; Ramilowski, J. A.; Huang, W.; Wang, L.-S.; Boldyrev, A. I. *J. Am. Chem. Soc.* **2010**, *132*, 14104–14112.

(45) Averkiev, B. B.; Boldyrev, A. I. *Russ. J. Gen. Chem.* **2008**, *78*, 769–773.

(46) Guo, J. C.; Yao, W. Z.; Li, Z.; Li, S. D. *Sci. China Ser. B* **2009**, *52*, 566–570.

(47) Islas, R.; Heine, T.; Ito, K.; Schleyer, P. v. R.; Merino, G. *J. Am. Chem. Soc.* **2007**, *129*, 14767–14774.

(48) Pu, Z. F.; Ge, M. F.; Li, Q. S. *Sci. China Ser. B* **2010**, *53*, 1737–1745.

(49) Alexandrova, A. N.; Zhai, H. J.; Wang, L.-S.; Boldyrev, A. I. *Inorg. Chem.* **2004**, *43*, 3552–3554.

(50) Zhai, H.-J.; Alexandrova, A. N.; Birch, K. A.; Boldyrev, A. I.; Wang, L.-S. *Angew. Chem. Int. Ed.* **2003**, *42*, 6004–6008.

(51) Ito, K.; Pu, Z.; Li, Q. S.; Schleyer, P. v. R. *Inorg. Chem.* **2008**, *47*, 10906–10910.

(52) Luo, Q. *Sci. China Ser. B* **2008**, *51*, 607–613.

(53) Miao, C.; Guo, J.; Li, S. *Sci. China Ser. B* **2009**, *52*, 900–904.

(54) Pu, Z.; Ito, K.; Schleyer, P. v. R.; Li, Q.-S. *Inorg. Chem.* **2009**, *48*, 10679–10686.

(55) Romanescu, C.; Galeev, T. R.; Li, W.-L.; Boldyrev, A. I.; Wang, L.-S. *Angew. Chem. Int. Ed*. **2011**, *50*, 9334–9337.

(56) Li, W.-L.; Romanescu, C.; Galeev, T. R.; Piazza, Z. A.; Boldyrev, A. I.; Wang, L.-S. *J. Am. Chem. Soc*. **2012**, *134*, 165–168.

(57) Galeev, T. R.; Romanescu, C.; Li, W.-L.; Wang, L.-S.; Boldyrev, A. I. *Angew. Chem. Int. Ed*. **2012**, *51*, 2101–2105.

(58) Haiges, R.; Schneider, S.; Schroer, T.; Christe, K. O. *Angew. Chem. Int. Ed*. **2004**, *43*, 4919–4924.

(59) Saeed, M. A.; Pramanik, A.; Wong, B. M.; Haque, S. A.; Powell, D. R.; Chandd, D. K.; Hossain, M. *Chem. Commun*. **2012**, *48*, 8631–8633.

(60) Markovich, G.; Pollack, S.; Giniger, R.; Cheshnovsky, O. J. *Chem. Phys*. **1994**, *101*, 9344–9353.

(61) Wang, Q.-Q.; Day, V. W.; Bowman-James, K. *J. Am. Chem. Soc.* **2013**, *135*, 392–399.

(62) Watson, J. D.; Crick, F. H. C. *Nature* **1953**, *171*, 737–738.

(63) Meurer, K. P.; Vogtle, F. *Top. Curr. Chem.* **1985**, *127*, 1.

(64) Wu, H.-C. H.; Sarko, A. *Carbohydr. Res*. **1978**, *61*, 27–40.

(65) Fersht, A. *Structure and Mechanism in Protein Science*; W. H. Freeman: New York, 1998.

(66) Albrecht, M. *Chem. Rev*. **2001**, *101*, 3457−3497.

(67) Meyer, B. *Chem. Rev*. **1976**, *76*, 367−388.

(68) Weinhold, F.; Landis, C. R. *Valency and Bonding: A Natural Bond Orbital Donor-Acceptor Perspective*, Cambridge University Press: Cambridge, U.K., 2005

(69) Lewis, G. N. *J. Am. Chem. Soc*. **1916**, *38*, 762–785.

(70) Galeev, T. R.; Boldyrev, A. I. Aromaticity and Antiaromaticity in Inorganic Chemistry. In *Comprehensive Inorganic Chemistry II (Second Edition)*; Reedijk, J.; Poeppelmeier, K., Eds.; Elsevier: Amsterdam, 2013; pp. 245–275.

(71) Walter, M. G.; Rudine, A. R.; Wamser, C. C. *J. Porphyrins Phthalocyanines* **2010**, *14*, 759–792.

(72) Hückel, E. *Z. Phys.* **1931**, *70*, 204–286.

(73) Zhdankin, V. V. *Hypervalent Iodine Chemistry: Preparation, Structure, and Synthetic Applications of Polyvalent Iodine Compounds*; Wiley: Chichester, 2013.

(74) Varvoglis, A. *Hypervalent Iodine in Organic Synthesis*, Academic Press: London, 1997.

(75) Brand, J. P.; Gonzalez, D. F.; Nicolai, S.; Waser, J. *Chem. Commun*. **2011**, *47*, 102–115.

(76) Duschek, A.; Kirsch, S. F. *Angew. Chem*. **2011**, *123*, 1562–1590.

(77) Miro, P.; Audiffred, M.; Heine, T. *Chem. Soc. Rev*. **2014**, *43*, 6537–6554.

(78) Bersuker, I. B. *Chem. Rev*. **2013**, *113*, 1351–1390.

(79) Bersuker, I. B. *The Jahn-Teller Effect*, Cambridge University Press: Cambridge, U.K., 2006.

(80) Bersuker, I. B.; Gorinchoi, N. N.; Polinger, V. Z. *Theor. Chim. Acta*. **1984**, *66*, 161–172.

(81) Algara-Siller, G.; Severin, N.; Chong, S. Y.; Björkman, T.; Palgrave, R. G.; Laybourn, A.; Antonietti, M.; Khimyak, Y. Z.; Krasheninnikov, A. V.; Rabe, J. P.; et al. *Angew. Chem. Int. Ed.* **2014**, *53*, 7450–7455.

(82) Dinadayalane, T. C.; Priyakumar, U. D.; Sastry, G. N. *J. Phys. Chem. A* **2004**, *108*, 11433–11448.

(83) Jacobsen, H.; Ziegler, T. *J. Am. Chem. Soc*. **1994**, *116*, 3667–3679.

(84) Nagase, S.; Kobayashi, K.; Takagi, N. J. *Organomet. Chem*. **2000**, *611*, 264–271.

(85) Frenking, G.; Krapp, A.; Nagase, S.; Takagi, N.; Sekiguchi, A. *Chem. Phys. Chem*. **2006**, *7*, 799–800.

(86) Power, P. P. *Chem. Rev*. **1999**, *99*, 3463–3504.

(87) Nagase, S.; Teramae, H.; Kudo, T. *J. Chem. Phys*. **1987**, *86*, 4513–4517.

(88) Galeev, T. R.; Boldyrev, A. I. *Phys. Chem. Chem. Phys*. **2011**, *13*, 20549–20556.

(89) Scherer, O. J.; Sitzmann, H.; Wolmershauser, G. *Angew. Chem. Int. Ed*. **1985**, *24*, 351–353.

(90) Novoselov, K. S.; Jiang, D.; Schedin, F.; Booth, T. J.; Khotkevich, V. V.; Morozov, S. V.; Geim, A. K. *Proc. Natl. Acad. Sci. USA* **2005**, *102*, 10451–10453.

CHAPTER 2

MOLECULAR WHEEL TO MONOCYCLIC RING TRANSITION IN BORON–CARBON MIXED CLUSTERS $C_2B_6^-$ AND $C_3B_5^-$ [1]

Abstract

In this joint experimental and theoretical work we present a novel type of structural transition occurring in the series of $C_xB_{8-x}^-$ (x = 1-8) mixed clusters upon increase of the carbon content from x = 2 to x = 3. The wheel to ring transition is surprising because it is rather planar-to-linear type of transition to be expected in the series since B_8, B_8^-, B_8^{2-} and CB_7^- are known to posses wheel-type global minimum structures while C_8 is linear.

Carbon and boron being neighbours in The Periodic Table have very different geometric structures of their small clusters. Small carbon clusters are either linear or cyclic,[1] whereas, those of boron are either planar or quasiplanar.[2] Thus, one can expect peculiar transitions from planar to linear structures upon increasing the number of carbon atoms in mixed boron-carbon clusters. An example of such planar-to-linear structural transition as a function of the number of carbon atoms has been found to occur in the mixed boron-carbon clusters, $C_xB_{5-x}^-$ (x = 1-5) between x = 2 and 3.[3] Larger boron-carbon mixed clusters have been computationally proposed to exemplify unusual hexa-, hepta and octa-coordinated planar carbon species (CB_6^{2-},[4] CB_7^-,[5] and CB_8[6]). However, it was shown later in joint experimental and theoretical works[7-9] that carbon avoids the central

[1] Coauthored by Timur R. Galeev, Alexander S. Ivanov, Constantin Romanescu, Wei-Li Li, Konstantin V. Bozhenko, Lai-Sheng Wang, and Alexander I. Boldyrev. Reproduced from *Phys. Chem. Chem. Phys.* **2011**, *13*, 8805-8810 with permission from the PCCP Owner Societies.

position in those wheel-type global minimum geometries and occupies the peripheral position instead. It is known that the B_8 , B_8^- and B_8^{2-} clusters[10-14] and the CB_7^- cluster[8] have wheel-type heptagon structures with one boron atom in the center. The C_8 cluster has a linear global minimum structure with the cyclic isomer being about 10 kcal mol^{-1} higher.[1,15,16] Therefore, a planar-to-linear transition could be expected in the $C_xB_{8-x}^-$ (x = 1-8) series upon increasing the carbon content in the clusters. Surprisingly, we found a novel structural transition that has never been observed before – wheel-to-ring transition between $C_2B_6^-$ and $C_3B_5^-$ structures of the series. We would like to point out that ring-like structures have been previously reported in a theoretical study by Shao *et. al.*[17] for the neutral C_nB_3 (n = 4-8) clusters.

The $C_2B_6^-$ and $C_3B_5^-$ clusters were investigated by photoelectron spectroscopy (PES) and *ab initio* calculations. The experiment was performed with a laser-vaporization cluster source and a magnetic-bottle photoelectron spectrometer (see Experimental Section). [18]

The photoelectron spectra of the $C_2B_6^-$ cluster are presented in Fig. 2-1 and the photoelectron spectra of $C_3B_5^-$ are shown in Fig. 2-2. The experimentally observed vertical detachment energies (VDEs) for the clusters are given in Tables 2-1 and 2-2 and are compared to the theoretically calculated data.

Fig. 2-1 shows the PES spectra of $C_2B_6^-$ at three photon energies. The 193 nm spectrum of $C_2B_6^-$ reveals six well-resolved features labelled A-F (Fig. 2-1b). At the low binding energy side, we observe a very broad feature (X, X′) corresponding to photodetachment from the two lowest lying isomers of $C_2B_6^-$. The ninth band (G) can be tentatively identified, but the signal-to-noise ratios are poor at the high binding energy

side. The spectra recorded at 266 nm (Fig. 2-1a) reveal fine vibrational features for the A and B electronic bands. For the A band we measured a vibrational spacing of 330±30 cm^{-1} using the PES measured at 355 nm (see the inset of Fig. 2-1a). The B band shows fine structure both at 193 nm and 266 nm, however, the measurement of the vibrational spacing is complicated by the existence of two nearly isoenergetic photodetachment channels.

The spectra of $C_3B_5^-$ are shown in Fig. 2-2. The VDE of the X band was measured to be 3.94 ± 0.03 eV. The intensity change between the X and the A bands confirms that there are two features rather than a vibrational progression. The X band shows a short vibrational progression with a spacing of 380 ± 30 cm^{-1}.

Computationally, we first performed the global minimum structure search for the $C_2B_6^-$ ion using the Coalescence Kick (CK)[19–21] program written by Averkiev. The CK method subjects large populations of randomly generated structures to a coalescence procedure in which all atoms are pushed gradually to the molecular center of mass to avoid generation of fragmented structures and then optimized to the nearest local minima. The CK calculations were performed at the B3LYP/3-21G level of theory. All the low-lying (ΔE < 25 kcal mol^{-1}) isomers revealed were reoptimized with follow up frequency calculations at the B3LYP/6-311+G* level of theory. Single point calculations for the lowest energy structures were performed at the RCCSD(T)/6-311+G(2df) level of theory using the B3LYP/6-311+G* optimized geometries. The relative energies of a series of representative isomers are given in Fig. 2-3.

The CK search revealed that the cyclic structure I.6 is the lowest isomer with the structures I.1–I.5 being 12–25 kcal mol^{-1} higher at the B3LYP/3-21G level of theory.

However, when we reoptimized all the low-lying structures at the B3LYP/6-311+G* level of theory we found a significantly different order of the isomers with the wheel-type structure I.1 being the lowest isomer and the cyclic structure I.6 lying 9.1 kcal mol^{-1} higher (Fig. 2-3). Therefore, the set of isomers for subsequent investigation should be formed of all the structures lying in the range of about 20 kcal mol^{-1} relative energies at this level of theory as it was done in the current work. Moreover, the B3LYP/6-311+G* calculated results were further corrected by the single point calculations at the RCCSD(T)/6-311+G(2df)//B3LYP/6-311+G* level of theory (Fig. 2-3). Thus, according to our most accurate calculations the wheel-type structure I.1 is the global minimum for the $C_2B_6^-$cluster. In order to verify this theoretical prediction we calculated theoretical VDEs for the global minimum structure I.1 at three levels of theory: TD-B3LYP/6-311+G(2df), UOVGF/6-311+G(2df) and R(U)CCSD(T)/6-311+G(2df) all at the B3LYP/6-311+G* optimized geometries. We also calculated VDEs for the second lowest structure I.2 at the same three levels of theory and found out that it also contributes to the experimental PES of $C_2B_6^-$. Results of the VDEs calculations are summarized in Table 2-1.

The broad feature X(X′) in the experimental spectrum of $C_2B_6^-$ (Fig. 2-1) can be assigned to the electron detachment from the singly-occupied HOMO $7a_1$ of the global minimum structure I.1. The broad shape of the peak is an indication of a large geometry change upon the electron detachment, which was confirmed by geometry optimization of the neutral C_2B_6 cluster (see Fig. 2-4) The electron detachment from the singly occupied HOMO 11a′ of the I.2 isomer can also contribute to this peak since the first VDE is very close to that of I.1. None of the calculated VDEs of I.1 could be assigned to the

experimental feature at ~3.2 eV. This peak confirms the presence of the second-lowest isomer I.2 of $C_2B_6^-$ in the molecular beam since it can be clearly explained by the electron detachment from 3a″ of I.2 leading to the final $^3A''$ state. Electron detachment processes with final triplet states are expected to be more prominent in the experimental spectra, therefore, we discuss only the transitions leading to the final triplet states. The feature at 3.54 eV in the experimental PES is due to the electron detachment from HOMO − 1 $2b_1$ with the final state $^3B_1$. The next feature (4.35 eV) corresponds to the electron detachment from HOMO − 2 $1a_2$ to the final $^3A_2$ state. Both of these detachment channels are of isomer I.1. The features at 4.68 and 4.77 eV can be explained only by the electron detachment from 2a″ and 10a′ of I.2 corresponding to two final states: $^3A'$ and $^3A''$. The sharp peak at 4.96 eV is due to the detachment from HOMO − 3 $6a_1$ leading to the $^3A_1$ state of I.1. The broad feature at about 6 eV can be assigned to two detachments of electrons from HOMO − 4 $4b_2$ of I.1 and from HOMO − 4 9a′ of I.2 with the final states $^3B_2$ and $^3A'$, respectively. The excellent agreement between the experimentally observed and the theoretically calculated VDEs confirms the predicted structures of the two lowest-lying isomers I.1 and I.2 contributing to the experimental PES of $C_2B_6^-$.

According to the CK search the global minimum structure of the $C_3B_5^-$cluster is a cyclic isomer II.1 with the lowest wheel-type structure II.5 being 62.1 kcal mol^{-1} higher at the B3LYP/3-21G level of theory (Fig. 2-5).

Geometry optimization for the low-lying isomers ($\Delta E<25$ kcal mol^{-1}) and the lowest-found wheel-type structure II.5 at the B3LYP/6-311+G* level of theory with subsequent single point calculations at the RCCSD(T)/6-311+G(2df)//B3LYP/6-311+G*

level revealed the presented (Fig. 2-5) order. Thus, according to our calculations the global minimum is the cyclic isomer II.1 and the structural transition from the wheel-type structure to monocyclic ring occurs between $C_2B_6^-$ and $C_3B_5^-$. The lowest wheel-type structure II.5 is 28.8 kcal mol^{-1} higher than the global minimum (RCCSD(T)/6-311+G(2df)//B3LYP/6-311+G*).

Again, we calculated VDEs of the proposed structure II.1 to compare those with the experimental PES. Only the isomer II.1 is expected to contribute to the experimental PES of the $C_3B_5^-$ cluster, since the lowest alternative isomer II.2 is 13 kcal mol^{-1} higher than II.1. The VDE calculations were performed at the same three levels of theory: TD-B3LYP/6-311+G(2df), ROVGF/6-311+G(2df) and RCCSD(T)/6-311+G(2df) all at the B3LYP/6-311+G* optimized geometry. The VDEs calculated are summarized in Table 2-2. Our calculations revealed two very close transitions corresponding to the electron detachments from HOMO ($5b_2$) and HOMO-1 ($1a_2$). The first VDE is 0.1-0.2 eV lower than that assigned to the detachment from HOMO-1 according to all the three theory levels. These two transitions are responsible for the features X and A in the experimental spectra of the $C_3B_5^-$ cluster (Fig. 2-2). There is a big gap between these two transitions and the transition corresponding to electron detachment from HOMO-2 ($2b_1$) which varies from 1.0 eV (TD-DFT) to 1.3 eV (RCCSD(T)). This computational prediction is confirmed by the experimental spectra, showing the gap of 1.2 eV between feature A and feature B. The fourth electron detachment occurs from HOMO-3 ($6a_1$) and the calculated VDE agrees well with the experimental value (5.47 eV). The sharp shape of the first peak in the PES spectra of the $C_3B_5^-$ cluster is consistent with the calculated small geometry change upon the electron detachment (see Fig. 2-4). The perfect agreement between the

experimental and the theoretical VDEs confirms the global minimum structure II.1 for the $C_3B_5^-$ cluster.

In order to trace structural change from the wheel-type structure to the monocyclic ring structure we calculated the monocyclic structure for the cluster CB_7^-. The calculated relative energy of the wheel-type global minimum structure with respect to the monocyclic ring structure is presented in Fig. 2-6 as well as the corresponding relative energies of the monocyclic ring and wheel-type structures for the $C_2B_6^-$ and $C_3B_5^-$clusters.

One can see that the energy difference between the wheel-type and monocyclic ring isomers dropped from 79.0 to 20.5 kcal mol^{-1} (at RCCSD(T)/6-311+G(2df)//B3LYP/6-311+G*) upon transition from CB_7^- to $C_2B_6^-$. The substitution of another boron by a carbon atom in $C_3B_5^-$ leads to the inversion of the wheel-type and monocyclic structures with the monocyclic structure being now the global minimum. It was proposed by Zubarev and Boldyrev[22] that the wheel-type structures appear in boron clusters beginning from B_8 since the dangling electron density at the center of the monocyclic cluster cannot be supported by the valence charge of the boron atoms. Migration of one of the boron atoms into the center of the ring provides the necessary electrostatic field stabilization in the wheel-type structures and that is the reason why those structures are the global minima. The substitution of boron atoms in the peripheral ring by carbon atoms provided additional electrostatic field stabilization at the center of the ring due to the higher valence charge of carbon, which eventually leads to the higher stability of the monocyclic structures over the wheel-type structures in the mixed carbon–boron clusters.

It was previously shown[7] that the global minimum wheel-type structure of CB_7^- is doubly aromatic. The CB_7^- monocyclic structure has a conflicting aromaticity. The chemical bonding is consistent with the higher stability of the doubly aromatic wheel-type structure relative to the monocyclic structure with the conflicting aromaticity.

We performed chemical analysis in the studied clusters using the Adaptive Natural Partitioning method (AdNDP) developed by Zubarev and Boldyrev.[23] Results of the AdNDP analysis are summarized Fig. 2-7 and 2-8. According to our AdNDP analysis, chemical bonding in the wheel-type structure of the $C_2B_6^-$cluster in Fig. 2-7 can be described as a combination of three 2c–2e σ B–B bonds, four 2c–2e σ C–B bonds, three delocalized π-bonds (responsible for π-aromaticity), three delocalized doubly-occupied σ-bonds and one delocalized singly-occupied σ-bond. Here and elsewhere the terms delocalized σ-bonds and delocalized π-bonds mean that those bonds cannot be reduced to 2c–2e bonds by the AdNDP method. It was previously proposed[24] to name cases like the one we have here with an odd number of electrons for σ-delocalized bonds as ½-σ-antiaromatic. "½" is used as a label and means that the σ-system with singly occupied delocalized bond is half way down to being σ-antiaromatic in the wheel-type structure of the doubly-charged $C_2B_6^{2-}$ ion. The ½-σ-antiaromatic nature of the global minimum structure I.1 of the $C_2B_6^-$cluster is consistent with relatively low first VDE of the cluster. When the extra electron in the $C_2B_6^-$cluster is removed from the singly-occupied orbital the resulting neutral C_2B_6 species becomes a doubly-aromatic system which is consistent with the round structure of the neutral species (Fig. 2-7).

The chemical bonding in the monocyclic structure I.6 of the $C_2B_6^-$cluster can be described as follows. There are four 2c–2e σ B–B bonds, four 2c–2e σ C–B bonds, three

delocalized π-bonds (responsible for π-aromaticity), two delocalized doubly-occupied σ-bonds and one delocalized singly-occupied σ-bond. Thus, the structure I.6 is ½-σ-aromatic since the singly occupied delocalized bond is half way down to being σ-aromatic in the monocyclic ring-type structure of the doubly-charged $C_2B_6^{2-}$ ion (see Fig. 2-7). The presence of ½-σ-antiaromaticity in the wheel-type structure and of the ½-σ-aromaticity in the monocyclic structure explains the relatively low energy difference compared to that of the CB_7^- structures (Fig. 2-6).

The global minimum monocyclic structure II.1 of the $C_3B_5^-$cluster (Fig. 2-8) is doubly-aromatic with two 2c–2e σ B–B bonds, six 2c–2e σ C–B bonds, three delocalized π-bonds (responsible for π-aromaticity), three delocalized σ-bonds (responsible for σ-aromaticity). The doubly-aromatic nature of the global minimum structure $C_3B_5^-$ is consistent with the rather high first VDE of this cluster.

Chemical bonding analysis of the lowest-lying wheel-type isomer II.5 (Fig. 2-8) revealed one 2c–2e σ B–B bond, six 2c–2e σ C–B bonds, three delocalized π-bonds (responsible for π-aromaticity) and four delocalized σ-bonds (responsible for σ-antiaromaticity). The σ-antiaromaticity leads to deformation of the heptagon structure into the hexagon structure with one carbon atom coordinated to the edge of the hexagon. As a result of that we have three σ-bonds delocalized over the hexagon and one 3c–2e σ-bond delocalized over the external carbon atom and the two edge boron atoms see Fig. 2-8). The structure II.5 possessing conflicting aromaticity is higher in energy than the doubly-aromatic global minimum structure II.1.

In the above discussion we presented chemical bonding explanation for different stabilities of the wheel-type and monocyclic ring-type structures. With the chemical

bonding analysis we can explain why the $C_2B_6^-$cluster has relatively low first VDE compared to that of the $C_3B_5^-$cluster. However we would like to stress that we believe that the transition from the wheel-type to the ring-type structures in the series occurs due to the increase of the stabilizing electrostatic field at the center of the cluster as a result of the increased number of carbon atoms in $C_3B_5^-$, which makes the presence of the central boron atom unnecessary.

2-1. Experimental section

The experiment was performed using a magnetic-bottle PES apparatus equipped with a laser vaporization cluster source, details of which have been published elsewhere.[25,26] Briefly, the carbon-doped boron clusters were produced by laser vaporization of a disk target made of isotopically enriched ^{10}B (~6% wt), C (~0.6% wt), and Bi. The clusters were entrained by the helium carrier gas supplied by two pulsed Jordan valves and underwent a supersonic expansion to form a collimated molecular beam. The cluster composition and the cooling were controlled by the time delay between the pulsed beam valves and the vaporization laser. The negatively charged clusters were extracted from the cluster beam and analyzed with a time-of-flight mass spectrometer. The clusters of interest were mass selected and decelerated before being intercepted by the probe photodetachment laser beam: 193 nm (6.424 eV) from an ArF excimer laser and 355 nm (3.496 eV) or 266 nm (4.661 eV) from a Nd:YAG laser. Photoelectrons were collected at nearly 100% efficiency by a magnetic bottle and analyzed in a 3.5 m long electron flight tube. The cluster PE spectra were calibrated using the known spectra of

Bi^-. The kinetic energy resolution of the magnetic bottle apparatus, $\Delta E/E$, was typically better than 2.5%, *i.e.* ~25 meV for 1 eV electrons.

2-2. Theoretical section

We searched for the global minimum of the $C_2B_6^-$ and $C_3B_5^-$clusters using the Coalescence Kick (CK) program[19–21] with the B3LYP/3-21G method for energy and gradient calculations. Then we reoptimized the geometries and performed frequency calculations for the lowest isomers (E < 25 kcal mol^{-1}) at the B3LYP/6-311+G* level of theory and recalculated total energies of the isomers at the RCCSD(T)/6-311+G(2df)//B3LYP/6-311+G* level of theory. The VDEs for the global minima I.1 and II.1 and the low-lying isomer I.2 were calculated using the R(U)CCSD(T)/6-311+G(2df) method, the outer-valence Green Function method (R(U)OVGF/6-311+G(2df)) and the time-dependent DFT method (TD B3LYP/6-311+G(2df) at the B3LYP/6-311+G* geometries. The calculations were performed with the Gaussian 03[27] and Molpro[28] software. Molecular orbitals were visualized with the MOLDEN 3.4[29] and Molekel 5.4.0.8[30] programs.

Notes and references

1 A. V. Orden, R. J. Saykally, *Chem. Rev.* 1998, **98**, 2313.

2 A. N. Alexandrova, A. I. Boldyrev, H. J. Zhai and L. S. Wang. *Coord. Chem. Rev*. 2006, **250**, 2811.

3 L. M. Wang, B. B. Averkiev, J. A. Ramilowski, W. Huang, L. S. Wang and A. I. Boldyrev. *J. Am. Chem. Soc.* 2010, **132**, 14104.

4 K. Exner and P. v. R. Shleyer, *Science*, 2000, **290**, 1937.

5 Z. X. Wang and P. v. R. Shleyer, *Science*, 2001, **292**, 2456.

6 R. M. Minyaev, T. N. Gribanova, A. G. Starikov and V. I. Minkin, *Mendeleev Commun.* 2001, **11**, 213.

7 B. B. Averkiev, D. Yu. Zubarev, L. M. Wang, W. Huang, L. S. Wang and A. I. Boldyrev, *J. Am. Chem. Soc*. 2008, **120**, 9248.

8 L. M. Wang, W. Huang, B. B. Averkiev, A. I. Boldyrev and L. S. Wang, *Angew. Chem. Int. Ed.* 2007, **46**, 4550.

9 B. B. Averkiev, L. M. Wang, W. Huang, L. S. Wang and A. I. Boldyrev, *Phys. Chem. Chem. Phys*. 2009, **11**, 9840.

10 I. Boustani, *Phys. Rev. B.* 1997, **55**, 233.

11 V. Bonacic-Koutecky, P. Fantucci and J. Koutecky, *Chem. Rev*. 1991, **91**, 1035.

12 H.-J. Zhai, A. N. Alexandrova, K. A. Birch and A. I. Boldyrev, L. S. Wang, Angew. *Chem. Int. Ed. Engl*. 2003, **42**, 6004.

13 A. N. Alexandrova, H.-J. Zhai, L .S. Wang and A. I. Boldyrev, *Inorg. Chem.* 2004, **43**, 3552.

14 Q. S. Li, Y. Zhao, W. Xu and N. Li, *Int. J. Quant. Chem.* 2005, **101**, 219.

15 J. M. L. Martin and P. R. J. Taylor, *Phys. Chem.* 1996, **100**, 6047.

16 Yu. Shlyakhter and S. Sokolova, *J. Chem. Phys.* 1999, **110**, 10725.

17 J. Shao, C. He, R. Shi, C. Wang, X. Zhu and X. Lu, *J. Mol. Struct: THEOCHEM*, 2010, **961**, 17.

18 L. S. Wang, H. S. Cheng and J. Fan, *J. Chem. Phys.* 1995, **102**, 9480.

19 B. B. Averkiev, PhD thesis, Utah State University (USA), 2009.

20 W. Huang, A. P. Sergeeva, H.-J. Zhai, B. B. Averkiev, L. S. Wang and A. I. Boldyrev, *Nat. Chem.* 2010, **2**, 202.

21 M. Saunders, *J. Comput. Chem.* 2004, **25**, 621.

22 D. Yu. Zubarev and A. I. Boldyrev, *J. Comput. Chem.* 2007, **28**, 251

23 D. Yu. Zubarev and A. I. Boldyrev, *Phys. Chem. Chem. Phys.* 2008, **10**, 5207.

24 D. Yu. Zubarev, A. P. Sergeeva and A. I. Boldyrev, in *Chemical Reactivity Theory. A Density Functional View.* (Ed: P. K.Chattaraj) CRC Press, Taylor & Francis Group, New York, 2009; pp. 439-452.

25 J. W. Fan and L. S. Wang, *J. Chem. Phys.* 1995, **102**, 8714-8717

26 L.-S. Wang and X. Li, in *Proc. Int. Symp. on Clusters and Nanostructure Interfaces (Oct. 25-28, 1999, Richmond, VA)* (Eds.: P. Jena, S. N. Khanna, B. K. Rao), World Scientific, River Edge, New Jersey, 2000, pp. 293-300.

27 M. J. Frisch, G. W. Trucks, H. B. Schlegel, G. E. Scuseria, M. A. Robb, J. R. Cheeseman, J. A. Montgomery, Jr., T. Vreven, K. N. Kudin, J. C. Burant, J. M. Millam, S. S. Iyengar, J. Tomasi, V. Barone, B. Mennucci, M. Cossi, G. Scalmani, N. Rega, G. A. Petersson, H. Nakatsuji, M. Hada, M. Ehara, K. Toyota, R. Fukuda, J. Hasegawa, M. Ishida, T. Nakajima, Y. Honda, O. Kitao, H. Nakai, M. Klene, X. Li, J. E. Knox, H. P. Hratchian, J. B. Cross, V. Bakken, C. Adamo, J. Jaramillo, R. Gomperts, R. E. Stratmann, O. Yazyev, A. J. Austin, R. Cammi, C. Pomelli, J. W. Ochterski, P. Y. Ayala, K. Morokuma, G. A. Voth, P. Salvador, J. J. Dannenberg, V. G. Zakrzewski, S. Dapprich, A. D. Daniels, M. C. Strain, O. Farkas, D. K. Malick, A. D. Rabuck, K. Raghavachari, J. B. Foresman, J. V. Ortiz, Q. Cui, A. G. Baboul, S. Clifford, J. Cioslowski, B. B. Stefanov, G. Liu, A. Liashenko, P.

Piskorz, I. Komaromi, R. L. Martin, D. J. Fox, T. Keith, M. A. Al-Laham, C. Y. Peng, A. Nanayakkara, M. Challacombe, P. M. W. Gill, B. Johnson, W. Chen, M. W. Wong, C. Gonzalez, and J. A. Pople, Gaussian, Inc., Wallingford, CT, 2004.

27 H.-J. Werner, P. J. Knowles, F. R. Manby, M. Schütz, P. Celani, G. Knizia, T. Korona, R. Lindh, A. Mitrushenkov, G. Rauhut, T. B. Adler, R. D. Amos, A. Bernhardsson, A. Berning, D. L. Cooper, M. J. O. Deegan, A. J. Dobbyn, F. Eckert, E. Goll, C. Hampel, A. Hesselmann, G. Hetzer, T. Hrenar, G. Jansen, C. Köppl, Y. Liu, A. W. Lloyd, R. A. Mata, A. J. May, S. J. McNicholas, W. Meyer, M. E. Mura, A. Nicklaß, P. Palmieri, K. Pflüger, R. Pitzer, M. Reiher, T. Shiozaki, H. Stoll, A. J. Stone, R. Tarroni, T. Thorsteinsson, M. Wang, and A. Wolf, *MOLPRO, version 2006.1*.

29 G. Schaftenaar, *MOLDEN 4.3*, CAOS/CAMM Center, The Netherlands, 1998.

30 Varetto, U. *Molekel 5.4.0.8,* Swiss National Supercomputing Centre: Manno, Switzerland, 2009.

Table 2-1 Comparison of the experimental VDEs with calculated values for the structure I.1. C_{2v} ($^2A_1$) and I.2. C_s ($^2A'$) of the $C_2B_6^-$ cluster. All energies are in eV.

Feature	VDE (exp)[a]	Final State and electronic configuration	VDE (theor.)		
			TD-B3LYP[b]	UOVGF[c]	R(U)CCSD(T)[d]
		I.1. C_{2v} ($^2A_1$)			
X'	2.3(1)	$^1A_1$, {...$5a_1^{(2)}4b_2^{(2)}6a_1^{(2)}1a_2^{(2)}2b_1^{(2)}7a_1^{(0)}$}	2.26	2.59 (0.89)	2.17
B	3.54(3)	$^3B_1$, {...$5a_1^{(2)}4b_2^{(2)}6a_1^{(2)}1a_2^{(2)}2b_1^{(1)}7a_1^{(1)}$}	3.51	3.54 (0.89)	3.64
		$^1B_1$, {...$5a_1^{(2)}4b_2^{(2)}6a_1^{(2)}1a_2^{(2)}2b_1^{(1)}7a_1^{(1)}$}	3.91	[e]	[e]
C	4.35(5)	$^3A_2$, {...$5a_1^{(2)}4b_2^{(2)}6a_1^{(2)}1a_2^{(1)}2b_1^{(2)}7a_1^{(1)}$}	4.25	4.25 (0.88)	4.41
		$^1A_2$, {...$5a_1^{(2)}4b_2^{(2)}6a_1^{(2)}1a_2^{(1)}2b_1^{(2)}7a_1^{(1)}$}	4.46	[e]	[e]
F	4.96(5)	$^3A_1$, {...$5a_1^{(2)}4b_2^{(2)}6a_1^{(1)}1a_2^{(2)}2b_1^{(2)}7a_1^{(1)}$}	4.93	4.88 (0.89)	5.06
G	5.7(2)	$^3B_2$, {...$5a_1^{(2)}4b_2^{(1)}6a_1^{(2)}1a_2^{(2)}2b_1^{(2)}7a_1^{(1)}$}	5.58	5.72 (0.89)	5.79
		$^1A_1$, {...$5a_1^{(2)}4b_2^{(2)}6a_1^{(1)}1a_2^{(2)}2b_1^{(2)}7a_1^{(1)}$}	5.66	[e]	[e]
		$^1B_2$, {...$5a_1^{(2)}4b_2^{(1)}6a_1^{(2)}1a_2^{(2)}2b_1^{(2)}7a_1^{(1)}$}	5.93	[e]	[e]
		I.2. C_s ($^2A'$)			
X	2.2(1)	$^1A'$, {...$9a'^{(2)}10a'^{(2)}2a''^{(2)}3a''^{(2)}11a'^{(0)}$}	2.19	[f]	2.09
A	3.23(2)	$^3A''$, {...$9a'^{(2)}10a'^{(2)}2a''^{(2)}3a''^{(1)}11a'^{(1)}$}	3.12	[f]	3.28
		$^1A''$, {...$9a'^{(2)}10a'^{(2)}2a''^{(2)}3a''^{(1)}11a'^{(1)}$}	3.52	[f]	[e]
D	4.68(5)	$^3A'$, {...$9a'^{(2)}10a'^{(1)}2a''^{(2)}3a''^{(2)}11a'^{(1)}$}	4.62	[f]	4.81
E	4.77(5)	$^3A''$, {...$9a'^{(2)}10a'^{(2)}2a''^{(1)}3a''^{(2)}11a'^{(1)}$}	4.69	[f]	[e]
		$^1A''$, {...$9a'^{(2)}10a'^{(2)}2a''^{(1)}3a''^{(2)}11a'^{(1)}$}	4.91	[f]	[e]
		$^1A'$, {...$9a'^{(2)}10a'^{(1)}2a''^{(2)}3a''^{(2)}11a'^{(1)}$}	5.31	[f]	[e]
G	5.7(2)	$^3A'$, {...$9a'^{(1)}10a'^{(2)}2a''^{(2)}3a''^{(2)}11a'^{(1)}$}	5.90	[f]	[e]

[a] Numbers in parentheses represent the uncertainty in the last digit. [b] VDEs were calculated at the TD-B3LYP/6-311+G(2df)//B3LYP/6-311+G* level of theory. [c] VDEs were calculated at the UOVGF/6-311+G(2df)// B3LYP/6-311+G* level of theory. Values in parentheses represent the pole strength of the OVGF calculation. [d] VDEs were calculated at the R(U)CCSD(T)/6-311+G(2df)// B3LYP/6-311+G* level of theory. [e] VDE value cannot be calculated at this level of theory. [f] These VDEs are not presented because of large spin contamination at the UHF/6-311+G(2df) level of theory.

Table 2-2 Comparison of the experimental VDEs with calculated values for the structure II.1. C_{2v} ($^1A_1$) of the $C_3B_5^-$ cluster. All energies are in eV.

Feature	VDE (exp)[a]	Final State and electronic configuration	VDE (theor.)		
			TD-B3LYP[b]	ROVGF[c]	RCCSD(T)[d]
X	3.94(3)	$^2B_2$ {...$5a_1^{(2)}1b_1^{(2)}6a_1^{(2)}2b_1^{(2)}1a_2^{(2)}5b_2^{(1)}$}	3.82	3.99 (0.87)	3.94
A	4.04(3)	$^2A_2$ {...$5a_1^{(2)}1b_1^{(2)}6a_1^{(2)}2b_1^{(2)}1a_2^{(1)}5b_2^{(2)}$}	4.03	4.09 (0.88)	4.11
B	5.26(5)	$^2B_1$ {...$5a_1^{(2)}1b_1^{(2)}6a_1^{(2)}2b_1^{(1)}1a_2^{(2)}5b_2^{(2)}$}	5.06	5.26 (0.87)	5.38
C	5.47(5)	$^2A_1$ {...$5a_1^{(2)}1b_1^{(2)}6a_1^{(1)}2b_1^{(2)}1a_2^{(2)}5b_2^{(2)}$}	5.41	5.55 (0.85)	5.53

[a] Numbers in parentheses represent the uncertainty in the last digit. [b] VDEs were calculated at TD-B3LYP/6-311+G(2df)//B3LYP/6-311+G* level of theory. [c] VDEs were calculated at ROVGF/6-311+G(2df)// B3LYP/6-311+G* level of theory. Values in parentheses represent the pole strength of the OVGF calculation. [d] VDEs were calculated at RCCSD(T)/6-311+G(2df)// B3LYP/6-311+G* level of theory.

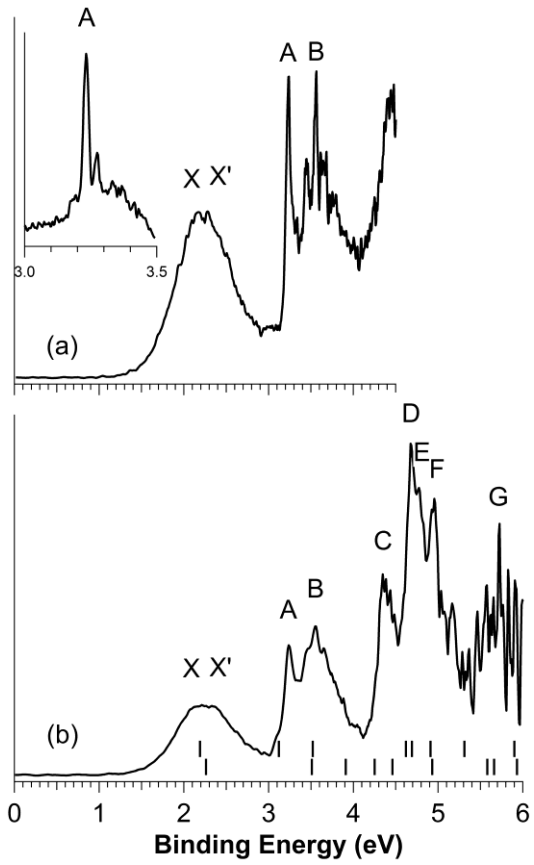

Fig. 2-1 Photoelectron spectra of $C_2B_6^-$ at a) 266 nm (4.661 eV) and b) 193 nm (6.424 eV). The inset shows a partial PES at 355 nm (3.455 eV). The short vertical lines represent the TD-B3LYP values of VDE for structure I.1(bottom) and I.2 (top).

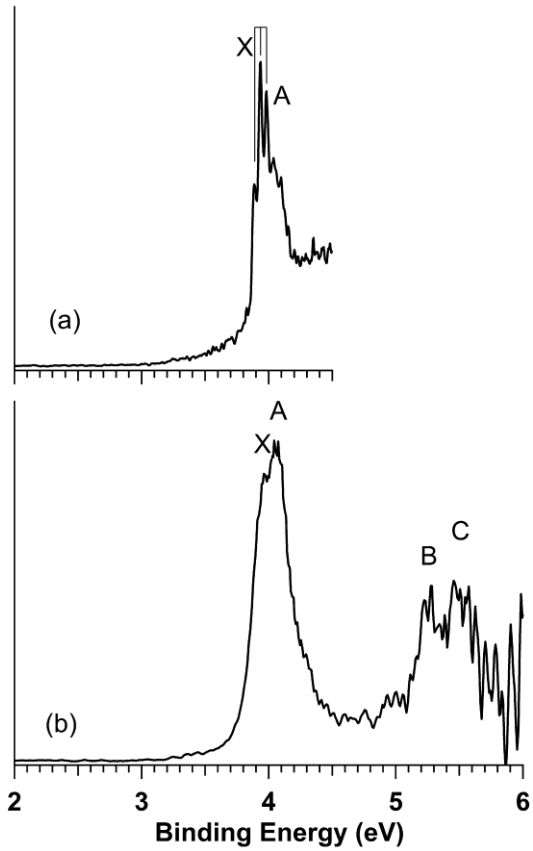

Fig. 2-2 Photoelectron spectra of $C_3B_5^-$ at (a) 266 nm (4.661 eV) and (b) 193 nm (6.424 eV).

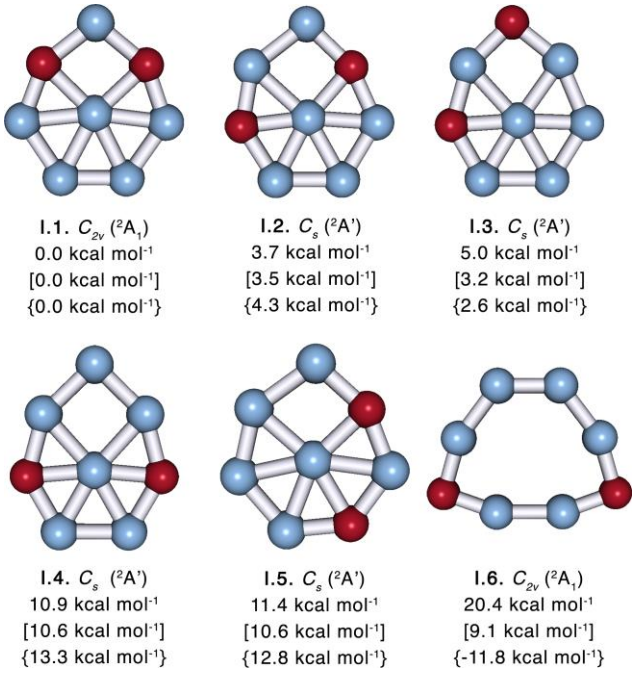

Fig. 2-3 Representative optimized isomers of the $C_2B_6^-$ cluster, their point group symmetries, spectroscopic states and relative energies. The ZPE corrected energies are given at the RCCSD(T)/6-311+G(2df)//B3LYP/6-311+G*, B3LYP/6-311+G* (in square brackets), and B3LYP/3-21G (in curly brackets) levels of theory.

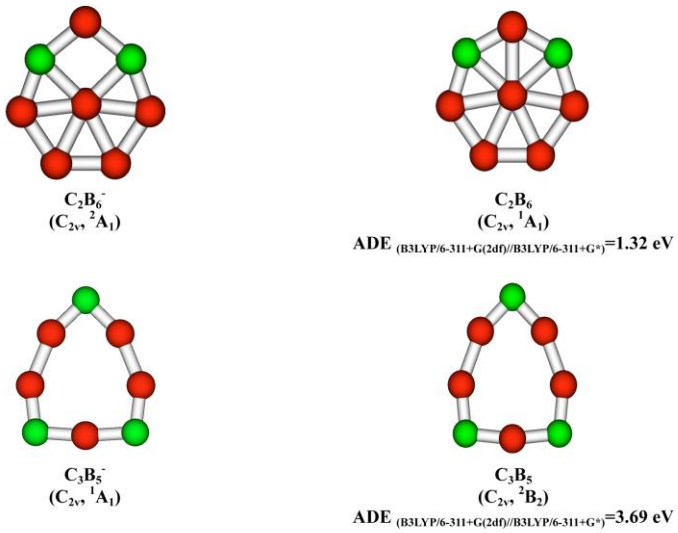

Fig. 2-4 Adiabatic Detachment Energies (ADE) of the $C_2B_6^-$ and $C_3B_5^-$ clusters.

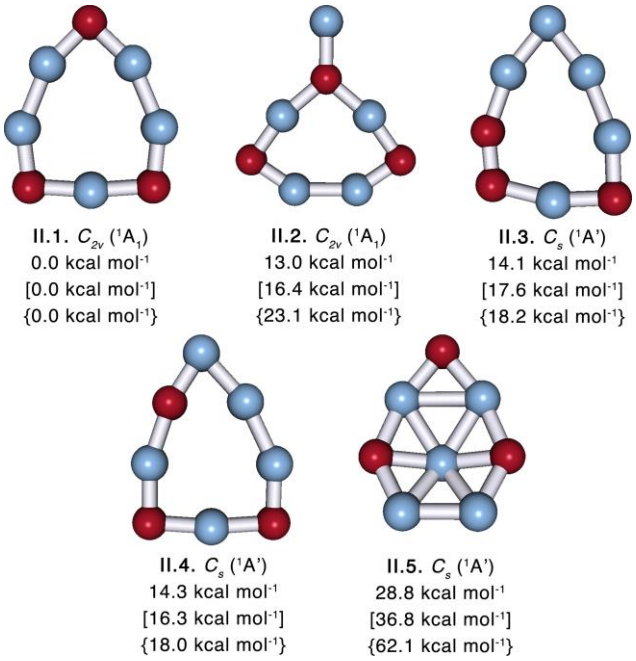

Fig. 2-5 Optimized isomers of the $C_3B_5^-$ cluster, their point group symmetries, spectroscopic states and relative energies. The ZPE corrected energies are given at the RCCSD(T)/6-311+G(2df)//B3LYP/6-311+G*, B3LYP/6-311+G* (in square brackets), and B3LYP/3-21G (in curly brackets) levels of theory.

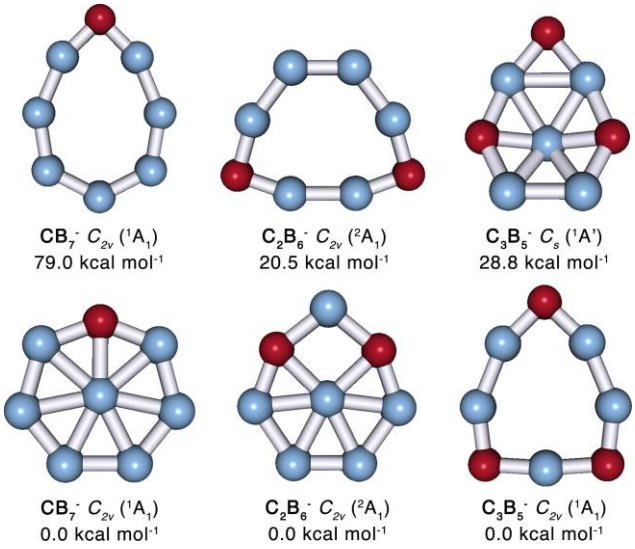

Fig. 2-6 Wheel-type to monocyclic ring structural transition in the series of the $C_xB_{8-x}^-$ (x=1-3) clusters. Relative energies are given at RCCSD(T)/6-311+G(2df)//B3LYP/6-311+G*.

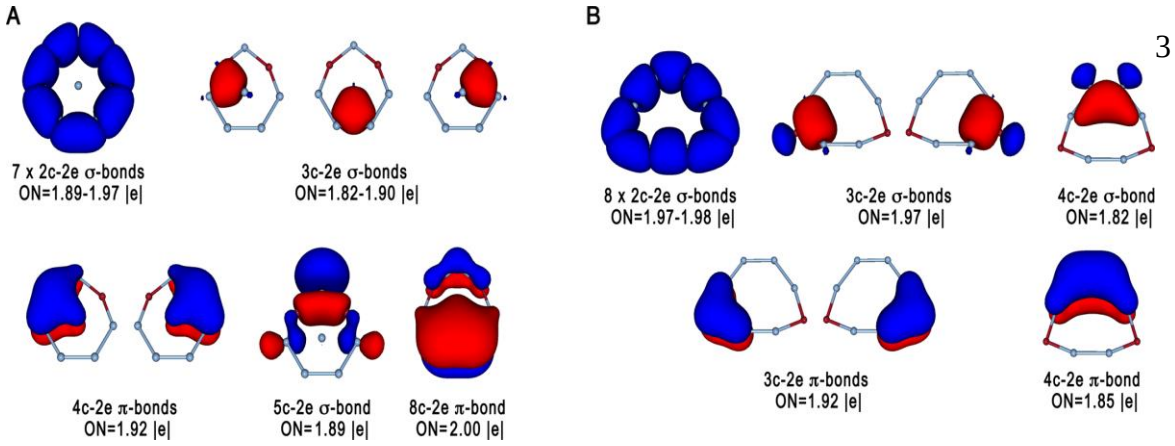

Fig. 2-7 The chemical bonding patterns revealed by the AdNDP analysis for the $C_2B_6^{2-}$ cluster at the optimized geometries of the global minimum wheel-type structure I.1 (**A**) and lowest ring isomer I.6 (**B**) of the $C_2B_6^-$ cluster. The extra electron was added in order to avoid complications of the chemical bonding picture caused by spin polarization in the open-shell $C_2B_6^-$ cluster. The 2c-2e C-B and B-B bonds of both isomers are superimposed on a single molecular framework.

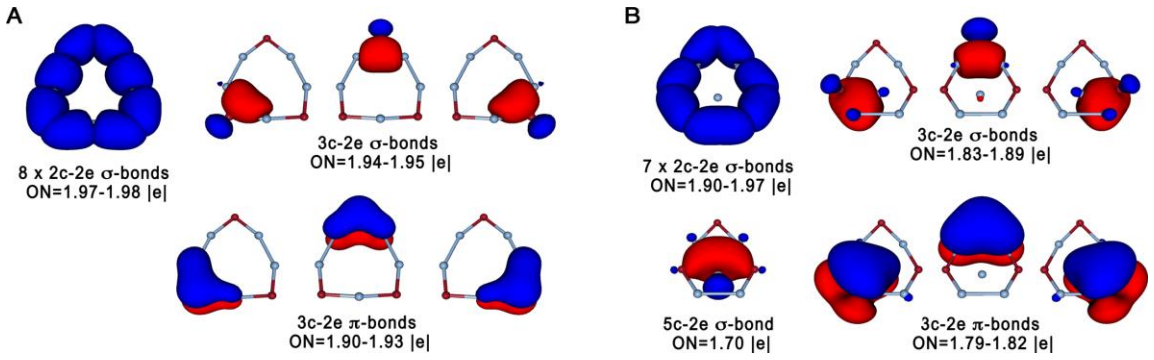

Fig. 2-8 The chemical bonding patterns revealed by the AdNDP analysis for the global minimum ring isomer II.1 (**A**) and the lowest wheel-type isomer II.5 (**B**) of the $C_3B_5^-$ cluster. The 2c-2e C-B and B-B bonds of both isomers are superimposed on a single molecular framework.

CHAPTER 3

ON THE WAY TO THE HIGHEST COORDINATION NUMBER IN THE PLANAR METAL-CENTRED AROMATIC $Ta©B_{10}^-$ CLUSTER: EVOLUTION OF THE STRUCTURES OF TaB_n^- (n = 3 – 8)[1]

Abstract

The structures and chemical bonding of TaB_n^- (n = 3–8) clusters are investigated systematically to elucidate the formation of the planar metal-centred aromatic borometallic cluster, $Ta©B_{10}^-$ (the © sign is used to designate the central position of the doped atom in monocyclic structures in $M©B_n$-type planar clusters), which was found previously to have the highest coordination number for a metal atom in a planar geometry. Photoelectron spectroscopy is combined with *ab initio* calculations to determine the global minima of the TaB_n^- clusters. We find that from TaB_3^- to TaB_5^- the boron atoms nucleate around the central Ta atom to form fan-like structures. A structural transition occurs at TaB_6^-, which is found to have a hexagonal structure, but with a boron atom in the centre and the Ta atom on the periphery. TaB_7^- is shown to have a three-dimensional boat-like structure, which can be viewed as a Ta atom coordinated to an elongated B_7 cluster from above. The global minimum of the TaB_8^-cluster is found to be pyramidal with the Ta atom interacting with a B_8 monocyclic ring. Starting from this structure, additional boron atoms simply enlarge the boron ring to form the slightly pyramidal TaB_9^- cluster and eventually the perfectly planar Ta-centred B_{10}-ring aromatic cluster, $Ta©B_{10}^-$. It is shown that boron atoms do not nucleate

[1] Coauthored by Wei-Li Li, Alexander S. Ivanov, Jozef Federič, Constantin Romanescu, Ivan Černušák, Alexander I. Boldyrev and Lai-Sheng Wang. Reprinted with permission from *J. Chem. Phys.* **2013**, 139, 104312. Copyright 2013, AIP Publishing LLC.

smoothly around a Ta atom on the way to the decacoordinated $Ta©B_{10}^-$ molecular wheel, but rather the competition between B–B interactions and Ta–B interactions determines the most stable structures of the smaller TaB_n^- (n = 3–8) clusters.

3-1. Introduction

As a second-row element, boron has some unique properties that differentiate it from its neighbours in Group 13 and from the rest of the metalloids in the Periodic Table. The peculiar features of boron chemistry can be attributed to its electron deficiency (four valence atomic orbitals with only three valence electrons). Owing to this electron configuration ($2s^2 2p^1$), boron favours multi-centre bonds with pairs of electrons shared among three or more atoms, resulting in interesting three-dimensional (3D) cage structures in bulk boron and boranes. However, joint photoelectron spectroscopy (PES) and computational studies over the past decade have shown that bare boron clusters (B_n) are planar or quasi-planar at least up to n = 23 for anions.[1–12] Neutral boron clusters become 3D at B_{20},[7] which have been reaffirmed by recent computational studies.[13,14] Positively charged boron clusters have been shown to become 3D at B_{16}^+.[15] Small planar boron clusters starting from n = 7 are composed of a periphery featuring strong covalent two-centre two-electron (2c-2e) B–B σ-bonds and one or more inner atoms, which interact with the periphery through delocalized σ and π bonding.[16] Two anionic clusters B_8^{2-} (D_{7h}) and B_9^- (D_{8h}) were found to be perfectly symmetric and doubly (π and σ) aromatic molecular wheels with a central B atom.[2,17] Chemical bonding analyses revealed that in both clusters each B atom in the periphery contributes two electrons to the B–B peripheral covalent bonds and one electron to the delocalized bonds, whereas the central B atom contributes all its valence

electrons to the delocalized bonds.[18–20] An intriguing question arose: is it possible to substitute the central boron atom in the B_8^{2-} and B_9^- molecular wheels with a heteroatom, thus creating highly coordinated monocyclic boron clusters? CB_6^{2-} and CB_7^- were proposed computationally to form carbon-centred molecular wheels.[21,22] However, the reported high-symmetry CB_6^{2-} and CB_7^- structures were only local minima, as confirmed by joint experimental and theoretical studies that the carbon atom (being more electronegative than boron) avoids hyper-coordination in binary B_xC_y clusters.[20,23–25] Subsequent computational studies on silicon-centred clusters suggested that planar structures could be obtained by consecutively adding B atoms to the periphery of a Si-centred C_{2v}-$B_nSi_2Si^-$ molecular fan.[26] A perfect planar octacoordinated-Si is achieved at B_8Si (D_{8h}).[22,27] These examples indicate the plausibility of nonmetal-centred monocyclic boron clusters, albeit none has been experimentally confirmed. Some attention has been turned to replacing the central boron atom with a metal atom. We have shown previously that valence isoelectronic substitution of the central boron atom by aluminium in $B_8^{2-}$and B_9^- led to umbrella-type structures for AlB_7^- (C_{6v}) and AlB_8^- (C_{7v}),[28] in which the Al atom forms ionic bonds within a quasi-planar B_7^{3-} or B_8^{2-} moiety and does not participate in delocalized bonding. Formation of ionic bonds in Al-doped boron clusters was also observed for larger AlB_n^- (n = 9–11) clusters.[29,30] Hence, it appears unlikely that main group atoms are capable of forming molecular wheels with boron rings other than the boron atom itself.

A number of computational studies have examined the possibility of substituting the central B atom in B_8^{2-} and B_9^- by a transition metal atom.[31] Recently, we have experimentally and theoretically characterized the first transition metal centred boron

wheels,[32]which led to the proposal of a design principle based on π and σ double aromaticity and the "©" symbol to designate the structures of this type of molecular wheels.[33] The design principle, derived from the bonding model of the doubly aromatic B_8^{2-} ($B©B_7^{2-}$) and B_9^- ($B©B_8^-$) clusters,[2] requires that, in order to form a stable M-centred $M^{(x)}©B_n^{q-}$ molecular wheel, the bonding electrons in the system ($3n + x + q$) participate in n 2c-2e B–B peripheral bonds and two sets of aromatic delocalized bonds (π and σ), each fulfilling the Hückel's rule for aromaticity ($4N + 2$ electrons), where n is the number of peripheral boron atoms, x is the formal valence of the transition metal, q is the cluster's charge, and N is an integer. Stable planar molecular wheels of this type that fill the design principle and that have been characterized both experimentally and theoretically thus far include: $Fe©B_8^-$ and $Fe©B_9^-$,[34]$Co©B_8^-$ and $Ru©B_9^-$,[32] $Ta©B_{10}^-$ and $Nb©B_{10}^-$,[35] and $Rh©B_9$ and $Ir©B_9$.[36] In addition to the electronic requirement, we have found that the geometric fitness is also essential. For instance, in a recent study we showed that even though the VB_{10}^- system fulfils the electronic requirement to form a D_{10h}-$V©B_{10}^-$ aromatic molecular wheel, the V atom is too small to stabilize the ten-membered boron ring.[37] On the other hand, the B_9 ring fits well a V atom to form a perfectly planar $V©B_9^{2-}$ wheel, whereas it is too small to fit a Nb or Ta atom.[38] Global minimum searches for planar boron wheels with a central hypercoordinate atom ($M©B_n$, where M is a second or third row element) revealed that most of the boron wheels are only local minima.[39] Among the experimentally characterized $M©B_n^-$ wheels, the $Ta©B_{10}^-$ and $Nb©B_{10}^-$ clusters represent the highest coordination number achieved for planar systems.[35,40] It would be interesting to understand atom-by-atom how these remarkable structures are formed. Theoretical

calculations on TiB_n (n = 1–10) clusters showed that planar two-dimensional (2D) fan- and wheel-type structures are more stable than three-dimensional pyramidal structures.[41] However, the calculations were done at relatively low level of theory and whether these structures are true global minima on their potential energy surfaces was not addressed. Furthermore, the viability of Ti-containing molecular wheels of any size has not been examined experimentally. Beside a recent study on $Ta_2B_n^-$ (n = 2–5),[42] there have been no prior studies of the small TaB_n^- clusters. An interesting question arises, concerning the structures of these precursors to the decacoordinated $Ta©B_{10}^-$: do the boron atoms nucleate around the Ta atom in fan-like structures on the way to the highest coordinate Ta or are there non-planar structures and structural transitions?

In this article we provide an extensive and systematic experimental and theoretical studies on a series of $Ta©B_n^-$ (n = 3–8) clusters to examine how boron atoms nucleate around the Ta atom to form the highest coordination molecular wheel in $Ta©B_{10}^-$. We found that in the small $Ta©B_n^-$ (n = 3–5) clusters the B atoms form a fan structure around the Ta atom, as expected. However, the cluster structure takes a different turn at TaB_6^-, which has a B-centred hexagonal structure with Ta on the periphery, whereas TaB_7^- has a 3D structure. Only at TaB_8^- is a complete B_8 ring formed with a pyramidal structure. From then on, the boron ring enlarges with each additional B atom until the perfect decagonal wheel-type structure is achieved at the $Ta©B_{10}^-$ (D_{10h}) cluster.

3-2. Experimental and computational methods

3-2.1. Photoelectron spectroscopy method

The experiment was performed using a magnetic-bottle photoelectron spectroscopy (PES) apparatus equipped with a laser vaporization cluster source, details of

which have been published in Ref.[43] Briefly, the TaB_n^- clusters were produced by laser vaporization of a composite disk target made of ~10% isotopically-enriched ^{11}B and ~15% Ta balanced by Bi or Ag. The latter acted as a binder and also provided atomic Bi^- or Ag^- anions as calibrants for the PES experiment. The clusters were entrained by a He carrier gas seeded with 5% Ar and underwent a supersonic expansion to form a collimated and cold cluster beam. The negatively charged clusters were analyzed with a time-of-flight mass spectrometer. The species of interest were mass-selected and decelerated before being photodetached by a pulsed laser beam at 193 nm (6.424 eV) from an ArF excimer laser; 266 nm (4.661 eV), 355 nm (3.496 eV) and 532 nm (2.331 eV) from a Nd:YAG laser. Photoelectrons were collected at nearly 100% efficiency by a magnetic bottle and analyzed in a 3.5 m long electron flight tube. The resolution of the apparatus, $\Delta E_k/E_k$, was 2.5%, i.e. ~25 meV for 1 eV electrons.

3-2.2. Global optimization methods

The search for the global minimum structures of TaB_n^- (n = 3–8) stoichiometries with different (singlet, doublet, triplet, quartet, quintet, and sextet) electronic states was performed using the Coalescence Kick (CK) program.[10] The CK method subjects large populations of randomly generated structures to a coalescence procedure in which all atoms are pushed gradually to the molecular center of mass to avoid generation of fragmented structures and then optimized to the nearest local minima. These calculations were performed at the PBE0/LANL2DZ[44-46] level of theory. The lowest energy isomers (ΔE<30 kcal mol^{-1}) were then reoptimized at PBE0/Ta/Stuttgart/ B/aug-cc-pVTZ[47-51] and single-point calculations for the selected isomers were performed using the CCSD(T)/Ta/Stuttgart/B/aug-cc-pVTZ level of theory. Theoretical vertical detachment

energies (VDEs) were calculated at the ROPBE0/Ta/Stuttgart/B/ aug-cc-pVTZ and ROCCSD(T)/Ta/Stuttgart/B/aug-cc-pVTZ// PBE0/Ta/Stuttgart/B/aug-cc-pVTZ levels of theory. Chemical bonding analyses (PBE0/LANL2DZ) of the global minimum structures were performed using the AdNDP method.[19] All calculations were done using Gaussian 09.[52] Molekel 5.4.0.8 was used for molecular orbitals visualization.[53]

3-3. Experimental results

The photoelectron spectra of TaB_n^- (n = 3–8) at 193 and 266 nm are shown in Figure 3-1. For the smaller clusters, we have also obtained spectra at 355 nm (n = 3–7) and 532 nm (n = 3), which are given in Figs. 3-7–3-11.[55] The observed detachment transitions are labeled by letters. The VDEs for the observed PES bands are compared with the theoretical data in Tables 1–6 for n = 3–8, respectively. In each spectrum, the X band represents the transition from the anionic to the neutral ground states. The A, B, … bands denote transitions to the first, second … excited states of the neutral species, etc.

The 193 nm spectrum of TaB_3^- (Figure 3-1a) is relatively congested with at least eight resolved detachment bands (X, A–G). The A band is resolved as a shoulder in the 266 nm spectrum (Figure 3-1b). We also obtained the spectra of TaB_3^- at 355 and 532 nm at slightly better resolution (Figure 3-7). Vibrational fine features are partially resolved at 532 nm for the X band with an average spacing of 670 ± 30 cm^{-1}. The VDE of the X band is measured from the 532 nm spectrum to be 1.87 ± 0.03 eV. The VDE of the A band is measured from the 355 nm spectrum as 2.03 ± 0.04 eV (Figure 3-7b). The VDEs of the remaining spectral bands are measured from the peak maxima and all the VDEs are given in Table 3-1.

The 193 nm spectrum of TaB_4^- (Figure 3-1c) reveals four prominent PES bands (X, A–C). A shoulder (A') is resolved on the lower energy side of the X band in the 266 nm spectrum (Figure 3-1d), where a low binding energy tail (X') is also discernible. This tail becomes more recognizable in the 355 nm spectrum (Figure 3-8). As will be shown later, the X' tail, the A' feature, and the weak B' band are all due to a low-lying isomer of TaB_4^-. The VDEs of all the observed features are given in Table 3-2.

The 193 nm spectrum of TaB_5^- (Figure 3-1e) shows five PES bands (X, A–D) plus a weak low binding energy tail (X'). The A band is relatively weak, while the relative intensities of the B and C bands also decreased significantly at 266 nm (Figure 3-1f). The 355 nm spectrum of TaB_5^- (Figure 3-9) is not significantly improved. The VDEs of all the observed PES bands are given in Table 3-3.

The 193 nm spectrum of TaB_6^- is quite complicated with many PES transitions (Figure 3-1g). More PES bands (X", A", B") are resolved at 266 nm (Figure 3-1h). As will be shown below, there are two low-lying isomers, which can potentially contribute to the observed spectra and result in the congested spectra observed. The VDEs of all the resolved PES bands are given in Table 3-4.

The 193 nm spectrum of TaB_7^- (Figure 3-1i) is relatively simple with four well-resolved bands (X, A–C). Bands B and C are quite broad and may contain multiple electronic transitions. The X band defines a relatively low VDE of 2.05 eV for TaB_7^-. The spectra of TaB_7^- suggest that they come from a single stable isomer without any appreciable contribution from low-lying isomers. The observed VDEs for TaB_7^- are given in Table 3-5. The 193 nm spectrum of TaB_8^- (Figure 3-1k) displays five relatively sharp PES bands (X, A–D). The band A is better resolved in the 266 nm spectrum (Figure

3-1l), which shows possible vibrational structures for band X. Very weak signals at lower binding energies (labeled as *) are seen in the 266 nm and they may come from a weakly populated isomer. The VDEs of all the observed PES bands for TaB_8^- are given in Table 3-6. Overall, the binding energy increases from TaB_3^- to TaB_5^- and then drops at TaB_6^- and reaches a minimum at TaB_7^- before increasing again at TaB_8^-. This observation may suggest a structural change at TaB_6^- and TaB_7^-. The spectra of TaB_8^- exhibit some similarity to those of TaB_9^- and TaB_{10}^- with systematic increasing VDEs,[35,38] suggesting that TaB_8^- may show structural similarities to the larger $Ta©B_9^-$ and $Ta©B_{10}^-$ molecular wheels.

3-4. Theoretical results

3-4.1. TaB_3^-

The unbiased global minimum searches for TaB_3^- in different spin states led to three low energy isomers (Figure 3-2a). The C_{2v} ($^4A_2$) structure I.3 was found to be the lowest energy isomer at the PBE0/Ta/Stuttgart/B/aug-cc-pVTZ level of theory. However, single point calculations at CCSD(T)/Ta/Stuttgart/B/aug-cc-pVTZ and CCSD(T)/Ta/Stuttgart/B/aug-cc-pVQZ for all the low-lying isomers of TaB_3^- (Figure 3-10) showed that the C_{2v} ($^4B_1$) fan-type structure I.1 is the true global minimum on the potential energy surface of TaB_3^-, although isomers I.2 and I.3 are very close in energy to I.1, only 0.2 and 1.6 kcal/mol higher at the CCSD(T)/Ta/Stuttgart/B/aug-cc-pVTZ level of theory.

3-4.2. TaB_4^-

Our global minimum search revealed that the fan-like structure (II.1 in Figure 3-2b) is the global minimum for TaB_4^-. Single point calculations at CCSD(T)/Ta/Stuttgart/B/aug-cc-pVTZ showed that a similar triplet isomer is only 2.7 kcal/mol higher (Figure 3-2b, II.2). The II.2 isomer is not completely planar, but the deviation from planarity is very small. A low-symmetry 3D isomer (II.3 in Figure 3-11) is 8.7 kcal/mol above the global minimum. The global minimum of TaB_4^- continues the fan-like structure observed for TaB_3^-.

3-4.3 TaB_5^-

The global minimum of TaB_5^- is also a planar fan-like structure (III.1 in Figure 3-2c). The second lowest isomer (III.2 in Figure 3-2c) which is similar to isomer II.3 of TaB_4^-, is only 1.4 kcal/mol higher in energy at CCSD(T)/Ta/Stuttgart/B/aug-cc-pVTZ. A more extensive set of alternative isomers found in our global minimum search for TaB_5^- is summarized in Figure 3-12.

Thus, TaB_5^- continues the fan-growth mode, which is now half way on to the $Ta©B_{10}^-$ molecular wheel. However, some subtle structural trends can be seen from TaB_3^- to TaB_5^-: the B−B bond lengths seem to decrease, whereas the Ta−B bond lengths increase. This trend suggests that the interaction between Ta and individual B atoms decreases, while the boron ring motif is taking shape.

3-4.4. TaB_6^-

The fan-growth mode is disrupted at TaB_6^-. Our global search showed that the most stable structure of TaB_6^- (IV.1 in Figure 3-2d) is planar with a hexagonal shape, but

with a B atom in the centre. We also found two boat-like 3D isomers (IV.2 and IV.3 in Figure 3-2d), which are competitive, lying within 3 kcal/mol of isomer IV.1 (CCSD(T)/Ta/Stuttgart/B/aug-cc-pVTZ). The expected fan-shaped structure (IV.5 in Figure 3-13) is only the fifth lowest isomer of TaB_6^-, being 9.8 kcal/mol above IV.1. It seems that the B−B interactions prevail over Ta−B bonding in TaB_6^-.

3-4.5. TaB_7^-

We found that the global minimum of TaB_7^- is a very stable boat-like 3D structure (Figure 3-3a), which can be viewed as being formed from the IV.3 isomer of TaB_6^-. The fan-like structure (V.9 in Figure 3-14) is now a much higher isomer by 20.2 kcal/mol above the global minimum. Interestingly, the second lowest isomer of TaB_7^- is heptagonal pyramidal structure (V.2 in Figure 3-14), which is higher than the global minimum by 4.9 kcal/mol (CCSD(T)/Ta/Stuttgart /B/aug-cc-pVTZ). This isomer can be viewed as Ta atom interacting with a B_7 ring. Thus, starting from n = 7, a boron-ring based isomer becomes energetically favorable, even though the global minimum of TaB_7^- is 3D.

3-4.6. TaB_8^-

According to our CK search, the global minimum of TaB_8^- is a pyramidal structure with a triplet spin state (Figure 3-3b), in which the Ta atom is interacting with a B_8 ring. Ta atom is obviously too large to fit in the centre of the B_8 ring to form the planar octacoordinated Ta. Our calculations at the PBE0 level of theory showed that the global minimum VI.1 represents only a low-symmetry C_s structure. However, optimization with follow-up frequency calculations using the exchange-correlation

potential PW91PW91[56] and the hybrid meta-exchange-correlation functional M06-2X[57] confirmed the C_{8v} structure VI.1 to be the global minimum. However, the distortion in the C_s structures relative to the C_{8v} symmetry is small and our chemical bonding analyses yielded very similar results for either C_s or C_{8v} symmetry. The second low-lying isomer is also a pyramidal structure with a singlet spin state and C_{4v} symmetry (VI.2 in Figure 3-15), in which four boron atoms are slightly pulled out from the molecular framework. The VI.2 isomer is 4.1 kcal/mol higher than the global minimum and all other isomers (Figure 3-15) are at least 18 kcal/mol higher.

3-5. Interpretation of the photoelectron spectra

3-5.1. TaB_3^-

According to the relative energies calculated at the CCSD(T) level, isomer I.1 is the global minimum and should be responsible for the observed PES spectra of TaB_3^-. Isomers I.2 and I.3 are quite low-lying (Figure 3-2a) and may be present in the cluster beam and make minor contributions to the PES spectra.

Isomer I.1 is open shell with a quartet ground state ($^4B_1$). The calculated VDEs for TaB_3^- are compared with the experimental data in Table 3-1. Three molecular orbitals are singly occupied in isomers I.1, yielding triplet or quintet neutral final states upon electron detachment. The first VDE corresponds to the electron detachment from the $3b_2$ orbital to produce the $^3A_2$ final state. The calculated VDE of 1.82 eV (all the calculated values discussed in this section are at ROCCSD(T) level of theory) is in excellent agreement with the experimental value of 1.87 ± 0.03 eV. All the other calculated VDEs agree well with the observed major PES bands. There is a small tail in front of peak X at ~1.6-1.7

eV (Figure 3-7), which might come from I.2 and I.3. The calculated first VDEs for I.2 and I.3 are 1.64 eV and 1.60 eV, respectively, at the CCSD(T) level of theory. The calculated VDEs for higher energy detachment channels for isomers I.2 and I.3 are given in Table 3-7. The almost negligible signals in the low binding energy tail in the experimental spectra suggest that the populations of isomers I.2 and I.3 are minor, if at all. Thus, their relative energies may be even higher than the CCSD(T) results indicate.

3-5.2. TaB_4^-

The global minimum (II.1) of TaB_4^- is closed shell with a singlet ground state (Figure 3-2b). The triplet isomer II.2 is only 2.7 kcal/mol higher in energy and may be present in the cluster beam and contribute to the photoelectron spectra. The calculated VDE from the $3b_2$ HOMO of II.1 is 2.66 eV (Table 3-2), corresponding to the ground state detachment band X at 2.78 eV. The VDE of the next detachment channel from the $1a_2$ HOMO-1 is calculated to be 3.09 eV, in good agreement with the band A at 3.14 eV. The VDEs from HOMO-2 and HOMO-3 are calculated to be 3.49 eV and 4.21 eV, consistent with the observed bands B (VDE = 3.46 eV) and C (VDE = 4.07 eV), respectively.

Hence, the weak features X', A', and B' must come from the low-lying isomer II.2. This isomer has a triplet ground electronic state, which can yield doublet and quartet final states, as shown in Table 3-2. The first VDE of II.2 is calculated to be 2.50 eV, which agrees well with the weak feature X' at ~2.5 eV. The second and third detachment channels were calculated to have very close VDEs of 2.80 and 2.82 eV, which should correspond to the A' feature. The next two detachment channel could not be calculated at the CCSD(T) level, one of the channels should correspond to the B' band. The sixth

detachment channel with a calculated VDE of 4.09 eV should contribute to the broad C band. Thus, the observed PES spectra can be explained well by isomers II.1 and II.2. Isomer II.2 is a triplet state, which is metastable and cannot relax readily to the singlet ground state in the cluster beam, which is why it was populated even though its energy is relatively high (by 2.7 kcal/mol) above isomer II.1.

3-5.3. TaB_5^-

The global minimum isomer III.1 of TaB_5^- (Figure 3-2c) is open shell with a doublet ground electronic state. The first detachment channel is from the fully occupied $3b_2$ MO producing a $^3B_2$ final state (Table 3-3). The calculated first VDE of 2.81 eV is in perfect agreement with the experimental result. The next two detachment channels from the $4b_2$ and $5a_1$ orbitals yielded similar VDEs of 2.86 and 2.89 eV, which should correspond to the broad A band. Following an energy gap, the next three detachment channels yielded VDEs in good agreement with bands B, C, and D in the experiment. The isomer III.2 is only 1.4 kcal/mol above III.1 and is expected to be present in the experiment. Indeed, the calculated first VDE from III.2 of 2.35 eV agrees well with the weak X' band in the low binding energy side. Higher energy detachment channels are likely buried in the broad features of isomer III.1.

3-5.4. TaB_6^-

The global minimum isomer IV.1 of TaB_6^- has a triplet ground state (Figure 3-2d), which can lead to both doublet and quartet final states in PES. The calculated first VDE of 2.43 eV from the $5b_2$ MO is in excellent agreement with band X at 2.49 eV (Table 3-4). The calculated VDEs for the next four detachment channels at the CCSD(T)

level are in excellent agreement with the observed bands A, B, C, and D, respectively. However, higher energy channels corresponding to bands E and F were unfortunately unable to be calculated at CCSD(T). The VDE from PBE at 4.44 eV is in good agreement with band E. These assignments leave several weaker features unaccounted for in the experimental spectra, which must come from low-lying isomers.

Our calculations suggested two 3D isomers (IV.2 and IV.3), which are within 3 kcal/mol of the global minimum (Figure 3-2d). Both are closed shell with singlet spin states and thus are metastable relative to the triplet ground state. They can be populated experimentally, even though their energies are relatively high. The calculated first VDE of isomer IV.2 is 2.32 eV, consistent with the low binding energy tail labeled as X' in Figure 3-1h. The second detachment channel of isomer IV.2 gives a calculated VDE of 2.73 eV, which may contribute to band A, whereas the third detachment channel of isomer IV.2 with a calculated VDE of 3.23 eV could contribute to band B". The higher detachment channels of isomer IV.2 from 4.68 to 4.85 eV should contribute to the nearly continuous signals in the corresponding spectral range in the 193 nm spectrum (Figure 3-1g).

The calculated VDEs from isomer IV.3 are in excellent agreement with the remaining weak features (X", A", B", C"), as shown in Table 3-4. The fourth detachment channel of IV.3 at 3.72 eV is likely buried in the intense C band. Overall, the complicated PES spectra of TaB_6^- are well explained by the global minimum and the two 3D low-lying isomers.

3-5.5. TaB_7^-

The global minimum 3D structure of TaB_7^- is very stable (Figure 3-3a) and the

nearest low-lying isomer is at least 4.9 kcal/mol higher in energy (Figure 3-14), thus unlikely to be present in the experiment. Indeed, the PES spectra of TaB_7^- are relatively simple with no hint of major low-lying isomer contributions. The first detachment channel from the global minimum V.1 isomer of TaB_7^- is from the 9a' singlet occupied MO, producing the neutral singlet ground state. The calculated VDE of 2.18 eV is in good agreement with band X at 2.05 eV (Table 3-5). The second detachment channel is from the fully occupied 8a' orbital with a calculated VDE of 3.32 eV, in excellent agreement with band A at 3.43 eV. The large X-A separation defines a large HOMO-LUMO gap (~1.4 eV) for the neutral TaB_7, suggesting it is a relatively stable cluster. The third detachment is from the 5a" MO with a calculated VDE of 3.91 eV, in good agreement with the observed band B at 3.80 eV. Even though the VDEs for deeper MOs could not be calculated at these level of theory, the good agreement between experiment and theory for the first three detachment channels provides strong support for the global minimum of TaB_7^-.

3-5.6. TaB_8^-

The global minimum of TaB_8^- has a triplet electronic state (either C_{8v} or C_s symmetry). The first and second detachment channels are from the fully occupied 5a" and 9a' MOs, producing two quartet final states. The calculated VDEs of 3.32 eV for these detachment channels are the same, in good agreement with band X at 3.35 eV (Table 3-6). Detachment from the two singly occupied 10a' and 6a" MOs, resulting in two doublet final states, also with very similar calculated VDEs, 3.42 and 3.43 eV, respectively, in good agreement with band A at 3.52 eV. The fifth detachment channel is from the 8a' MO, producing a quartet final state, with a calculated VDE of 4.48 eV in

good agreement with the observed band C at 4.42 eV. The VDEs for higher binding energy MOs could not be calculated at the current level of theory.

However, the above assignment still leaves the lower binding energy B band at 3.98 eV unaccounted for. This feature could be due to contributions from a low lying isomer. The second isomer TaB_8^- is a singlet state, 4.1 kcal/cal above the triplet global minimum (Figure 3-15). The first calculated VDE for isomer VI.2 is 3.23 eV (Table 3-6), which is consistent with the very weak tail around 3.2 eV (Figure 3-1l). However, this tail is almost negligible, suggesting that contributions from isomer VI.2 is negligible. Furthermore, there is no detachment channel from isomer VI.2 that agrees with the observed band B. We found that a two-electron detachment channel produced a VDE of 3.78 eV, in good agreement with the observed VDE of band B at 3.98 eV (Table 3-6). We also note a weak signal around 2.4 eV in the 266 nm spectrum of TaB_8^- (labeled as * in Figure 3-1l). But it is negligible in the 193 nm spectrum (Figure 3-1k). We attributed to it to an unknown impurity.

Overall, the computational results and the experimental data are in good agreement, lending considerable credence to the global minima and the low-lying isomers obtained for all the TaB_n^- (n = 3–8) clusters.

3-6. Structural evolution and chemical bonding in TaB_n^-

To understand the structural evolution and how boron atoms nucleate around the central Ta atom to form the highest coordination $Ta©B_{10}^-$ molecular wheel, we analyzed the chemical bonding in TaB_n^- (n = 3–8) using the Adaptive Natural Density Partitioning (AdNDP),[52] as shown in Figs. 3-4 – 3-6.

3-6.1. TaB_n^- (n = 3–5): nucleation of B around Ta

The AdNDP analysis for the global minimum TaB_3^- (C_{2v}, $^4B_1$) cluster (Figure 3-4, I.1) revealed four 2c-2e peripheral σ bonds (two B–B bonds and two Ta–B bonds) with occupation numbers (ON) ranging from 1.95 |e| to 1.98 |e|, one delocalized 4c-2e σ bond and one delocalized 4c-2e π bond (ON = 2.00 |e|). Since TaB_3^- has three unpaired electrons, the AdNDP analysis also showed one delocalized 4c-1e σ bond (ON = 1.00 |e|), one delocalized 4c-1e π bond (ON = 1.00 |e|), and one 1c-1e 6s lone-pair on Ta (ON = 1.00 |e|). The single electron delocalized σ and π bonds both describe Ta 5d bonding with the two terminal B atoms, rendering partial multiple bond characters for the two Ta–B bonds. This bonding picture is consistent with the short terminal Ta–B bond lengths (2.08 Å) and the relatively long bond length between Ta and the central B atom (2.32 Å). The latter is characterized by multicenter delocalized bonding only.

The bonding in the global minimum TaB_4^- (C_{2v}, $^1A_1$) consists of five localized 2c-2e σ peripheral bonds (three B–B bonds and two Ta–B bonds), two delocalized 3c-2e σ and π bonds (Figure 3-4, II.1). The two 3c-2e delocalized σ bonds describe bonding of Ta with two terminal B–B units, while the two delocalized π bonds mainly describe bonding between Ta and the terminal B atoms. Thus, the $Ta–B_{termial}$ bonds can be viewed as Ta=B double bonds, consistent with the very short Ta–B bond lengths (2.07 Å). From TaB_3^- to TaB_4^-, the bonding between Ta and the terminal B atoms is strengthened slightly. Again, the Ta bonding with the two middle B atom is through multicenter delocalized bonding only.

The chemical bonding picture in the TaB_5^- global minimum fan structure is similar to that in TaB_4^-. The AdNDP analysis recovered six localized 2c-2e peripheral σ

bonds (four B–B bonds and two Ta–B bonds), two delocalized 4c-2e σ and π bonds, and one 6c-1e σ bond (ON = 1.00 |e|) (Figure 3-4, III.1). Thus, the bonds between Ta and the two terminal B atoms contain multiple bond characters, whereas the bonding between Ta and the middle three B atoms are entirely via multicenter delocalized bonding.

3-6.2. TaB_6^- and TaB_7^-: structural excursions

The Ta atom in the global minimum of TaB_6^- (C_{2v}, $^3B_1$) is part of a hexagonal ring with a central B atom. Our AdNDP analysis revealed six localized 2c-2e σ peripheral bonds for the hexagonal ring, three delocalized 7c-2e σ bonds (ON = 2.00 |e|), two 7c-2e π bonds (ON = 2.00 |e|), one 1c-1e 5d lone-pair (ON = 1.00 |e|), and one delocalized 7c-1e π bond (ON = 1.00 |e|) (Figure 3-5, IV.1). The three delocalized 7c-2e σ bonds make TaB_6^- σ aromatic. The structure and bonding in TaB_6^- are reminiscent of those in AlB_6^-,[30] which has a similar structure with Al being part of the peripheral hexagonal ring and a central B atom. However, the Al atom is slightly out of plane due to π antiaromaticity because AlB_6^- only has four delocalized π electrons. Clearly, the additional delocalized π bond in TaB_6^- is sufficient for a perfect planar structure, even though it only has a single electron. Thus, TaB_7^- can be considered to be doubly aromatic. The AlB_6^- cluster was related to the pyramidal B_7^- cluster and the Al atom was considered as an isoelectronic substitute of a peripheral B atom.[30] The large size of the Al atom enlarges the hexagonal ring and planarizes the central B atom. However, because of the π antiaromaticity the Al atom is slightly bent out of plane in AlB_6^-. Thus, Ta can be considered as a better substitute of the peripheral B atom in the B_7^- cluster to yield the doubly aromatic and perfectly planar TaB_6^- cluster. This favourable bonding situation is

why the fan structure of TaB_6^- is not competitive.

The 3D global minimum structure of TaB_7^- has seven localized 2c-2e σ bonds (ON = 1.77-1.94 |e|), two delocalized 3c-2e σ bonds (ON = 1.85 |e|), one delocalized 8c-2e σ bond (ON = 1.99 |e|), three delocalized 8c-2e π bonds (ON = 2.00 |e|), and one completely delocalized 8c-1e σ bond (ON = 1.00 |e|) (Figure 3-5, V.1). The bonding pattern in this case is complicated and cannot be expressed in a simple manner. The term σ and π bonds are used loosely here. Clearly, the interactions between Ta and the boron atoms are optimized in the TaB_7^- global minimum structure.

3-6.3. TaB_8^-: on the way to $Ta©B_{10}^-$

Our calculations at different levels of theory found the pyramidal structure VI.1 to be the global minimum for TaB_8^- (Figure 3-3b). As mentioned above, the structure VI.1 has C_s point group symmetry at PBE0 level of theory and C_{8v} symmetry at the PW91PW91 and M06-2x levels of theory. However, regardless of C_s or C_{8v} symmetry, our AdNDP analysis recovered similar chemical bonding patterns for both structures (Figure 3-6), because the structural distortion in the C_s symmetry is very small.

While the TaB_8^- cluster is not planar, the deviation from planarity is not that large in order to interpret its bonding approximately in terms of σ and π bonds. The AdNDP analysis showed eight localized 2c-2e σ bonds (ON = 1.88-1.93 |e|) for the B_8 ring, three delocalized 9c-2e σ bonds (ON = 2.00 |e|), three delocalized 9c-2e π bonds (ON = 2.00 |e|), and two delocalized 9c-1e σ bonds (ON = 1.00 |e|) (Figure 3-6, VI.1). The delocalized bonds closely resemble the canonical molecular orbitals. Thus, TaB_8^- is π aromatic with 6 π electrons. Because the ground state of TaB_8^- is open shell, the eight

totally delocalized σ electrons occupy five MOs, rendering it σ-aromatic. Thus, TaB_8^- is doubly aromatic. The bonding of the triply TaB_8^- is consistent with the design principle for metal-centred aromatic wheel-type clusters.[32-35] Clearly the B_8 ring is too small to fit the Ta atom, resulting in the pyramidal structure. We showed recently even the B_9 ring is not large enough to host a Ta atom, resulting a slight pyramidal distortion in TaB_9^-.[38] Only the B_{10} ring is large enough for the Ta atom, resulting in the perfectly planar $Ta©B_{10}^-$ highest coordination borometallic molecular wheel. Thus, TaB_8^- is on the way to the $Ta©B_{10}^-$ cluster by successive additions of two boron atoms.

3-7. Conclusions

A comprehensive experimental and theoretical study is reported on the structures and bonding in a series of TaB_n^- (n = 3–8) clusters to elucidate the steps necessary to form the highest coordination $Ta©B_{10}^-$ molecular wheel. Photoelectron spectroscopy is combined with extensive global minimum searches to locate the most stable structures and low-lying isomers for each cluster. TaB_3^-, TaB_4^-, and TaB_5^- are found to have fan-like global minimum structures, in which the Ta atom interacts with the terminal boron atoms strongly with multiple Ta–B bond characters, whereas Ta interacts with the middle boron atom(s) via delocalized bonding. Thus, these clusters can also be viewed as ring structures with Ta being part of the ring. The fan growth mode is interrupted at TaB_6^-, which is found to have a planar hexagonal wheel-type structure with Ta being on the periphery of the wheel and a central B atom. The chemical bonding in the TaB_6^- cluster is found to be reminiscent of the AlB_6^- cluster and TaB_6^- can be viewed to be doubly aromatic. The TaB_7^- cluster is a three-dimensional boat-like global minimum structure, which seems to maximize Ta–B interactions. The global minimum of the TaB_8^- cluster is

found to be an octagonal pyramidal structure with Ta being out of the cyclic octagonal ring by about 1.1 Å. The B_8 ring is apparently too small to host a Ta atom, but the TaB_8^- cluster can be viewed as the precursor to the $Ta©B_{10}^-$ molecular wheel. Addition of one B atom will form the pyramidal TaB_9^- cluster, in which the Ta atom is only slightly above the B_9 ring.[38] And finally the B_{10} ring is perfect to host a Ta atom to form the doubly aromatic $Ta©B_{10}^-$ molecular wheel.[35] The current study shows that the competition between B−B interactions and Ta−B interactions determines the most stable structures of the TaB_n^- clusters. The structural evolution of the TaB_n^- clusters is not only important to understand the formation mechanisms for the highest known coordination number in planar species ($Ta©B_{10}^-$),[40] but also provides insights into the interactions between early transition metals with boron.

References

1 H. J. Zhai, L. S. Wang, A. N. Alexandrova and A. I. Boldyrev, *J. Chem. Phys.* **117**, 7917 (2002).

2 H. J. Zhai, A. N. Alexandrova, K.A. Birch, A. I. Boldyrev and L. S. Wang, *Angew. Chem. Int. Ed*. **42**, 6004 (2003).

3 H. J. Zhai, B. Kiran, J. Li and L. S. Wang, *Nat. Mater.* **2**, 827 (2003).

4 H. J. Zhai, L. S. Wang, A. N. Alexandrova, A. I. Boldyrev and V. G. Zakrzewski, *J. Phys. Chem. A* **107**, 9319 (2003).

5 A. N. Alexandrova, A. I. Boldyrev, H. J. Zhai, L. S. Wang, E. Steiner and P.W. Fowler, *J. Phys. Chem. A* **107**, 1359 (2003).

6 A. N. Alexandrova, A. I. Boldyrev, H. J. Zhai and L. S. Wang, *J. Phys. Chem. A* **108**, 3509 (2004).

[7] B. Kiran, S. Bulusu, H. J. Zhai, S. Yoo, X. C. Zeng and L. S. Wang, *Proc. Natl. Acad. Sci. U. S. A.* **102**, 961 (2005).

[8] A. P. Sergeeva, D. Y. Zubarev, H. J. Zhai, A. I. Boldyrev and L. S. Wang, *J. Am. Chem. Soc.* **130**, 7244 (2008).

[9] W. Huang, A.P. Sergeeva, H. J. Zhai, B.B. Averkiev, L. S. Wang and A. I. Boldyrev, *Nat. Chem.* **2**, 202 (2010).

[10] A. P. Sergeeva, B. B. Averkiev, H. J. Zhai, A. I. Boldyrev and L. S. Wang, *J. Chem. Phys.* **134**, 224304 (2011).

[11] Z. A. Piazza, W. L. Li, C. Romanescu, A. P. Sergeeva, L. S. Wang and A. I. Boldyrev, *J. Chem. Phys*. **136**, 104310 (2012).

[12] A. P. Sergeeva, Z. A. Piazza, C. Romanescu, W. L. Li, A. I. Boldyrev and L. S. Wang, *J. Am. Chem. Soc.* **134**, 18065 (2012).

[13] T. B. Tai, N. M. Tam and M. T. Nguyen, *Chem. Phys. Lett.* **530**, 71 (2012).

[14] F. Li, P. Jin, D.e. Jiang, L. Wang, S.B. Zhang, J. Zhao and Z. Chen, *J. Chem. Phys.* **136**, 074302 (2012).

[15] E. Oger, N.R.M. Crawford, R. Kelting, P. Weis, M.M. Kappes and R. Ahlrichs, *Angew. Chem. Int. Ed.* **46**, 8503 (2007).

[16] A. N. Alexandrova, A. I. Boldyrev, H. J. Zhai and L. S. Wang, *Coord. Chem. Rev*. **250**, 2811 (2006).

[17] A. N. Alexandrova, H. J. Zhai, L. S. Wang and A. I. Boldyrev, *Inorg. Chem*. **43**, 3552 (2004).

[18] P. W. Fowler and B. R. Gray, *Inorg. Chem*. **46**, 2892 (2007).

[19] D.Y. Zubarev and A. I. Boldyrev, *Phys. Chem. Chem. Phys.* **10**, 5207 (2008).

[20] B. B. Averkiev, L. M. Wang, W. Huang, L. S. Wang and A. I. Boldyrev, *Phys. Chem. Chem. Phys.* **11**, 9840 (2009).

[21] K. Exner and P. v. R. Schleyer, *Science*, 2000, **290**, 1937 (2000).

[22] Z. X. Wang and P. v. R. Schleyer, *Science*, 2001, **292**, 2465 (2001).

[23] L. M. Wang, W. Huang, B. B. Averkiev, A. I. Boldyrev and L. S. Wang, *Angew. Chem. Int. Ed*. **46**, 4550 (2007).

[24] B. B. Averkiev, D.Y. Zubarev, L. M. Wang, W. Huang, L. S. Wang and A. I. Boldyrev, *J. Am. Chem. Soc*. **130**, 9248 (2004).

[25] T. R. Galeev, A. S. Ivanov, C. Romanescu, W. L. Li, K.V. Bozhenko, L. S. Wang and A. I. Boldyrev, *Phys. Chem. Chem. Phys*. **13,** 8805 (2011).

[26] S. D. Li, C. Q. Miao, J. C. Guo and G. M. Ren, *J. Am. Chem. Soc.* **126**, 16227 (2004).

[27] (a) R. M. Minyaev, T. N. Gribanova, A. G. Starikov and V. I. Minkin, *Mendeleev Commun.*, 2001, **6**, 213 (2001); (b) V. I. Minkin, R. M. Minyaev and R. Hoffmann, *Russ. Chem. Rev*., 2002, **71**, 869 (2002).

[28] T. R. Galeev, C. Romanescu, W. L. Li, L. S. Wang and A. I. Boldyrev, *J. Chem. Phys*. **135**, 104301 (2011).

[29] W. L. Li, C. Romanescu, T.R. Galeev, L. S. Wang and A. I. Boldyrev, *J. Phys. Chem. A* **115**, 10391 (2011).

[30] C. Romanescu, A.P. Sergeeva, W. L. Li, A. I. Boldyrev and L. S. Wang, *J. Am. Chem. Soc.* **133**, 8646 (2011).

[31] (a) Q. Luo, *Sci. China Ser. B – Chem*. **51**, 607 (2008); (b) Q. Y. Wu, Y. P. Tang and X. H. Zhang, *Sci. China Ser. B – Chem*. **52**, 288 (2009); (c) K. Ito, Z. Pu, Q. S. Li and

P. v. R. Schleyer, *Inorg. Chem*. **47**, 10906 (2008); (d) Z. Pu, K. Ito, P. v. R. Schleyer and Q. S. Li, *Inorg. Chem*. **48**, 10679 (2009).

[32] C. Romanescu, T.R. Galeev, W. L. Li, A. I. Boldyrev and L. S. Wang, *Angew. Chem. Int. Ed.* **50**, 9334 (2011).

[33] C. Romanescu, T. R. Galeev, W. L. Li, A. I. Boldyrev and L. S. Wang, *Acc. Chem. Res*. **46**, 350 (2013).

[34] C. Romanescu, T. R. Galeev, A. P. Sergeeva, W. L. Li, L. S. Wang and A. I. Boldyrev, J. Organomet. Chem. **721-722**, 148 (2012).

[35] T. R. Galeev, C. Romanescu, W. L. Li, L. S. Wang and A. I. Boldyrev, *Angew. Chem. Int. Ed.* **51**, 2101 (2012).

[36] W. L. Li, C. Romanescu, T. R. Galeev, Z. A. Piazza, A. I. Boldyrev and L. S. Wang, *J. Am. Chem. Soc.* **134**, 165 (2012).

[37] W. L. Li, C. Romanescu, Z. A. Piazza and L. S. Wang, *Phys. Chem. Chem. Phys*. **14**, 13663 (2012).

[38] C. Romanescu, T. R. Galeev, W. L. Li, A. I. Boldyrev and L. S. Wang, *J. Chem. Phys*. **138**, 134315 (2013).

[39] Y. Liao, C. L. Cruz, P. v. R. Schleyer and Z. Chen, *Phys. Chem. Chem. Phys*. **14**, 14898 (2012).

[40] T. Heine and G. Merino, *Angew. Chem., Int. Ed*. **51**, 4275 (2012).

[41] I. Boustani and R. Pandey, *Solid State Sciences* **14**, 1591 (2012).

[42] L. Xie, W. L. Li, C. Romanescu, X. Huang and L. S. Wang, *J. Chem. Phys.* **138**, 034308 (2013).

[43] (a) L. S. Wang, H. S. Cheng and J. W. Fan, *J. Chem. Phys.* **102**, 9480 (1995). (b) L. S. Wang and X. Li, In advances in Metal and Semiconductor Clusters, edited by M. A. Duncan, (JAI, Greenwich, CT, 1998), Vol. 4, pp. 299-343.

[44] C. Adamo and V. Barone, *J. Chem. Phys*. **110**, 6158 (1999).

[45] J. P. Perdew, K. Burke and M. Ernzerhof, *Phys. Rev. Lett.* **77**, 3865 (1996).

[46] P. J. Hay and W. R. Wadt, *J. Chem. Phys*., 1985, **82**, 270.

[47] R. A. Kendall, T. H. Dunning, Jr. and R. J. Harrison, *J. Chem. Phys*. **96**, 6796 (1992).

[48] T. H. Dunning, Jr., *J. Chem. Phys*. **90**, 1007 (1989).

[49] A. Bergner, M. Dolg, W. Kuechle, H. Stoll and H. Preuss, *Mol. Phys.* **80**, 1431 (1993).

[50] M. Kaupp, P. v. R. Schleyer, H. Stoll and H. Preuss, *J. Chem. Phys*. **94**, 1360 (1991).

[51] M. Dolg, H. Stoll, H. Preuss and R. M. Pitzer, *J. Phys. Chem*. **97**, 5852 (1993).

[52] M. J. Frisch, G. W. Trucks, H. B. Schlegel *et al.*, *Gaussian09, Rev. B.01*, Gaussian, Inc, Wallingford, CT, 2009.

[53] U. Varetto, *Molekel 5.4.0.8*, Swiss National Supercomputing Centre, Manno, Switzerland, 2009.

[54] See supplementary material at http://dx.doi.org/ for the geometric structures and relative energies (CCSD(T)/Ta/Stuttgart/B/aug-cc-pVTZ, PBE0/Ta/Stuttgart/B/aug-cc-pVTZ, all at PBE0/Ta/Stuttgart/B/aug-cc-pVTZ optimized geometries) of all studied isomers. Cartesian coordinates of global minimum structures (PBE0/Ta/Stuttgart/B/aug-cc-pVTZ) for all considered stoichiometries

[55] J. P. Perdew, J. A. Chevary, S. H. Vosko, K. A. Jackson, M. R. Pederson, D. J. Singh and C. Fiolhais, *Phys. Rev. B* **46**, 6671 (1992).

[56] Y. Zhao and D. G. Truhlar, *Theor. Chem. Account* **120**, 215 (2008).

Table 3-1. Experimental vertical detachment energies (VDEs) compared with calculated VDEs for the global minimum structure I.1 (C_{2v}, $^4B_1$) of TaB_3^-. All energies are in eV.

Feature	VDE (exp)[a]	Final State and electronic configuration	VDE (theoretical)	
			ROPBE1PBE[b]	ROCCSD(T)[c]
I.1. C_{2v} ($^4B_1$)				
X	1.87(3)	$^3A_2$, $\{1a_1^{(2)}1b_2^{(2)}2a_1^{(2)}1b_1^{(2)}3a_1^{(2)}2b_2^{(2)}1a_2^{(1)}3b_2^{(0)}4a_1^{(1)}\}$	1.93	1.82
A	2.03(4)	$^3B_1$, $\{1a_1^{(2)}1b_2^{(2)}2a_1^{(2)}1b_1^{(2)}3a_1^{(2)}2b_2^{(2)}1a_2^{(1)}3b_2^{(1)}4a_1^{(0)}\}$	2.30	2.24
B	2.22(3)	$^3B_2$, $\{1a_1^{(2)}1b_2^{(2)}2a_1^{(2)}1b_1^{(2)}3a_1^{(2)}2b_2^{(2)}1a_2^{(0)}3b_2^{(1)}4a_1^{(1)}\}$	2.38	2.24
C	2.78(5)	$^5A_2$, $\{1a_1^{(2)}1b_2^{(2)}2a_1^{(2)}1b_1^{(2)}3a_1^{(2)}2b_2^{(1)}1a_2^{(1)}3b_2^{(1)}4a_1^{(1)}\}$	2.55	2.51
D	3.04(5)	$^5B_1$, $\{1a_1^{(2)}1b_2^{(2)}2a_1^{(2)}1b_1^{(2)}3a_1^{(1)}2b_2^{(2)}1a_2^{(1)}3b_2^{(1)}4a_1^{(1)}\}$	2.71	3.00
E	3.56(6)	$^5A_1$, $\{1a_1^{(2)}1b_2^{(2)}2a_1^{(2)}1b_1^{(1)}3a_1^{(2)}2b_2^{(2)}1a_2^{(1)}3b_2^{(1)}4a_1^{(1)}\}$	3.26	3.42
F	3.95(6)	$^5B_1$, $\{1a_1^{(2)}1b_2^{(2)}2a_1^{(1)}1b_1^{(2)}3a_1^{(2)}2b_2^{(2)}1a_2^{(1)}3b_2^{(1)}4a_1^{(1)}\}$	4.07	4.06
G	4.67(8)	$^5A_2$, $\{1a_1^{(2)}1b_2^{(1)}2a_1^{(2)}1b_1^{(2)}3a_1^{(2)}2b_2^{(2)}1a_2^{(1)}3b_2^{(1)}4a_1^{(1)}\}$	[d]	4.64

[a] Numbers in parentheses represent the uncertainty in the last digit.
[b]VDEs were calculated at ROPBE1PBE/Ta/Stuttgart/B/aug-cc-pVTZ//PBE1PBE/Ta/Stuttgart/B/aug-cc-pVTZ.
[c]VDEs were calculated at ROCCSD(T)/Ta/Stuttgart/B/aug-cc-pVTZ//PBE1PBE/Ta/Stuttgart/B/aug-cc-pVTZ.
[d]VDE could not be calculated at this level of theory.

Table 3-2. Experimentally VDEs compared with calculated VDEs for the II.1 (C_{2v}, $^1A_1$) global minimum and the II.2 (C_s, $^3A''$) low-lying isomer of TaB_4^-. All energies are in eV.

Feature	VDE (exp)[a]	Final State and electronic configuration	VDE (theoretical)	
			ROPBE1PBE[b]	ROCCSD(T)[c]
II.1. C_{2v} ($^1A_1$)				
X	2.78(3)	$^2B_2$, {…$3a_1^{(2)}2b_2^{(2)}1b_1^{(2)}4a_1^{(2)}1a_2^{(2)}3b_2^{(1)}$}	2.67	2.66
A	3.14(3)	$^2A_2$, {…$3a_1^{(2)}2b_2^{(2)}1b_1^{(2)}4a_1^{(2)}1a_2^{(1)}3b_2^{(2)}$}	3.01	3.09
B	3.46(3)	$^2A_1$, {…$3a_1^{(2)}2b_2^{(2)}1b_1^{(2)}4a_1^{(1)}1a_2^{(2)}3b_2^{(2)}$}	3.53	3.49
C	4.07(3)	$^2B_1$, {…$3a_1^{(2)}2b_2^{(2)}1b_1^{(1)}4a_1^{(2)}1a_2^{(2)}3b_2^{(2)}$}	4.09	4.21
II.2. C_s ($^3A''$)				
X‘	~ 2.5	$^2A''$, {…$3a'^{(2)}4a'^{(2)}5a'^{(2)}2a''^{(2)}3a''^{(2)}4a''^{(1)}6a'^{(0)}$}	2.53	2.50
		$^4A'$, {…$3a'^{(2)}4a'^{(2)}5a'^{(2)}2a''^{(2)}3a''^{(1)}4a''^{(1)}6a'^{(1)}$}	2.71	2.80
A’	2.91(4)	$^2A'$, {…$3a'^{(2)}4a'^{(2)}5a'^{(2)}2a''^{(2)}3a''^{(2)}4a''^{(0)}6a'^{(1)}$}	3.00	2.82
		$^4A'$, {…$3a'^{(2)}4a'^{(2)}5a'^{(2)}2a''^{(1)}3a''^{(2)}4a''^{(1)}6a'^{(1)}$}	3.25	[d]
B‘	3.71(4)	$^4A''$, {…$3a'^{(2)}4a'^{(2)}5a'^{(1)}2a''^{(2)}3a''^{(2)}4a''^{(1)}6a'^{(1)}$}	3.55	[d]
		$^4A''$, {…$3a'^{(2)}4a'^{(1)}5a'^{(2)}2a''^{(2)}3a''^{(2)}4a''^{(1)}6a'^{(1)}$}	3.87	4.09

[a] Numbers in parentheses represent the uncertainty in the last digit.
[b]VDEs were calculated at ROPBE1PBE/Ta/Stuttgart/B/aug-cc-pVTZ//PBE1PBE/Ta/Stuttgart/B/aug-cc-pVTZ.
[c]VDEs were calculated at ROCCSD(T)/Ta/Stuttgart/B/aug-cc-pVTZ//PBE1PBE/Ta/Stuttgart/B/aug-cc-pVTZ.
[d]VDE could not be calculated at this level of theory.

Table 3-3. Experimental VDEs compared with calculated VDEs for the III.1 (C_{2v}, $^2A_1$) global minimum and C_1 low-lying isomer of TaB_5^-. All energies are in eV.

Feature	VDE (exp)[a]	Final State and electronic configuration	VDE (theoretical)	
			ROPBE1PBE[b]	ROCCSD(T)[c]
III.1. C_{2v} ($^2A_1$)				
X	2.81(3)	$^3B_2$, {…$2b_2^{(2)}3a_1^{(2)}1b_1^{(2)}4a_1^{(2)}3b_2^{(1)}1a_2^{(2)}4b_2^{(2)}5a_1^{(1)}$}	[d]	2.81
A	3.09(5)	$^3B_2$, {…$2b_2^{(2)}3a_1^{(2)}1b_1^{(2)}4a_1^{(2)}3b_2^{(2)}1a_2^{(2)}4b_2^{(1)}5a_1^{(1)}$}	[d]	2.86
		$^1A_1$, {…$2b_2^{(2)}3a_1^{(2)}1b_1^{(2)}4a_1^{(2)}3b_2^{(2)}1a_2^{(2)}4b_2^{(2)}5a_1^{(0)}$}	2.84	2.89
B	3.89(8)	$^3A_2$, {…$2b_2^{(2)}3a_1^{(2)}1b_1^{(2)}4a_1^{(2)}3b_2^{(2)}1a_2^{(1)}4b_2^{(2)}5a_1^{(1)}$}	[d]	3.69
C	4.09(8)	$^3A_1$, {…$2b_2^{(2)}3a_1^{(2)}1b_1^{(2)}4a_1^{(1)}3b_2^{(2)}1a_2^{(2)}4b_2^{(2)}5a_1^{(1)}$}	[d]	4.12
D	4.65(5)	$^3B_1$, {…$2b_2^{(2)}3a_1^{(2)}1b_1^{(1)}4a_1^{(2)}3b_2^{(2)}1a_2^{(2)}4b_2^{(2)}5a_1^{(1)}$}	[d]	4.49
III.2. C_1 (^2A)				
X’	~ 2.4	^1A, {…$3a^{(2)}4a^{(2)}5a^{(2)}6a^{(2)}7a^{(2)}8a^{(2)}9a^{(2)}10a^{(2)}11a^{(0)}$}	2.20	2.35
		^3A, {…$3a^{(2)}4a^{(2)}5a^{(2)}6a^{(2)}7a^{(2)}8a^{(2)}9a^{(2)}10a^{(1)}11a^{(1)}$}	[d]	2.82

[a] Numbers in parentheses represent the uncertainty in the last digit.
[b]VDEs were calculated at ROPBE1PBE/Ta/Stuttgart/B/aug-cc-pVTZ//PBE1PBE/Ta/Stuttgart/B/aug-cc-pVTZ.
[c]VDEs were calculated at ROCCSD(T)/Ta/Stuttgart/B/aug-cc-pVTZ//PBE1PBE/Ta/Stuttgart/B/aug-cc-pVTZ.
[d]VDE could not be calculated at this level of theory.

Table 3-4. Experimental VDEs compared with calculated VDEs for the IV.1 (C_{2v}, $^3A_2$) global minimum, and IV.2 (C_{2v}, $^1A_1$) and IV.3 (C_{2v}, $^1A_1$) low-lying isomers of TaB_6^-. All energies are in eV.

Feature	VDE (exp)[a]	Final State and electronic configuration	VDE (theoretical)	
			ROPBE1PBE[b]	ROCCSD(T)[c]
IV.1. C_{2v} ($^3A_2$)				
X	2.49(3)	$^2B_1$, $\{...1b_1^{(2)}3b_2^{(2)}5a_1^{(2)}4b_2^{(2)}1a_2^{(2)}2b_1^{(1)}5b_2^{(0)}\}$	[d]	2.43
A	2.75(5)	$^2B_2$, $\{...1b_1^{(2)}3b_2^{(2)}5a_1^{(2)}4b_2^{(2)}1a_2^{(2)}2b_1^{(0)}5b_2^{(1)}\}$	2.86	2.81
B	3.07(4)	$^4A_1$, $\{...1b_1^{(2)}3b_2^{(2)}5a_1^{(2)}4b_2^{(2)}1a_2^{(1)}2b_1^{(1)}5b_2^{(1)}\}$	2.80	2.99
C	3.58(3)	$^4B_1$, $\{...1b_1^{(2)}3b_2^{(2)}5a_1^{(2)}4b_2^{(1)}1a_2^{(2)}2b_1^{(1)}5b_2^{(1)}\}$	3.55	3.56
D	3.77(5)	$^4A_2$, $\{...1b_1^{(2)}3b_2^{(2)}5a_1^{(1)}4b_2^{(2)}1a_2^{(2)}2b_1^{(1)}5b_2^{(1)}\}$	3.71	3.76
E	4.36(5)	$^4B_1$, $\{...1b_1^{(2)}3b_2^{(1)}5a_1^{(2)}4b_2^{(2)}1a_2^{(2)}2b_1^{(1)}5b_2^{(1)}\}$	4.44	[d]
F	5.08(8)		[d]	[d]
IV.2. C_{2v} ($^1A_1$)				
X'	~ 2.3	$^2B_2$, $\{\ldots2b_2^{(2)}4a_1^{(2)}1a_2^{(2)}2b_1^{(2)}5a_1^{(2)}6a_1^{(2)}3b_2^{(1)}\}$	2.21	2.32
		$^2A_1$, $\{\ldots2b_2^{(2)}4a_1^{(2)}1a_2^{(2)}2b_1^{(2)}5a_1^{(2)}6a_1^{(1)}3b_2^{(2)}\}$	2.62	2.73
		$^2A_1$, $\{\ldots2b_2^{(2)}4a_1^{(2)}1a_2^{(2)}2b_1^{(2)}5a_1^{(1)}6a_1^{(2)}3b_2^{(2)}\}$	3.20	3.23
		$^2B_1$, $\{\ldots2b_2^{(2)}4a_1^{(2)}1a_2^{(2)}2b_1^{(1)}5a_1^{(2)}6a_1^{(2)}3b_2^{(2)}\}$	4.66	4.68
		$^2A_2$, $\{\ldots2b_2^{(2)}4a_1^{(2)}1a_2^{(1)}2b_1^{(2)}5a_1^{(2)}6a_1^{(2)}3b_2^{(2)}\}$	4.72	4.73
		$^2A_1$, $\{\ldots2b_2^{(2)}4a_1^{(1)}1a_2^{(2)}2b_1^{(2)}5a_1^{(2)}6a_1^{(2)}3b_2^{(2)}\}$	4.83	4.85
IV.3. C_{2v} ($^1A_1$)				
X"	2.64(3)	$^2B_1$, $\{...4a_1^{(2)}2b_1^{(2)}2b_2^{(2)}5a_1^{(2)}3b_2^{(2)}3b_1^{(1)}\}$	2.50	2.56
A"	2.85(3)	$^2B_2$, $\{...4a_1^{(2)}2b_1^{(2)}2b_2^{(2)}5a_1^{(2)}3b_2^{(1)}3b_1^{(2)}\}$	2.86	2.84
B"	3.28(4)	$^2A_1$, $\{...4a_1^{(2)}2b_1^{(2)}2b_2^{(2)}5a_1^{(1)}3b_2^{(2)}3b_1^{(2)}\}$	3.13	3.28
		$^2B_2$, $\{...4a_1^{(2)}2b_1^{(2)}2b_2^{(1)}5a_1^{(2)}3b_2^{(2)}3b_1^{(2)}\}$	3.70	3.72
C"	4.00(5)	$^2B_1$, $\{...4a_1^{(2)}2b_1^{(1)}2b_2^{(2)}5a_1^{(2)}3b_2^{(2)}3b_1^{(2)}\}$	3.99	3.90
		$^2A_1$, $\{...4a_1^{(1)}2b_1^{(2)}2b_2^{(2)}5a_1^{(2)}3b_2^{(2)}3b_1^{(2)}\}$	4.90	4.86

[a] Numbers in parentheses represent the uncertainty in the last digit.
[b]VDEs were calculated at ROPBE1PBE/Ta/Stuttgart/B/aug-cc-pVTZ//PBE1PBE/Ta/Stuttgart/B/aug-cc-pVTZ.
[c]VDEs were calculated at ROCCSD(T)/Ta/Stuttgart/B/aug-cc-pVTZ//PBE1PBE/Ta/Stuttgart/B/aug-cc-pVTZ.
[d]VDE could not be calculated at this level of theory.

Table 3-5. Experimental VDEs compared with calculated VDEs for the V.1 (C_s, $^2A'$) global minimum of TaB_7^-. All energies are in eV.

Feature	VDE (exp)[a]	Final State and electronic configuration	VDE (theoretical)	
			ROPBE1PBE[b]	ROCCSD(T)[c]
V.1. C_s ($^2A'$)				
X	2.05(4)	$^1A'$, {…5a'$^{(2)}$6a'$^{(2)}$4a''$^{(2)}$5a''$^{(2)}$7a'$^{(2)}$8a'$^{(2)}$9a'$^{(0)}$}	2.09	2.18
A	3.43(8)	$^3A'$, {…5a'$^{(2)}$6a'$^{(2)}$4a''$^{(2)}$5a''$^{(2)}$7a'$^{(2)}$8a'$^{(1)}$9a'$^{(1)}$}	[d]	3.32
B	3.80(8)	$^3A''$, {…5a'$^{(2)}$6a'$^{(2)}$4a''$^{(2)}$7a'$^{(2)}$5a''$^{(1)}$8a'$^{(2)}$9a'$^{(1)}$}	[d]	3.91
C	4.9(1)		[d]	[d]

[a] Numbers in parentheses represent the uncertainty in the last digit.
[b]VDEs were calculated at ROPBE1PBE/Ta/Stuttgart/B/aug-cc-pVTZ//PBE1PBE/Ta/Stuttgart/B/aug-cc-pVTZ.
[c]VDEs were calculated at ROCCSD(T)/Ta/Stuttgart/B/aug-cc-pVTZ//PBE1PBE/Ta/Stuttgart/B/aug-cc-pVTZ.
[d]VDE could not be calculated at this level of theory.

Table 3-6. Experimental VDEs compared with calculated VDEs for the VI.1 (C_s, $^3A''$) global minimum and the VI.2 (C_{4v}, $^1A_1$) low-lying isomer of TaB_8^-. All energies are in eV.

Feature	VDE (exp)[a]	Final State and electronic configuration	VDE (theoretical)	
			ROPBE1PBE[b]	ROCCSD(T)[c]
VI.1. C_s ($^3A''$)				
X	3.35 (4)	$^4A'$, {…6a'$^{(2)}$7a'$^{(2)}$8a'$^{(2)}$4a''$^{(2)}$9a'$^{(2)}$5a''$^{(1)}$6a''$^{(1)}$10a'$^{(1)}$} $^4A''$, {…6a'$^{(2)}$7a'$^{(2)}$8a'$^{(2)}$4a''$^{(2)}$9a'$^{(1)}$5a''$^{(2)}$6a''$^{(1)}$10a'$^{(1)}$}	3.17 3.17	3.32 3.32
A	3.52 (3)	$^2A''$, {…6a'$^{(2)}$7a'$^{(2)}$8a'$^{(2)}$4a''$^{(2)}$9a'$^{(2)}$5a''$^{(2)}$6a''$^{(1)}$10a'$^{(0)}$} $^2A'$, {…6a'$^{(2)}$7a'$^{(2)}$8a'$^{(2)}$4a''$^{(2)}$9a'$^{(2)}$5a''$^{(2)}$6a''$^{(0)}$10a'$^{(1)}$}	3.52 3.52	3.42 3.43
B	3.98 (8)	$^2A''$, {…6a'$^{(2)}$7a'$^{(2)}$8a'$^{(2)}$4a''$^{(2)}$9a'$^{(2)}$5a''$^{(1)}$6a''$^{(2)}$10a'$^{(0)}$}[e]	3.84	3.78
C	4.42 (5)	$^4A''$, {…6a'$^{(2)}$7a'$^{(2)}$8a'$^{(1)}$4a''$^{(2)}$9a'$^{(2)}$5a''$^{(2)}$6a''$^{(1)}$10a'$^{(1)}$}	4.23[f]	4.48[f]
D	5.0 (1)		[d]	[d]
VI.2. C_{4v} ($^1A_1$)				
		$^2B_2$, {…1b$_2^{(2)}$2e$^{(4)}$2a$_1^{(2)}$1a$_2^{(2)}$3a$_1^{(2)}$3e$^{(4)}$4e$^{(4)}$2b$_2^{(1)}$}	3.29	3.23
		^2E, {…1b$_2^{(2)}$2e$^{(4)}$2a$_1^{(2)}$1a$_2^{(2)}$3a$_1^{(2)}$3e$^{(4)}$4e$^{(3)}$2b$_2^{(2)}$}	3.43	3.52
		^2E, {…1b$_2^{(2)}$2e$^{(4)}$2a$_1^{(2)}$1a$_2^{(2)}$3a$_1^{(2)}$3e$^{(3)}$4e$^{(4)}$2b$_2^{(2)}$}	4.41	[d]
		$^2A_1$, {…1b$_2^{(2)}$2e$^{(4)}$2a$_1^{(2)}$1a$_2^{(2)}$3a$_1^{(1)}$3e$^{(4)}$4e$^{(4)}$2b$_2^{(2)}$}	5.02	5.06
		$^2A_2$, {…1b$_2^{(2)}$2e$^{(4)}$2a$_1^{(2)}$1a$_2^{(1)}$3a$_1^{(2)}$3e$^{(4)}$4e$^{(4)}$2b$_2^{(2)}$}	5.59	5.38
		$^2A_1$, {…1b$_2^{(2)}$2e$^{(4)}$2a$_1^{(1)}$1a$_2^{(2)}$3a$_1^{(2)}$3e$^{(4)}$4e$^{(4)}$2b$_2^{(2)}$}	6.09	[d]

[a] Numbers in parentheses represent the uncertainty in the last digit.
[b] VDEs were calculated at ROPBE1PBE/Ta/Stuttgart/B/aug-cc-pVTZ//PBE1PBE/Ta/Stuttgart/B/aug-cc-pVTZ.
[c] VDEs were calculated at ROCCSD(T)/Ta/Stuttgart/B/aug-cc-pVTZ//PBE1PBE/Ta/Stuttgart/B/aug-cc-pVTZ.
[d] VDE could not be calculated at this level of theory.
[e] Peak B can only be explained by the shake-up.
[f] VDEs were calculated at UPBE1PBE/Ta/Stuttgart/B/aug-cc-pVTZ and at UCCSD(T)/Ta/Stuttgart/B/aug-cc-pVTZ. The values of 〈S2〉 are 3.79 (UPBE1PBE) and 4.11 (UCCSD(T)).

Table 3-7. Calculated VDEs for the I.2 (C_{2v}, $^2A_2$), and I.3 (C_{2v}, $^4A_2$) low-lying isomers of TaB_3^-. All energies are in eV.

		Final State and electronic configuration	VDE (theo)	
			ROPBE1PBE[a]	ROCCSD(T)[b]
I.2. C_{2v} ($^2A_2$)				
		$^3A_2$, {…$2b_2^{(2)}1b_1^{(2)}3a_1^{(2)}4a_1^{(1)}1a_2^{(1)}$}	[c]	1.64
		$^1A_1$, {…$2b_2^{(2)}1b_1^{(2)}3a_1^{(2)}4a_1^{(2)}1a_2^{(0)}$}	2.19	2.09
		$^3B_2$, {…$2b_2^{(2)}1b_1^{(1)}3a_1^{(2)}4a_1^{(2)}1a_2^{(1)}$}	[c]	4.26
I.3. C_{2v} ($^4A_2$)				
		$^3A_2$, {...$1b_2^{(2)}1b_1^{(2)}3a_1^{(2)}2b_2^{(2)}4a_1^{(1)}5a_1^{(0)}5a_2^{(1)}$}	[c]	1.60
		$^3A_1$, {...$1b_2^{(2)}1b_1^{(2)}3a_1^{(2)}2b_2^{(2)}4a_1^{(1)}5a_1^{(1)}5a_2^{(0)}$}	1.86	1.70
		$^5B_1$, {...$1b_2^{(2)}1b_1^{(2)}3a_1^{(2)}2b_2^{(1)}4a_1^{(1)}5a_1^{(1)}5a_2^{(1)}$}	2.76	2.68
		$^5A_2$, {...$1b_2^{(2)}1b_1^{(2)}3a_1^{(1)}2b_2^{(2)}4a_1^{(1)}5a_1^{(1)}5a_2^{(1)}$}	2.51	2.82
		$^5B_2$, {...$1b_2^{(2)}1b_1^{(1)}3a_1^{(2)}2b_2^{(2)}4a_1^{(1)}5a_1^{(1)}5a_2^{(1)}$}	3.52	3.70

[a]VDEs were calculated at ROPBE1PBE/Ta/Stuttgart/B/aug-cc-pVTZ//PBE1PBE/Ta/Stuttgart/B/aug-cc-pVTZ.
[b]VDEs were calculated at ROCCSD(T)/Ta/Stuttgart/B/aug-cc-pVTZ//PBE1PBE/Ta/Stuttgart/B/aug-cc-pVTZ.
[c]VDE could not be calculated at this level of theory.

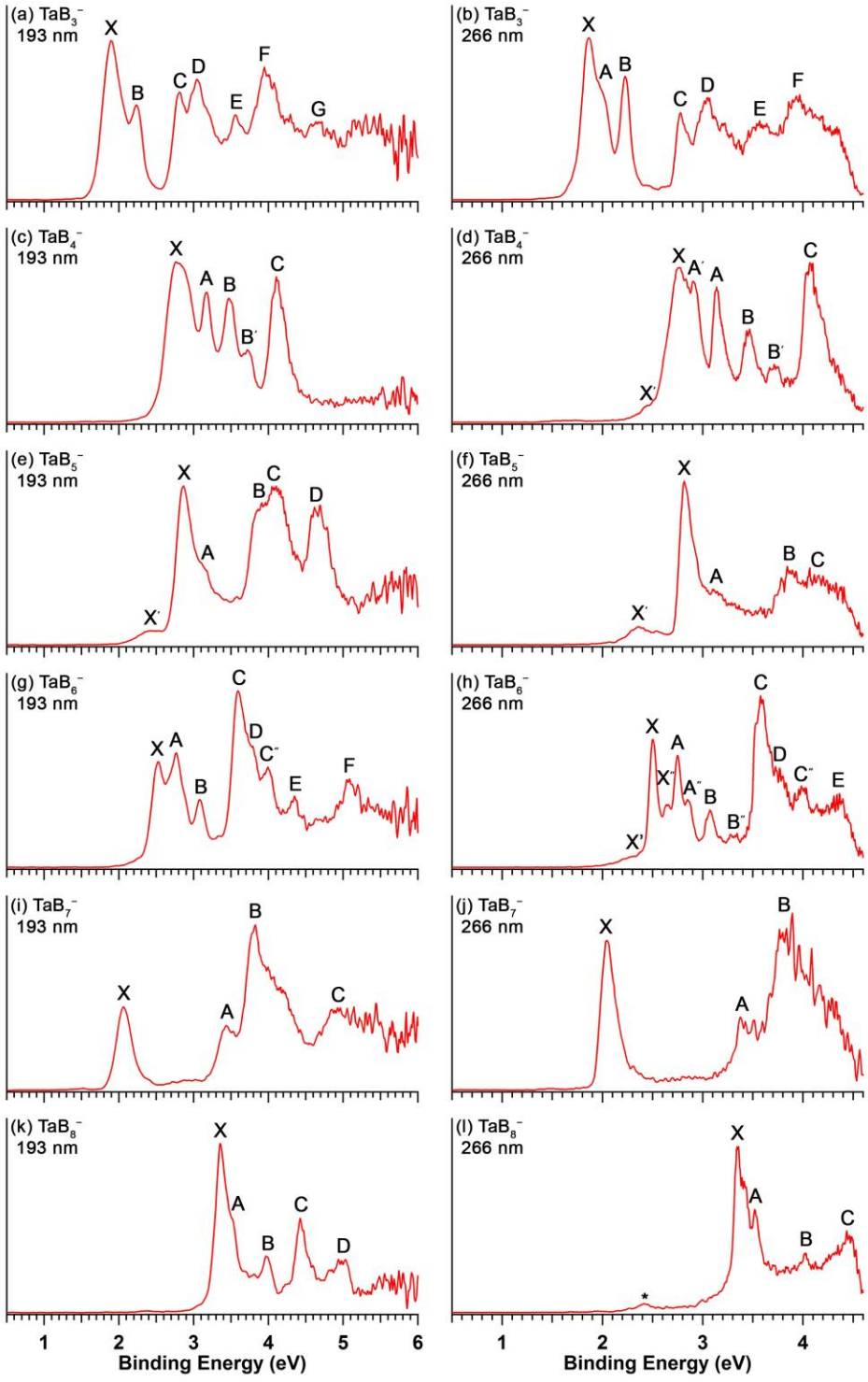

Figure 3-1. Photoelectron Spectra of TaB_n^- (n = 3–8) at 193 nm (left) and 266 nm (right).

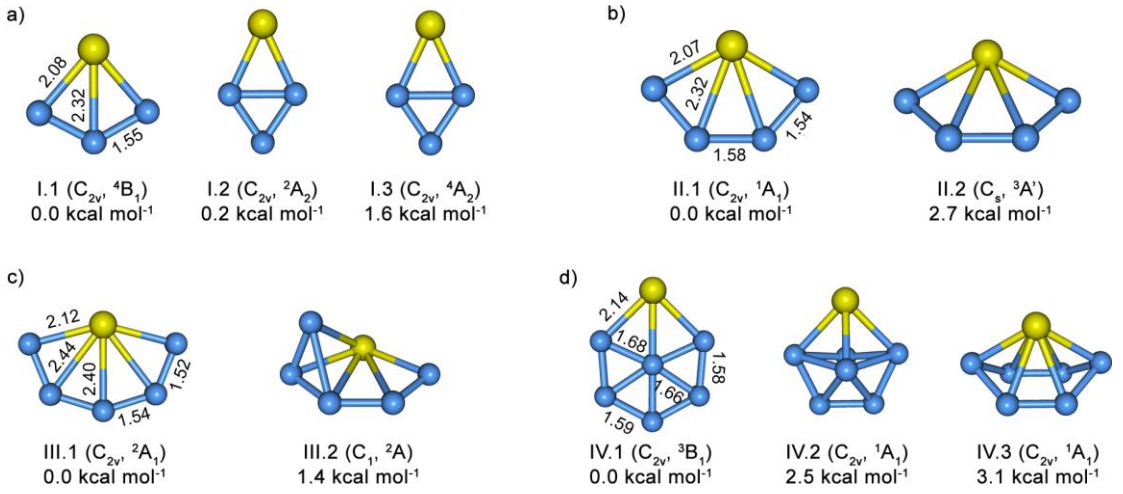

Figure 3-2. The global minimum structures and low-lying isomers of (a) TaB_3^-, (b) TaB_4^-, (c) TaB_5^-, and (d) TaB_6^-, optimized at the PBE0/Ta/Stuttgart/B/aug-cc-pVTZ level. Also given are the point group symmetries, spectroscopic states, and relative energies at the CCSD(T)/Ta/Stuttgart/B/aug-cc-pVTZ level with ZPE corrections at the PBE0/Ta/Stuttgart/B/aug-cc-pVTZ level. Bond lengths for the global minimum structures are given in Å.

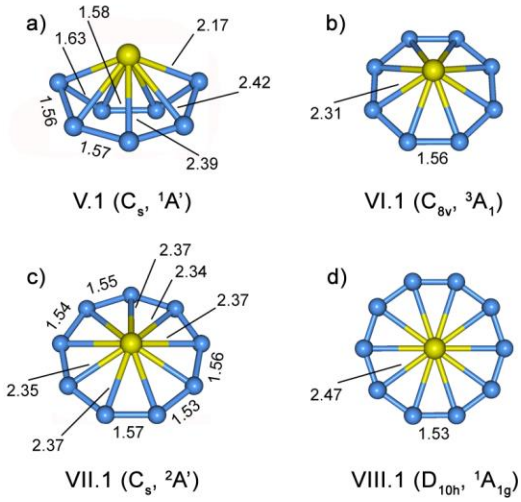

Figure 3-3. The global minimum structures of (a) TaB_7^-, (b) TaB_8^-, (c) TaB_9^-, and (d) TaB_{10}^-, optimized at PBE0/Ta/Stuttgart/B/aug-cc-pVTZ level. Bond lengths in Å, point group symmetries, and spectroscopic states are also shown. The structures of TaB_9^- and TaB_{10}^-, which were reported previously,[35, 38] are given for comparison.

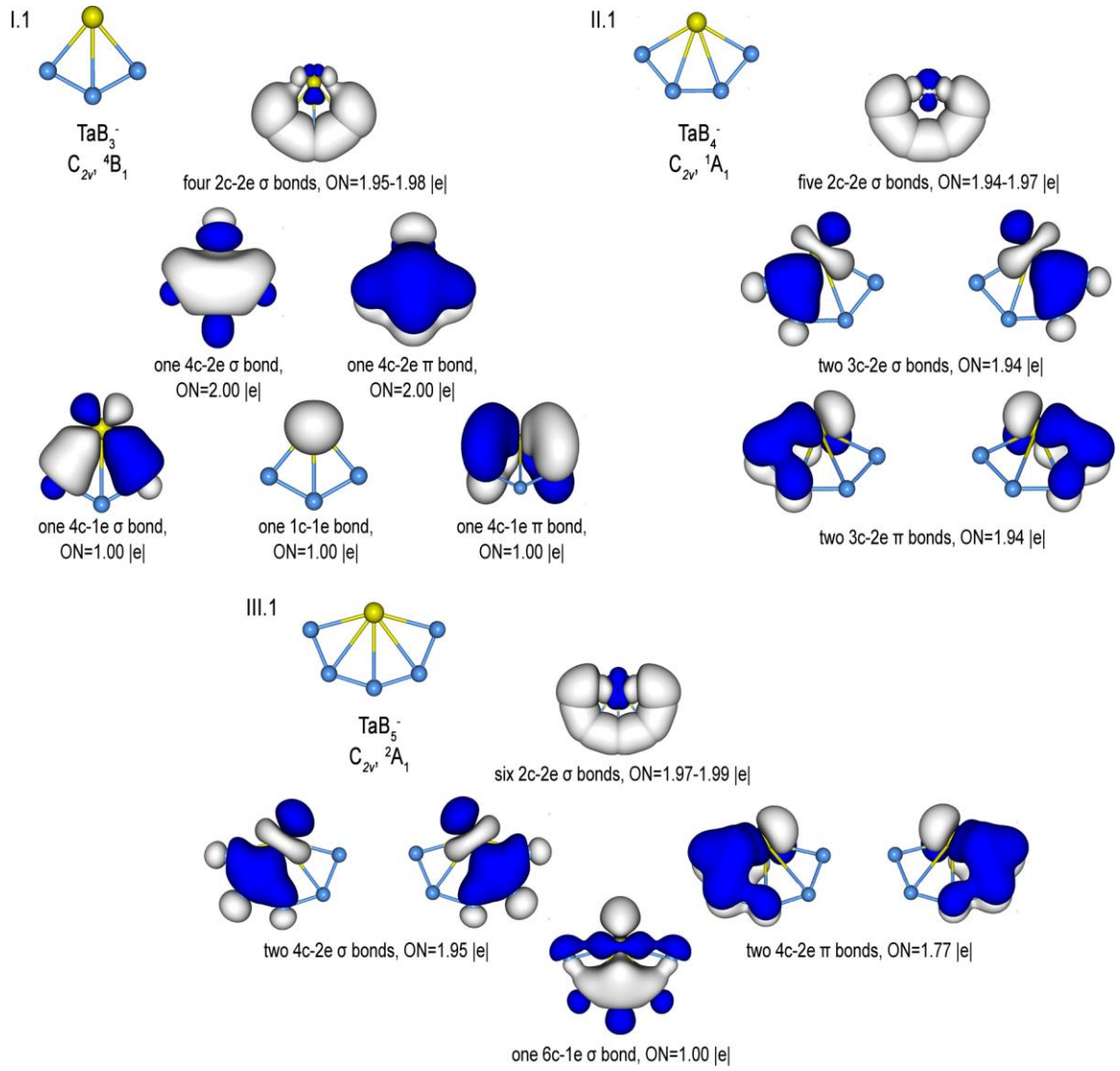

Figure 3-4. Results of AdNDP analyses for the global minimum structures of TaB_3^- (I.1), TaB_4^- (II.1), and TaB_5^- (III.1).

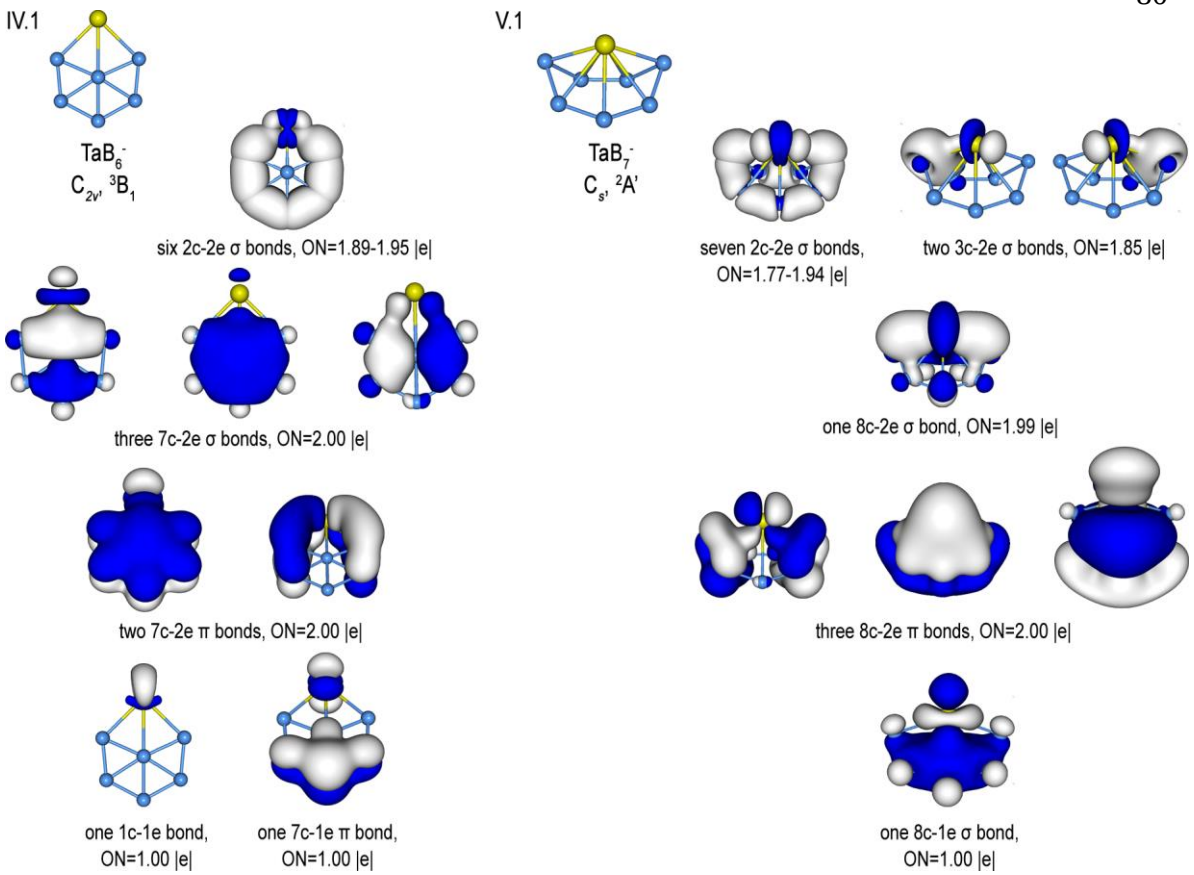

Figure 3-5. Results of AdNDP analyses for the global minimum structures of TaB_6^- (IV.1) and TaB_7^- (V.1).

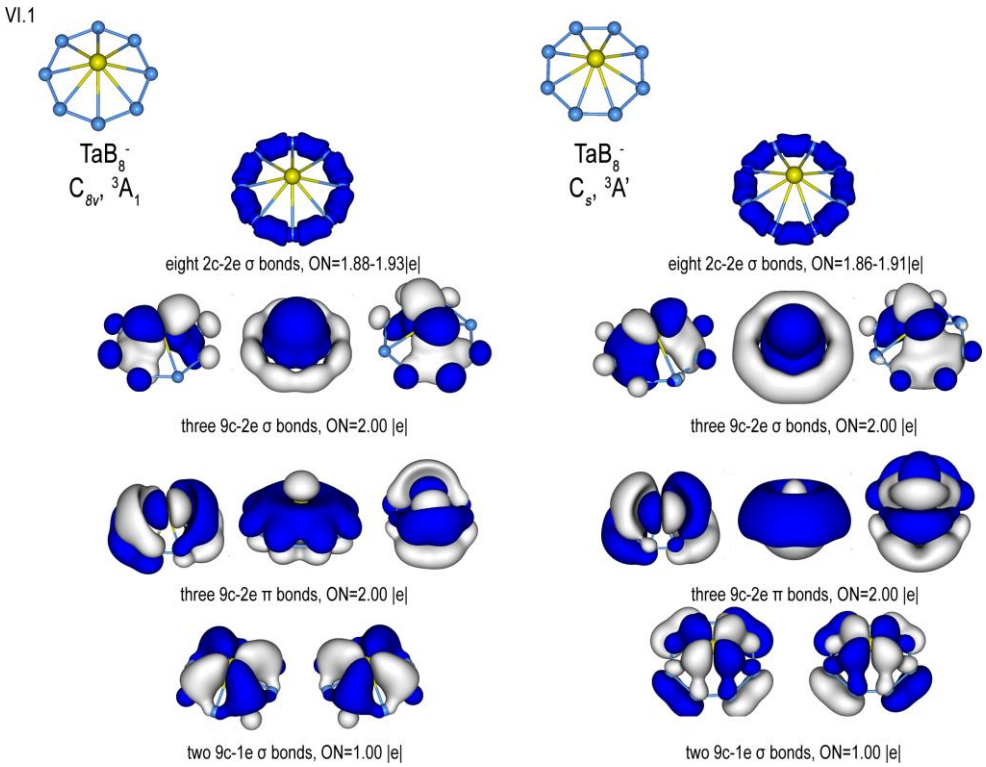

Figure 3-6. Results of AdNDP analyses for the C_{8v} and C_s TaB_8^-.

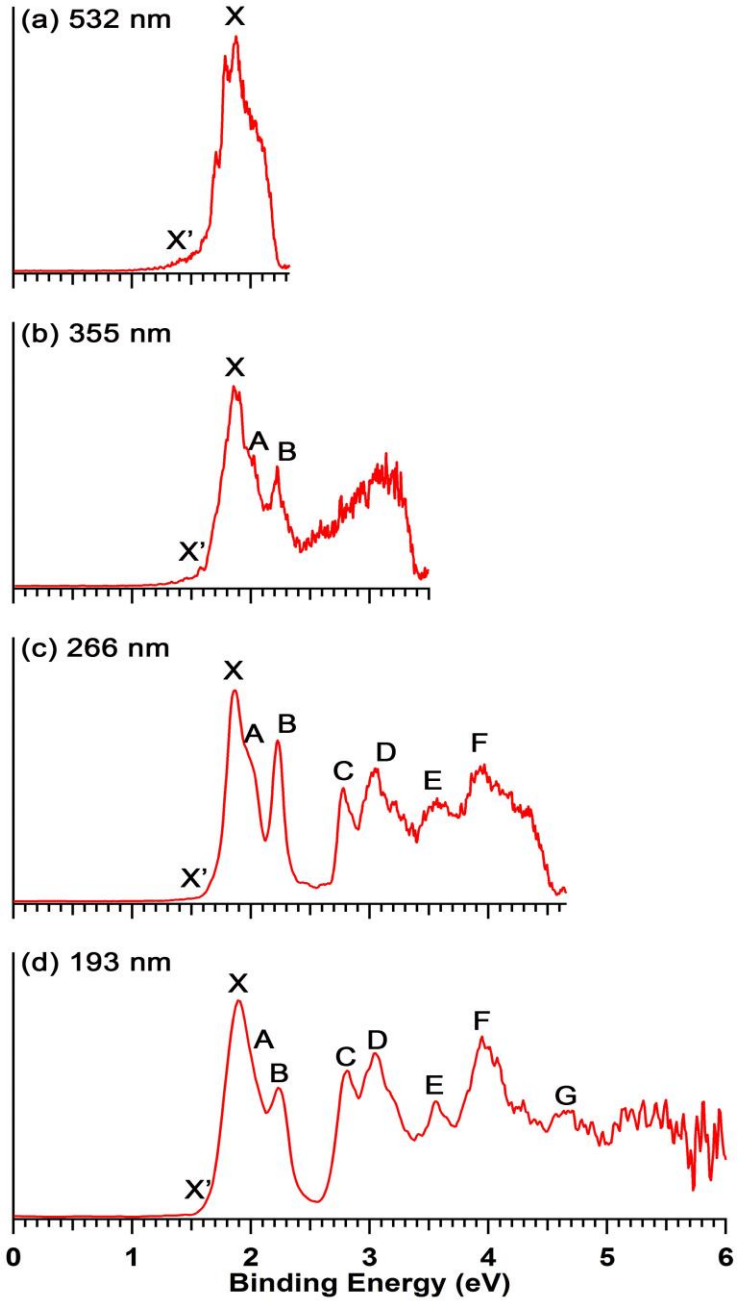

Figure 3-7. Photoelectron Spectra of TaB_3^- at (a) 532 nm, (b) 355 nm, (c) 266 nm, and (d) 193 nm.

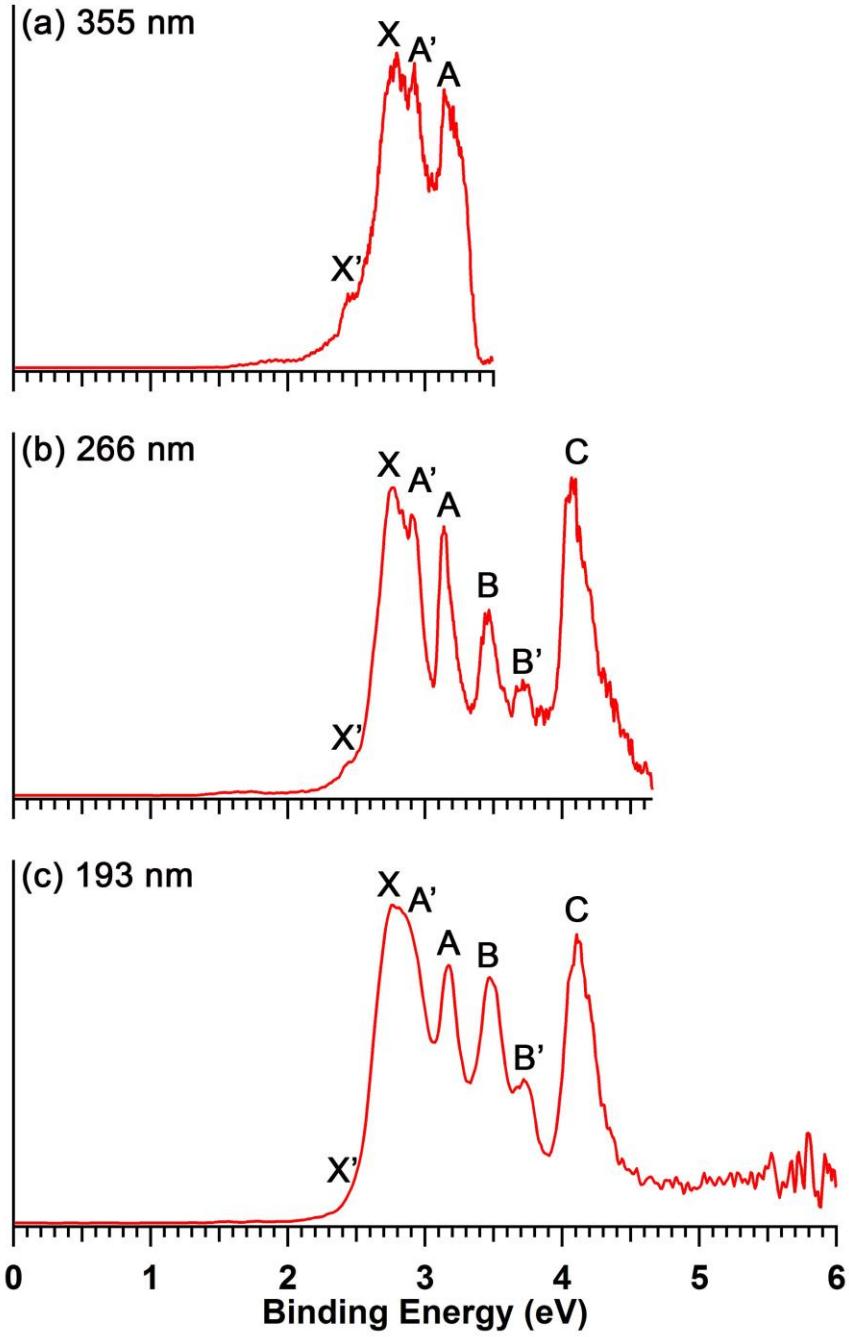

Figure 3-8. Photoelectron Spectra of TaB_4^- at (a) 355 nm, (b) 266 nm, and (c) 193 nm.

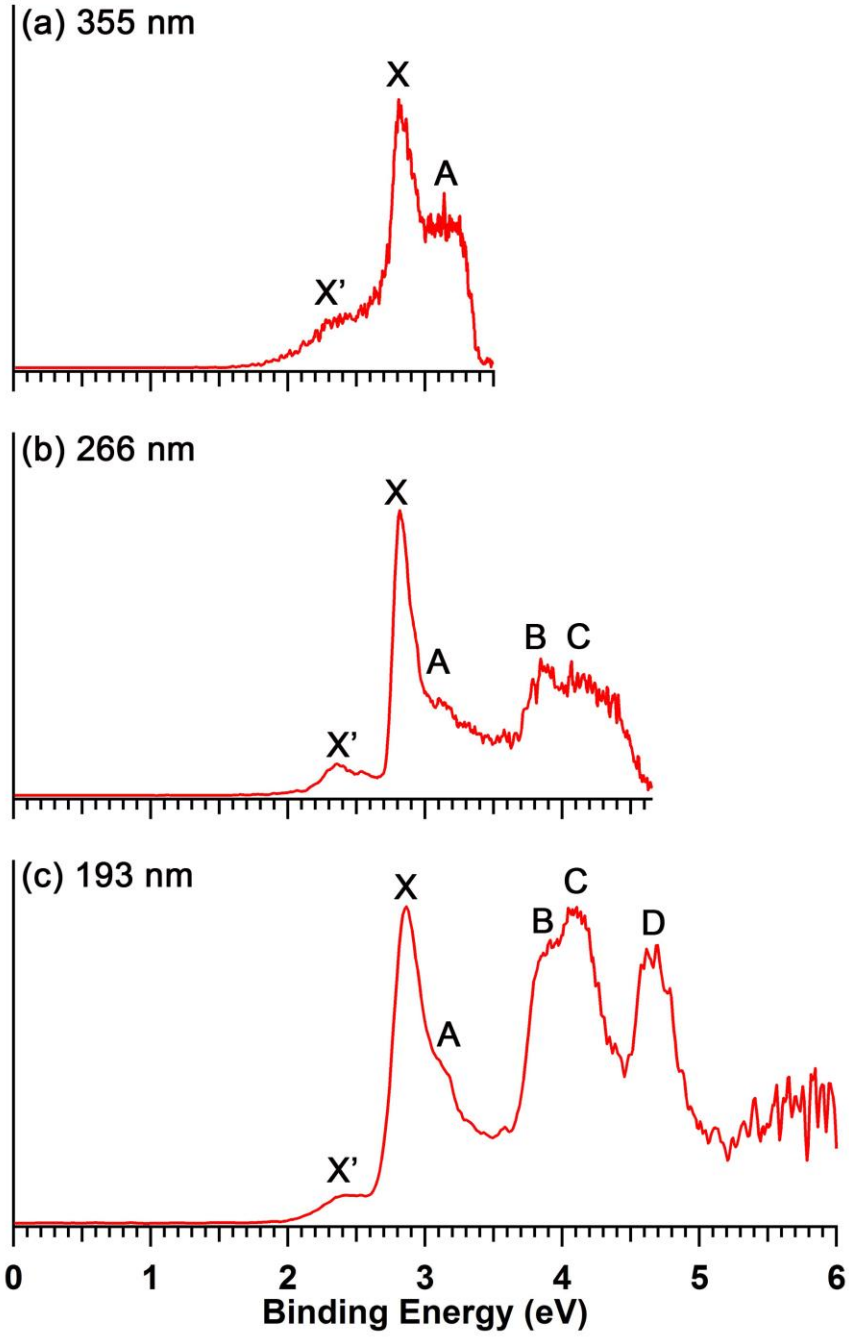

Figure 3-9. Photoelectron Spectra of TaB_5^- at (a) 355 nm, (b) 266 nm, and (c) 193 nm.

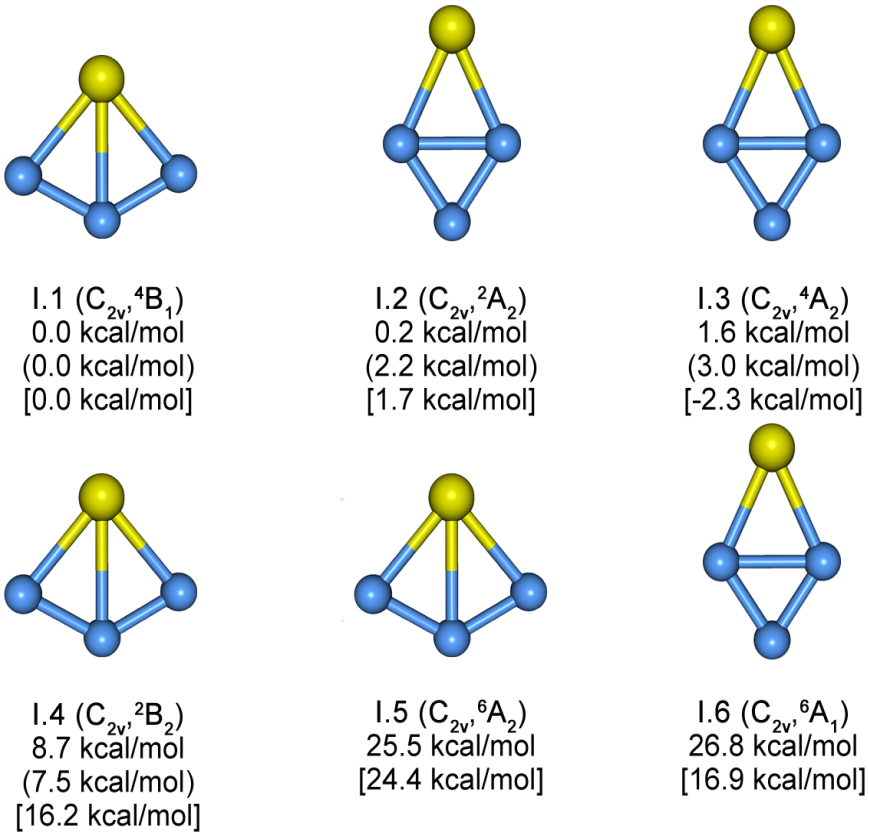

Figure 3-10. Low-lying structures of TaB_3^-, their point group symmetries, spectroscopic states and ZPE corrected relative energies. The energies are given at: CCSD(T)/Ta/Stuttgart/B/aug-cc-pVTZ (top), CCSD(T)/Ta/Stuttgart/B/aug-cc-pVQZ (in brackets), PBE0/Ta/Stuttgart/B/aug-cc-pVTZ (square brackets), all at PBE0/Ta/Stuttgart/B/aug-cc-pVTZ optimized geometries.

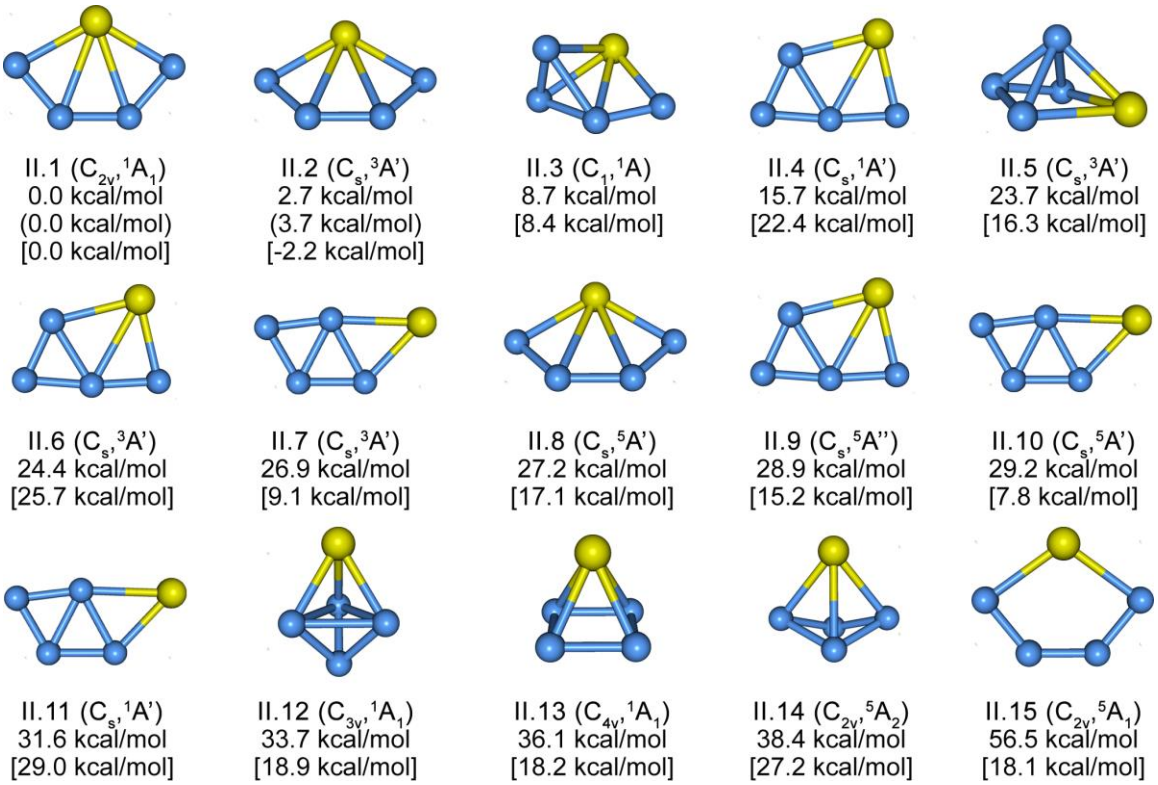

Figure 3-11. Low-lying structures of TaB_4^-, their point group symmetries, spectroscopic states and ZPE corrected relative energies. The energies are given at: CCSD(T)/Ta/Stuttgart/B/aug-cc-pVTZ (top), CCSD(T)/Ta/Stuttgart/B/aug-cc-pVQZ (in brackets), PBE0/Ta/Stuttgart/B/aug-cc-pVTZ (square brackets), all at PBE0/Ta/Stuttgart/B/aug-cc-pVTZ optimized geometries.

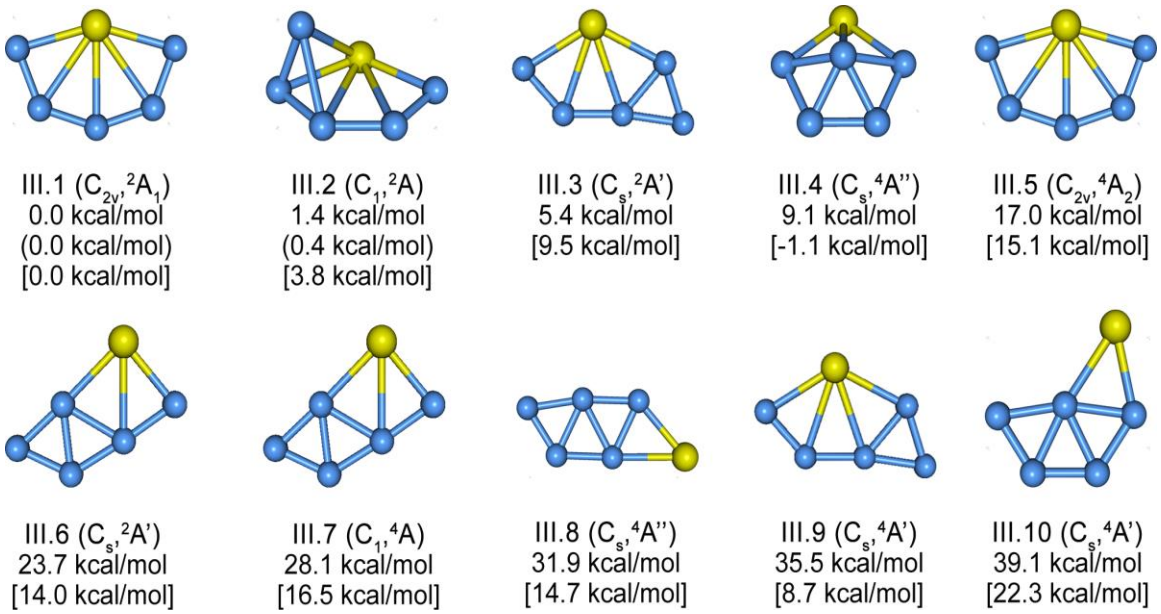

Figure 3-12. Low-lying structures of TaB_5^-, their point group symmetries, spectroscopic states and ZPE corrected relative energies. The energies are given at: CCSD(T)/Ta/Stuttgart/B/aug-cc-pVTZ (top), CCSD(T)/Ta/Stuttgart/B/aug-cc-pVQZ (in brackets), PBE0/Ta/Stuttgart/B/aug-cc-pVTZ (square brackets), all at PBE0/Ta/Stuttgart/B/aug-cc-pVTZ optimized geometries.

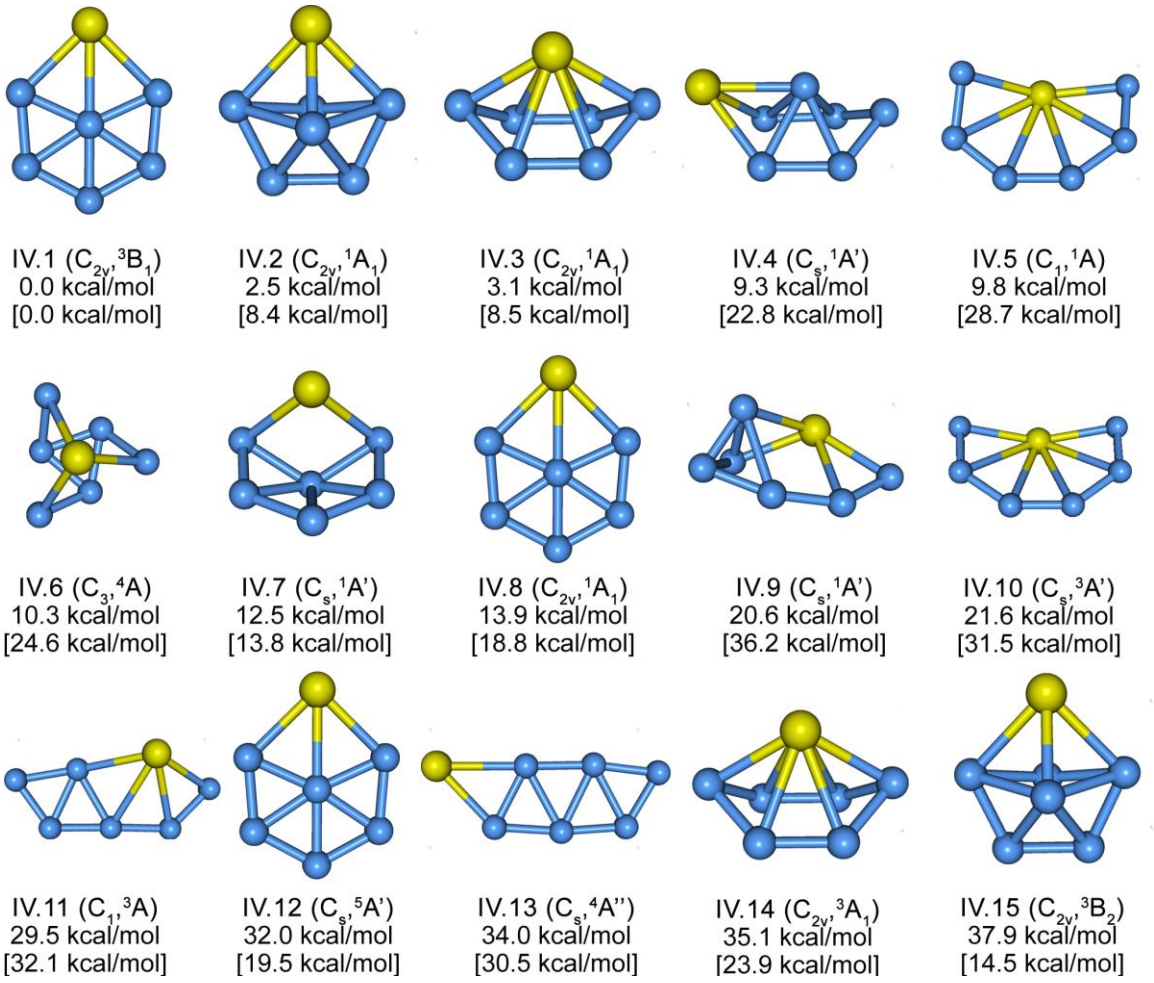

Figure 3-13. Low-lying structures of TaB_6^-, their point group symmetries, spectroscopic states and ZPE corrected relative energies. The energies are given at: CCSD(T)/Ta/Stuttgart/B/aug-cc-pVTZ (top), PBE0/Ta/Stuttgart/B/aug-cc-pVTZ (square brackets), all at PBE0/Ta/Stuttgart/B/aug-cc-pVTZ optimized geometries.

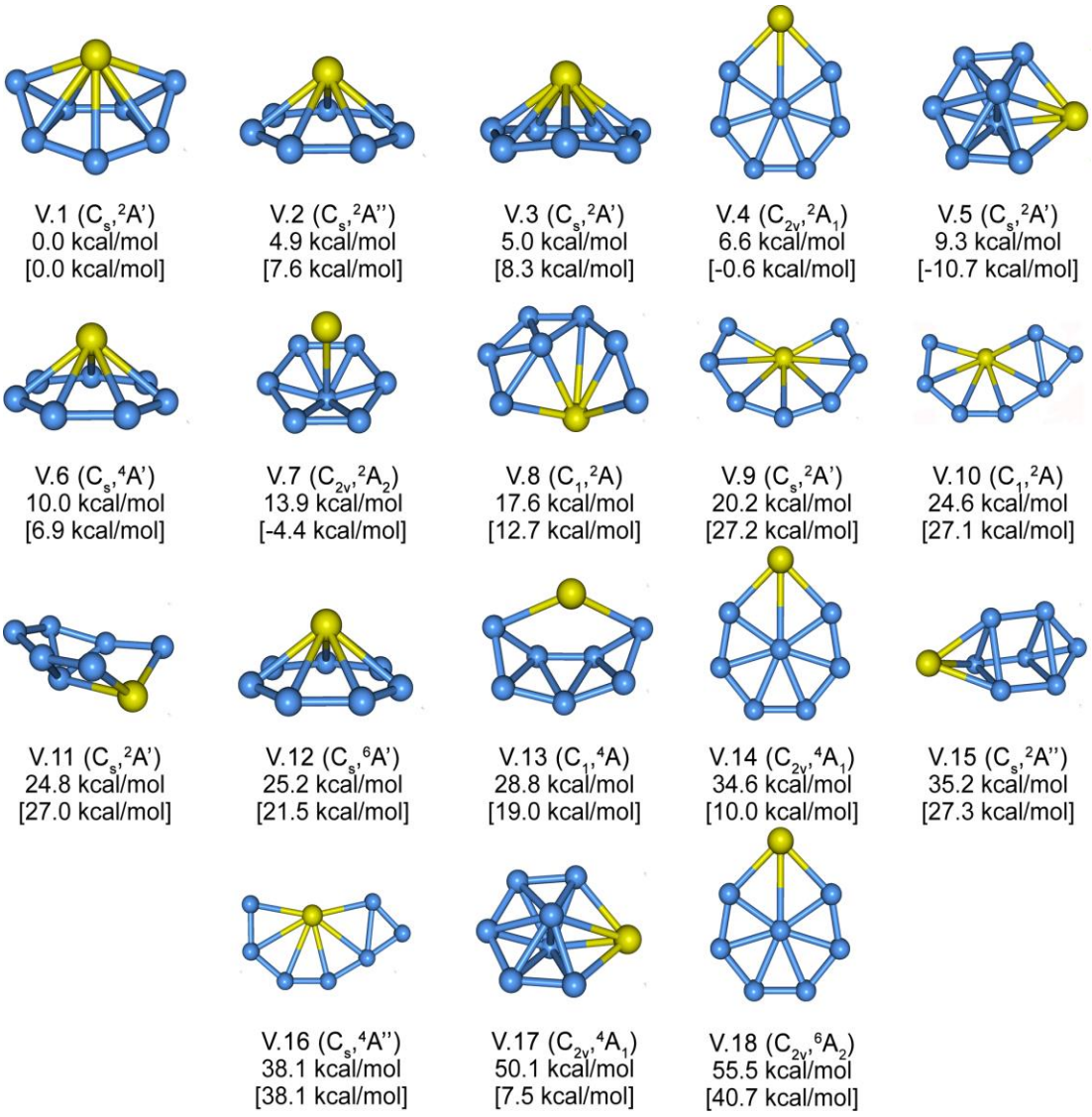

Figure 3-14. Low-lying structures of TaB_7^-, their point group symmetries, spectroscopic states and ZPE corrected relative energies. The energies are given at: CCSD(T)/Ta/Stuttgart/B/aug-cc-pVTZ (top), PBE0/Ta/Stuttgart/B/aug-cc-pVTZ (square brackets), all at PBE0/Ta/Stuttgart/B/aug-cc-pVTZ optimized geometries.

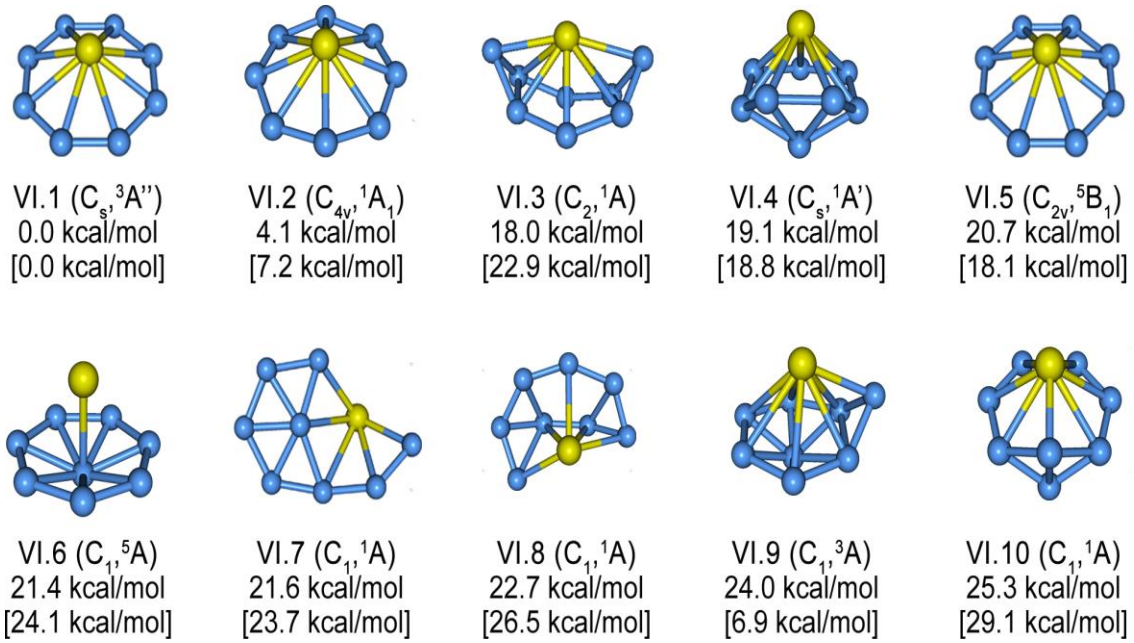

Figure 3-15. Low-lying structures of TaB_8^-, their point group symmetries, spectroscopic states and ZPE corrected relative energies. The energies are given at: CCSD(T)/Ta/Stuttgart/B/aug-cc-pVTZ (top), PBE0/Ta/Stuttgart/B/aug-cc-pVTZ (square brackets), all at PBE0/Ta/Stuttgart/B/aug-cc-pVTZ optimized geometries.

CHAPTER 4

ASSESSING INTENSITIES OF SPECTRAL LINES IN VIBRATIONALLY RESOLVED PHOTOELECTRON SPECTRA

Abstract

Anion photoelectron spectroscopy (PES) is a powerful method to study size-selected anion clusters, because it can provide unique information about the cluster structure and electronic properties. The photoelectron spectroscopic experiments are usually performed using a magnetic-bottle time-of-flight PES apparatus equipped with a laser vaporization supersonic cluster source.[1,2] Cluster anions are obtained by laser vaporization of an isotopically enriched disk target in the presence of a helium carrier gas. The produced cluster anions are then mass analyzed using a time-of-flight mass spectrometer and the cluster with a particular stoichiometric composition is mass selected. Photodetached electrons are collected by the magnetic-bottle and finally analyzed in a long electron time-of-flight tube. In this way the kinetic energy (KE) of the photodetached electrons can be measured and knowing the photon energy of the laser ($h\nu$), the binding energy (BE) of the electrons to the anion cluster can be determined using Einstein's photoelectric equation: BE = $h\nu$ − KE. High photon energy spectra are particularly important because they reveal more electronic transitions, while low photon energies in general produce better-resolved spectra that is essential for more accurate determination of adiabatic detachment energies of the neutral species and vibrational resolution.[3] However, the obtained photoelectron spectra is usually complex, moreover it is impossible to identify the carrier of the observed spectrum for a new species, due to

many structural isomers for a particular stoichiometry. Thus, theoretical *ab initio* calculations and spectral simulations are needed to help the interpretation of the photoelectron spectra and to elucidate the nature of the vibrational or electronic features. The program for the assignment of peaks in the vibrationally resolved photoelectron spectra has been developed. The algorithm of this program is based on the calculations of Franck-Condon harmonic oscillator overlap integrals using equations reported by Hutchisson.[4]

As it was shown by Condon,[5] the intensity (*I*) of a spectral line may be calculated by evaluating the integral of the product of the electric moment and the wave functions of the initial and final states where the integration is carried out over all of the coordinates of the electrons and the nuclei:

$$I = \iint M(x,r)\Psi'(x,r)\Psi''(x,r)dxdr$$

where *M (x, r)* is the electric moment; Ψ' and Ψ'' are the wave functions of the initial and final states (in the case of anion photoelectron spectroscopy Ψ' and Ψ'' are the wave functions of the anionic and neutral states respectively); *x* and *r* are the total coordinates of the electron and of the nuclei. According to the Born-Oppenheimer approximation (adiabatic approximation), the molecular wave function can be written as the product of an electronic wave function $\phi(x)$ and a vibrational wave function $\psi(r)$. Taking into account another approximation that the electronic transition probability is constant and doesn't influence intensity significantly (since the electronic transition probability is a slowly varying function of the nuclear coordinates), the relative intensity of a vibrational transition is proportional to the square of Franck-Condon factor ($\int \psi'(r)\psi''(r)dr$)[5,6]:

$$I \propto | \int \psi'(r)\psi''(r)dr \,|^2$$

If the normal modes in anionic and neutral states are independent (uncoupled in harmonic approximation), the wave functions can be represented as the product of one-dimensional wave functions in each normal coordinate:

$$\psi'(r) = \psi'_1(r_1)\psi'_2(r_2)\psi'_3(r_3)\psi'_4(r_4)\ldots\ldots \quad \text{and}$$

$$\psi''(r) = \psi''_1(r_1)\psi''_2(r_2)\psi''_3(r_3)\psi''_4(r_4)\ldots\ldots$$

In the parallel mode approximation the Franck-Condon overlap integral is simply the product of one dimensional overlap integrals and Franck-Condon factors are determined by displacements in each normal coordinate. The program calculates one dimensional harmonic overlap integrals using Hutchisson's analytic expressions for Franck-Condon factors.[4] Following the equations in reference 4, the value of Franck-Condon factors depends on two parameters: $\alpha = (\upsilon''/\upsilon')^{1/2}$ and $\delta = 2\pi/(h)^{1/2}(r' - r'')(\upsilon'')^{1/2}$, where υ'' and υ' are harmonic frequencies (expressed in cm^{-1}) of the anionic and the neutral electronic states respectively; $r' - r''$ is the displacement (in Angstroms) of the neutral electronic state relative to the anionic one along a mass weighted normal mode. So, the program uses only the *ab initio* data (optimized coordinates, vibrational frequencies, and normal mode matrices of the anionic and the neutral states) obtained from Gaussian 09 software.[7] It should be noted, however, that if the normal modes of the anionic and the neutral states differ significantly, the normal modes overlap matrix will not be diagonal, thus parallel mode approximation would not be applicable. In this case Duschinsky transformations[8] between the normal coordinates of the two states must be taken into account.

We tested the program on the B_3^- and B_5^- clusters. The vibrationally resolved photoelectron spectrum of the B_3^- cluster was recorded by Zhai et al.[9] B_3^- represents D_{3h} symmetric species with a $^1A_1'$ electronic state and $1a_1'^2 1e'^4 1a_2''^2 2a_1'^2$ electron configuration. An electron detachment from the highest occupied molecular orbital (HOMO) of B_3^- results in a D_{3h} structure of neutral B_3 with a $^2A_1'$ electronic state and $1a_1'^2 1e'^4 1a_2''^2 2a_1'^1$ electron configuration. Figure 4.1 (a) shows photoelectron spectrum of B_3^- at 355 nm photon energy. As one may see, the spectrum shows a strong and sharp peak (X) with a short vibrational progression and a hot band. The short vibrational progression suggests that there should be a little geometry change between the anionic and neutral ground states. Indeed, in accordance with our calculations there is only a slight elongation of B-B bond length in the neutral B_3 state, which indicates the removal of an electron from bonding $2a_1'$ molecular orbital of B_3^-. The simulated photoelectron spectrum of B_3^- is shown in Figure 4.1 (b). The peak positions in the simulated spectrum are given by: $E = -\mathrm{ADE} - v' + v''$, where ADE is adiabatic detachment energy (the energy difference between the ground vibrational states of the anionic and the neutral states), v'' and v' are the vibrational energies of the anion and the neutral states, respectively. The program found the most intense peak X, which corresponds to the 0-0 vibrational transition, as well as two peaks with rather weak intensities. Therefore, our simulation fits well the experimental photoelectron spectrum of B_3^-.

The vibrationally resolved photoelectron spectrum of B_5^- cluster was first reported by Zhai et al.[10] The global minimum of B_5^- is a planar C_{2v} symmetric structure having $1a_1^2 1b_2^2 2a_1^2 3a_1^2 1b_1^2 2b_2^2 4a_1^2 3b_2^2$ ($^1A_1$) electron configuration.[10] The detachment of one electron from the highest occupied molecular orbital of B_5^- yields a C_{2v} structure of

neutral B_5 species with $1a_1^2 1b_2^2 2a_1^2 3a_1^2 1b_1^2 2b_2^2 4a_1^2 3b_2^1$ ($^2B_2$) electron configuration. The experimental photoelectron spectrum of B_5^- with well-resolved vibrational progression is shown in Figure 4.2 (a). The observed vibrational progression indicates the change in the geometrical characteristics of the anionic and the neutral ground states. The HOMO of B_5^- represents a bonding orbital which covers the triangular fragments of the B_5^- global minimum structure. Logically, the detachment of an electron from the HOMO results in geometry relaxations within the triangular fragments. The simulated spectrum (Figure 4.2 (b)) confirms the existence of all peaks in the vibrational progression of the experimental photoelectron spectrum of B_5^-. According to our results the first peak corresponds to 0-0 vibrational transition. Interestingly, the w_3 (a_1) normal mode was found to be active and responsible for the geometry changes between the anionic and the neutral ground states. We also would like to emphasize that the simulation of the vibrational progression could be useful in establishing the right global minimum structure. For instance, the second lowest isomer of B_5^-, which is only ~5 kcal/mol higher than the global minimum,[10] has a completely different vibrational feature (Figure 4.3), and thus does not contribute to the photoelectron spectra. Therefore, the comparison of the vibrational features of closely lying isomers can serve as the second probe (after the comparison of theoretical and experimental vertical electron detachment energies) used to verify the validity of the theoretical predictions of new clusters.

References

(1) Wang, L. S.; Cheng, H.-S.; Fan. J. *J. Chem. Phys*. **1995**, *102*, 9480.

(2) Li, X.; Wu, H.; Wang, X. B.; Wang, L. S. *Phys. Rev. Lett*. **1998**, *81*, 1909.

(3) Alexandrova, A. N.; Boldyrev, A. I.; Zhai, H. J.; Wang, L.-S. *Coord. Chem. Rev*. **2006**, *250*, 2811.

(4) Hutchisson, E. *Phys. Rev*. **1930**, *36*, 410.

(5) Condon, E. *Phys. Rev*. **1926**, *28*, 1182.

(6) Franck, J. *Trans. Faraday Society* **1925**.

(7) Frisch, M. J.; Trucks, G. W.; Schlegel, H. B.; Scuseria, G. E.; Robb, M. A.; Cheeseman, J. R.; Scalmani, G.; Barone, V.; Mennucci, B.; Petersson, G. A. et al. *Gaussian 09*, Revision B.01; Gaussian, Inc.: Wallingford, CT, **2009**.

(8) Duschinsky, F. *Acta Physicochim. URSS* **1937**, *7*, 551.

(9) Zhai, H.-J.; Wang, L. S.; Alexandrova, A. N.; Boldyrev, A. I.; Zakrzewski, V. G. *J. Phys. Chem. A* **2003**, *107*, 9319.

(10) Zhai, H.-J.; Wang, L. S.; Alexandrova, A. N.; Boldyrev, A. I. *J. Chem. Phys. A* **2002**, *117*, 7917.

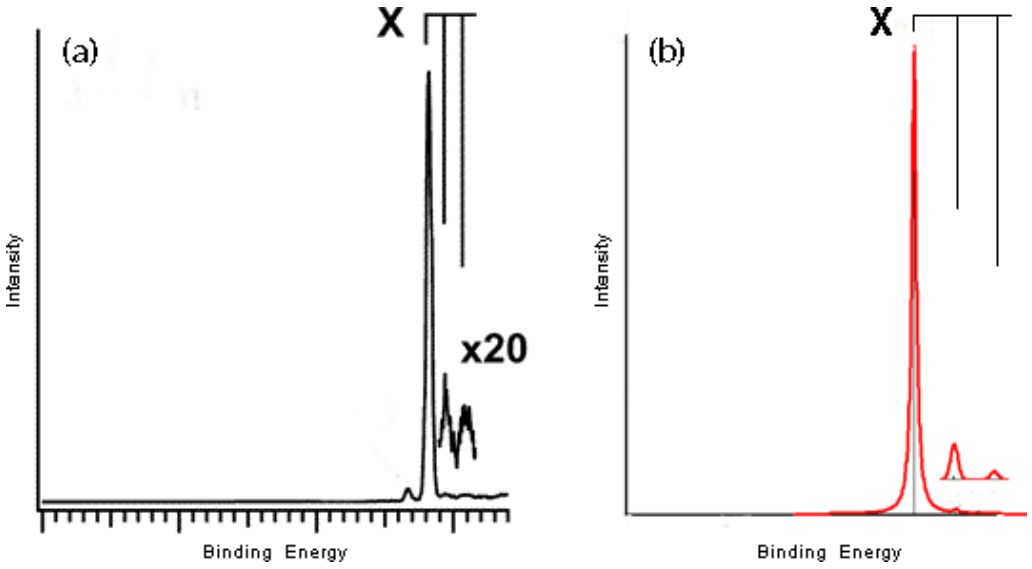

Figure 4-1. (a) Experimental photoelectron spectrum of B_3^- at 355 nm from reference 9, (b) simulated photoelectron spectrum of B_3^-.

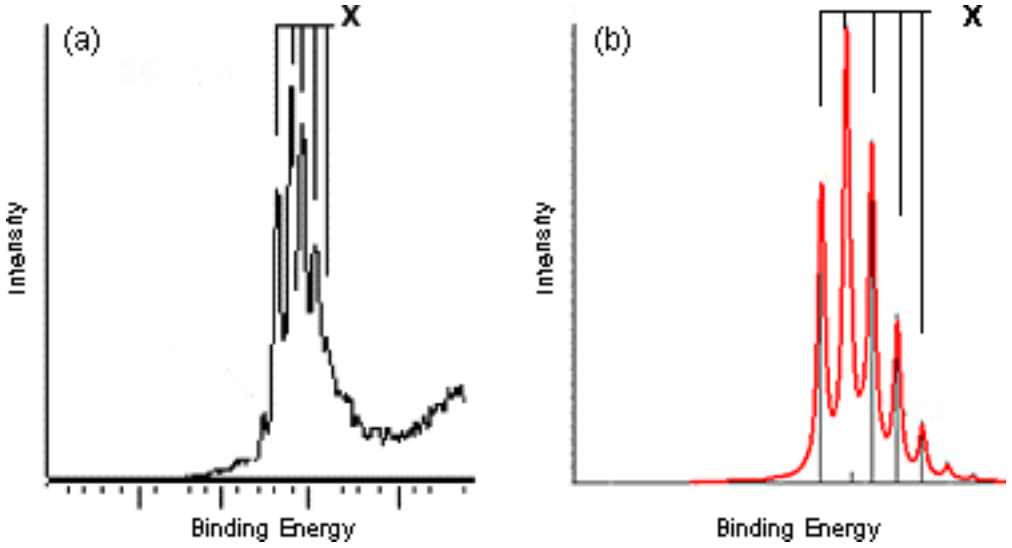

Figure 4-2. (a) Experimental photoelectron spectrum of B_5^- at 355 nm from reference 10, (b) simulated photoelectron spectrum of B_5^-.

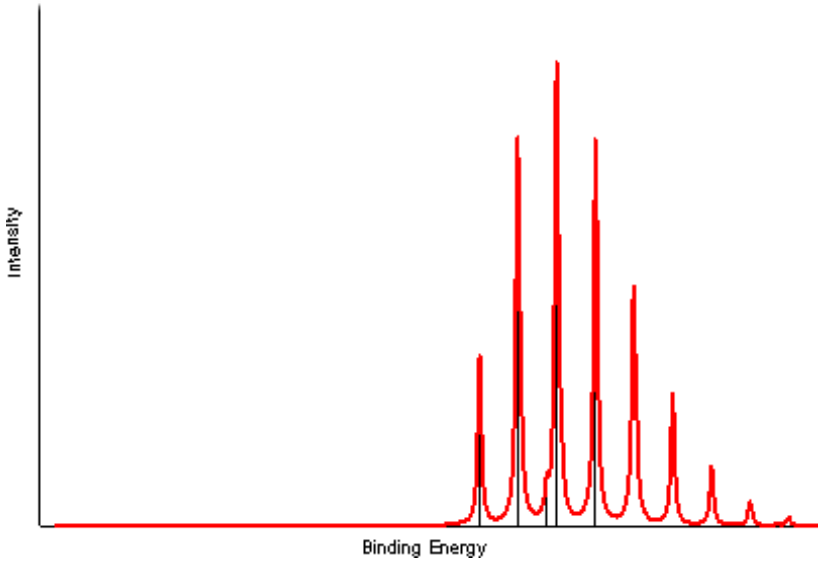

Figure 4-3. Simulated photoelectron spectrum of the second lowest isomer of B_5^- found in reference 10.

CHAPTER 5

ALL-NITROGEN ANALOGUE OF OZONE: Li_3N_3 SPECIES[1]

Abstract

A theoretical study of ozone isoelectronic Li_3N_3 species has been performed. Ab initio electronic structure calculations prove the viability of the ozone-like Li_3N_3 molecule that might become synthesized. The predicted Li_3N_3 species with a novel N_3^{3-} molecular motif possess structural and chemical bonding features similar to that of O_3 molecules and can thus be considered as an "all-nitrogen ozone".

5-1. Introduction

Nitrogen is not only one of the most abundant elements in air, forming about 80% of the Earth's atmosphere, but it is also widely spread in the universe, estimated at about seventh in total abundance in our galaxy and the Solar System. Since its discovery by Rutherford in 1772[1] the chemistry of nitrogen has primarily been driven by its property to form the extremely strong triple bond in the N_2 molecule, causing difficulty for both living organisms and industry to convert the N_2 into different compounds, but at the same time making the release of large amounts of often useful energy when the nitrogen substances explode, burn or decay back into nitrogen gas. Polynitrogen compounds are thus of great interest as promising candidates for high energy-density materials (HEDMs). However, despite the discovery of the azide anion (N_3^-) in 1890,[2] further attempts of chemists to synthesize stable polynitrogen compounds were unsuccessful. Only in 1999

[1] Coauthored by Jared K. Olson, Alexander S. Ivanov, and Alexander I. Boldyrev. Reprinted with permission from *Chem. Eur. J.* **2014**, 20, 6636 – 6640. Copyright © 2014 Wiley-VCH Verlag GmbH & Co. KGaA, Weinheim.

Christe et al.[3] showed that another nitrogen-rich species (the N_5^+ cation) could be produced in macroscopic quantities. Later, additional polynitrogen molecules were predicted and obtained in the gas phase, including experimental detection of the short-lived tetranitrogen N_4 species through the reduction of the gaseous N_4^+ molecule by neutralization-reionization (NR)-mass spectrometry;[4] pentazolate anion (cyclo-N_5^-),[5,6] and the N_5^+ combined compounds: $N_5^+[P(N_3)_6]^-$, $N_5^+[B(N_3)_4]^-$, $N_5^+[HF_2]^- \cdot nHF$, $N_5^+[BF_4]^-$, $N_5^+[PF_6]^-$, and $N_5^+[SO_3F]^-$ with the emphasis on their potential application as HEDMs.[7] As one can see, relatively few polynitrogen molecules have been synthesized or detected to date, mostly due to the experimental difficulties in the preparation and manipulation of high-energy nitrogen species.

Hydronitrogen compounds were proven to be effective HEDMs since the industrial application of well-known hydrazine (N_2H_4) as well as its derivatives (monomethylhydrazine (MMH) and 1,1-dimethylhydrazine (UDMH)) - very important chemical propellants which are intensively used presently for rocket propulsion and as precursors to blowing agents. In a related application, sodium azide (NaN_3), the gas-forming agent in air bags, can be produced from hydrazine by reaction with sodium nitrite. However, in spite of the use of alkali metal azides in a wide range of applications,[8-10] the reports of higher alkali metal substituted hydrazine derivatives are deficient. In 2001 Kniep et al.[11] synthesized binary diazenides SrN_2 and BaN_2, proving the existence of the homonuclear dinitrogen anion N_2^{2-}, which is a deprotonated diazene N_2H_2 with a N=N bond. Recently, Schnick et al.[12] experimentally confirmed the stability of the first alkali diazenide Li_2N_2 under high pressure/high temperature (HP/HT) conditions. As for theoretical reports, Bartlett et al.[13] using density functional theory

(DFT) calculations showed that lithium substitution on hydrogen positions of N_2H_4 – N_5H_5 hydrazines increases the specific impulse value – *Isp* (the force with respect to the amount of propellant used per unit of time) without lowering of the lowest dissociation frequency of these compounds, thus implying their potential use as HEDM molecules. The geometrical structures and spectroscopic characteristics of lithium-substituted hydrazine and its higher derivatives including Li_2N_4, Li_3N_3, Li_4N_4, and Li_5N_5 molecules have also been predicted. However, the global minimum searches for the corresponding stoichiometries have not been done in order to justify viability[14] of the proposed polynitrogen species. The above mentioned clusters Li_3N_3, Li_4N_4, and Li_5N_5 are valence-isoelectronic to O_3, O_4 and O_5. However, despite the usefulness of isoelectronic concept in predicting chemical reactions or existence of new compounds,[15] this concept fails as many times as it works. For example, the planar D_{6h} symmetric Si_6H_6 silabenzene molecule (isoelectronic to benzene C_6H_6) is not the most stable structure as it is in C_6H_6; moreover, it is not even a minimum on the potential energy surface.[16] This is why we proposed a more narrow version of this concept - so called "electronic transmutation principle", which assumes that elements, by acquiring an extra electron, begin to have the chemical bonding and geometric structure properties of compounds composed of neighboring elements.[17] There are plenty of examples of successful applications of this concept in predicting novel clusters and molecules.[17-25] Hence, the assessment of viability of the electronic transmutation principle is of great importance in order to predict new molecules and compounds.

Here we report a theoretical prediction of novel polynitrogen molecule - Li_3N_3 containing N_3^{3-} anion as a molecular motif, which is "all-nitrogen ozone" if we apply the

electronic transmutation approach to this molecule. As will be discussed below, the Li_3N_3 cluster represents a viable species, which is likely to be accessible experimentally. Chemical bonding analysis of Li_3N_3 reveals the same bonding pattern as in ozone molecule.

5-2. Results and discussion

According to the electronic transmutation concept,[17] nitrogen can form Li_xN_x compounds which have the same number of valence electrons (valence-isoelectronic) as oxygen species. Therefore our goal was to probe electronic transmutation for the smallest Li_3N_3 clusters by making bonded structures (where the less electronegative lithium atom donates an electron to the more electronegative nitrogen atom, resulting in each nitrogen bearing a negative charge) with the anticipation that structures similar to ozone would be formed. In Figure 5-1 we present the global minimum structure I.1 (Figure 5-1) and three lowest isomers for the Li_3N_3 species. A more extensive set of alternative isomers found in our global minimum search is summarized in Figures 5-5.

Interestingly, ozone-like structures I.3 and I.4 were found to be almost degenerate with the global minimum I.1, being only 0.6 and 0.1 kcal/mol higher in energy at the B3LYP/aug-cc-pvTZ level of theory; however, they are the third and the fourth lowest isomers, respectively, at CCSD(T)/6-311++G** and CCSD(T)/aug-cc-pvTZ//B3LYP/aug-cc-pvTZ. The global minimum structure I.1 (Figure 5-1) represents N_3^- azide anion connected with an aromatic triangle of Li_3^+ cation.[26] Structure I.2, in which Li_3^+ triangle is located above the "stick" of nitrogen atoms, is just an isomer of the global minimum, being only 1.2 kcal/mol higher in energy (CCSD(T)/6-311++G**). Bent structures I.3 and I.4 (Figure 5-1) with the kernel N_3^{3-} similar to ozone molecule

were found to be 6.2 and 8.1 kcal/mol higher, respectively, at the CCSD(T)/6-311++G** level of theory.

According to our results, azide anion with lithium cation triangle structures are more energetically favorable species for Li_3N_3 stoichiometry than ozone-like structures. However, molecules do not have to possess the global minimum structure in order to be isolated experimentally. Structures that are not global minima can also be viable species[14] if they are separated from other isomers by large enough barriers. Figure 5-2 shows the calculated energetic barriers, which separate the individual minima from the global minimum. In spite of the fact that we found two Li_3N_3 structures with similar nitrogen motif (structures I.3 and I.4 in Figure 5-1) we assessed the value of the transition state for the interconversion between the global minimum and structure I.4 specifically, because I.4 is the lowest isomer which has the same symmetry (C_{2v}) as that of ozone molecule. As one may see from Figure 5-2, the interconversion barrier value (28 kcal/mol) is large enough for structure I.4 to exist as an individual molecule. The computed barrier between two degenerate structures I.1 and I.2 was found to be only 5.6 kcal/mol and it corresponds to the displacement of Li_3^+ fragment relative to N_3^-.

To further investigate the viability of ozone-like structure I.4 (Figure 5-1) we analyzed its electronic properties and vibrational frequencies. The simulated vibrational spectrum of I.4 at the CCSD(T)/6-311++G** level of theory is shown in Figure 5-3 and may be helpful for possible experimental detection and characterization of this exotic molecule. Imaginary vibrational frequencies have not been observed, verifying that structure I.4 is indeed a local minimum on the potential energy surface. The lowest frequency is observed at 159 cm^{-1}. The most prominent feature in the spectrum is a strong

transition at 1221 cm^{-1} which describes the symmetric bend of N_3^{3-} molecular fragment analogous to the symmetric bend vibration observed for O_3 molecule at 1057 cm^{-1}.[27] The next strong transitions are at 1021 cm^{-1} and 853 cm^{-1}. These vibrations are responsible for symmetric and anti-symmetric stretches of N_3^{3-} fragment, respectively; this is similar to the corresponding vibrations of O_3 (1152 and 717 cm^{-1}).

The highest occupied molecular orbital–lowest unoccupied molecular orbital (HOMO—LUMO) energy separation serves as a simple measure of chemical stability.[28] The calculated HOMO—LUMO energy gap for structure I.4 is relatively large, ΔHL = 1.91 eV, conferring stability on the ozone-like Li_3N_3 cluster. The first electron excitation from the simulated time-dependent DFT (TD-DFT) spectrum of Li_3N_3 (Figure 5-6) is 1.82 eV, which is consistent with the HOMO—LUMO gap value. Additionally, the vertical ionization energy is 5.90 eV. Similar to hydrazine, azides, and ozone molecules, Li_3N_3 is predicted to be metastable species, decomposing to give nitrogen gas. The dissociation energies described by the following equations: 1) $Li_3N_3 \rightarrow 3/2N_2 + Li_3$ and 2) $Li_3N_3 \rightarrow N_2 + Li_3N$ were found to be 1) 4.7 kcal/mol and 2) 10.0 kcal/mol exothermic. However, it is worthy to note that the Li_3N_3 ozone-like cluster is 29.9 kcal/mol more stable relative to the infinitely separate molecule of lithium azide and lithium dimer cluster ($LiN_3 + Li_2$), as well as the decomposition of Li_3N_3 into neutral N_3 and Li_3 species ($Li_3N_3 \rightarrow N_3 + Li_3$) was found to be quite unfavorable process, being 102.4 kcal/mol endothermic.

As we introduced the link between ozone-like clusters I.3 and I.4 of Li_3N_3 and ozone molecule it would be useful to compare their structural features. The N-N bond lengths and N-N-N angle in N_3^{3-} fragment of Li_3N_3 structure I.4 are 1.32 Å and 128.3°,

respectively (for structure I.3 of Li_3N_3, the N-N bond lengths are 1.28 Å and 1.45 Å (C_s symmetry), the N-N-N angle is 128.3°). The corresponding parameters of O_3 molecule, which has been optimized with the same method and basis (CCSD(T)/6-311++G**), are almost analogous (1.28 Å for O-O distances and 117.1° for O-O-O angle). To gain more insight into the structure and chemical bonding in the ozone-like structures of Li_3N_3 species, we performed Natural Bond Orbital (NBO)[29] and Adaptive Natural Density Partitioning (AdNDP)[30] analyses. According to NBO analysis for Li_3N_3 C_{2v} bent structure I.4, the bonding between lithium and nitrogen atoms is quite ionic with effective atomic charges ranging from +0.65 on the side lithium atoms to +0.73 on the central lithium atom and -0.89 on the two side nitrogens to -0.26 on the central nitrogen atom. Interestingly, NBO analysis for ozone molecule shows slightly negative (-0.14) charges on the ozone side atoms, while the central oxygen bears moderately positive charge (+0.27). In literature, the bonding in O_3 is usually expressed as a resonance hybrid with a single bond on one side of the molecule and double bond on the other, producing an overall bond order of about 1.5 for each side.[31] The NBO method revealed one of the resonance structures for ozone as expected. However, it failed to describe chemical bonding in the ozone-like Li_3N_3 molecule in terms of resonance structures. Thus, in order to interpret bonding in Li_3N_3 species we used the AdNDP method which achieves seamless chemical bonding description of systems without invoking the concept of resonance. The results of the AdNDP analysis for Li_3N_3 structure I.4 and O_3 molecule are shown in Figure 5-4.

For Li_3N_3 isomer I.4 the AdNDP revealed the presence of two N-N double bonds with occupation numbers (ON) equal to 1.98 |e| for σ bonds and 1.93 |e| for π bonds; one

lone pair on the central nitrogen (ON = 1.72 |e|), and two lone pairs of s- and p type on each side nitrogen atoms with ON ranging from 1.71 |e| to 1.86 |e| (Figure 5-4, a)). As one may see from Figure 5-4, the recovered chemical bonding pattern of the Li_3N_3 cluster is almost identical to that of ozone molecule. Lower values of occupation numbers for the Li_3N_3 suggest that the s- and p lone pairs are more diffuse than that of O_3 due to the presence of lithium atoms. Hence, from chemical bonding point of view, the N_3^{3-} molecular fragment in the Li_3N_3 cluster can be considered as a nitrogen analogue of ozone. We also performed the AdNDP analysis of chemical bonding in isomer I.3, which is another ozone-like structure of Li_3N_3 stoichiometry. The AdNDP results (Figure 5-7) showed the same bonding picture as for ozone and Li_3N_3 structure I.4, confirming that structure I.3 of Li_3N_3 is also analogous to O_3 molecule.

5-3. Conclusions

In conclusion, based on the results of electronic structure calculations, we predicted a new ozone-like polynitrogen molecule Li_3N_3 with unusual N_3^{3-} molecular motif, which represents a viable species and is expected to be structurally stable. The predicted molecule has no imaginary frequencies and the computed vibrational spectrum suggests a way in which this novel molecule could be experimentally characterized. To date, there are no experimental reports on the existence of higher lithium substituted hydrazine derivatives. However, there are some facts that should be noted. As it was mentioned, lithium diazenide Li_2N_2 (valence-isoelectronic to oxygen) has successfully been obtained under HP/HT conditions by decomposition of LiN_3. Hence, there is a hope that fully lithium substituted triazenes: lithium triazenides Li_3N_3 may also be produced at rather specific experimental conditions. There are known examples, when the higher

energy isomers were experimentally obtained before the global minimum structures. For instance, hexasilaprismane is only the third lowest isomer for the Si_6H_6 stoichiometry, being 30.7 kcal/mol higher than the global minimum structure,[16b] yet it was synthesized[32] two decades before the experimental characterization of the global minimum structure.[33] Thus, we believe that the ozone-like polynitrogen molecule Li_3N_3 with unusual N_3^{3-} molecular motif can also be made. The calculations of this work demonstrate a conceptually new interesting bonding motif in chemistry of polynitrogen compounds, and, if Li_3N_3 with the N_3^{3-} kernel, a nitrogen analogue of ozone, is prepared experimentally, it would be a potentially useful species, possessing new, yet unexplored physical and chemical properties.

5-4. Computational and theoretical methods

We performed an unbiased quantum-chemical search for Li_3N_3 species (initially at the B3LYP/aug-cc-pvDZ level of theory) in order to find the global minimum and low lying structures on the Li_3N_3 potential energy surface (PES) using a Coalescence Kick program.[34] The Coalescence Kick method subjects large populations of randomly generated structures to a coalescence procedure in which all atoms are pushed gradually to the molecular center of mass to avoid the generation of fragmented structures and then optimizes them to the nearest local minima. All low-lying isomers found by this method were re-optimized with follow-up frequency calculations at the B3LYP[35] level of theory using the aug-cc-pvTZ basis set. Finally, the total energies of the lowest isomers were calculated at the CCSD(T)/aug-cc-pvTZ//B3LYP/aug-cc-pvTZ level of theory. To examine the robustness of the prediction made with the B3LYP functional we also re-optimized the structures of four lowest isomers with frequency calculations at

CCSD(T)/6–311++G**. To examine the applicability of the CCSD(T) and B3LYP methods for our system we performed single-point calculations of the C_2vsymmetric Li_3N_3 ozone-like structure at the CASSCF(12,14)/6–311++G** level of theory. According to these calculations the Hartree–Fock coefficient in the CASSCF expansion (4510506 configurations) is 0.970. Thus, both B3LYP and CCSD(T) methods are valid. The vertical ionization energy was calculated using electron propagator method, outer-valence green's function (OVGF).[36] All calculations were performed using the Gaussian 09 program.[37] Molecular structure visualization was performed with the Chemcraft[38] and MOLEKEL 5.4.0.8.[39] programs.

References

[1] M. E. Weeks, *J. Chem. Ed.* **1930**, *9*, 215.

[2] T. Curtius, *Berichte Dtsch. Chem. Ges*. **1890**, *23*, 3023.

[3] K. O. Christe, W. W. Wilson, J. A. Sheehy, J. A. Boatz, *Angew. Chem. Int. Ed.* **1999**, *38*, 2004.

[4] F. Cacace, G. de Petris, A. Troiani, *Science* **2002**, *295*, 480.

[5] A. Vij, J. G. Pavlovich, W. W. Wilson, V. Vij, K. O. Christe, *Angew. Chem. Int. Ed*. **2002**, *114*, 3177.

[6] H. Ostmark, S. Wallin, T. Brinck, P. Carlqvist, R. Claridge, E. Hedlund, L. Yudina, *Chem. Phys. Lett.* **2003**, *379*, 539.

[7] R. Haiges, S. Schneider, T. Schroer, K. O. Christe, *Angew. Chem. Int. Ed.* **2004**, *43*, 4919.

[8] H. D. Fair, R. F. Walker, *Energetic Materilas, Vol. 1*; Plenum Press: New York, **1977**.

[9] F. P. Bowden, A. D. Yoffe, *Fast Reactions in Solids*, Butterworth: London, U.K., **1958**.

[10] C. E. Housecroft, A. G. Sharpe, *Inorganic Chemistry*; Prentice Hall: Harlow, **2001**.

[11] G. Auffermann, Y. Prots, R. Kniep, *Angew. Chem.* **2001**, *113*, 565; *Angew. Chem. Int. Ed.* **2001**, *40*, 547.

[12] S. B. Schneider, R. Frankovsky, W. Schnick, *Angew. Chem. Int. Ed.* **2012**, *51*, 1873.

[13] M. Tobita, R. J. Bartlett, Quantum Theory Project, University of Florida, Gainesville, FL, http://www.qtp.ufl.edu/~bartlett/

[14] a) R. Hoffmann, P. v. R. Schleyer, H. F. Schaefer III, *Angew. Chem.* **2008**, *120*, 7276; *Angew. Chem. Int. Ed.* **2008**, *47*, 7164; b) A. S. Ivanov, A. I. Boldyrev, *Phys. Chem. Chem. Phys.* **2012**, *14*, 15943.

[15] R.-C. Geoff, *Found. Chem*. **2009**, *11*, 123.

[16] a) M. Moteki, S. Maeda, K. Ohno, *Organometallics* **2009**, *28*, 2218; b) A. S. Ivanov, A. I. Boldyrev, *J. Phys. Chem. A* **2012**, *116*, 9591.

[17] J. K. Olson, A. I. Boldyrev, *Chem. Phys. Lett.* **2012**, *523*, 83.

[18] J. Nagamatsu, N. Nakagawa, T. Muranaka, Y. Zenitani, J. Akimitsu, *Nature* **2001**, *410*, 63.

[19] A. N. Alexandrova, K. A. Birch, A. I. Boldyrev, *J. Am. Chem. Soc*. **2003**, *125*, 10787.

[20] H. Fahlquist, D. Noréus, M. H. Sorby, *Inorg. Chem*., **2013**, *52*, 4771.

[21] H. Fahlquist, D. Noréus, S. Callear, W. I. F. David, B. C. Hauback,´ *J. Am. Chem. Soc*. **2011**, *133*, 14574.

[22] H. Fahlquist, D. Noréus, *Inorg. Chem*., **2013**, *52*, 7125.

[23] a) B. H. Boo, S.-J. Kim, M. H. Lee, N. Nishi, *Chem. Phys. Lett*. **2008**, *453*, 150; b) N. Perez-Peralta, A. I. Boldyrev, *J. Phys. Chem. A* **2011**, *115*, 11551.

[24] A. S. Ivanov, A. J. Morris, K. V. Bozhenko, C. J. Pickard, A. I. Boldyrev, *Angew. Chem*. **2012**, *124*, 8455; *Angew. Chem. Int. Ed*. **2012**, *51*, 8330.

[25] O. Degtyareva, E. Gregoryanz, M. Somayazulu, P. Dera, H. K. Mao, R. J. Hemley, *Nat. Mater.* **2005**, *4*, 152.

[26] A. N. Alexandrova, A. I. Boldyrev, *J. Chem. Theory Comput*. **2005**, *1*, 566.

[27] T. J. Lee, G. E. Scuseria, *J. Chem. Phys*. **1990**, *93*, 489.

[28] B. A. Hess, L. J. Schaad, *J. Am. Chem. Soc*. **1971**, *93*, 2413.

[29] J. P. Foster, F. Weinhold, *J. Am. Chem. Soc.* **1980**, *102*, 7211.

[30] D. Yu. Zubarev, A. I. Boldyrev, *Phys. Chem. Chem. Phys*. **2008**, *10*, 5207.

[31] E. Miliordos, S. S. Xantheas, *J. Am. Chem. Soc.* **2014**, DOI: 10.1021/ja410726u

[32] A. Sekiguchi, T. Yatabe, C. Kabuto, H. Sakurai, *J. Am. Chem. Soc*. **1993**, *115*, 5853.

[33] K. Abersfelder, A. J. P. White, R. J. F. Berger, H. S. Rzepa, D. Scheschkewitz, *Angew. Chem., Int. Ed*. **2011**, *50*, 7936.

[34] A. P. Sergeeva, B. B. Averkiev, H. J. Zhai, A. I. Boldyrev, L. S.Wang, *J. Chem. Phys*. **2011**, *134*, 224304.

[35] a) R. G. Parr, W. Yang, *Density-Functional Theory of Atoms and Molecules*; Oxford University Press: Oxford, **1989**; b) A. D. Becke, *J. Chem. Phys.* **1993**, *98*,

5648; c) J. P. Perdew, J. A. Chevary, S. H. Vosko, K. A. Jackson, M. R. Pederson, D. J. Singh, C. Fiolhais, *Phys. Rev. B* **1992**, *46*, 6671.

[36] V. G. Zakrzewski, O. Dolgounitcheva, A. V. Zakjevskii, J. V. Ortiz, *Ann. Rev. Comput. Chem*. **2010**, *6*, 79.

[37] Gaussian09, Revision B.0.1, M. J. Frisch, G. W. Trucks, H. B. Schlegel, G. E. Scuseria, M. A. Robb, J. R. Cheeseman, G. Scalmani, V. Barone, B. Mennucci, G. A. Petersson, H. Nakatsuji, M. Caricato, X. Li, H. P. Hratchian, A. F. Izmaylov, J. Bloino, G. Zheng, J. L. Sonnenberg, M. Hada, M. Ehara, K. Toyota, R. Fukuda, J. Hasegawa, M. Ishida, T. Nakajima, Y. Honda, O. Kitao, H. Nakai, T. Vreven, J. A. Montgomery, Jr., J. E. Peralta, F. Ogliaro, M. Bearpark, J. J. Heyd, E. Brothers, K. N. Kudin, V. N. Staroverov, R. Kobayashi, J. Normand, K. Raghavachari, A. Rendell, J. C. Burant, S. S. Iyengar, J. Tomasi, M. Cossi, N. Rega, J. M. Millam, M. Klene, J. E. Knox, J. B. Cross, V. Bakken, C. Adamo, J. Jaramillo, R. Gomperts, R. E. Stratmann, O. Yazyev, A. J. Austin, R. Cammi, C. Pomelli, J. W. Ochterski, R. L. Martin, K. Morokuma, V. G. Zakrzewski, G. A. Voth, P. Salvador, J. Dannenberg, S. Dapprich, A. D. Daniels, Ö. Farkas, J. B. Foresman, J. V. Ortiz, J. Cioslowski, D. J. Fox, Gaussian, Inc., Wallingford CT, **2009**.

[38] http://www.chemcraftprog.com

[39] U. Varetto, Molekel 5.4.0.8, Swiss National Supercomputing Centre: Manno, Switzerland, **2009**.

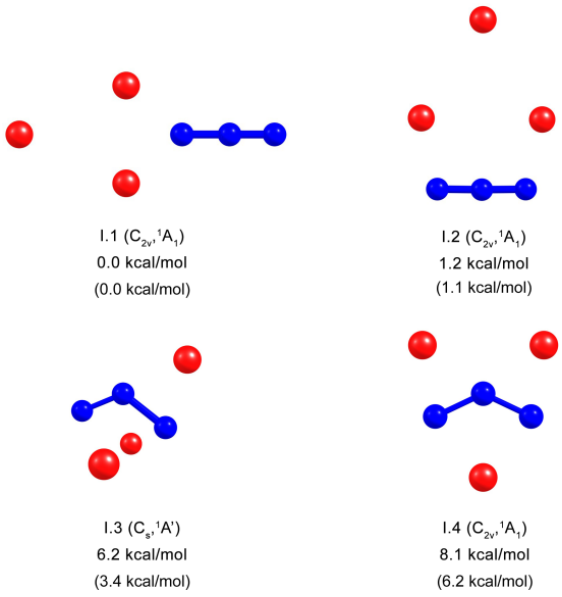

Figure 5-1. Representative optimized isomers of Li_3N_3 species, their point group symmetries, spectroscopic states, and zero-point energy (ZPE) corrected energies. The relative energies are given at: CCSD(T)/6-311++G**//CCSD(T)/6-311++G** (bold) and CCSD(T)/aug-cc-pvTZ//B3LYP/aug-cc-pvTZ (in brackets). Here and elsewhere the red and blue spheres represent lithium and nitrogen atoms, respectively.

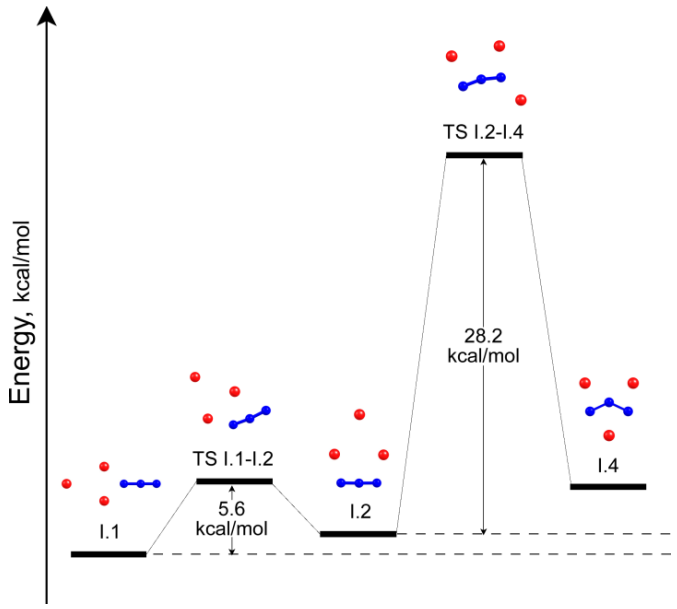

Figure 5-2. The transition state barriers diagram, showing large energy separation between isomers I.2 and I.4. The energies of the barriers are given at the CCSD(T)/aug-cc-pvTZ//B3LYP/aug-cc-pvTZ level of theory.

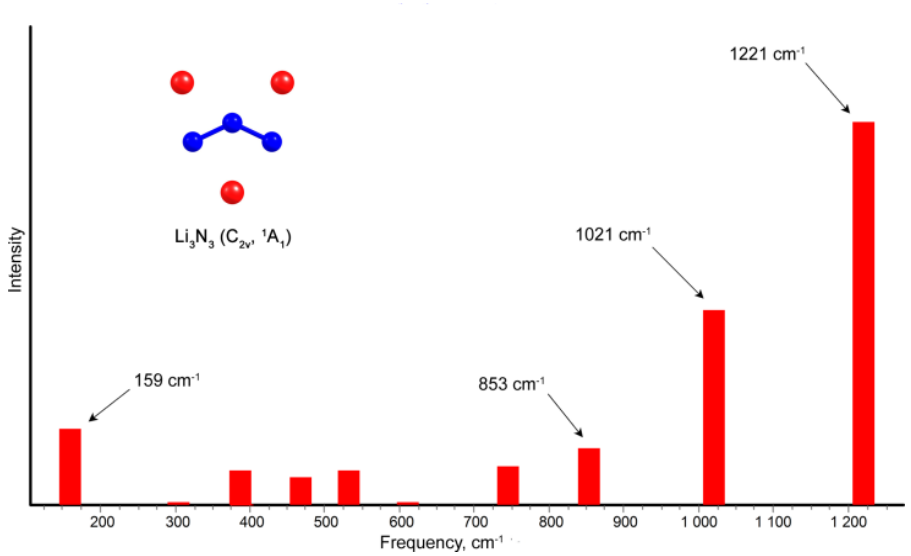

Figure 5-3. Simulated vibrational spectrum of the ozone-like (C_{2v}) cluster at the CCSD(T)/6-311++G** level of theory. Corresponding wavenumbers are presented for the most intense transitions.

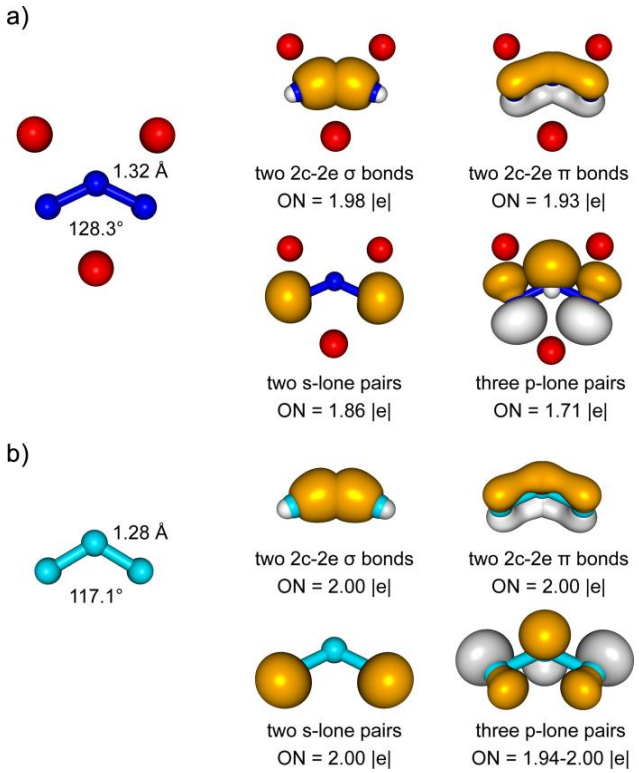

Figure 5-4. Chemical bonding pattern of a) Li_3N_3 and b) O_3 structures revealed by the AdNDP analysis. ON stands for occupation number.

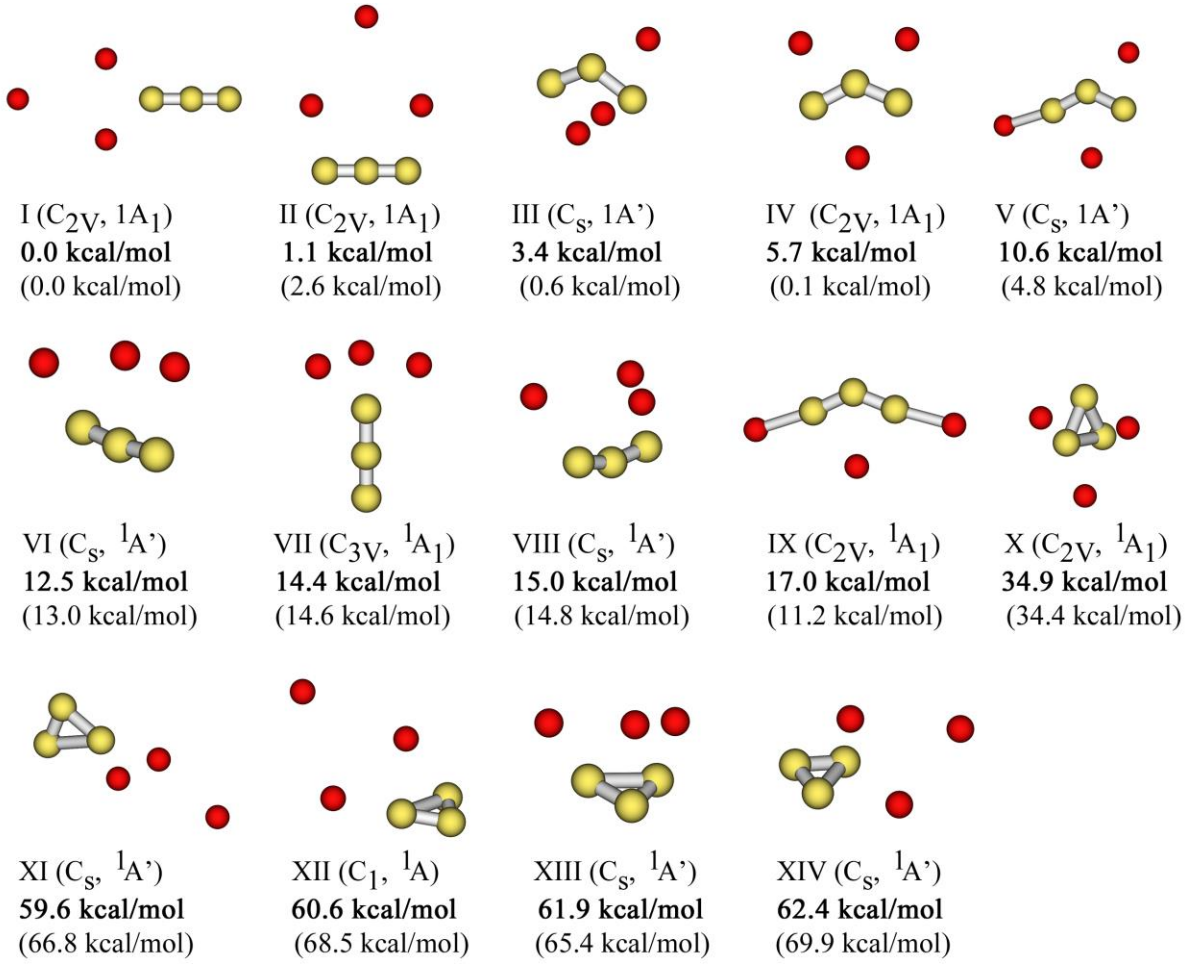

Figure 5-5. Lowest-lying structures of Li_3N_3, their point group symmetries, spectroscopic states and ZPE corrected relative energies. The energies are given at: CCSD(T)/aug-cc-pvTZ (bold) and B3LYP/aug-cc-pvTZ (in brackets) levels of theory, all at B3LYP/aug-cc-pvTZ optimized geometries. Here the red and yellow spheres represent lithium and nitrogen atoms, respectively.

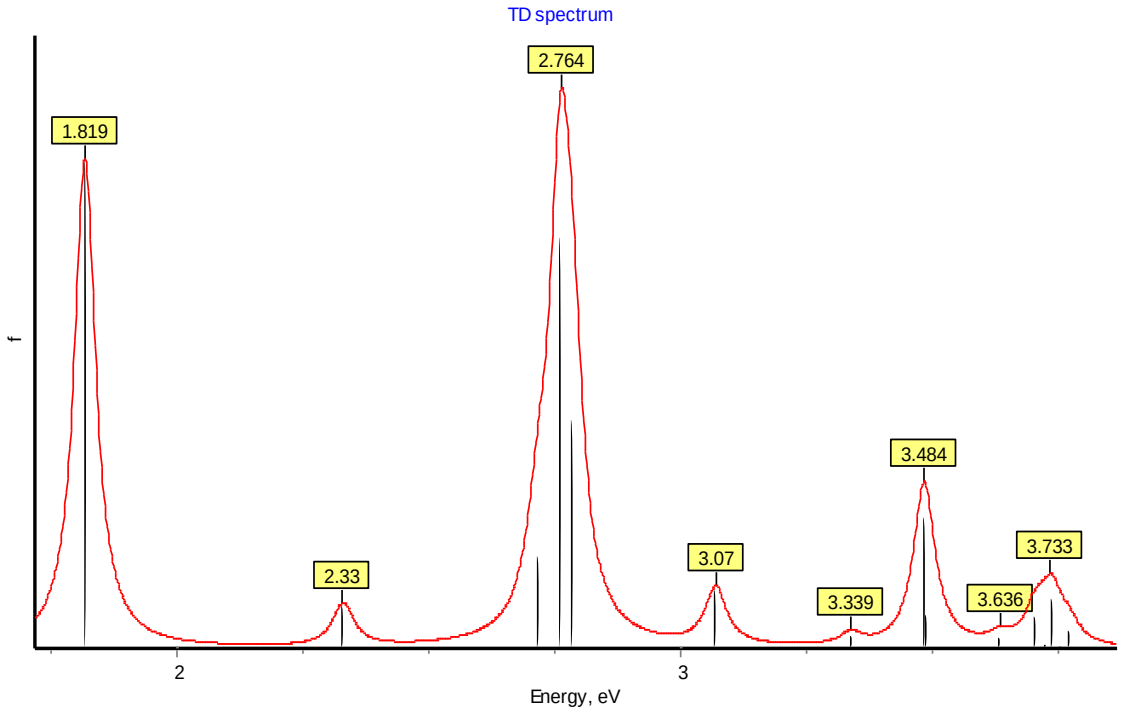

Figure 5-6. Computed UV-visible absorption spectrum for C_{2v} Li_3N_3 ozone-like cluster at the B3LYP/aug-cc-pvTZ level of theory.

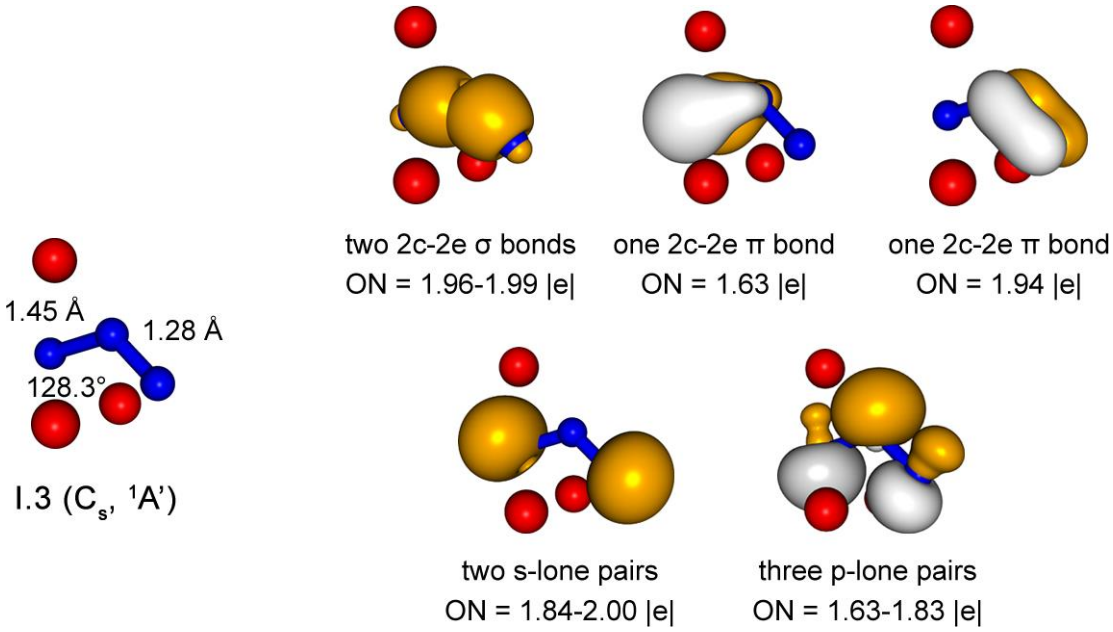

Figure 5-7. Chemical bonding pattern of Li_3N_3 structure I.3 revealed by the AdNDP analysis and structural parameters of I.3 at CCSD(T)/6-311++G**. Significantly lower occupation numbers (ON) have been obtained for the first N-N π bond due to the close location of lithium atoms that make this pi bond delocalized over the lithium atoms.

CHAPTER 6

STABILIZATION OF $Cl^- - Cl^-$ ANION PAIR IN THE GAS PHASE: AB INITIO MICROSOLVATION STUDY[1]

Abstract

Despite the confirmation of $Cl^-{-}Cl^-$ association in aqueous solution and crystalline state, there were no reports about the existence of stable dichloride anion pair in the gas phase. In the current work we performed a systematic *ab initio* study of microsolvation of dichloride anion pair. The stepwise solvation mechanism observed for free gaseous $[Cl_2(H_2O)_n]^{2-}$ (n = 2-10) clusters was found to be quite interesting. The lowest structure for dichloride hexahydrate closely resembles cubic water octamer W8 in which two water molecules in the corners of the cube are substituted by two chloride anions. We have also shown that $Cl^-{-}Cl^-$ pair may be completely stabilized by about 36 water molecules in the gas phase. Stabilization of the pair leads to formation of cyclic H_2O structures that bridge the Cl^- ions. It has been predicted that the large clusters of $[Cl_2(H_2O)_{36}]^{2-}$ and $[Cl_2(H_2O)_{40}]^{2-}$ may exhibit properties analogous to bulk aqueous solutions, therefore they could become good molecular models for understanding complicated processes of solvation of Cl^- in the bulk.

6-1. Introduction

The understanding of many physical and chemical processes which involve fluids in the Earth's crust and reactions in oceanic and atmospheric environments requires a

[1] Coauthored by Alexander S. Ivanov, Gernot Frenking, and Alexander I. Boldyrev. Reprinted with permission from *J. Phys. Chem. A*, **2014**, 118 (35), pp 7375–7384. Copyright 2014 American Chemical Society.

detailed knowledge of the mechanisms in which ions and molecules are solvated. Particularly, the hydrated chloride anions are of great significance in a variety of processes since they are the most common anions in nature playing an important role in numerous chemical, environmental, and biological systems.[1-3] Therefore, the systematic study of the structures of chloride−water clusters at the molecular level can provide valuable insight into solvation phenomena,[4] electrical phenomena in the troposphere and ionosphere, ion selectivity of ion channels in biological membranes, and processes on different water/membrane interfaces.[5] Indeed, there are a lot of experimental and theoretical works on halide−water clusters, where most of these studies are devoted to hydrated monochloride anions $[Cl(H_2O)_n]^-$. These hydrated anions have been characterized within lattices of organic hosts and metal complexes.[6-9] For $[Cl(H_2O)_n]^-$ (n = 1-7) clusters in the gas phase experimental photoelectron spectra have been recorded.[10] Thus, properties such as coordination numbers, the stability and structures of the complexes, their infrared spectra have been thoroughly investigated. However, theoretical and experimental studies on like-charged ion dihalide hydrates are rare and only recently became an attractive area of research. To the best of our knowledge, only five dichloride water clusters of $[Cl_2(H_2O)_2]^{2-}$,[11] $[Cl_2(H_2O)_4]^{2-}$,[12,13] $[Cl_2(H_2O)_6]^{2-}$,[14,15] $[Cl_2(H_2O)_{10}]^{2-}$,[16] and $[Cl_2(H_2O)_{14}]^{2-}$ [17] have been obtained in the solid state as discrete units. Their salts were structurally characterized by low-temperature X-ray and neutron diffraction studies, and the corresponding clusters $[Cl_2(H_2O)_n]^{2-}$ (n = 2, 4, 6, 10, 14) were also investigated by single crystal infrared spectroscopy. Gao et al.[18] conducted combined study of crystallographic analyses and *ab initio* calculations providing strong support of the possible existence of dichloride ion pair in water. It was also found that the bridging

effect of water between the two anions can stabilize these clusters. X-ray diffraction[19] and neutron scattering experiments[20] provided further evidence for the existence of halide ion pairs in high salt concentration solution.

As one can see, despite some advances have been achieved for the preparation of the solids with dichloride hydrate clusters and confirmation of the stable Cl^-–Cl^- anion pairs in solution, reports of $[Cl_2(H_2O)_n]^{2-}$ in the gas phase are scarce. We were not able to find any experimental work on such systems in the gas phase. As for theoretical studies of stable Cl^-–Cl^-, there is only one paper published in 1996, which is devoted to molecular dynamic simulations of dichloride anion pair in steam.[21] Therefore it seems that gaseous dihalide hydrates have been almost completely ignored, probably because of the expectation that the electrostatic repulsion between the two anions would make the formation of dihalide hydrates in the gas phase unfavorable. This would mean that such species would be of little relevance to natural systems. However, many widely spread ions such as SO_4^{2-} or CO_3^{2-} are not stable in the gas phase[22] (like Cl^-–Cl^-) due to the tremendous intramolecular Coulomb repulsion. But they are stabilized in solution by the solvent. For example, it was found that both SO_4^{2-} and $C_2O_4^{2-}$ require a minimum of three water molecules to be stabilized and observed by means of photoelectron spectroscopy in the gas phase.[23,24] The study of such multiply charged ions is of great importance, since solvated clusters can provide molecular models to understand complicated processes of solvation in the bulk.[25]

In this work we present a systematic study of microsolvation of dichloride anion pair. Though the term “like-charged ion pair” is usually referred for aqueous solutions in order to emphasize nearly contact distance between the two ions, here we use the term

"stable Cl^-−Cl^- pair" meaning that two chlorides do not repel each other and may coexist in a stable $Cl^-(H_2O)_nCl^-$ cluster. Various experiments have confirmed Cl^-−Cl^- association in aqueous solution, however, an experimental and theoretical understanding of stabilization of Cl^-−Cl^- in the gas phase has not been established. The main goal of the current study is to trace microsolvation of dichloride pair and find the number of water molecules that would be sufficient to make like-charged Cl^-−Cl^- pair stable and assessable for the experimental photoelectron spectroscopy studies.

6-2. Computational and theoretical methods

Finding the global minimum structure on potential energy surface (PES) was one of the main goals of our study, because the experimental conditions of thermodynamic equilibrium allow detecting only the global minimum structure or isomers that are very close in energy to their ground state.[26] A computational search for the lowest lying structures of $[Cl_2(H_2O)_n]^{2-}$ (n = 2–10), $[Cl_2(H_2O)_{36}]^{2-}$, and $[Cl_2(H_2O)_{40}]^{2-}$ systems was performed using the Coalescence Kick (CK) program written by Averkiev.[27] In the CK method, a random structure is first checked for connectivity: if all atoms in the structure belong to one fragment, then the structure is considered connected, and the Berny algorithm[28] for geometry optimization procedure is applied to it. However, in most cases, a randomly generated structure is fragmented; that is, the structure contains several fragments not bonded with each other, including cases with just one atom not being connected. In these cases, the coalescence procedure is applied to the fragmented structure: all of the fragments are pushed to the center of mass simultaneously. The magnitude of shift should be small enough so that atoms or molecules do not approach each other too closely but large enough so that the procedure converges in a reasonable

amount of time. The obtained structure is checked for connectivity again, and the procedure repeats. When two fragments approach each other close enough, they "coalesce" to form a new fragment, which will be pushed as a whole in the following steps. Obviously, at some point, all fragments are coalesced. This method does not deal with cases when, in a randomly generated structure, two atoms are too close to each other. To avoid this problem, the initial structures are generated in a very large box with all three linear dimensions being 4* (the sum of atomic covalent radii). Hence, usually an initially generated random structure consists of separated atoms as initial fragments. The current version of the program is designed for the global minimum searches of both single molecules of desired composition and complexes of molecules like solvated anions (e.g., $SO_4^{2-}\cdot 4H_2O$),[29] where the initial geometry of each molecular unit is specified in the input file. In the latter case, the two molecular units of the complex are considered as connected in a fragment if the distances between two of their atoms are less than the sum of the corresponding van der Waals radii. In the current study, the CK method for solvated Cl^-–Cl^- anion pair (with the initial setup distance of 5.0 Å between two chloride ions) was used. The CK calculations for $[Cl_2(H_2O)_{36}]^{2-}$ and $[Cl_2(H_2O)_{40}]^{2-}$ systems become extremely computationally expensive. For the large $[Cl_2(H_2O)_{36}]^{2-}$ and $[Cl_2(H_2O)_{40}]^{2-}$ systems, we generated a large number (~1000) of reasonable cluster structures within a box to avoid the generation of unnecessary structures. In the first step, the single-point energy calculations of the generated structures have been performed exclusively. The lowest structures (100 structures) were then optimized to the nearest local minima to reveal the lowest energy isomers. Taking into account the fact that the number of lowest isomers, which are different in energy by only 1–2 kcal/mol, is growing

exponentially with increasing number of water molecules in the system, it is difficult to explore the PES thoroughly. Therefore, we do not insist that the found lowest structures of the large chloride hydrate clusters can be represented solely by a global minimum structure. In fact, a large number of structures will contribute to the average geometry, which should be treated by statistical mechanical methods.

The CK calculations were performed at the M06-2X level of theory using the aug-cc-pvDZ basis set for $[Cl_2(H_2O)_n]^{2-}$ (n = 2–10) and the 3-21G basis set for $[Cl_2(H_2O)_{36}]^{2-}$, $[Cl_2(H_2O)_{40}]^{2-}$ cluster systems.[30,31] Low-lying isomers were reoptimized with follow up frequency calculations at the M06-2X level of theory using the aug-cc-pvTZ ($[Cl_2(H_2O)_n]^{2-}$ (n = 2–10)) and the aug-cc-pvDZ ($[Cl_2(H_2O)_{36}]^{2-}$ and $[Cl_2(H_2O)_{40}]^{2-}$) basis sets.[32-34] The final relative energies of the found low-lying isomers were calculated at the CCSD(T)/aug-cc-pvDZ level. The global minim geometrical structures for monochloride hydrates $[Cl(H_2O)_n]^-$ (n = 1–10, 18, 20) have been obtained from previous experimental and theoretical reports,[35-38] and optimized with follow-up frequency calculations using the same methods as for the studied $[Cl_2(H_2O)_n]^{2-}$ systems in order to trace the change in dissociation energies of $[Cl_2(H_2O)_n]^{2-}$ at different numbers of water molecules (n).

The vertical detachment electron energies (VDEs) of the lowest isomers were calculated using the electron propagator method, outer-valence Green's function (OVGF).[39-40] The adiabatic detachment energies calculations were performed using the M06-2X level of theory. The 6-311++G** basis was used in the electron propagator calculations and aug-cc-pvDZ basis for M06-2X calculations.[41-43] All pole strengths (OVGF) exceeded 0.90.

The atomic charges on chloride anions were calculated using natural population analysis (NPA)[44] at the M06-2X/aug-cc-pvTZ level. All ab initio calculations were done using the Gaussian 09 program.[45] Molecular structure visualization was performed with the Chemcraft program.[46]

6-3. Results and discussion

It is obvious that the two like-charged ions of Cl^- with eight electrons in the outer shell (a complete octet) repel each other. However it is possible to overcome such repulsion between two chlorides by sequentially adding water molecules. We first performed an *ab initio* random search for the lowest lying structures of $[Cl_2(H_2O)_n]^{2-}$ (n = 2-10), using the M06-2X/aug-cc-pvDZ level of theory. Then low-lying isomers were reoptimized at higher level of theory (M06-2X/aug-cc-pvTZ) and single-point CCSD(T)/aug-cc-pvDZ calculations were made in order to compare their final relative energies. By adding one water molecule to the chlorides we did not find any isomer on the potential energy surface, because $Cl^-(H_2O)Cl^-$ complex immediately dissociates into Cl^- and $Cl^-(H_2O)$ anions. However, starting from $Cl^-(H_2O)_2Cl^-$ all the chloride anion pair clusters considered in the current work were found to be local minima, in spite of the strong electrostatic repulsion between the two Cl^- ions. This was confirmed by frequency calculations which yielded all positive vibrational frequencies for these structures. The calculated stabilization energies of $Cl^-(H_2O)_n$ (n = 1-10) and $[Cl_2(H_2O)_n]^{2-}$ (n = 2-10) clusters relative to the infinitely separate species were determined by the following processes (equations (1), (2)) and are given in Table 6-1 and Table 6-2, respectively.

$$Cl^- + nH_2O \rightarrow Cl^-(H_2O)_n \qquad (1)$$

$$2Cl^- + nH_2O \rightarrow Cl^-(H_2O)_nCl^- \qquad (2)$$

As one can see from Table 6-1, Cl^- already forms a stable complex with water: $Cl^-(H_2O)_n$ at n = 1. The computed stabilization energies are generally in agreement with experimental data (column 5 in Table 6-1), thus confirming the choice of the theoretical methods and basis sets employed for the current study of water-chloride systems.

The results from Table 6-2 demonstrate that the hydrogen-bonding interaction involving two water molecules was not sufficient to compensate the Coulombic repulsion between two chloride ions. However, we found small negative complexation energy of −3.7 kcal/mol (CCSD(T)/aug-cc-pvDZ level of theory) for $Cl^-(H_2O)_nCl^-$ complex at n = 3. The complex is further stabilized by −22.6 kcal/mol (Table 6-2) by adding another water molecule. Addition of more waters makes the stabilization energies of dichloride clusters comparable to those of monochloride complexes. In spite of this fact, it is necessary to evaluate the dissociation energies of dichloride hydrate clusters in order to make a conclusion about their stability in the gas phase. Therefore, we calculated the reaction energy for the dissociation process defined by eq (3):

$$Cl^-(H_2O)_nCl^- \rightarrow Cl^-(H_2O)_m + Cl^-(H_2O)_k \qquad (3)$$

The results of our calculations at different levels of theory are shown in Table 6-3. The dissociation energies for $[Cl_2(H_2O)_n]^{2-}$ (n = 2–10) systems were found to be 27–45 kcal/mol exothermic. Consequently, small $[Cl_2(H_2O)_n]^{2-}$clusters are highly unstable and would not exist in the gas phase due to more energetically favorable decomposition of $Cl^-(H_2O)_nCl^-$ into two negatively charged monochloride hydrates. The calculated barrier (M06-2X/aug-cc-pvTZ) for the smallest $Cl^-(H_2O)_2Cl^-$ cluster appeared to be only 1.1 kcal/mol, further confirming instability of the $Cl^-(H_2O)_nCl^-$ (n = 2–10) complexes.

First, we will describe local minima structures of $[Cl_2(H_2O)_n]^{2-}$ (n = 2-10) clusters in order to obtain a more qualitative picture about how Cl^-−Cl^- pair is solvated by H_2O leading to the stabilization of dichloride anion pair in the gas phase, and then move on to the determination of the number of water molecules needed for the dissociation process (equation 3) to become endothermic.

6-3.1. $[Cl_2(H_2O)_2]^{2-}$ clusters

Our CK search found only one D_{2h} structure I.1 (Figure 6-1, A)) to be a local minimum for $[Cl_2(H_2O)_2]^{2-}$ stoichiometry. Structure I.1 represents two chloride ions connected through two bridged water molecules. The Cl^-−Cl^- distance was found to be 5.77 Å at M06-2X/aug-cc-pvTZ. Despite this structure has positive stabilization energy of 15.4 kcal/mol (Table 6-2), it is interesting that already two water molecules are able to hold two negative chloride anions together. Moreover, structure I.1 is vertically and adiabatically electronically stable, which has been confirmed by vertical detachment electron energy (VDE) and adiabatic detachment electron energy (ADE) calculations (Table 6-4). The VDE and ADE for $[Cl_2(H_2O)_2]^{2-}$ cluster I.1 are 1.62 eV and 1.43 eV, respectively. It is also worthy to note that Basu et al.[11] has recently shown the encapsulation of an analogous D_{2h} planar cyclic tetrameric chloride water cluster $[Cl_2(H_2O)_2]^{2-}$ within the dimeric capsular assembly of a conformationally flexible tripodal amide receptor, where $[Cl_2(H_2O)_2]^{2-}$ has acted as a template in the formation of the dimeric capsular complexes.

6-3.2. $[Cl_2(H_2O)_3]^{2-}$ clusters

According to the results of the CK search for $[Cl_2(H_2O)_3]^{2-}$ stoichiometry structure II.1 (Figure 6-1, B)) is 0.9 kcal/mol (CCSD(T)/aug-cc-pvDZ) lower than three water bridged D_{3h} structure II.2. The separation distance between two chloride anions is now 5.67 Å which is only 0.1 Å shorter than the corresponding distance in $[Cl_2(H_2O)_2]^{2-}$ cluster. The results show that two water bridged structure II.1 is slightly more energetically favorable than three water bridged structure II.2 and structure II.3, in which two water molecules connect two chlorides and the third water forms hydrogen bonds with the other water molecules (Figure 6-1, B)). As it was mentioned above, the stabilization energy for $[Cl_2(H_2O)_3]^{2-}$ is -3.7 kcal/mol, so addition of three water molecules is sufficient to offset Coulombic repulsion between the two anions and to observe $Cl^-\ldots Cl^-$ aggregate in aqueous solution.[18] The VDE and ADE values for the lowest structure II.1 are 1.89 eV and 1.00 eV, respectively.

6-3.3. $[Cl_2(H_2O)_4]^{2-}$ clusters

From the CK search for $[Cl_2(H_2O)_4]^{2-}$ we found that structure III.1 (Figure 6-1, C)) without bridged water molecules and the highest $Cl^-{-}Cl^-$ separation distance (11.69 Å) is the lowest energy dichloride tetrahydrate. D_{4h} symmetric four water bridged structure III.4 is 9.6 kcal/mol higher in energy. Therefore, although Gao et al.[18] revealed that water-bridged hydrogen bonds with two chloride ions in addition to interactions with counterions play a major role in the stabilization of the $Cl^-{-}Cl^-$ pair in the crystalline state, it is not the case for the gas phase. The VDE and ADE values (2.89 eV and 1.17

eV) for $[Cl_2(H_2O)_4]^{2-}$ are becoming higher compared to the smaller dichloride hydrate clusters.

Our results for the three structures of water bridged chloride clusters (structures I.1, II.2, and III.4 (Figure 6-1)) are in agreement with previous calculations performed by Gao et al.,[18] where the corresponding like-ion chloride clusters were optimized in order to support the theoretical finding of the possible existence of a stable Cl_2^{2-} aggregate in water.

6-3.4. $Cl_2(H_2O)_5]^{2-}$ clusters

The CK search of the $[Cl_2(H_2O)_5]^{2-}$ species revealed that the potential energy surface has more low-lying structures than that of $[Cl_2(H_2O)_n]^{2-}$ (n = 2-4) (Figure6-2, D)). In the lowest structure IV.1 water molecules again avoid the formation of bridges between two negatively charged chloride ions. However, three water bridged structure IV.2 with the Cl^-−Cl^- distance of 5.02 Å is higher than the lowest structure IV.1 on just 1.6 kcal/mol. The maximum number (5) of bridged waters and the smallest separation distance between two Cl^- (4.19 Å) is observed for D_{5h} structure IV.8 (Figure 6-2, D)), which is 14.6 kcal/mol less energetically favorable than structure IV.1.

6-3.5. $[Cl_2(H_2O)_6]^{2-}$ clusters

For $[Cl_2(H_2O)_6]^{2-}$ stoichiometry we unexpectedly found that structure V.1 (Figure 6-2, E)) of S_6 symmetry is the lowest one among other dichloride hexahydrates. Thus, for $[Cl_2(H_2O)_6]^{2-}$ we observe a new type of coordination of water molecules between the chloride anions, where the water molecules tend to adopt a cubic arrangement in the space between two Cl^-. The Cl^-−Cl^- distance in structure V.1 is now balanced (6.52 Å)

that is contrary to what we saw for structure III.1 of $[Cl_2(H_2O)_4]^{2-}$ and structure IV.1 of $[Cl_2(H_2O)_5]^{2-}$ clusters, in which the largest separation between two Cl^- was the most preferable. Interestingly, in 1991 K. D. Jordan using *ab initio* and model-potential calculations predicted[49] and later characterized by spectroscopic studies[50] the lowest energy structure for $(H_2O)_8$ – the cubic water octamer (W8), with the eight tricoordinated water molecules taking up positions at the corners of the cube. Therefore, the lowest structure V.1 depicted on Figure 6-2, E) can be viewed as water octamer W8 where two water molecules in the corners of the cube are substituted by two chloride anions. The structure of such dichloride hexahydrate cube, $[Cl_2(H_2O)_6]^{2-}$, as a salt with the tris(diisopropylamino)-cyclopropenium cation, $[C_3(NiPr_2)_3]^+$, has been determined and well characterized by low-temperature X-ray and neutron diffraction studies by Butchard et al.[14,15] Our calculations of VDE and ADE for cubic hexahydrate V.1 also confirmed its vertical and adiabatic electronic stability (Table 6-4). However, despite the negative stabilization energy (Table 6-2) $[Cl_2(H_2O)_6]^{2-}$ clusters are still far from being able to be detected in the gas phase (the computed dissociation energy (equation (3)) remains highly exothermic (-34.1 kcal/mol for m=3, k=3 dissociation channel (Table 6-3)).

6-3.6. $[Cl_2(H_2O)_7]^{2-}$, $[Cl_2(H_2O)_8]^{2-}$ clusters

The low-lying structures for $[Cl_2(H_2O)_7]^{2-}$, $[Cl_2(H_2O)_8]^{2-}$ clusters identified by the CK search are shown in Figure 6-3. The number of isomers grows very fast with the cluster size. Almost all of the local minimum structures now have isomers (not shown) that differ only by relative orientations of the dangling H atoms on water molecules. These isomers are all found within 0.5-1 kcal/mol from one another. However, the barriers to the interconversion of structures of each type achieved through the flipping

motion of dangling hydrogen atoms appeared to be smaller than 1 kcal/mol (M06-2X/aug-cc-pvTZ), which is below the zero-point energy of these clusters. Hence, such hydrogen flips are thermally allowed at room temperature, and these clusters would be indistinguishable. Importantly, however, the nature of the coordination of water molecules and the relative energies of typical isomers are preserved for $[Cl_2(H_2O)_7]^{2-}$ and $[Cl_2(H_2O)_8]^{2-}$ clusters. Since the M062x/aug-cc-pvTZ level of theory results for the energy sequence of $[Cl_2(H_2O)_n]^{2-}$ (n = 3-6) structures are generally in agreement with CCSD(T)/aug-cc-pvDZ, we did not perform single-point CCSD(T)/aug-cc-pvDZ calculations for $[Cl_2(H_2O)_n]^{2-}$ (n = 7-10) systems. The lowest structures found by our search are structure VI.1 of $[Cl_2(H_2O)_7]^{2-}$ and structure VII.1 of $[Cl_2(H_2O)_8]^{2-}$ (Figure 6-3, F), G)) with a cubic arrangement between two Cl^- similarly to the structure of the lowest dichloride hexahydrate. The addition of one ($[Cl_2(H_2O)_7]^{2-}$) or two water molecules ($[Cl_2(H_2O)_8]^{2-}$) does not destruct the cubic pattern of the corresponding clusters. In structure VI.1 (Figure 6-3, F)) the water molecule forms hydrogen bond with one of the chloride anions, and in structure VII.1 (Figure 6-3, G)) there are two water molecules that are hydrogen bonded to each of Cl^- in trans-position. We did not find any structures with seven ($[Cl_2(H_2O)_7]^{2-}$) or eight ($[Cl_2(H_2O)_8]^{2-}$) water-bridged hydrogen bonds between chloride ions. It seems that adding more bridged waters to the chlorides causes repulsion between the adjacent water molecules and such structures become significantly unstable.

6-3.7. $[Cl_2(H_2O)_9]^{2-}$, $[Cl_2(H_2O)_{10}]^{2-}$ clusters

Starting with the clusters containing nine water molecules, the total number of found isomers becomes almost unmanageable. However, the lowest structures (VIII.1,

and IX.1) again preserve cubic arrangement of the solvent water molecules between two Cl^- (Figure 6-4, H), I)). Analogous to $[Cl_2(H_2O)_7]^{2-}$ and $[Cl_2(H_2O)_8]^{2-}$ clusters, the additional waters are coordinated directly to the chloride anions. It is interesting to note that the Cl^-−Cl^- separation distance (~6.5 Å) is almost the same for all lowest structures of $[Cl_2(H_2O)_n]^{2-}$ starting from n = 6 until n = 10. Structure IX.4 of $[Cl_2(H_2O)_{10}]^{2-}$ which is 6.3 kcal/mol higher than the dichloride decahydrate IX.1 (Figure 6-4, I)) has been observed in a solid-state structure of $\{[Na_2(H_2O)_6(H_2O@TMEQ[6])]\cdot 2(C_6H_5NO_3)\}Cl_2(H_2O)_{10}\}$, (TMEQ[6] = α,α′,δ,δ′-tetramethylcucurbit[6]uril and can be viewed as a connection of two $[Cl(H_2O)_3]^-$ clusters with a uudd cyclic water tetramer through hydrogen-bonding interactions.[16] One may see that for $[Cl_2(H_2O)_9]^{2-}$ and $[Cl_2(H_2O)_{10}]^{2-}$ stoichiometries there are many structures with cyclic water trimers and tetramers above and under the plane of chloride ions (Figure 6-4, H), I)).

The results for the dissociation energies of $[Cl_2(H_2O)_n]^{2-}$ (n = 2-10) shown in Table 6-3 demonstrate that the above studied cluster systems of dichloride hydrates are unstable in the gas phase. However, as the solvent H_2O number increases the $[Cl_2(H_2O)_n]^{2-}$ clusters are gradually being stabilized. According to our calculations, the addition of first three water molecules stabilizes dichloride hydrate complex by as much as 10.0 kcal/mol (CCSD(T)/aug-cc-pvDZ). The complex is then further stabilized by approximately 0.5-2 kcal/mol (Table 6-3) by adding more and more water molecules. Consequently, the dissociation energy of our largest $[Cl_2(H_2O)_{10}]^{2-}$ cluster (structure IX.1, Figure 6-4, I)) is -27.2 kcal/mol. Thus, dichloride hydrate complexes should gain additional stabilization energy of about 28 kcal/mol in order to exist as a stable gaseous

Cl^-−Cl^- pair. We believe that the repulsion between two Cl^- ions is significant since there is no sufficient dielectric screening to the electrostatic interaction between these chloride anions. Hence, to overcome such a strong electrostatic repulsion each chloride ion in $[Cl_2(H_2O)_n]^{2-}$ cluster must be fully solvated. Kemp et al.[35] using the effective fragment potential (EFP) method, coupled with Monte Carlo simulations as well as HF, and MP2 calculations predicted that 18 water molecules are required to form a complete solvation shell around a Cl^- anion. Therefore, we searched for the most stable structure of $[Cl_2(H_2O)_{36}]^{2-}$ stoichiometry. Figure 6-5 (structure X) shows the global minimum structure optimized at the M06-2X/aug-cc-pvDZ level of theory. Interestingly, the computed dissociation energy (M06-2X/aug-cc-pvDZ) determined by the following equation:

$$Cl^-(H_2O)_{36}Cl^- \rightarrow Cl^-(H_2O)_{18} + Cl^-(H_2O)_{18} \qquad (4)$$

is now +4.5 kcal/mol making process (4) endothermic and disadvantageous for the decomposition into two $Cl^-(H_2O)_{18}$ clusters. Taking into account the fact that one of the most favorable dissociation channels for $[Cl_2(H_2O)_n]^{2-}$ (n = 2-10) has been observed for m=k, where m + k = n (Table 6-3 and equation 3) we think it is enough to consider only one dissociation process in order to make a conclusion about the stability of gaseous $[Cl_2(H_2O)_{36}]^{2-}$. Therefore, 36 water molecules are likely needed to obtain stable Cl^-−Cl^- pair in the gas phase. Kemp et al.[35] also found that interior Cl^- ion of $Cl^-(H_2O)_n$ is even more solvated at n = 20. Hence, the calculations were also performed with the Cl^-−Cl^- dianion pair and a water cluster with 40 water molecules to confirm the findings for n = 36. It turned out that $[Cl_2(H_2O)_{40}]^{2-}$ cluster (Figure 6-5, structure XI) is now more

stabilized (+15.2 kcal/mol) than $[Cl_2(H_2O)_{36}]^{2-}$ with respect to the dissociation into two $Cl^-(H_2O)_{20}$. The high stability of $Cl^-{-}Cl^-$ pairs in the large $[Cl_2(H_2O)_{36}]^{2-}$ and $[Cl_2(H_2O)_{40}]^{2-}$ clusters may be attributed to the delocalization of charge from the Cl^- species to the surrounding waters. To quantify the charge delocalization, the atomic charges on Cl^- ions in the clusters were calculated at the M06-2X/aug-cc-pVTZ level and are summarized in Table 6-5. Due to the geometric symmetries of some lowest $[Cl_2(H_2O)_n]^{2-}$ clusters, the charges on the two ions were identical within a given cluster. As one may see from Table 6-5, the amount of charge delocalization increased with an increasing number of water molecules for $[Cl_2(H_2O)_{36}]^{2-}$ and $[Cl_2(H_2O)_{40}]^{2-}$ clusters: the calculated charge on Cl^- ranges from -0.98 |e| with two waters bound, to -0.85 |e| in the complex with forty waters.

$[Cl_2(H_2O)_{36}]^{2-}$ and $[Cl_2(H_2O)_{40}]^{2-}$ clusters shown in Figure 6-5 and the structure formed by water molecules in the space between the $Cl^-{-}Cl^-$ pair may not be characterized as compact clusters. So, we do not observe two or three water bridged structures between two chlorides; instead, however, the shared waters are oriented in such a manner to create a cyclic structure that eventually bridges the Cl^- ions. Interestingly, Choi et al.[51] using QM/EFP MD (quantum mechanics/effective fragment potential molecular dynamics) simulations in solution recently showed that only one-water bridged structures were dominant at the local minimum, implying a weak dependency of ion pair structures on locally bridged waters. In $[Cl_2(H_2O)_{36}]^{2-}$ and $[Cl_2(H_2O)_{40}]^{2-}$ clusters the separation distance between $Cl^-{-}Cl^-$ is 8.86-8.87 Å, which corresponds to 37.3 kcal/mol (M06-2X/aug-cc-pvTZ) of the Coulomb repulsion energy between bare Cl^- ions at that distance. The addition of 36 and 40 water molecules helps to overcome this high

Coulomb repulsion energy. The water molecules lying in the space between the Cl^- ions are predominantly oriented in a way that the hydrogen atoms in the molecule are father from Cl^- than the oxygen atoms due to hydrogen bonding between the shared water molecules. Also, structures formed by waters in the $[Cl_2(H_2O)_{36}]^{2-}$ and $[Cl_2(H_2O)_{40}]^{2-}$ complexes can be considered as interlacing of rings containing mostly four, five, six and seven water molecules.

The electron binding energies VDE (Table 6-4) were observed to increase monotonically with the solvent number. The VDE values for $[Cl_2(H_2O)_n]^{2-}$ at n=36 and n=40 are as much as 6.62 eV and 6.86 eV, respectively. But what is the nature of the high VDE binding energy feature in these large solvated clusters? The dimensions of our largest solvated clusters $[Cl_2(H_2O)_{36}]^{2-}$ and $[Cl_2(H_2O)_{40}]^{2-}$ are greater than 1 nm. It was observed that such water nanodroplets doped with a single solute molecule began to exhibit electronic properties similar to bulk electrolyte solutions.[25] Similarly to the large solvated $SO_4^{2-}(H_2O)_n$ and $C_2O_4^{2-}(H_2O)_n$ clusters[25] the high VDE feature in $[Cl_2(H_2O)_{36}]^{2-}$ and $[Cl_2(H_2O)_{40}]^{2-}$ complexes must correspond to a new detachment channel, which may be attributed to ionization of the solvent. The ionization potentials of water clusters should be between that of gaseous water molecules at 12.6 eV and that of liquid water at 10.06 eV.[52] Because our solvated clusters are negatively charged, the ionization potentials of water should be lowered. Indeed, it was observed that the ionization potential of a water molecule was reduced from 12.6 eV to about 6.1 eV in the $F^-(H_2O)$ complex,[53] because of the strong Coulomb repulsion experienced by the valence electrons in H_2O from F^- ion. Therefore, stable $[Cl_2(H_2O)_{36}]^{2-}$ and $[Cl_2(H_2O)_{40}]^{2-}$ dichloride hydrates may behave analogous to bulk aqueous solutions. However, thorough

experimental photoelectron studies on gaseous $[Cl_2(H_2O)_n]^{2-}$ are needed to confirm the predicted stabilities and electronic properties of these clusters.

6-4. Conclusions

We presented a systematic ab initio study of microsolvation of dichloride anion pair by water molecules. For small $[Cl_2(H_2O)_n]^{2-}$ (n = 2–10) clusters, we obtained a clear picture of stepwise solvation and stabilization processes. We see a delicate balance between H_2O–Cl^- interactions and H_2O–H_2O interactions. When the solvent number is between 2 and 10 H_2O, the negative charges on Cl^- attract water strongly enough that more H-bonds are formed between Cl^- ions and waters. As the solvent number increases (n = 36, 40), the negative charges on chlorides are sufficiently screened that both H-bonds plus H_2O–H_2O interactions, are favored. According to our results, at n = 6 the lowest structure of $[Cl_2(H_2O)_n]^{2-}$ represents a cube that closely resembles water octamer W8 in which two water molecules in the corners of the cube are substituted by two chloride anions. Also, adding more waters does not destruct the cubic pattern of the corresponding $[Cl_2(H_2O)_n]^{2-}$ (n = 7–10) clusters.

It was found that the lowest structures of all studied dichloride hydrates are vertically and adiabatically electronically stable; therefore they may exist in the solid state as discrete units. However, $[Cl_2(H_2O)_n]^{2-}$ (n = 2–10) clusters are significantly unstable with the reaction energy for the dissociation process being highly exothermic. Thus, they would not exist in the gas phase. We predicted that the stabilization of the gaseous $[Cl_2(H_2O)_n]^{2-}$ may likely be achieved at n = 36. The complex $[Cl_2(H_2O)_{36}]^{2-}$ is further stabilized by adding four water molecules. The only stable anion pairs of Cl^- are in fact hydrogen-bonded clusters of $Cl^-(H_2O)_n$. Hence, they are not real dianions, but

anion clusters which are large enough that the hydrogen bonds of the outer water molecules are stronger than the Coulombic repulsion between two Cl^-.

The stability of the large $[Cl_2(H_2O)_{36}]^{2-}$ and $[Cl_2(H_2O)_{40}]^{2-}$ clusters may be attributed to the delocalization of charge from the Cl^- species to the surrounding waters. It was also found that in these large $[Cl_2(H_2O)_{36}]^{2-}$ and $[Cl_2(H_2O)_{40}]^{2-}$ clusters, stabilization of the Cl^-–Cl^- pair leads to formation of cyclic H_2O structures. The water molecules formed rings or interlacing of rings depending on the size of the system. The waters in the space between two Cl^- were organized in such a way that bridged the Cl^-–Cl^- pair. According to our calculations, $[Cl_2(H_2O)_{36}]^{2-}$ and $[Cl_2(H_2O)_{40}]^{2-}$ complexes possess the high VDE binding energies, which is the characteristic feature for bulk electrolyte solutions. We think that the association of stable gaseous Cl^-–Cl^-anion pairs may play an important role in nucleation of industrial steam or geothermal steam from the Geysers wells.[54] Moreover, the studied solvated chloride clusters may be viewed as molecular models for understanding physicochemical processes in aqueous solutions containing Cl^- ions.

References

(1) Ohtaki, H.; Radnai, T. Structure and Dynamics of Hydrated Ions. *Chem. Rev*. **1993**, *93*, 1157.

(2) Marcus, Y. *Ion Solvation*, Wiley: Chichester, 1986.

(3) Richens, D. T. *The Chemistry of Aqua Ions*, Wiley: Chichester, 1997.

(4) Castleman, A. W.; Bowen, K. H. Clusters: Structure, Energetics, and Dynamics of Intermediate States of Matter. *J. Phys. Chem*. **1996**, *100*, 12911.

(5) Roux, B.; Berneche, S.; Egwolf, B.; Lev, B.; Noskov, S. Y.; Rowley, C. N.; Yu, H. B. Ion Selectivity in Channels and Transporters. *J. Gen. Physiol*. **2011**, *137*, 415.

(6) Custelcean, R.; Gorbunova, M. G. A Metal-Organic Framework Functionalized with Free Carboxylic Acid Sites and its Selective Binding of a $Cl(H_2O)_4^-$ Cluster. *J. Am. Chem. Soc*. **2005**, *127*, 1636.

(7) Wang, Q.-Q.; Day, V. W.; Bowman-James, K. Chemistry and Structure of a Host Guest Relationship: The Power of NMR and X-ray Diffraction in Tandem. *J. Am. Chem. Soc*. **2013**, *135*, 392.

(8) Wang, Q.-Q.; Day, V. W.; Bowman-James, K. Supramolecular Encapsulation of Tetrahedrally Hydrated Guests in a Tetrahedron Host. *Angew. Chem. Int. Ed*. **2012**, *51*, 2119.

(9) Saeed, M. A.; Pramanik, A.; Wong, B.M.; Haque, S. A.; Powell, D. R.; Chandd, D. K.; Hossain, M. A. Self-Assembly of Ordered Water Tetramers in an Encapsulated $[Br(H_2O)_{12}]^-$ Complex. *Chem. Commun*. **2012**, *48*, 8631.

(10) Markovich, G.; Pollack, S.; Giniger, R.; Cheshnovsky, O. J. Photoelectron Spectroscopy of Cl^-, Br^-, and I^- Solvated in Water Clusters. *Chem. Phys.* **1994**, *101*, 9344.

(11) Basu, A.; Das, G. Encapsulation of a Discrete Cyclic Halide Water Tetramer $[X_2(H_2O)_2]^{2-}$, X = Cl^-/Br^- within a Dimeric Capsular Assembly of a Tripodal Amide Receptor. *Chem. Commun*. **2013**, *49*, 3997.

(12) Kopylovich, M. N.; Tronova, E. A.; Haukka, M.; Kirillov, A. M.; Kukushkin, V. Yu.; Fraústo da Silva, J. J. R.; Pombeiro, A. J. L. Identification of Hexameric Water and Hybrid Water–Chloride Clusters Intercalated in the Crystal Hosts of (Imidoylamidine)nickel(II) Complexes. *Eur. J. Inorg. Chem.* **2007**, *29*, 4621.

(13) Casas, J. S.; Couce, M. D.; Sánchez, A.; Sordo, J.; López, E. M. V. Hydrogen Bonded Water–Halide $\{[(H_2O)_4X_2]^{2-}\}_n$ (X=Cl, Br) Tapes as Organizing Units in Crystals Containing $[SnMe_2(MePN–H)]_2^{2+}$ Cations (MePN=N-methylpyridoxine). *Inorg. Chem. Commun.* **2013**, *30*, 156.

(14) Butchard, J. R.; Curnow, O.J.; Garrett, D. J.; Maclagan, R. G. A. R. Structure of a Discrete Dichloride Hexahydrate Cube as a Tris(diisopropylamino)cyclopropenium Salt. *Angew. Chem. Int. Ed*. **2006**, *45*, 7550.

(15) Butchard, J. R.; Curnow, O. J.; Garrett, D. J.; Maclagan, R. G. A. R.; Libowitzky, E.; Piccolic, P. M. B.; Schultz, A. J. Structural, Theoretical and Spectroscopic Studies of the Dichloride Hexahydrate Cube $[Cl_2(H_2O)_6]^{2-}$. *Dalton Trans*. **2012**, *41*, 11765.

(16) Chen, W-j.; Long, L. S.; Huang, R. B.; Zheng, L. S. A Dihalide−Decahydrate Cluster of $[X_2(H_2O)_{10}]^{2-}$ in a Supramolecular Architecture of $\{[Na_2(H_2O)_6(H_2O@TMEQ[6])]\cdot 2(C_6H_5NO_3)\}X_2(H_2O)_{10}$ (TMEQ[6] = α,α′,δ,δ′-Tetramethylcucurbit[6]uril; X = Cl, Br). *Cryst. Growth Des.* **2013**, *13*, 2507.

(17) Ghosh, A. K.; Ghoshal, D.; Ribas, J.; Mostafa, G.; Chaudhuri, N. R. Hydrogen-Bonded Assembly of Water and Chloride in a 3D Supramolecular Host. *Cryst. Growth Des.* **2006**, *6*, 36.

(18) Gao, J.; Boudon, S.; Wipff, G. Ab Initio and Crystal-Structure Analysis of Like-Charged Ion-Pairs. *J. Am. Chem. Soc*. **1991**, *113*, 9610.

(19) Smith, L. S.; Wertz, D. L. Solute Structuring in Aqueous Lanthanum (III) Chloride Solutions. *J. Am. Chem. Soc*. **1975**, *97*, 2365.

(20) Copestake, A. P.; Neilson, G. W.; Enderby, J. E. The Structure of a Highly Concentrated Aqueous-Solution of Lithium-Chloride. *J. Phys. C: Solid State Phys*. **1985**, *18*, 4211.

(21) Galashev, A. E.; Sigon, F.; Servida, A. Molecular Dynamic Study of Stabilization of the Cl^{-}−Cl^{-} Anion Pair in Steam. *J. Struct. Chem.* **1996**, *37*, 252.

(22) Boldyrev, A. I.; Simons, J. Isolated SO_4^{2-} and PO_4^{3-} Anions Do Not Exist. *J. Phys. Chem*. **1994**, *98*, 2298.

(23) Wang, X. B.; Nicholas, J. B.; Wang L. S. Electronic Instability of Isolated SO_4^{2-} and Its Solvation Stabilization. *J. Chem. Phys*. **2000**, *113*, 10837.

(24) Wang, X. B.; Yang, X.; Nicholas, J. B.;Wang, L. S. Photodetachment of Hydrated Oxalate Dianions in the Gas Phase, $C_2O_4^{2-}(H_2O)_n$ (n = 3−40) – From Solvated Clusters to Nano Droplet. *J. Chem. Phys.* **2003**, *119*, 3631.

(25) Wang, X. B.; Yang, X.; Nicholas, J. B.;Wang, L. S. Bulk-Like Features in the Photoemission Spectra of Hydrated Doubly-Charged Anion Clusters. *Science* **2001**, *294*, 1322.

(26) Ivanov, A. S.; Boldyrev, A. I. Reliable Predictions of Unusual Molecules. *Phys. Chem. Chem. Phys*. **2012**, *14*, 15943.

(27) Sergeeva, A. P.; Averkiev, B. B.; Zhai, H. J.; Boldyrev, A. I.; Wang, L. S. All-boron Analogues of Aromatic Hydrocarbons: B_{17}^- and B_{18}^-. *J. Chem. Phys.* **2011**, *134*, 224304.

(28) Schlegel, H. B. Optimization of Equilibrium Geometries and Transition Structures. *J. Comput. Chem.* **1982**, *3*, 214.

(29) Wang, X. B.; Sergeeva, A. P.; Yang, J.; Xing, X. P.; Boldyrev, A. I.; Wang, L. S. Photoelectron Spectroscopy of Cold Hydrated Sulfate Clusters, $SO_4^{2-}(H_2O)_n$ (n = 4-7): Temperature-dependent Isomer Populations. *J. Phys. Chem. A* **2009**, *113*, 5567.

(30) Zhao, Y.; Truhlar, D. G. The M06 Suite of Density Functionals for Main Group Thermochemistry, Thermochemical Kinetics, Noncovalent Interactions, Excited States, and Transition Elements: Two New Functionals and Systematic Testing of Four M06-Class Functionals and 12 Other Functionals. *Theor. Chem. Acc*. **2008**, *120*, 215.

(31) Woon, D. E.; Dunning, T. H., Jr. Gaussian Basis Sets for Use in Correlated Molecular Calculations. III. The Second Row Atoms, Al-Ar. *J. Chem. Phys*. **1993**, *98*, 1358.

(32) Kendall, R. A.; Dunning, T. H.; Harrison, R. J. Electron Affinities of the First-Row Atoms Revisited. Systematic Basis Sets and Wave Functions. *J. Chem. Phys*. **1992**, *96*, 6796.

(33) Dunning, T. H. Gaussian Basis Sets for Use in Correlated Molecular Calculations. I. The Atoms Boron through Neon and Hydrogen. *J. Chem. Phys*. **1989**, *90*, 1007.

(34) Wilson, A.; van Mourik, T.; Dunning, T. H. Gaussian Basis Sets for Use in Correlated Molecular Calculations. VI. Sextuple-zeta Correlation-Consistent Sets for Boron through Neon. THEOCHEM **1997**, *388*, 339.

(35) Kemp, D. D.; Gordon, M. S. Theoretical Study of the Solvation of Fluorine and Chlorine Anions by Water. *J. Phys. Chem. A* **2005**, *109*, 7688.

(36) Lee, H. M.; Kim, D; Kim, K. S. Structures, Spectra, and Electronic Properties of Halide-Water Pentamers and Hexamers, $X^-(H_2O)_{5,6}$ (X = F, Cl, Br, I): Ab Initio Study. *J. Chem. Phys*. **2002**, *116*, 5509.

(37) Kim, J.; Lee, H. M.; Suh, S. B.; Majumdar, D.; Kim, K. S. Comparative Ab Initio Study of the Structures, Energetics and Spectra of $X^-(H_2O)_{n=1-4}$ [X = F, Cl, Br, I] Clusters. *J. Chem. Phys*. **2000**, *113*, 5259.

(38) Perera, L.; Berkowitz, M. L. Structures of $Cl^-(H_2O)_n$, and $F^-(H_20)_n$ (n = 2,3,…,15) C!usters. Molecular, Dynamics Computer Simulations. *J. Chem. Phys*. **1994**, 100, 3085.

(39) von Niessen, W.; Schirmer, J.; Cederbaum, L. S. Computational Methods for the One-Particle Green's Function. *Comput. Phys. Rep*. **1984**, *1*, 57.

(40) Zakrzewski, V. G.; Dolgounitcheva, O.; Zakjevskii, A. V.; Ortiz, J. V. Ab Initio Electron Propagator Methods: Applications to Fullerenes and Nucleic Acid Fragments. *Ann. Rev. Comput. Chem*. **2010**, *6*, 79.

(41) Rassolov, V. A.; Ratner, M. A.; Pople, J. A.; Redfern, P. C.; Curtiss, L. A. 6-31G* Basis Set for Third-Row Atoms *J. Comput. Chem.* **2001**, *22*, 976.

(42) Gordon, M. S.; Binkley, J. S.; Pople, J. A.; Pietro, W. J.; Hehre, W. J. Self-Consistent Molecular Orbital Methods. 22. Small Split-Valence Basis Sets for Second-Row Elements. *J. Am. Chem. Soc.* **1982**, *104*, 2797.

(43) Pietro, W. J.; Francl, M. M.; Hehre, W. J.; Defrees, D. J.; Pople, J. A.; Binkley, J. S. Self-Consistent Molecular Orbital Methods. 24. Supplemented Small Split-Valence Basis Sets for Second-Row Elements. *J. Am. Chem. Soc.* **1982**, *104*, 5039.

(44) Reed, A. E.; Weinstock, R. B.; Weinhold, F. Natural Population Analysis. *J. Chem. Phys*. **1985**, *83*, 735.

(45) Frisch, M. J.; Trucks, G. W.; Schlegel, H. B.; Scuseria, G. E.; Robb, M. A.; Cheeseman, J. R.; Scalmani, G.; Barone, V.; Men-nucci, B.; Petersson, G. A.; Nakatsuji, H.; Caricato, M.; Li, X.; Hratchian, H. P.; Izmaylov, A. F.; Bloino, J.; Zheng, G.; Sonnen-berg, J. L.; Hada, M.; Ehara, M.; Toyota, K.; Fukuda, R.; Hasega-wa, J.; Ishida, M.; Nakajima, T.; Honda, Y.; Kitao, O.; Nakai, H.; Vreven, T.; Montgomery, J. A., Jr.; Peralta, J. E.; Ogliaro, F.; Bearpark, M.; Heyd, J. J.; Brothers, E.; Kudin, K. N.; Staroverov, V. N.; Kobayashi, R.; Normand, J.; Raghavachari, K.; Rendell, A.; Burant, J. C.; Iyengar, S. S.; Tomasi, J.; Cossi, M.; Rega, N.; Millam, N. J.; Klene, M.; Knox, J. E.; Cross, J. B.; Bakken, V.; Adamo, C.; Jaramillo, J.; Gomperts, R.; Stratmann, R. E.; Yazyev, O.; Austin, A. J.; Cammi, R.; Pomelli, C.; Ochterski, J. W.; Martin, R. L.; Morokuma, K.; Zakrzewski, V. G.; Voth, G. A.; Salvador, P.; Dannenberg, J. J.;

Dapprich, S.; Daniels, A.D.; Farkas,O.; Foresman,J.B.; Ortiz,J.V.; Cioslowski,J.; Fox, D. J. *Gaussian 09*, Revision B.01; Gaussian, Inc.: Wallingford, CT, **2010**.

(46) http://www.chemcraftprog.com

(47) Perera, L; Berkowitz, M. L. Stabilization Energies of Cl^-, Br^-, and I^- Ions in Water Clusters. *J. Chem. Phys.* **1993**, *99*, 4222.

(48) Kebarle, P. Ion Thermochemistry and Solvation from Gas Phase Ion Equilibria. *Annu. Rev. Phys. Chem.* **1977**, *28*, 445.

(49) Tsai, C. J.; Jordan, K. D. Monte Carlo simulation of $(H_2O)_8$: Evidence for a Low-energy S_4 Structure and Characterization of the Solid ↔ Liquid Transition. *J. Chem. Phys*. **1991**, *95*, 3850.

(50) Gruenloh, C. J.; Carney, J. R.; Arrington, C. A.; Zwier, T. S.; Fredericks, S. Y.; Jordan, K. D. Infrared Spectrum of a Molecular Ice Cube: The S_4 and D_{2d} Water Octamers in Benzene-$(Water)_8$. *Science* **1997**, *276*, 1678.

(51) Choi, C. H.; Re, S.; Rashid, M. H. O.; Li, H.; Feig, M.; Sugita, Y. Solvent Electronic Polarization Effects on Na^+−Na^+ and Cl^-−Cl^- Pair Associations in Aqueous Solution. *J. Phys. Chem. B* **2013**, *117*, 9273.

(52) Delahay, P. Photoelectron Emission Spectroscopy of Aqueous Solutions. *Acc. Chem. Res*., **1982**, *15*, 40.

(53) Yang, X.; Wang, X. B.; Wang, L. S. Photodetachment of $F^-(H_2O)_n$ (n=1–4): Observation of Charge-Transfer states $[F^-(H_2O)^+_n]$ and the Transition State of F^+H_2O Hydrogen Abstraction Reaction. *J. Chem. Phys*. **2001**, *115*, 2889.

(54) Hirtz, P.; Buck, C.; Kunzman, R. *Current Techniques in Acid-Chloride Corrosion Control and Monitoring at The Geysers*, Sixteenth Workshop on Geothermal Reservoir Engineering, Stanford Geothermal Program, **1991**, p. 83.

Table 6-1. Calculated Stabilization Energies of $Cl^-(H_2O)_n$ Clusters (kcal/mol) at Different Levels of Theory.

$Cl^-(H_2O)_n$	M062X/ aug-cc-pvDZ	M062X/ aug-cc-pvTZ	CCSD(T)/ aug-cc-pvDZ	exp.[47]
$Cl^-(H_2O)$	-15.2	-15.3	-14.6	-17.5/ -13.1[48]
$Cl^-(H_2O)_2$	-31.1	-31.4	-29.7	-31.4
$Cl^-(H_2O)_3$	-49.1	-49.5	-46.3	-43.6
$Cl^-(H_2O)_4$	-64.2	-64.2	-61.2	-
$Cl^-(H_2O)_5$	-75.4	-75.8	-72.1	-
$Cl^-(H_2O)_6$	-91.6	-91.6	-88.5	-
$Cl^-(H_2O)_7$	-103.0	-103.2	-100.1	-
$Cl^-(H_2O)_8$	-116.5	-116.3	-113.3	-
$Cl^-(H_2O)_9$	-127.1	-127.0	-123.9	-
$Cl^-(H_2O)_{10}$	-140.6	-140.4	-139.2	-

Table 6-2. Calculated Stabilization Energies of $[Cl_2(H_2O)_n]^{2-}$ (n = 2-10) Clusters (kcal/mol) at Different Levels of Theory.

$Cl^-(H_2O)_nCl^-$	symm	M062X/ aug-cc-pvDZ	M062X/ aug-cc-pvTZ	CCSD(T)/ aug-cc-pvDZ
$Cl^-(H_2O)_2Cl^-$	D_{2h}	15.5	14.8	15.4
$Cl^-(H_2O)_3Cl^-$	C_1	-4.3	-5.1	-3.7
$Cl^-(H_2O)_4Cl^-$	C_1	-27.7	-28.0	-26.3
$Cl^-(H_2O)_5Cl^-$	C_1	-43.6	-44.1	-41.6
$Cl^-(H_2O)_6Cl^-$	S_6	-62.9	-63.7	-61.8
$Cl^-(H_2O)_7Cl^-$	C_1	-79.4	-80.1	-78.1
$Cl^-(H_2O)_8Cl^-$	S_2	-95.2	-96.0	-94.3
$Cl^-(H_2O)_9Cl^-$	C_1	-109.8	-110.5	-108.5
$Cl^-(H_2O)_{10}Cl^-$	S_2	-123.8	-124.5	-122.3

Table 6-3. Calculated Dissociation Energies for Different Dissociation Channels $Cl^-(H_2O)_nCl^- \rightarrow Cl^-(H_2O)_m + Cl^-(H_2O)_k$, where m + k = n (kcal/mol).

Method/ Basis	m=1, k=1	m=1, k=2	1)m=1,k=3 2)m=2, k=2	1) m=1, k=4 2) m=2, k=3	1) m=1, k=5 2) m=2, k=4 3) m=3, k=3	1) m=1, k=6 2) m=2, k=5 3) m=3, k=4	1) m=1, k=7 2) m=2, k=6 3) m=3, k=5 4) m=4, k=4	1) m=1, k=8 2) m=2, k=7 3) m=3, k=6 4) m=4, k=5	1) m=1, k=9 2) m=2, k=8 3) m=3, k=7 4) m=4, k=6 5) m=5, k=5
M06-2X/ aug-cc-pv-DZ	-45.8	-41.3	1) -36.6 2) -34.5	1) -35.3 2) -36.1	1) -27.6 2) -32.4 3) -35.3	1) -27.4 2) -27.1 3) -34.0	1) -23.1 2) -27.7 3) -29.4 4) -33.3	1) -22.0 2) -24.3 3) -31.0 4) -29.8	1) -18.5 2) -23.9 3) -28.3 4) -28.6 5) -27.0
M06-2X/ aug-cc-pv-TZ	-45.5	-41.6	1) -36.8 2) -34.8	1) -35.4 2) -36.7	1) -27.4 2) -31.9 3) -35.2	1) -26.9 2) -27.0 3) -33.6	1) -22.7 2) -27.2 3) -29.4 4) -32.7	1) -21.2 2) -24.0 3) -30.6 4) -29.5	1) -17.8 2) -23.2 3) -28.1 4) -28.4 5) -27.0
CCSD(T)/ aug-cc-pv-DZ	-44.6	-40.7	1) -34.6 2) -33.2	1) -34.2 2) -34.5	1) -26.1 2) -30.7 3) -34.1	1) -25.6 2) -26.1 3) -32.3	1) -21.2 2) -26.5 3) -31.1 4) -31.8	1) -19.9 2) -22.7 3) -29.5 4) -28.4	1) -16.5 2) -22.1 3) -27.0 4) -27.2 5) -26.3

Table 6-4. Calculated Adiabatic (ADE) and Vertical (VDE) Electron Binding Energies for $[Cl_2(H_2O)_n]^{2-}$ (n = 2-10) in eV.

$Cl^-(H_2O)_nCl^-$	VDE (OVGF/6-311++G**)	VDE (M062X/aug-cc-pvDZ)	ADE (M062X/aug-cc-pvDZ)
$Cl^-(H_2O)_2Cl^-$	1.62	1.49	1.43
$Cl^-(H_2O)_3Cl^-$	1.89	1.88	1.00
$Cl^-(H_2O)_4Cl^-$	2.89	2.77	1.17
$Cl^-(H_2O)_5Cl^-$	2.60	2.72	1.22
$Cl^-(H_2O)_6Cl^-$	2.86	2.79	1.83
$Cl^-(H_2O)_7Cl^-$	3.09	3.01	2.27
$Cl^-(H_2O)_8Cl^-$	3.56	3.42	2.44
$Cl^-(H_2O)_9Cl^-$	3.78	3.74	2.59
$Cl^-(H_2O)_{10}Cl^-$	4.42	4.38	2.76

Table 6-5. Atomic Charges |e| on Ions Calculated with Natural Population Analysis (NPA).

$Cl^-(H_2O)_nCl^-$	Charge on the first Cl atom	Charge on the second Cl atom
$Cl^-(H_2O)_2Cl^-$	-0.9759	-0.9759
$Cl^-(H_2O)_3Cl^-$	-0.9557	-0.9647
$Cl^-(H_2O)_4Cl^-$	-0.9563	-0.9396
$Cl^-(H_2O)_5Cl^-$	-0.9633	-0.9298
$Cl^-(H_2O)_6Cl^-$	-0.9286	-0.9285
$Cl^-(H_2O)_7Cl^-$	-0.9187	-0.9230
$Cl^-(H_2O)_8Cl^-$	-0.9136	-0.9136
$Cl^-(H_2O)_9Cl^-$	-0.9083	-0.9083
$Cl^-(H_2O)_{10}Cl^-$	-0.9034	-0.9034
$Cl^-(H_2O)_{36}Cl^-$	-0.8600	-0.8570
$Cl^-(H_2O)_{40}Cl^-$	-0.8464	-0.8531

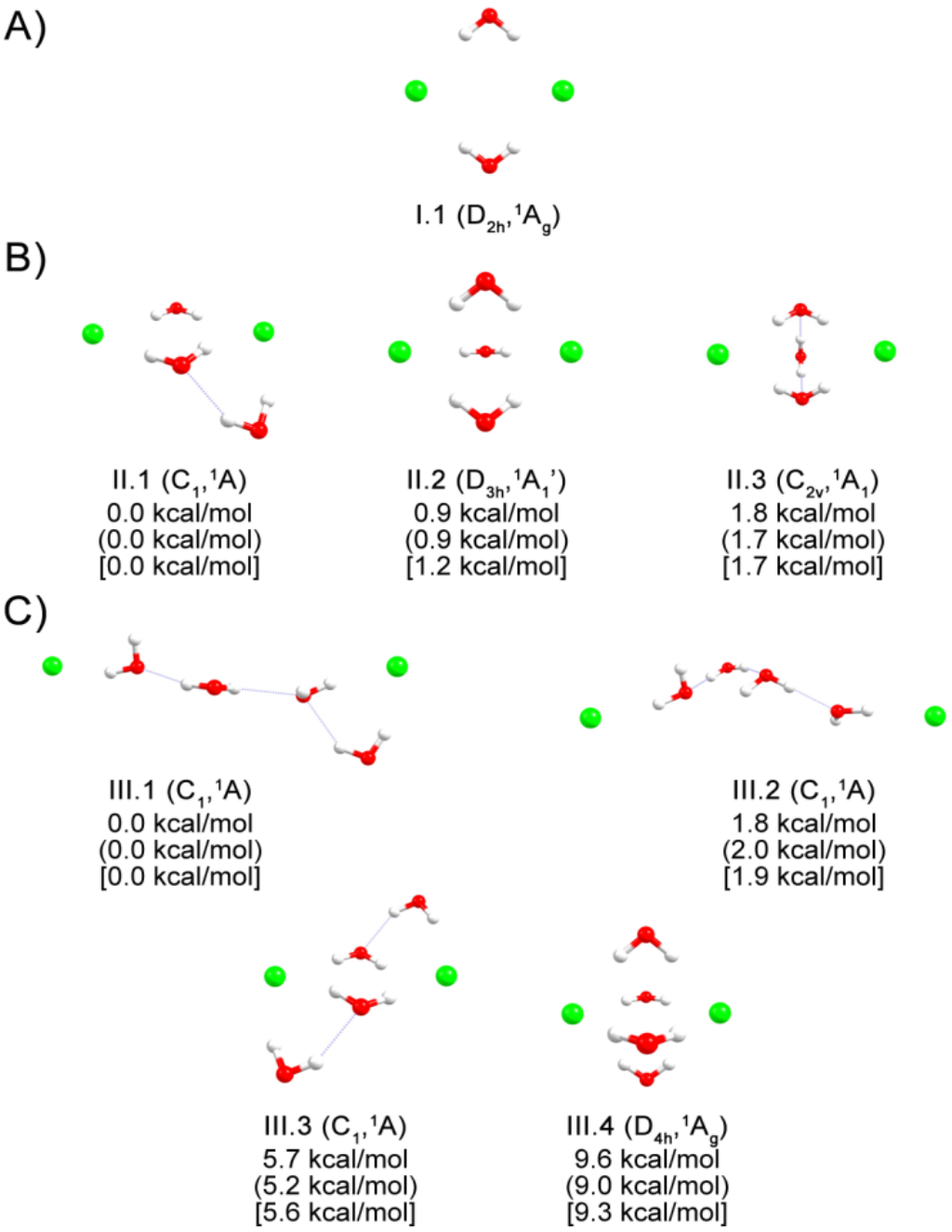

Figure 6-1. Representative optimized structures of A) $[Cl_2(H_2O)_2]^{2-}$, B) $[Cl_2(H_2O)_3]^{2-}$, and C) $[Cl_2(H_2O)_4]^{2-}$, their point group symmetries, spectroscopic states and ZPE (M06-2X/aug-cc-pvTZ) corrected relative energies. The energies are given at: CCSD(T)/aug-cc-pvDZ (bold), M06-2X/aug-cc-pvTZ (in brackets), M06-2X/aug-cc-pvDZ (square brackets). Here and elsewhere hydrogen bonds between adjacent water molecules are marked with tiny blue lines.

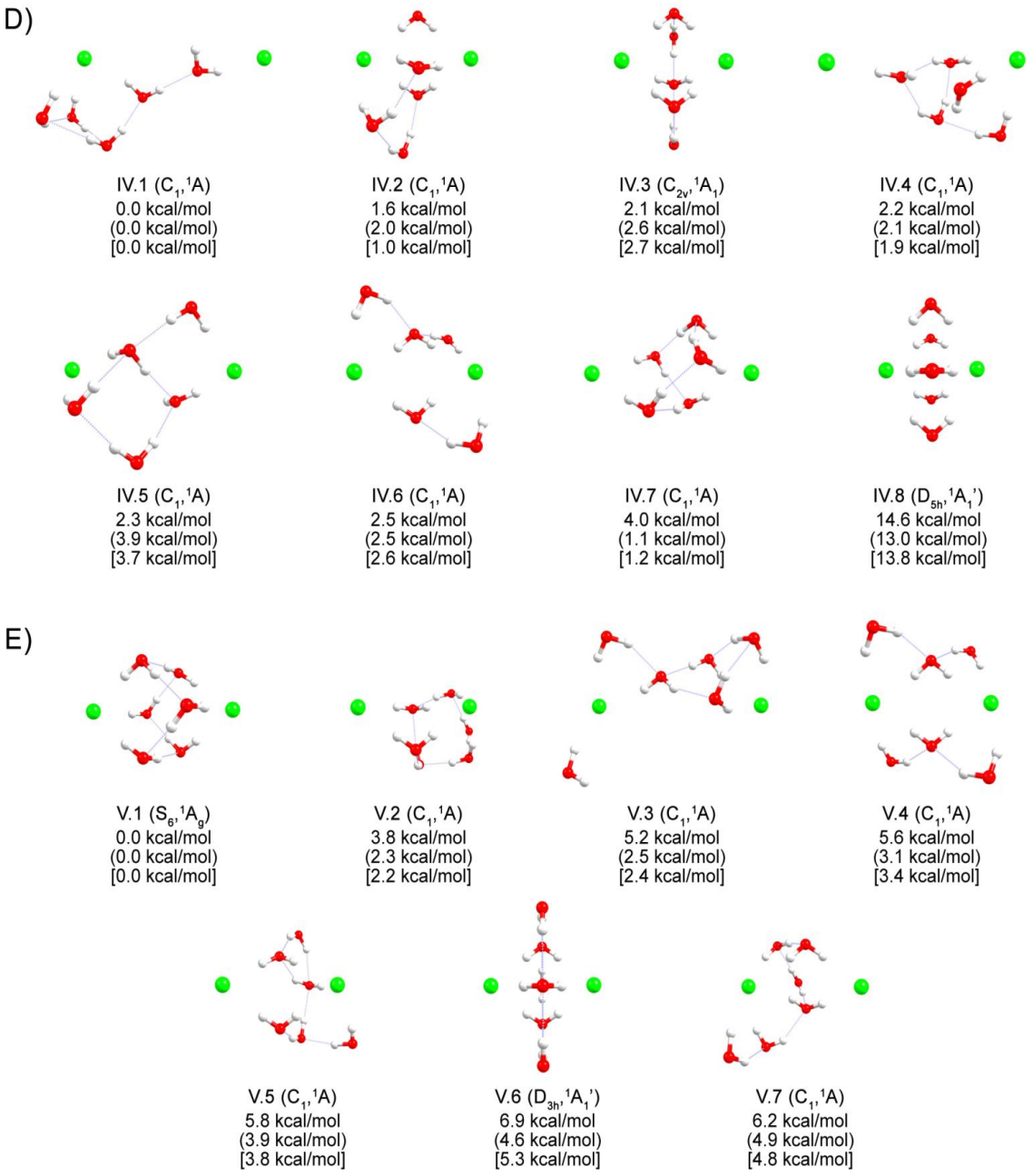

Figure 6-2. Representative optimized structures of D) $[Cl_2(H_2O)_5]^{2-}$ and E) $[Cl_2(H_2O)_6]^{2-}$, their point group symmetries, spectroscopic states and ZPE (M06-2X/aug-cc-pvTZ) corrected relative energies. The energies are given at: CCSD(T)/aug-cc-pvDZ (bold), M06-2X/aug-cc-pvTZ (in brackets), M06-2X/aug-cc-pvDZ (in square brackets).

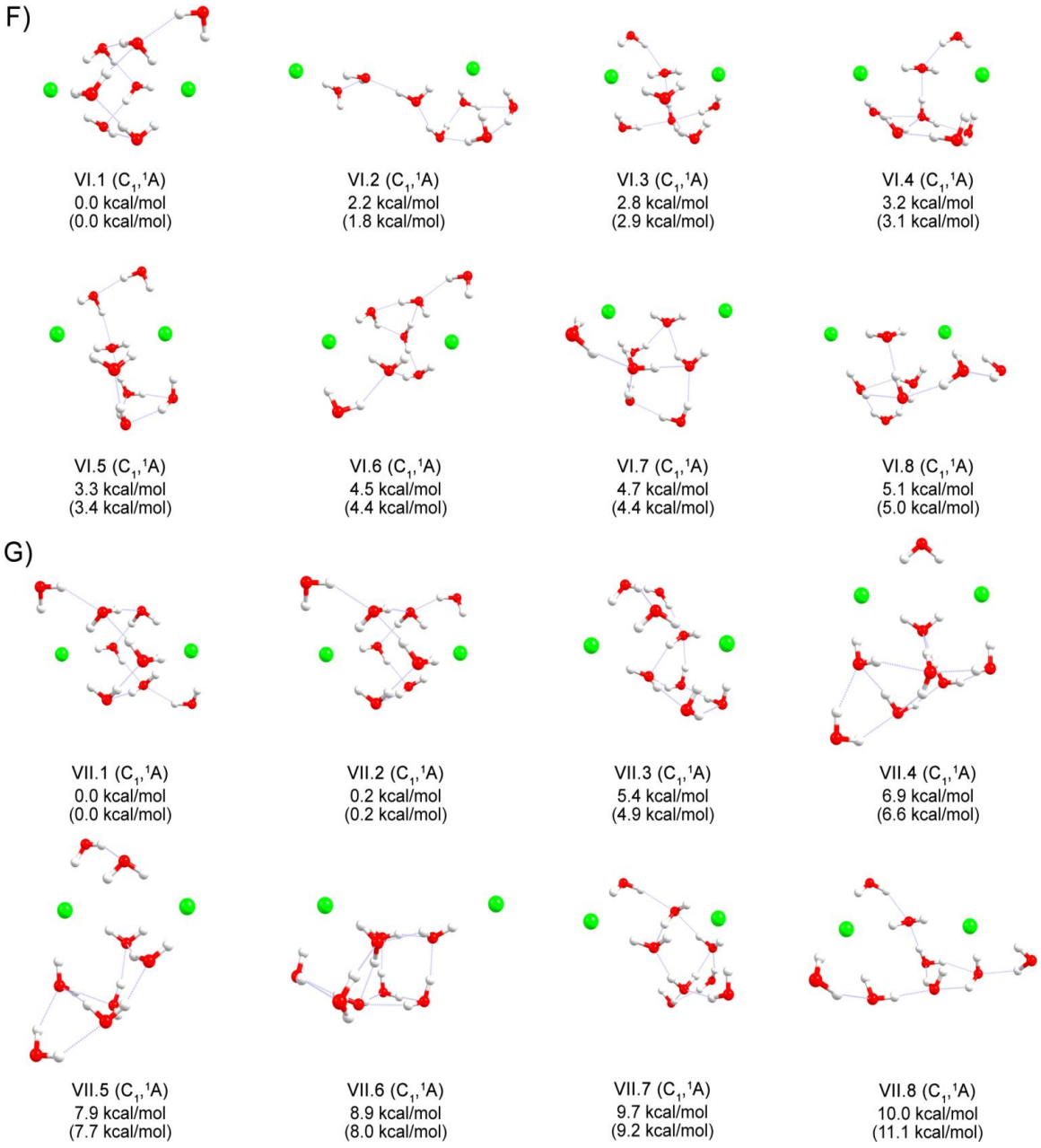

Figure 6-3. Representative optimized structures of F) $[Cl_2(H_2O)_7]^{2-}$ and G) $[Cl_2(H_2O)_8]^{2-}$, their point group symmetries, spectroscopic states and ZPE corrected relative energies. The energies are given at: M06-2X/aug-cc-pvTZ (bold), M06-2X/aug-cc-pvDZ (in brackets).

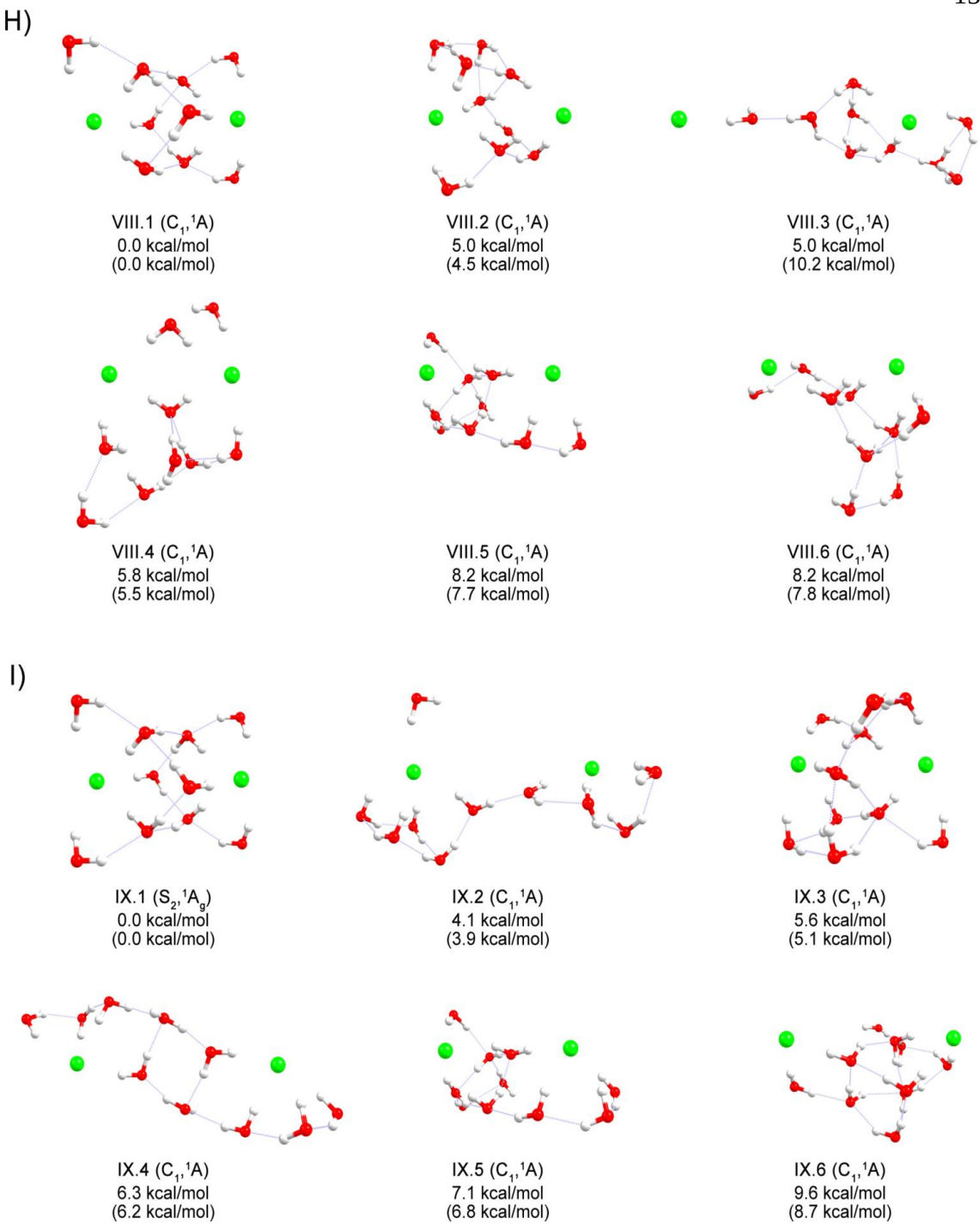

Figure 6-4. Representative optimized structures of H) $[Cl_2(H_2O)_9]^{2-}$ and I) $[Cl_2(H_2O)_{10}]^{2-}$, their point group symmetries, spectroscopic states and ZPE corrected relative energies. The energies are given at: M06-2X/aug-cc-pvTZ (bold), M06-2X/aug-cc-pvDZ (in brackets).

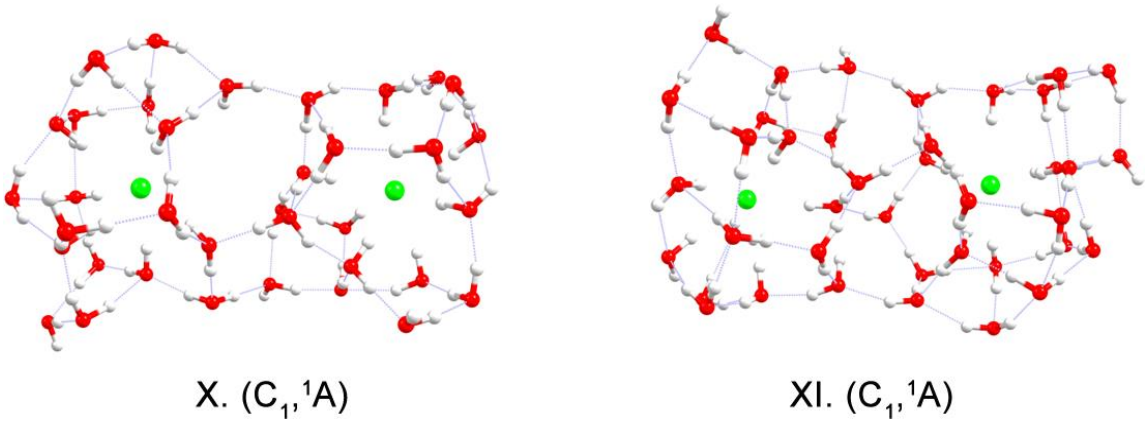

Figure 6-5. Optimized (M06-2X/aug-cc-pvDZ) structures of $[Cl_2(H_2O)_{36}]^{2-}$ (left) and $[Cl_2(H_2O)_{40}]^{2-}$ (right) clusters, their point group symmetries and spectroscopic states.

CHAPTER 7

INORGANIC DOUBLE HELIX STRUCTURES OF UNUSUALLY SIMPLE Li-P SPECIES[1]

Abstract

The existence of inorganic double-helix structures at the atomic level is theoretically predicted. An unbiased quantum-chemical search for the global minimum structures of Li_xP_x (x=5–9) species is performed. For the Li_7P_7–Li_9P_9 stoichiometries the global minimum structure has a peculiar double-helix form.

7-1. Introduction

The double helix represents one of the most fascinating geometric structures in nature. Helical structures can be either right-handed or left-handed depending on the direction of the rotation. In other words they possess the chirality property, which is vital for every living organism. Chiral molecules lack an internal plane of symmetry and thus have a nonsuperposable mirror image. It turns out that for organic compounds nature decides by itself whether the most preferable structure will be right-handed or left-handed, but questions regarding such differentiation in the inorganic world have not yet been answered.

In chemistry and biology, the term double helix usually refers to the structure formed by double-stranded molecules of nucleic acids such as DNA, discovered by Watson and Crick,[1] and RNA. Watson and Crick stressed: "It has not escaped our notice

[1] Coauthored by Alexander S. Ivanov, Andrew J. Morris, Konstantin V. Bozhenko, Chris J. Pickard and Alexander I. Boldyrev. Reprinted with permission from *Angew. Chem. Int. Ed.* **2012**, 51, 8330 –8333.

that the specific pairing we have postulated immediately suggests a possible copying mechanism for the genetic material." There are many other organic polymers with helical structures and proteins which have substructures known as α-helices. In spite of the diversity and significance of the role of double-helix structures in evolution and metabolism, they are very rare in inorganic chemistry. In 1993 V. Soghomonian et al. showed that very complicated inorganic solids can be self-assembled from structurally simple precursors by the hydrothermal synthesis of vanadium phosphate and $[(CH_3)_2NH_2]K_4[V_{10}O_{10}(H_2O)_2(OH)_4(PO_4)_7]\cdot 4\,H_2O$, which contains chiral double helices formed from interpenetrating spirals of vanadium oxo pentamers bonded together by P_5^+ ions[2] After that, there were also many successful syntheses of inorganic compounds with helical structures.[3,4] Thus, while some advances have been achieved for inorganic materials with a single-helical geometry, reports of counterparts with the double-helix structure are deficient. Recently, double-helical silicon microtubes and double-helical carbon nanotube (CNT) arrays were prepared.[5,6] However, there is no structural model at the atomic level to explain the Si and C tubular double helices.

Here we report the theoretical prediction of the existence of double-helix structures in the series of Li_xP_x (x=5–9) clusters and in an infinite LiP chain and compare them with bulk phases of LiP. It was surprising to discover the double-helix structures in rather simple species consisting of only two elements: lithium and phosphorus. Our initial goal was to probe electronic transmutation for Li_xP_x clusters by making bonded structures[7,8] which obey the Zintl-rule (where the less electronegative lithium atom donates an electron to the more electronegative phosphorus atom, resulting in each phosphorus bearing a negative charge) with the anticipation that structures similar to

sulfur compounds would be formed.[8] However, the unexpected double helices were found to be either global minimum structures or low-lying isomers.

7-2. Results and discussion

We performed an unbiased quantum-chemical search for Li_xP_x (x=5–9) clusters using a Coalescence Kick[9] program written by B. B. Averkiev initially at the B3LYP/3-21G level of theory. The Coalescence Kick method subjects large populations of randomly generated structures to a coalescence procedure in which all atoms are pushed gradually to the molecular center of mass to avoid the generation of fragmented structures and then optimizes them to the nearest local minima. All low-lying isomers found by this method were reoptimized with follow-up frequency calculations at the B3LYP level of theory using the 6-311+G* basis set. The total energies of the lowest isomers of Li_5P_5, Li_6P_6, and Li_7P_7 stoichiometries were calculated at the CCSD(T)/CBS//B3LYP/6-311+G* level of theory by extrapolating CCSD(T)/cc-pvDZ//B3LYP/6-311+G* and CCSD(T)/cc-pvTZ//B3LYP/6-311+G* to the infinite basis set using the Truhlar formula.[10] Additional calculations of the three lowest isomers for each stoichiometry were also performed (see the Theoretical Section).

In Figure 7-1 we present the right- and left-handed double helices for the Li_5P_5, Li_6P_6, Li_7P_7, Li_8P_8, and Li_9P_9 species.

A more extensive set of alternative isomers found in our global minimum search is summarized in Figures 7-5 – 7-9. For the Li_5P_5 stoichiometry the double-helix structure is the second lowest isomer, which is 5.6 kcal mol^{-1} higher than the global minimum (Figure 7-5). For the Li_6P_6 stoichiometry, the helical structure is the third isomer and is 12.6 kcal mol^{-1} higher than the global minimum structure (Figure 7-6). Our search for the

global minimum in the Li_7P_7 stoichiometry revealed that the double-helix structure (Figure 7-2 and Figure 7-7) is the global minimum with the second isomer containing a seven-membered ring similar to sulfur clusters.[11]

We also performed a search for the global minimum S_7 cluster and found two low-lying isomers: *exo* and *endo* isomers with the second one being 3.4 kcal mol^{-1} higher in energy than the global minimum *exo* isomer (Figure 7-8). Our search also revealed a helical isomer of S_7 which is 34.1 kcal mol^{-1} higher in energy than the global minimum. The helical structure of the S_7 isomer is very similar to the helical phosphorus strand in the double-helix structure of Li_7P_7. The double helices were found to be the global minimum structures for both the Li_8P_8 and Li_9P_9 stoichiometries (Figures 7-9 and 7-10).

n-Membered rings are the most stable structures for sulfur clusters. It was recently reported, however, that there are two phases having helical structures with triangular and squared chains of sulfur, which are stable at 1.5 GPa and temperatures from 300 K to 1100 K.[12] The same authors also showed that selenium can form the helix squared chain structures similar to sulfur.[12] Another representative of group VI-A elements, oxygen, is able to form analogous helical structures under the pressure of metallization according to the latest theoretical reports.[13,14]

Because of their small size and unique properties, clusters could become good samples for describing a structural model of the double helix at the atomic level. Therefore, to gain additional insight into the structure and chemical bonding of the double-helix structure of Li_xP_x species, we performed natural bond orbital analysis (NBO).[15] According to NBO analysis for the Li_5P_5 double helix, the bonding between lithium and phosphorus atoms is quite ionic with effective atomic charges for Li ranging

from +0.4 to +0.7|e|. Additionally, NBO analysis revealed the presence of two P–Li σ-bonds with occupation numbers (ON) equal to 1.84–1.86|e|, four P—P σ bonds with ON ranging from 1.92–1.96|e|, one double bond with ON=1.83|e| for the π bond, and one triple bond with ON=1.80|e| and ON=1.30|e| for two π bonds, respectively (Figure 7-11). For the Li_6P_6 double-helix structure, we found the following bonding picture: the effective atomic charges on Li range from +0.5 to +0.8|e|; four Li—P σ bonds with ON=1.63–1.68|e|; five P—P σ bonds with ON=1.94–1.96|e|; one double bond with ON=1.86|e| for the P—P π bond. Starting from Li_7P_7 and up to Li_9P_9 double helices have a similar chemical bonding pattern: effective charges on Li range from +0.8 to +0.9|e|; there are no more Li—P σ bonds, there are six (Li_7P_7), seven (Li_8P_8), and eight (Li_9P_9) P—P σ bonds with ON=1.95–1.98|e|; there is one double bond at the end of phosphorus chain with ON=1.93–1.94|e| for the π bond (see Figures 7-12 – 7-15). We see from this data that when the bonding between the Li and P atoms is ionic, beginning from Li_7P_7 to Li_9P_9, the double-helix structures are much more favourable relative to other isomers. We believe that for the smaller clusters, termination effects are responsible for the double-helix structures being less stable. Thus, the electronic transmutation takes place in the case of Li_xP_x (x=5–9) clusters, but in a rather strange way. The presence of lithium cations seems to be working similar to high pressure and high temperature in the helix phases of sulfur and selenium. Though NBO analysis does not show any significant direct Li—Li covalent bonding, in our graphical representation of double-helix structures, we connected adjacent Li atoms to make the double-helix structure more apparent. From our point of view, the helix structure formed by lithium cations because of favourable electrostatic interactions with neighboring phosphorus anions.

To further test the viability[16] of our double-helix structures we checked their lowest frequencies and the HOMO–LUMO gaps. The lowest frequencies for Li_5P_5, Li_6P_6, Li_7P_7, Li_8P_8, and Li_9P_9 are 102, 89, 61, 82, and 75 cm^{-1}, respectively, which are comparable to the lowest theoretically calculated frequency at the same level of theory (102 cm^{-1}) in the $Li_3Al_4^-$ anion observed in a molecular beam.[17] The HOMO–LUMO gap for the clusters are as follows: Li_5P_5 (2.27 eV), Li_6P_6 (2.14 eV), Li_7P_7 (2.24 eV), Li_8P_8 (1.90 eV), and Li_9P_9 (1.71 eV) (HOMO/LUMO=highest occupied/lowest unoccupied molecular orbital). All data presented (calculated at the B3LYP/6-311+G* level of theory) are comparable to the HOMO–LUMO gap (2.02 eV, B3LYP/cc-pvTZ/Ta/Stuttgart/B/aug-cc-pVTZ) in the TaB_{10}^- wheel-type Ta-centered anionic cluster, which was recently prepared in a molecular beam.[18]

To further investigate the existence of double-helix structures we performed a solid-state study using plane-wave density functional theory (see the Theoretical Section), on the LiP infinite double-helix chain and two bulk phases of LiP of different symmetry. The LiP infinite double-helix chain was found to be stable (Figure 7-3). The structure comprises four functional units (FU) of Li_1P_1 per turn and is 6.00 kcal mol^{-1} lower in energy than Li_9P_9. Atomic chained helices of this kind were first found by Cromer in the Zintl phases, LiAs and NaSb[19,20] and exist in XY (X=Li,Na,K,Rb,Cs, Y=P,As,Sb).[21] Using ab initio random structure searching (AIRSS)[22,23] we recovered the *P*21/*c*symmetric Li_1P_1 bulk phase comprising of packed double helices[24] where adjacent helices are of opposite sense and 9.69 kcal mol^{-1}lower in energy than the infinite double-helix chain (Figure 7-4). Using AIRSS a metastable bulk phase of $P2_12_12_1$ symmetry, in which all helices have the same sense, similar to

Na_1P_1[25] was also uncovered which was 0.24 kcal mol^{-1} higher in energy than the *P*21/*c*symmetric phase.

7-3. Conclusions

The structures presented for Li_xP_x (*x*=5–9) are simple molecules which possess a double-helix structure comprising only two kinds of atoms. From solid-state calculations the LiP infinite double-helix chain was also found to be stable. Our solid-state calculations showed that the *P*21/*c* symmetric Li_1P_1 bulk phase comprising of packed double helices has an energy that is lower than the infinite double-helix chain. We believe that although the Li atoms are not connected by chemical bonding it is the positions of the Li atoms in space that make the structures double helical. The structures of XY (X=Li,Na,K,Rb,Cs, Y=P,As,Sb) Zintl phase compounds[21] may then also be interpreted as double helical. Our results extended the family of double-helical solids and we hope that other inorganic double-helix structures which obey the Zintl rule may be found.

7-4. Computational and theoretical methods

Additional calculations including geometry optimization and frequency calculations for the lowest three isomers of Li_5P_5, Li_6P_6, Li_7P_7, Li_8P_8, and Li_9P_9 stoichiometries were performed at the PBE1PBE/6-311+G* and M06/6-311+G* levels of theory. The results of these two levels of theory are generally consistent with the results at the B3LYP/6-311+G* level of theory. To test the applicability of the CCSD(T) and B3LYP methods for our systems we performed single-point calculations of the Li_7P_7 double-helix structure at the CASSCF(10,12)/6-311+G* level of theory. According to these calculations the Hartree–Fock coefficient in the CASSCF expansion (314028

configurations) is 0.973. Thus, both B3LYP and CCSD(T) methods are valid. Chemical bonding analysis was performed using the natural bond orbital (NBO) analysis. All quantum-chemical calculations were performed using the Gaussian 09 program.[26] Molecular visualization was performed using the Molekel 4.3 program.[27]

The solid-state study was performed using the plane-wave density functional theory code CASTEP[28] and the PBE exchange-correlation functional, ultrasoft pseudopotentials, and a Brillouin zone sampling finer than $2\pi\times0.05$ Å^{-1}. The valence states were described by a basis set containing plane waves with energies up to 400 eV. The infinite chain was relaxed in a supercell which had 10 Å between each periodic repetition. The structure was fully geometry-optimized and phonon calculations were performed to demonstrate its stability (see Figure 7-16).

References

[1] J. D. Watson, F. H. C. Crick, *Nature* **1953**, *171*, 737.

[2] V. Soghomonian, Q. Chen, R. C. Haushalter, J. Zubieta, C. J. O'Connor, *Science* **1993**, *259*, 1596.

[3] M. Yang, N. A. Kotov, J. *Mater. Chem*. **2010**, *21*, 6775.

[4] S.-H. Yu, H. Cölfen, K. Tauer, M. Antonietti, *Nat. Mater*. **2005**, *4*, 51.

[5] H. Morito, H. Yamane, *Angew. Chem.* **2010**, *122*, 3720; *Angew. Chem. Int. Ed*. **2010**, *49*, 3638.

[6] Q. Zhang, M.-Q. Zhao, D.-M. Tang, F. Li, J.-Q. Huang, B. Liu, W.-C. Zhu, Y.-H. Zhang, F. Wei, *Angew. Chem*. **2010**, *122*, 3724; *Angew. Chem. Int. Ed.* **2010**, *49*, 3642.

[7] R. Nesper, Prog. *Solid State Chem.* **1990**, *20*,1.

[8] J. K. Olson, A. I. Boldyrev, *Chem. Phys. Lett*. **2012**, *523*, 83.

[9] A. P. Sergeeva, B. B. Averkiev, H. J. Zhai, A. I. Boldyrev, L. S. J. Wang, J. *Chem. Phys*. **2011**, *134*, 224304.

[10] D. G. Truhlar, *Chem. Phys. Lett*. **1998**, *294*, 45.

[11] F. A. Cotton, G. Wilkinson, C. A. Murillo, M. Bochmann, *Advanced Inorganic Chemistry, 6 ed*., Wiley, New-York, **1999**, pp. 499 – 502.

[12] O. Degtyareva, E. Gregoryanz, M. Somayazulu, P. Dera, H. K. Mao, R. J. Hemley, *Nat. Mater*. **2005**, *4*, 152.

[13] Z. Wang, Y. Wang, G. Zou, H.-K. Mao, Y. Ma, *Proc. Natl. Acad. Sci. USA* **2012**, *109*, 751.

[14] J. Sun, M. Martinez-Canales, D. D. Klug, C. J. Pickard, R. J. Needs, *Phys. Rev. Lett.* **2012**, *108*, 045503.

[15] J. P. Foster, F. Weinhold, J. *Am. Chem. Soc*. **1980**, *102*, 7211.

[16] R. Hoffmann, P. v. R. Schleyer, H. F. Schaefer III, *Angew. Chem.* **2008**, *120*, 7276; *Angew. Chem. Int. Ed.* **2008**, *47*, 7164.

[17] A. E. Kuznetsov, K. A. Birch, A. I. Boldyrev, X. Li, H.-J. Zhai, L. S. Wang, *Science* **2003**, *300*, 622.

[18] T. R. Galeev, C. Romanescu, W.-L. Li, L. S. Wang, A. I. Boldyrev, Angew. *Chem. Int. Ed*. **2012**, *51*, 2101.

[19] D. T. Cromer, *Acta Cryst*. **1959**, *12*, 36.

[20] D. T. Cromer, *Acta Cryst*. **1959**, *12*, 41.

[21] C. X. Cui, M. Kertesz, J. *Am. Chem. Soc*. **1989**, *111*, 4216.

[22] C. J. Pickard, R. J. Needs, *Phys. Rev. Lett.* **2006**, *97*, 045504.

[23] C. J. Pickard, R. J. Needs, J. *Phys. Condens. Matter* **2011**, *23*, 053201.

[24] W. Hçnle, H. G. von Schnering, *Z. Kristallogr.* **1981**, *155*, 307.

[25] H. G. von Schnering, W. Hoenle, Z. *Anorg. Allg. Chem.* **1979**, *456*, 194.

[26] M. J. Frisch, G. W. Trucks, H. B. Schlegel, G. E. Scuseria, M. A. Robb, J. R. Cheeseman, G. Scalmani, V. Barone, B. Mennucci, G. A. Petersson, H. Nakatsuji, M. Caricato, X. Li, H. P. Hratchian, A. F. Izmaylov, J. Bloino, G. Zheng, J. L. Sonnenberg, M. Hada, M. Ehara, K. Toyota, R. Fukuda, J. Hasegawa, M. Ishida, T. Nakajima, Y. Honda, O. Kitao, H. Nakai, T. Vreven, J. A. Montgomery, Jr., J. E. Peralta, F. Ogliaro, M. Bearpark, J. J. Heyd, E. Brothers, K. N. Kudin, V. N. Staroverov, R. Kobayashi, J. Normand, K. Raghavachari, A. Rendell, J. C. Burant, S. S. Iyengar, J. Tomasi, M. Cossi, N. Rega, J. M. Millam, M. Klene, J. E. Knox, J. B. Cross, V. Bakken, C. Adamo, J. Jaramillo, R. Gomperts, R. E. Stratmann, O. Yazyev, A. J. Austin, R. Cammi, C. Pomelli, J. W. Ochterski, R. L. Martin, K. Morokuma, V. G. Zakrzewski, G. A. Voth, P. Salvador, J. Dannenberg, S. Dapprich, A. D. Daniels, Ö. Farkas, J. B. Foresman, J. V. Ortiz, J. Cioslowski, and D. J. Fox, *Gaussian, Inc.*, Wallingford, CT, **2009**.

[27] U. Varetto, *Molekel 5.4.0.8*, Swiss National Supercomputing Centre: Manno, Switzerland, **2009**.

[28] S. J. Clark, M. D. Segall, C. J. Pickard, P. J. Hasnip, M. I. J. Probert, K. Refson, M. C. Payne, *Z. Kristallogr*. **2005**, *220*, 567.

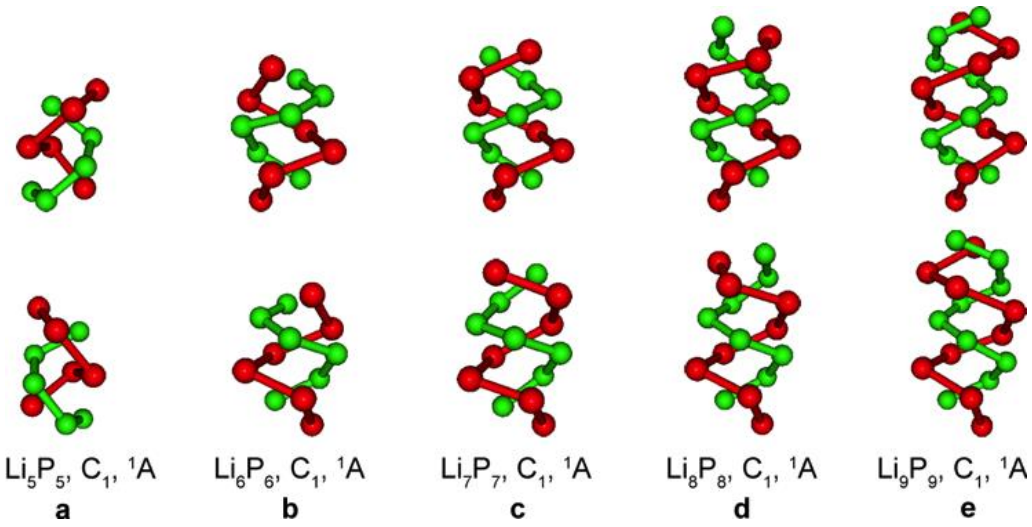

Figure 7-1. Optimized structures of Li_5P_5, Li_6P_6, Li_7P_7, Li_8P_8 and Li_9P_9 helices. a) Li_5P_5 (C_1, ^1A), b) Li_6P_6 (C_1, ^1A), c) Li_7P_7 (C_1, ^1A), (d) Li_8P_8 (C_1, ^1A), e) Li_9P_9 (C_1, ^1A).

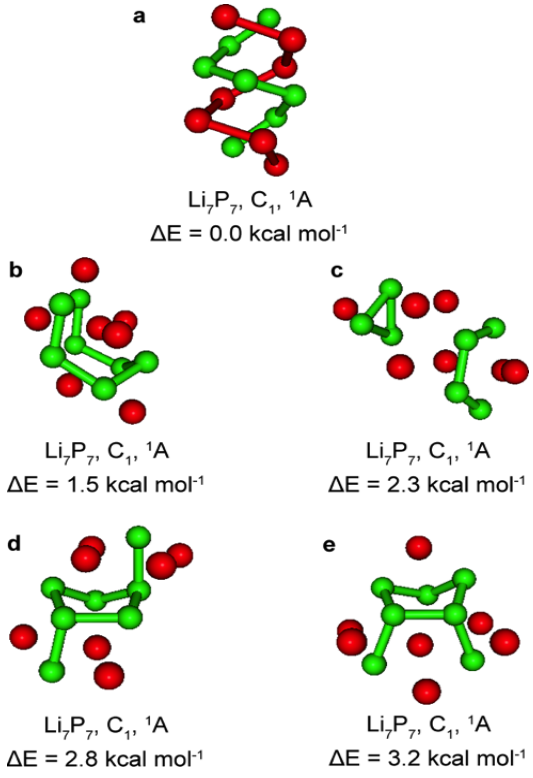

Figure 7-2. Representative optimized structures of Li_7P_7, their point group symmetries, spectroscopic states, and zero-point energy (ZPE) corrected (B3LYP/6-311+G*) relative energies at the CCSD(T)/CBS//B3LYP/6-311+G* level of theory.

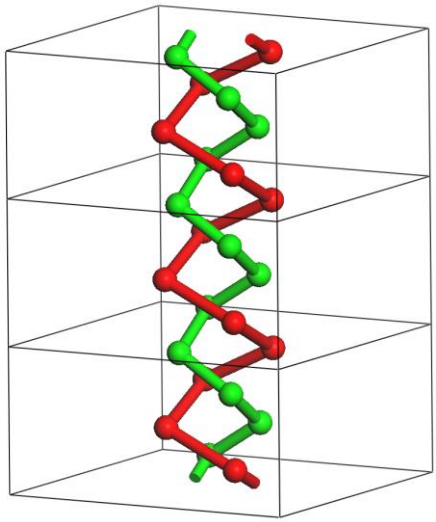

Figure 7-3. Three periodic repetitionsof the LiP infinite double-helix chain geometry optimized at the DFT-PBE level of theory.

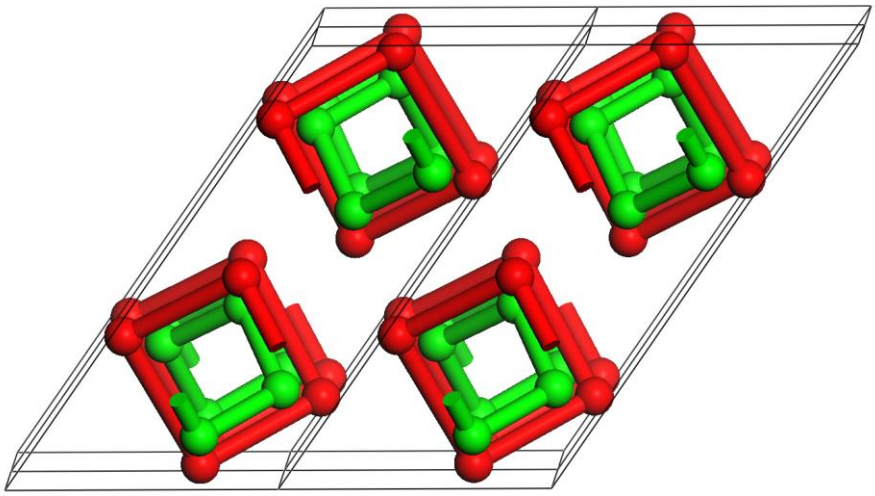

Figure 7-4. A 2X2 supercell containing a *P*21/*c* symmetric Li_1P_1 bulk phase comprising of packed double helices.

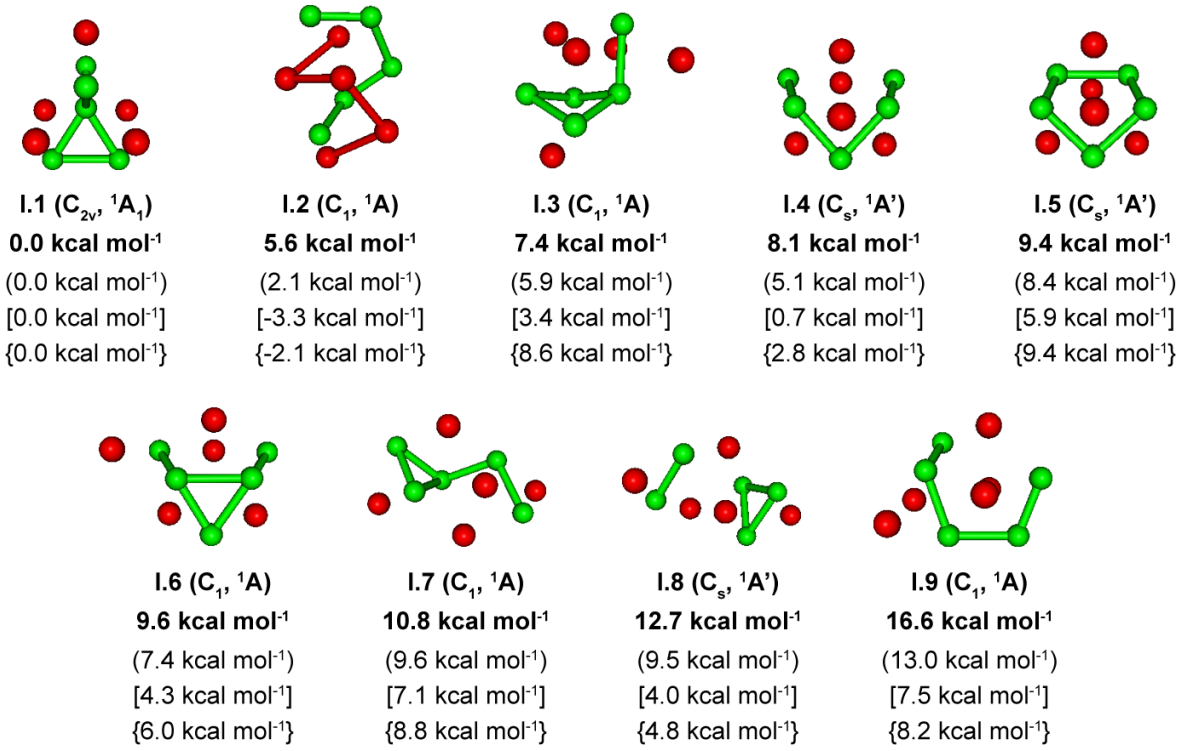

Figure 7-5. Lowest-lying structures of Li_5P_5, their point group symmetries, spectroscopic states and ZPE corrected relative energies. The energies are given at: CCSD(T)/CBS (bold), CCSD(T)/cc-pvTZ (in brackets), CCSD(T)/cc-pvDZ (square brackets), and B3LYP/6-311+G* (curly brackets) levels of theory, all at B3LYP/6-311+G* optimized geometries.

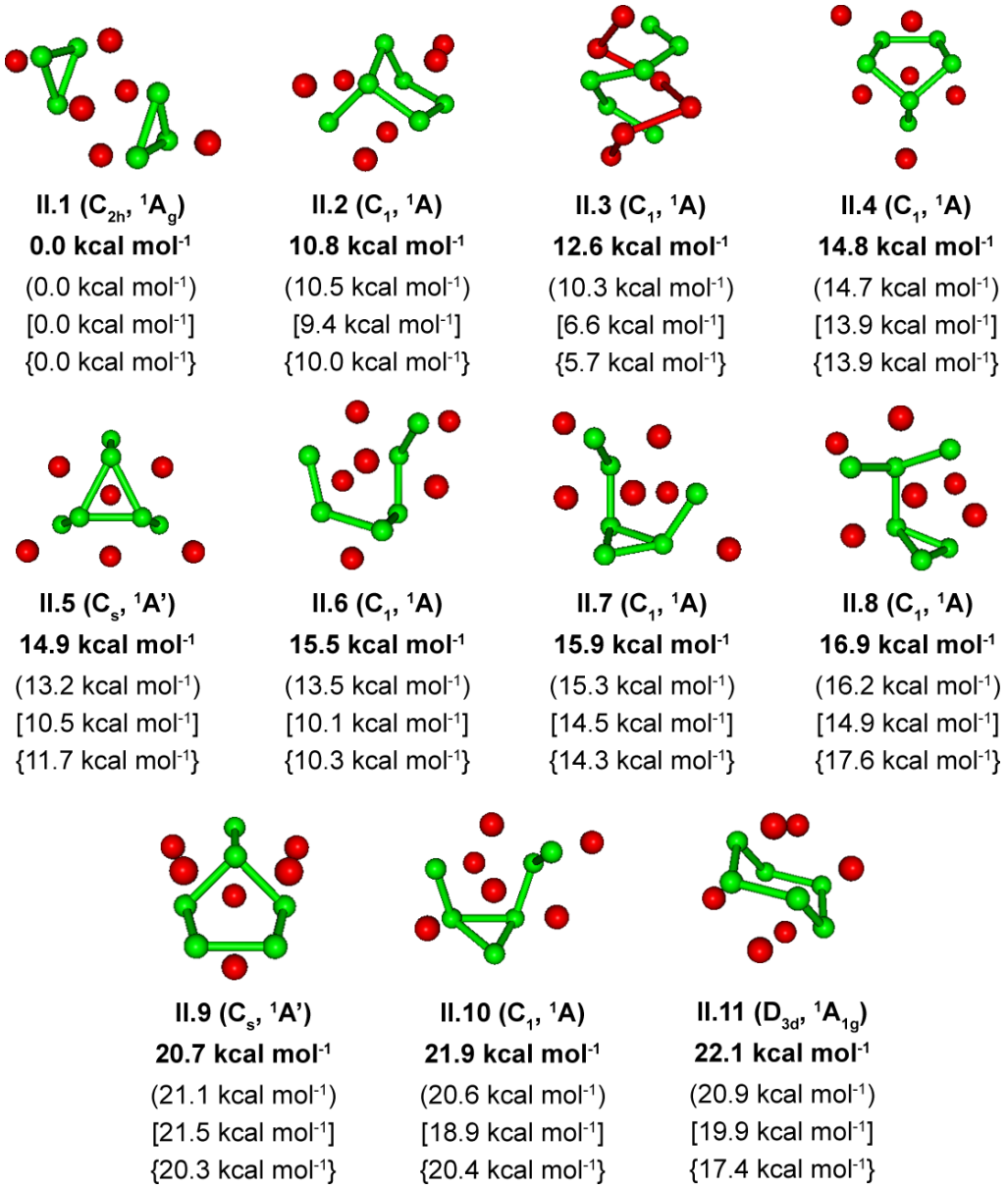

Figure 7-6. Lowest-lying structures of Li_6P_6, their point group symmetries, spectroscopic states and ZPE corrected relative energies. The energies are given at: CCSD(T)/CBS (bold), CCSD(T)/cc-pvTZ (in brackets), CCSD(T)/cc-pvDZ (square brackets), and B3LYP/6-311+G* (curly brackets) levels of theory, all at B3LYP/6-311+G* optimized geometries.

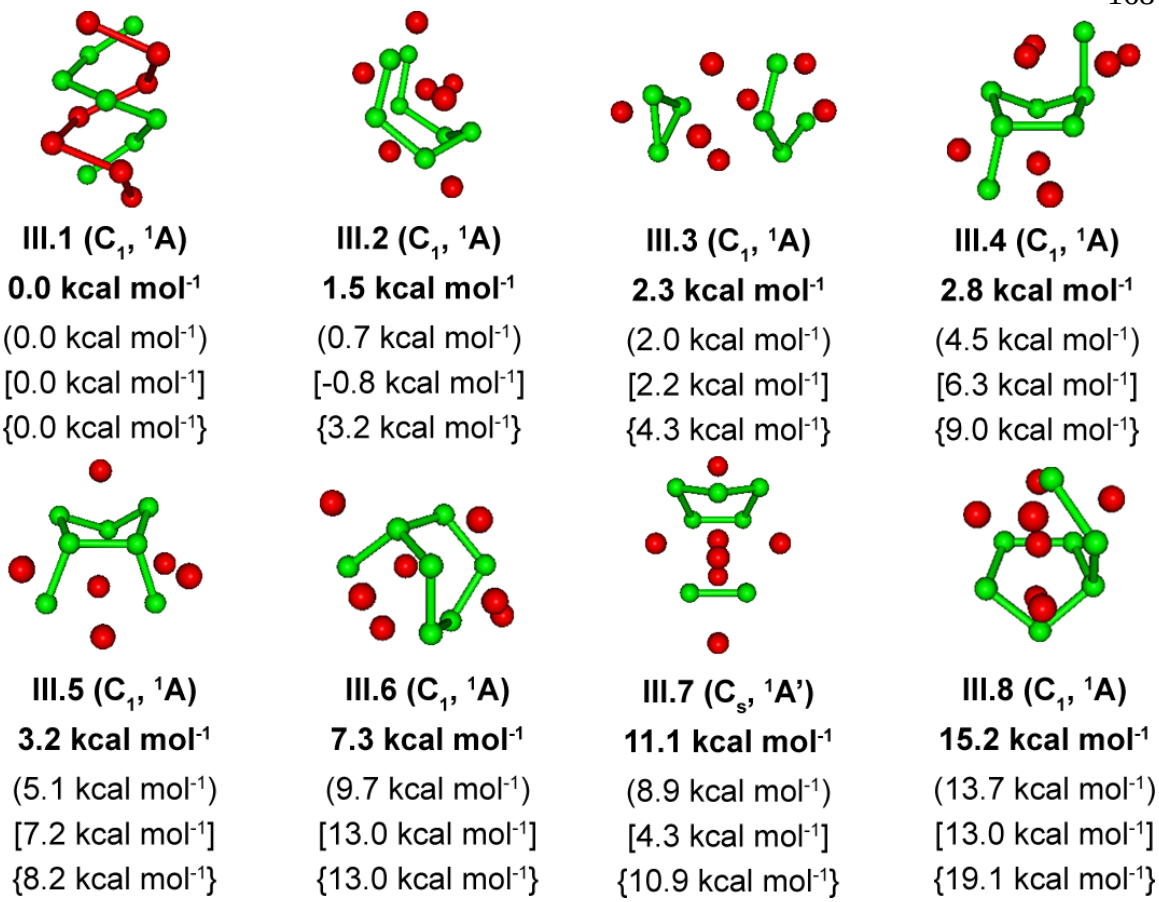

Figure 7-7. Lowest-lying structures of Li_7P_7, their point group symmetries, spectroscopic states and ZPE corrected relative energies. The energies are given at: CCSD(T)/CBS (bold), CCSD(T)/cc-pvTZ (in brackets), CCSD(T)/cc-pvDZ (square brackets), and B3LYP/6-311+G* (curly brackets) levels of theory, all at B3LYP/6-311+G* optimized geometries.

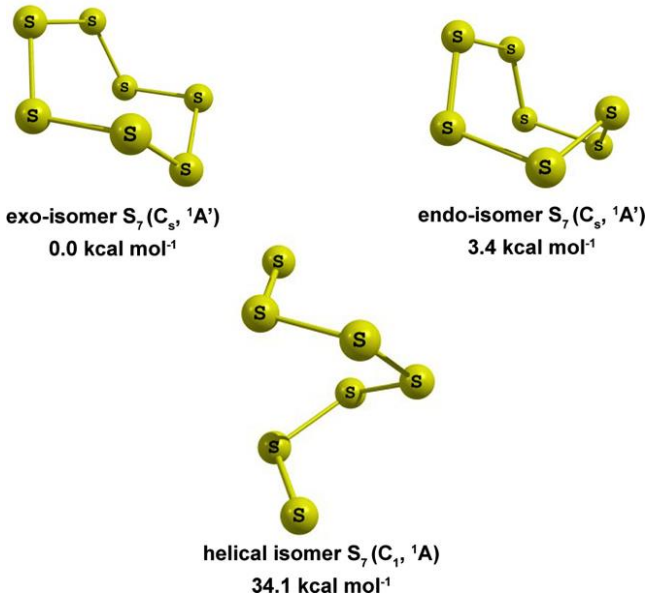

Figure 7-8. Global minimum exo and edo isomers of S_7 and helical isomer S_7, their point group symmetries, spectroscopic states and ZPE corrected relative energies. The energies are given at B3LYP/6-311+G* level of theory, all at B3LYP/6-311+G* optimized geometries.

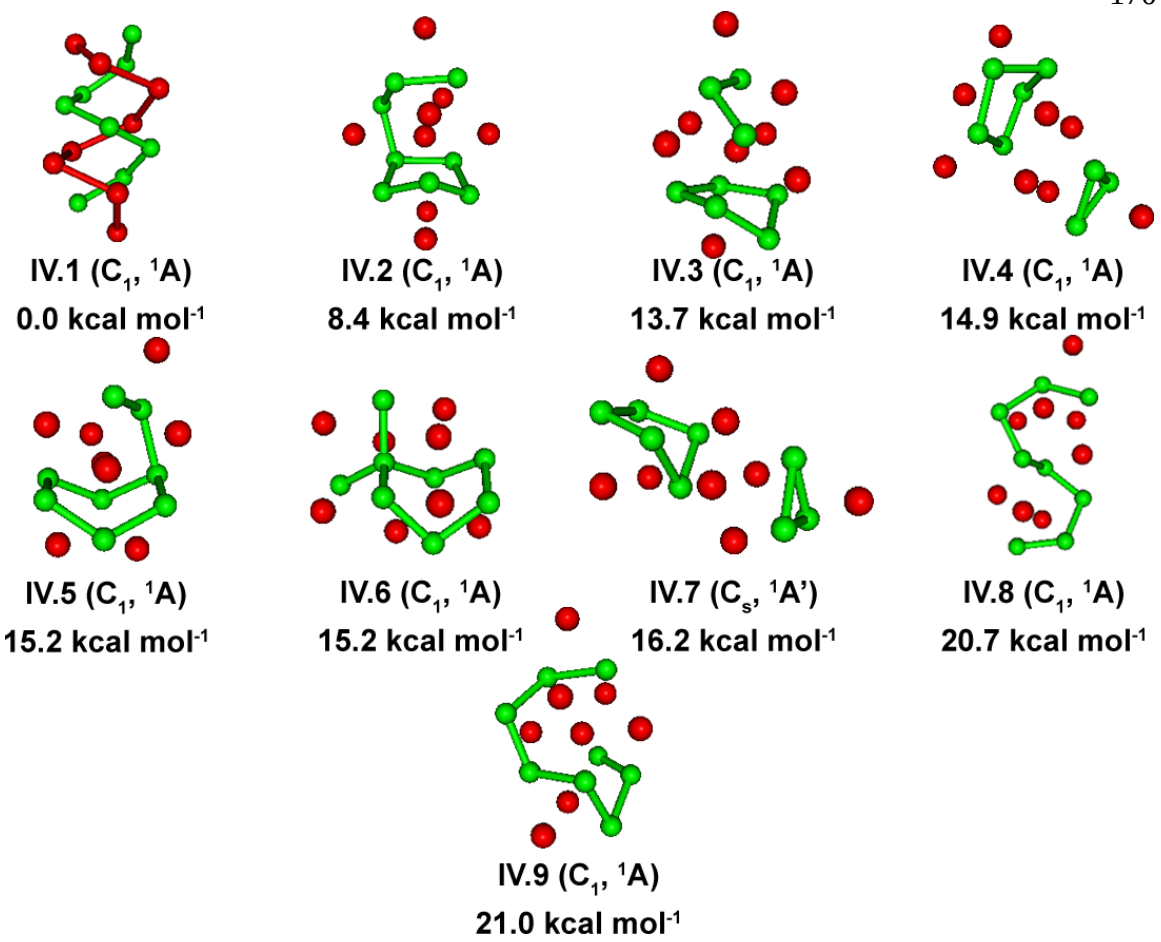

Figure 7-9. Lowest-lying structures of Li_8P_8, their point group symmetries, spectroscopic states and ZPE corrected relative energies. The energies are given at the B3LYP/6-311+G* level of theory, all at B3LYP/6-311+G* optimized geometries.

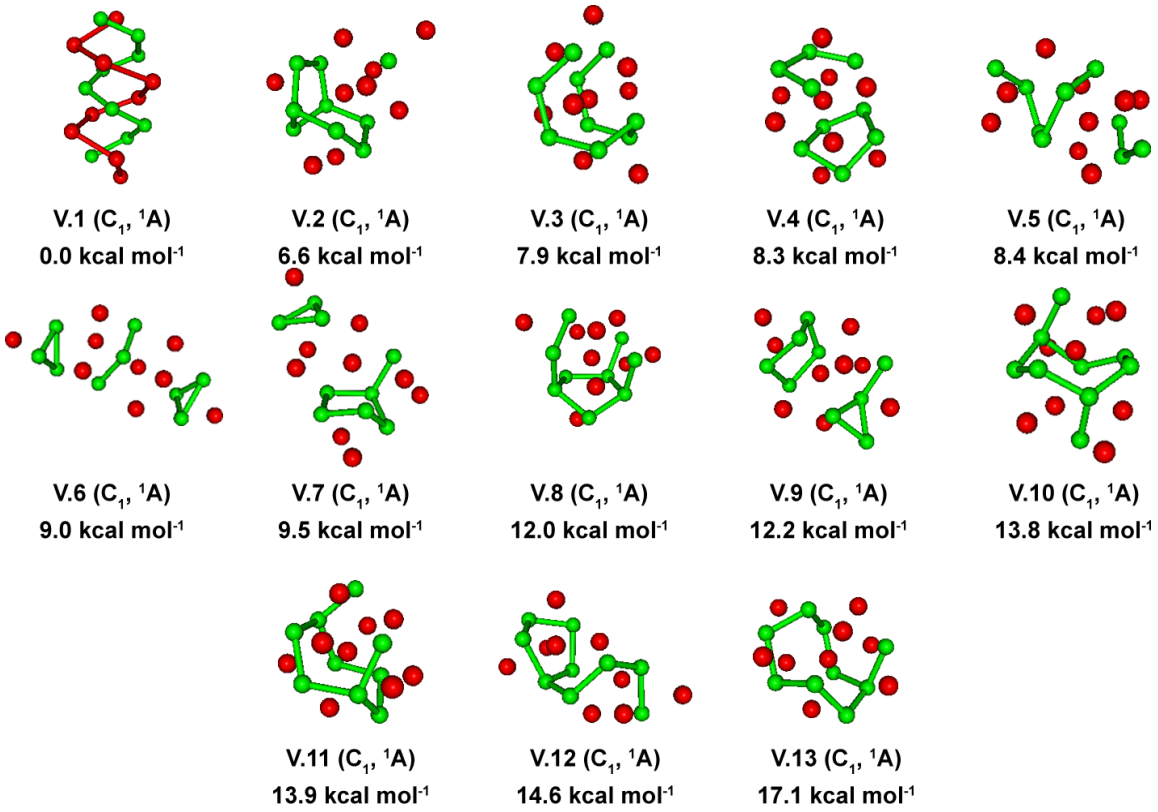

Figure 7-10. Lowest-lying structures of Li_9P_9, their point group symmetries, spectroscopic states and ZPE corrected relative energies. The energies are given at the B3LYP/6-311+G* level of theory, all at B3LYP/6-311+G* optimized geometries.

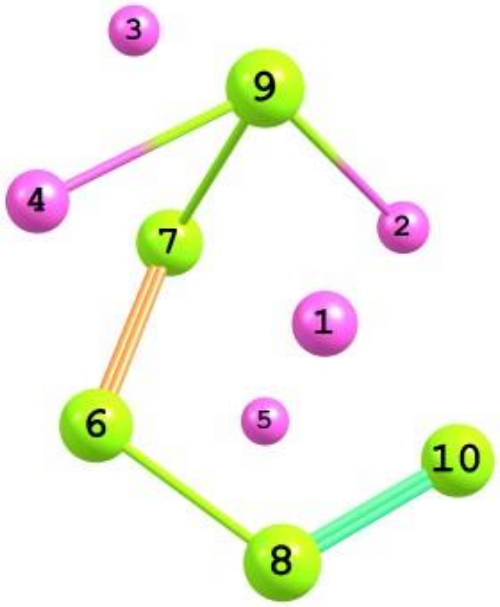

Figure 7-11. The results of NBO analysis for L_5P_5 double helix structure (here and elsewhere P is green, Li is violet).

NBO analysis recovered: two Li-P σ-bonds: Li4-P9 (ON=1.84 |e|) and Li2-P9 (ON=1.86 |e|), though they are essentially lone pairs on P9 atom [Li (7%), P (93%)]; four P-P σ-bonds (ON=1.92-1.96 |e|); three P-P π-bonds (ON=1.34-1.83 |e|); lone pairs on phosphorus atoms: one lone pair on P6 (ON=1.89 |e|), one lone pair on P7 (ON=1.84 |e|), one lone pair on P8 (ON=1.92 |e|), one lone pair on P9 (ON=1.63 |e|), two lone pairs on P10 (ON=1.60-1.89 |e|).

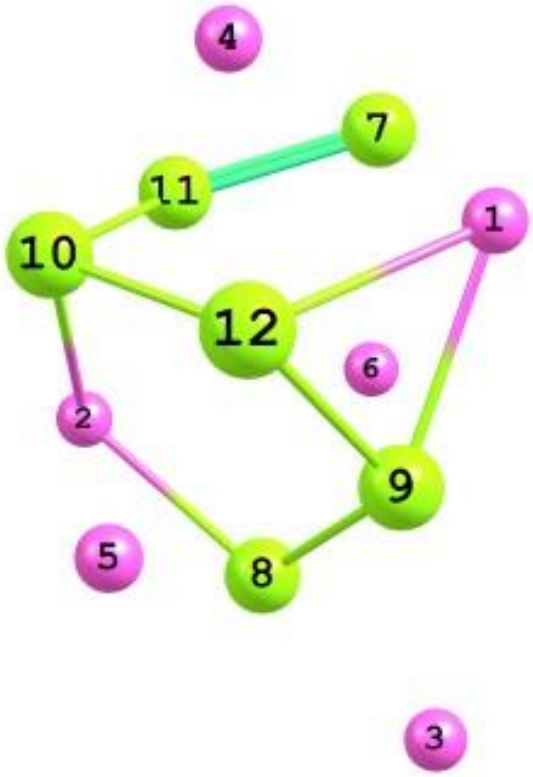

Figure 7-12. The results of NBO analysis for L_6P_6 double helix structure.

NBO analysis recovered: four Li-P σ-bonds: Li1-P9 (ON=1.65 |e|), Li1-P12 (ON=1.68 |e|), Li2-P10 (ON=1.64 |e|), Li2-P8 (ON=1.63 |e|), though they are essentially lone pairs on P8 [Li(3%), P(97%)], P9 [Li(4%), P(96%)], P10 [Li(4%), P(96%)], and P12 [Li(5%), P(95%)] atoms; five P-P σ-bonds (ON=1.94-1.96 |e|); one P11-P7 π-bond (ON=1.86 |e|); lone pairs on phosphorus atoms: two lone pairs on P7 (ON=1.64-1.87 |e|), two lone pairs on P8 (ON=1.70-1.79 |e|), one lone pair on P9 (ON=1.82 |e|), one lone pair on P10 (ON=1.85 |e|), one lone pair on P11 (ON=1.85 |e|), one lone pair on P12 (ON=1.86 |e|).

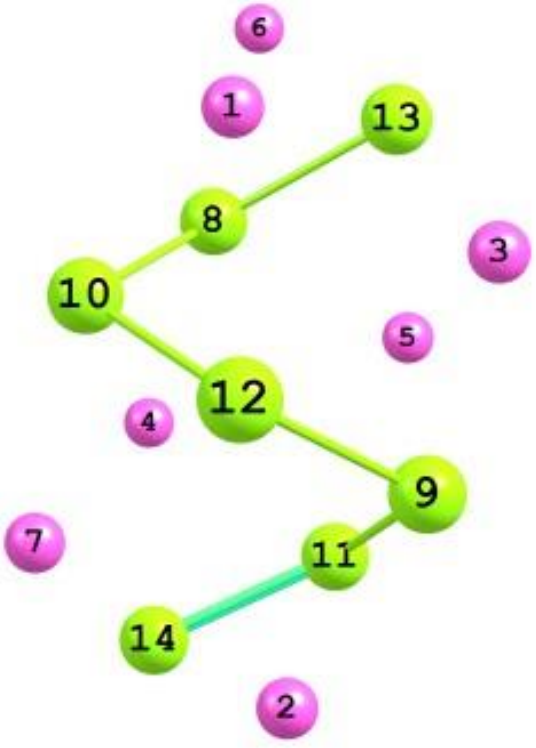

Figure 7-13. The results of NBO analysis for L_7P_7 double helix structure.

NBO analysis recovered: six P-P σ-bonds (ON=1.95-1.98 |e|); one P11-P14 π-bond (ON=1.94 |e|); lone pairs on phosphorus atoms: two lone pairs on P8 (ON=1.7-1.90 |e|), two lone pairs on P9 (ON=1.70-1.90 |e|), two lone pairs on P10 (ON=1.70-1.90 |e|), one lone pair on P11 (ON=1.91 |e|), two lone pairs on P12 (ON=1.74-1.93 |e|), three lone pairs on P13 (ON=1.75-1.90 |e|), two lone pairs on P14 (ON=1.78-1.91 |e|).

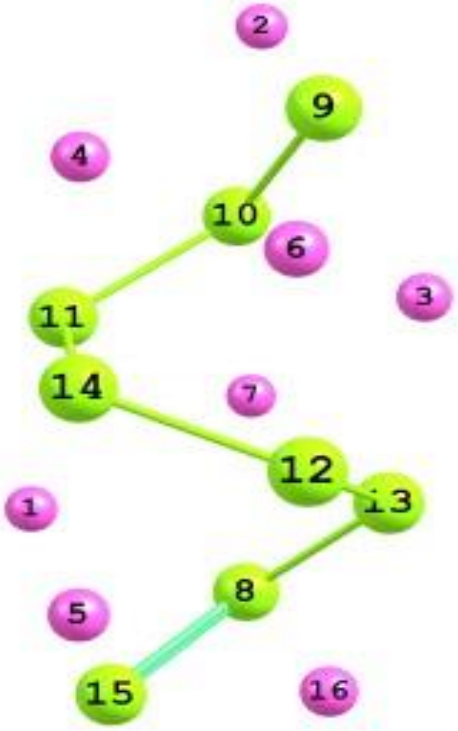

Figure 7-14. The results of NBO analysis for L_8P_8 double helix structure.

NBO analysis recovered: seven P-P σ-bonds (ON=1.95-1.98 |e|); one P8-P15 π-bond (ON=1.93 |e|); lone pairs on phosphorus atoms: one lone pair on P8 (ON=1.92 |e|), three lone pairs on P9 (ON=1.75-1.90 |e|), two lone pairs on P10 (ON=1.81-1.91 |e|), two lone pairs on P11 (ON=1.70-1.90 |e|), two lone pairs on P12 (ON=1.78-1.91 |e|), three lone pairs on P13 (ON=1.61-1.90 |e|), two lone pairs on P14 (ON=1.77-1.90 |e|), two lone pairs on P15 (ON=1.76-1.91 |e|).

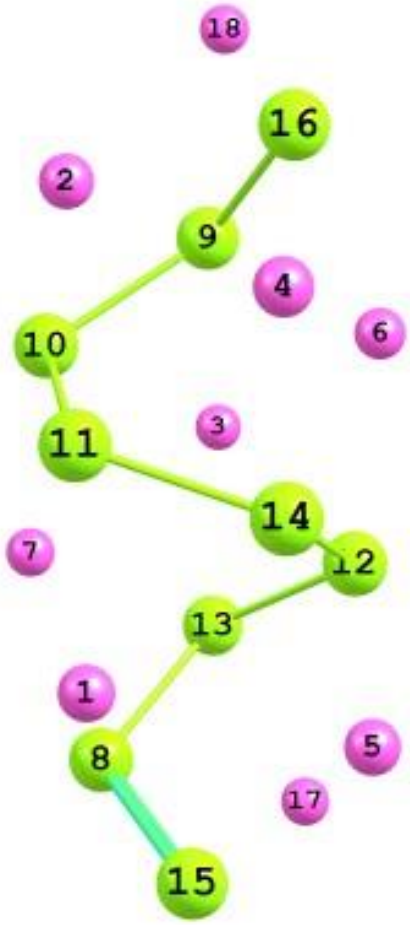

Figure 7-15. The results of NBO analysis for L_9P_9 double helix structure.

NBO analysis recovered: eight P-P σ-bonds (ON=1.95-1.98 |e|); one P8-P15 π-bond (ON=1.94 |e|); lone pairs on phosphorus atoms: one lone pair on P8 (ON=1.91 |e|), two lone pairs on P9 (ON=1.86-1.90 |e|), two lone pairs on P10 (ON=1.77-1.90 |e|), two lone pairs on P11 (ON=1.74-1.90 |e|), two lone pairs on P12 (ON=1.72-1.90 |e|), two lone pairs on P13 (ON=1.65-1.90 |e|), two lone pairs on P14 (ON=1.76-1.88 |e|), two lone pairs on P15 (ON=1.77-1.91 |e|), three lone pairs on P16 (ON=1.76-1.90 |e|),

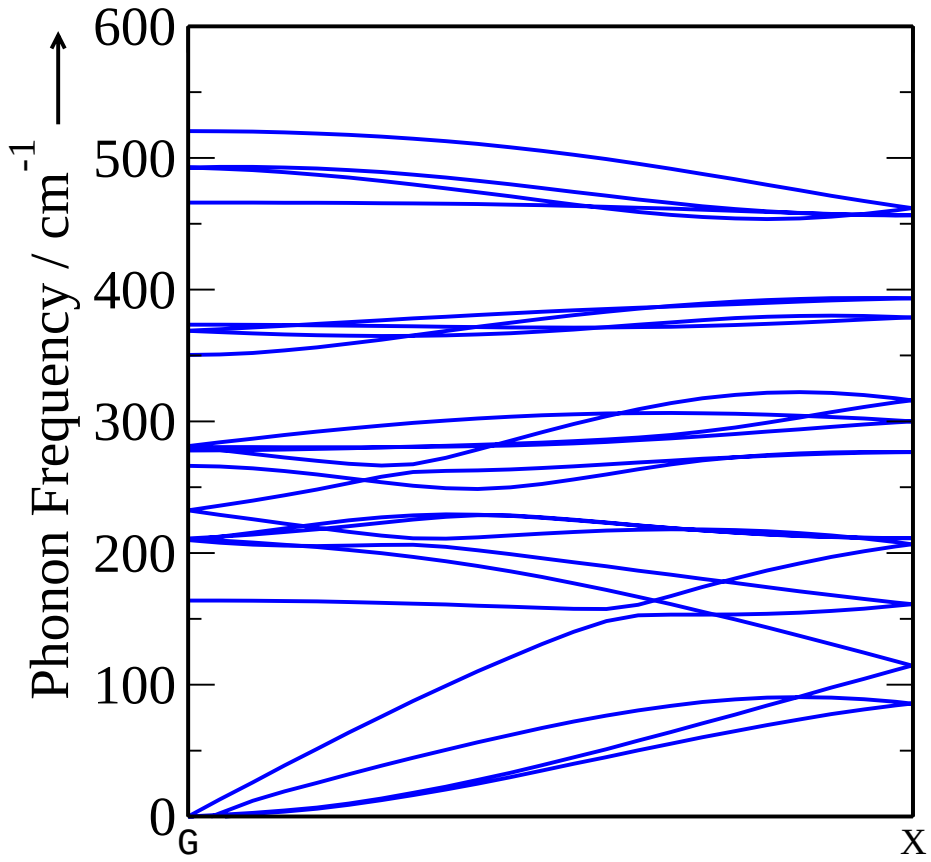

Figure 7-16. Phonon dispersion of the infinite chain using the local-density approximation and norm-conserving pseudopotentials with a basis set containing plane-waves with energies up to 500 eV. The structure is stable to distortions hence a local minimum. There is a vibrational mode with small negative frequency (~ -6 cm^{-1}) at the Gamma point, which is a torsional mode associated with the orientation of the chain within the finite supercell.

CHAPTER 8

INORGANIC DOUBLE-HELIX NANOTOROID OF SIMPLE LITHIUM-PHOSPHORUS SPECIES[1]

Abstract

A theoretical study of $Li_{90}P_{90}$, which possesses a circular double-helix structure that resembles the Watson–Crick DNA structure, is reported. This is a new bonding motif in inorganic chemistry. The calculations show that the molecule might become synthesized and that it could be a model for other inorganic species which possess a double-helix structure.

8-1. Introduction

When most people think of a double helix, they think of DNA structure—a now familiar image, thanks to Watson and Crick's landmark 1953 discovery of the double-stranded molecules of nucleic acids.[1] It was initially believed that all DNA molecules are linear and have two free ends. Indeed, the chromosomes of eukaryotic cells each contain a single (extremely long) DNA molecule. But now we know that some DNAs are circles. For example, the chromosome of the small monkey DNA virus SV40[2] is a circular, double-helical DNA molecule of about 5000 base pairs. Also, most (but not all) bacterial chromosomes are circular; *Escherichia coli* has a circular chromosome of about five million base pairs.[3] Additionally, many bacteria have small autonomously replicating genetic elements known as plasmids,[4] which are generally circular DNA

[1] Coauthored by Alexander S. Ivanov, Alexander I. Boldyrev, and Gernot Frenking. Reprinted with permission from *Chem. Eur. J.* **2014**, 20, 2431 – 2435. Copyright © 2014 Wiley-VCH Verlag GmbH & Co. KGaA, Weinheim.

molecules. The distinctive feature of closed circular molecules is that its topological state cannot be altered by any conformational rearrangement short of breaking DNA strands. This topological constraint is the basis for the characteristic properties of closed circular DNA, which have fascinated biologists, chemists, physicists and mathematicians for the past 50 years.

The double-helix and circular double-helix geometric structures play a significant role in metabolism and evolution. Although they appear in great and small forms in varied organisms and viruses, they are very rare in inorganic chemistry. After the introduction of the first inorganic doubly stranded helicate by Lehn et al.[5] in 1987, a number of artificial single-helical supramolecular assemblies[6-12] based on different predesigned ligands have been extensively reported due to both their aesthetically appealing topologies and their potential applications, such as asymmetric catalysis and nonlinear optical materials. Thus, while some advances have been achieved for inorganic materials with a single-helical geometry, reports of counterparts with double-helix structure are deficient, not to mention circular double-helix structures. It seems that, because of the lack of guiding principles for the construction of toroids, researchers have not widely studied the self-assembly of toroidal nanostructures compared with the work on other supramolecular architectures. Besides synthesized metal string complexes $[Ni_4(\mu_4\text{-phdpda})_4]$ and $[Ni_7Cl_2(\mu_7\text{-teptra})_4]$[13] ($H_2$phdpda=*N*-phenyldipyridyldiamine and H_3teptra=tetrapyridyltriamine) with the ligands wrapping themselves around the metal wire in a helical arrangement, we were not able to find any examples of inorganic double-helical ring structure in the literature.

In 1959 Cromer determined the crystal structures of LiAs and NaSb.[14,15] It was found that LiAs and NaSb represent monoclinic solids with eight formula units in space group *P*21/*c*. The arsenic and antimony atoms form singly bonded infinite spiral chains in the corresponding structures, whereas the lithium and sodium atoms are in positions defined approximately by a spiral coaxial with the arsenic and antimony chains, respectively, but with a larger radius. Recently, we published a study[16] that reported the first theoretical evidence of the existence of small inorganic double-helix Li_nP_n chiral clusters. For Li_7P_7—Li_9P_9 stoichiometries the global minimum structure has a peculiar double-helix form containing two strands, one composed of lithium cations and one composed of phosphorus anions, which run in opposite directions to each other and are therefore antiparallel. To further investigate the existence of the double helices in the solid state, we performed an ab initio random solid-state structure search using the AIRSS program.[17.18] We recovered the *P*21/*c* symmetric Li_1P_1 bulk phase comprising of packed double helices in which adjacent helices are of opposite sense and 9.69 kcal mol^{-1} lower in energy than the infinite double-helix chain.[16] Later, Datta et al.[19] analyzed the nature of bonding in these Li_nP_n (n=7–9) double helices. It was shown that the simple inorganic double helices present a bonding picture very similar to that of nature's double-helical DNA. Analogous to DNA, which is stabilized by interstrand H bonding and intrastrand base stacking, Li_nP_n strands are held together by weak Li—P and P—P noncovalent interactions. It is known that in some cases DNA is able to circularize by base-pairing between single-stranded regions that protrude from the ends of the DNA and that have complementary sequences. Taking cues from nature, a few interesting questions arise concerning inorganic Li_nP_n double helix motif: is it possible to design a

circular inorganic double helix, would it be stable and what kind of chemical bonding would play a major role in its stabilization?

Here we report theoretical results on the existence of the first stable inorganic double-helix toroid made of remarkably simple lithium—phosphorus (Li—P) species. The predicted structure comprises two antiparallel strands of 90 Li and 90 P atoms with the linking number (the number of times one strand would have to be passed through the other strand in order for the two strands to be entirely separated from each other) of 18 (Figure 8-1). Therefore, it can be considered as chiral, topologically constrained (two ends of a double-helix structure are covalently closed to form a circle) molecule. In this study, we investigate the structural stability, electronic properties, and chemical bonding of this $Li_{90}P_{90}$ inorganic circular double-helix structure using quantum chemical density functional theory (DFT) and solid state calculations.

8-2. Results and discussion

We modeled the $Li_{90}P_{90}$ toroid-like structure with the anticipation that the large circle of ninety Li_1P_1 units will be stable due to low strain energy in such a ring. Indeed using the B3LYP/STO-3G level of theory, we found that the "donut" structure is a minimum on the potential energy surface, which possesses C_6 symmetry (Figure 8-5). We then reoptimized $Li_{90}P_{90}$ with follow-up frequency calculations using different pure/hybrid exchange-correlation potentials and larger basis sets in order to assess the stability of the $Li_{90}P_{90}$ toroid structure at various levels of theory (see the Experimental Section). The $Li_{90}P_{90}$ structure was found to be stable in all cases. It should be noted that the exact number of atoms (90 Li and 90 P) may be not critical in the stability of the circular arrangement and analogous double-helical toroids with smaller or larger number

of Li and P atoms can possibly be found. However, in this work our aim is not finding the smallest or largest size at which the ring of Li and P atoms would be stable, but to show the possibility of the existence of such double-helical toroids. Figure 8-1 shows the double-helical ring of $Li_{90}P_{90}$ at the BP86/6-31G(d) level of theory. The results obtained at B3LYP/6-31G(d) are summarized in Figure 8-5. It is interesting to note that the double-helical toroid exhibits C_2 symmetry at BP86/6-31G(d), however, the deviation from the C_6 atomic orientation is quite low (0.0056 Å; Figure 8-1).

We compared the structural parameters of $Li_{90}P_{90}$ circular double helix with smaller straight double helices: Li_7P_7, Li_8P_8, Li_9P_9 (global minimum structures for their stoichiometries), and the infinite chain of Li and P atoms, which was also found to be stable.[16] The values of the corresponding distances between adjacent P—P, Li—Li atoms and Li—P atoms of the opposite Li and P strands are summarized in Table 8-1. The P—P distance for all helices, including the LiP infinite double-helix chain (not shown in Table 8-1) with a P—P distance of 2.25 Å (optimized using solid-state calculations and plane-wave density functional theory)[16] is about the same, apart from one P—P terminal π bond distance (~2.13 Å) that is present in Li_7P_7—Li_9P_9 helical structures. The same trend is traced in the distances between corresponding Li and P atoms of the opposite Li and P chains. However, in the $Li_{90}P_{90}$ ring structure, the distance between two Li atoms is a little bit lower than for the infinite LiP and Li_7P_7—Li_9P_9 structures.

The calculated harmonic vibrational frequencies of $Li_{90}P_{90}$ at the BP86/6-31G(d) level of theory are shown in Figure 8-2. Imaginary vibrational frequencies have not been observed at another level of theory (B3LYP/6-31G(d)), verifying that our structure is

indeed a local minimum. The highest occupied molecular orbital–lowest unoccupied molecular orbital (HOMO–LUMO) energy separation serves as a simple measure of chemical stability.[20] The calculated HOMO–LUMO energy gap for our circular double helix is relatively large, ΔHL=1.08 eV, conferring stability on the $Li_{90}P_{90}$ cluster. The first electron excitation from the simulated time-dependent DFT (TD-DFT) spectrum of $Li_{90}P_{90}$ (Figure 8-7) is 1.09 eV, which is consistent with the HOMO–LUMO gap value. In addition, vertical ionization potential is 4.12 eV, and vertical electron affinity is 1.93 eV.

Since we established the link between straight Li*n*P*n* double-helical chains and circular $Li_{90}P_{90}$ double-helix structure, it is useful to compare their relative stability. We made additional calculations on some $Li_{10}P_{10}$, $Li_{11}P_{11}$, $Li_{13}P_{13}$, $Li_{14}P_{14}$, $Li_{20}P_{20}$, $Li_{21}P_{21}$, $Li_{22}P_{22}$, $Li_{25}P_{25}$, $Li_{27}P_{27}$, $Li_{30}P_{30}$, $Li_{35}P_{35}$, $Li_{40}P_{40}$ clusters at the BP86/6-31G(d) level of theory. We have plotted the cohesive energy (E_c) of several Li*n*P*n* structures versus the number of Li_1P_1 units (*n*; see the Experimental Section for details) in Figure 8-3. In the same figure we have also included the E_c value of $Li_{90}P_{90}$ double-helical toroid. From Figure 8-3 we can see that the E_c values of Li*n*P*n* chains monotonically increase from the value of 5.23 eV per unit for the smallest Li_5P_5 helix to the value of 5.87 eV per unit for the infinite length LiP double helix (shown by the dotted horizontal line). Consequently, the most stable structure among all straight Li*n*P*n* helices is the infinite chain (computed with the same method). We were not able to obtain E_c value for the $Li_{90}P_{90}$ stick, because in the process of optimization it started to bend and we did not achieve any local minima. However, according to the curve that shows a trend line in our graph (Figure 8-3), the $Li_{90}P_{90}$ double-helical toroid (E_c=5.75 eV per unit) is lying lower in energy than the

possible $Li_{90}P_{90}$ stick and only 0.12 eV less stable than the infinite chain of lithium and phosphorus atoms (E_c=5.87 eV per unit). The limit for the stability of all double helices is symmetric Li_1P_1 bulk phase composed of packed double helices and it is 9.69 kcal mol^{-1} lower in energy than the infinite double-helix chain.[16]

In order to gain additional insight into the structure and chemical bonding in the double-helix toroid-like structure of Li—P species, we performed natural bond orbital (NBO)[21] and adaptive natural density partitioning (AdNDP)[22] analyses. According to the NBO analysis of the $Li_{90}P_{90}$ circular double-helix structure, bonding between lithium and phosphorus atoms is quite ionic with effective atomic charges ranging from +0.5 to +0.7 and −0.4 to −0.8 on Li and P, respectively. Additionally, NBO analysis revealed the presence of ninety P—P σ bonds with occupation numbers (ON) equal to 1.92–1.95 |e|, and two lone pairs of s- and p-type on each phosphorus atom with ON ranging from 1.72 to 1.84 |e|. The results of the AdNDP analysis are generally in agreement with the NBO results (Figure 8-4). According to the Zintl concept[23] $Li_{90}P_{90}$ is an electron balanced structure, having two homonuclear bonds and two electron lone pairs, thus realizing an electron octet. Therefore, Li*x*P*x* helices are isoelectronic to sulfur S*x* compounds. However, the coil formation is unlikely for S contrary to Li*x*P*x*. In order to understand this phenomenon we analyzed chemical bonding (Figure 8-7) in a helical isomer of S_7 (isoelectronic to the smallest Li_7P_7 double helix) which is 34.1 kcal mol^{-1} higher in energy than the chair-like global minimum structure for S_7 stoichiometry. The AdNDP analysis for S_7 and Li_7P_7 revealed the same bonding pattern, however, the s- and p lone pairs of Li_7P_7 are more diffuse than that of S_7 due to the presence of lithium atoms, making Li*x*P*x* coil and form double helix, whereas S*x* have less tendency to do so. As one

can see, in Li_7P_7 double helix the electron transfer from Li to P is not complete and electron density is delocalized over both P and Li atoms. Therefore, the presence of particularly lithium, or other monovalent metal, seems to be a very important factor in phosphorus chain helical formation. Indeed, according to the crystal structures of different polyphosphides,[24] the infinite phosphorus (P^-) chains exhibit high configurational and conformational variability, which is dictated mostly by the size and coordination of surrounding metals.[25]

We estimated the stabilization energy $E^{(2)}$ for $Li_{90}P_{90}$ toroid using second-order perturbation theory, which is associated with electron delocalization between the donor and acceptor orbitals. The NBO analysis for $Li_{90}P_{90}$ toroid revealed some Li — P interactions that play an important role in stabilizing the circular double helix similar to Li_7P_7–Li_9P_9 helices.[19] The stabilization energy $E^{(2)}$ for $BD^*_{P\text{-}P} \rightarrow LP^*_{Li}$, $BD_{P\text{-}P} \rightarrow LP^*_{Li}$, and $LP_P \rightarrow LP^*_{Li}$ interactions vary from 1.2 to 1.8 kcal mol^{-1}, 9.3 to 18.6 kcal mol^{-1}, and 7.2 to 34.04 kcal mol^{-1}, respectively. For instance, the calculated energy sequence ($E_{n \rightarrow \sigma}$) of the H bonds stabilizing the adenine–thymine (A–T-OH_2^+) base pair, is almost in the same range (−14.5, −31.8, and −0.43 kcal mol^{-1} for N—H···O, N—H···N, and C—H···O interactions, respectively, at the B3P86/6-311++G(d,p) level).[26] Therefore, the Li—P interactions make a valuable impact in holding together the lithium and phosphorus strands of $Li_{90}P_{90}$ circular double helix similar to hydrogen bonds, which are important for stabilizing the 3D structure of DNA. The NBO analysis does not show any significant direct covalent bonding between Li atoms, and we think the formation of helical Li strand is due to favorable electrostatic interactions between lithium cations and neighboring phosphorus anions. However, the stabilization energies indicate significant interactions

among the Li atoms. Several $LP^*_{Li} \rightarrow LP^*_{Li}$ and $CR_{Li} \rightarrow LP^*_{Li}$ interactions with $E^{(2)}$ ranging from 6.4 to 80.2 kcal mol^{-1} and from 2.1 to 4.1 kcal mol^{-1} are observed for $Li_{90}P_{90}$. Overall, we see that the noncovalent P—P, Li—P, and Li—Li interactions significantly stabilize the circular double-helix framework, and that the ionic character of the system is responsible for wrapping Li and P helical strands around each other, forming a double-helical toroid-like structure.

8-3. Conclusions

There are no experimental reports about the existence of free double-helical Li_nP_n clusters. However, there are some facts related to this topic that should be noted. As it was mentioned, atomic chained helices were first found by Cromer in the Zintl phases, LiAs and NaSb[14,15] and exist in XY solids (X=Li, Na, K, Rb, Cs; Y=P, As, Sb).[27] The $Li_{90}P_{90}$ toroid is isoelectronic to the S_{90} cluster. It is well known that a chain of sulfur atoms could bite its own tail and produce a stable ring structure with the smallest unstrained ring consisting of only eight S atoms. Although the largest circular sulfur clusters experimentally identified so far contain no more than 18 atoms,[28] it is likely that with proper choice of conditions larger rings should form. The presented work on $Li_{90}P_{90}$ singles out the circular double helix as a stable cluster with unusual inorganic chemistry topology, and therefore suggests that it possibly appears as a result of self-assembly of lithium and phosphorus atoms, though such aggregation may only occur at rather specific experimental conditions, which cannot be derived from the present work. We believe that because of their small size and unique properties, clusters could become good samples for describing a structural model of the circular double helix at the atomic level. Thus, further investigation of the topologies of such clusters can provide a

fundamental approach towards the development of artificial double-helical toroids. If the inorganic $Li_{90}P_{90}$ toroid is confirmed experimentally, it would be the first example in nature, with a circular, unusually simple, bielemental, and distinctive double-helical structure.

8-4. Computational and theoretical methods

Additional calculations including geometry optimization and frequency calculations for the $Li_{90}P_{90}$ were performed at the BP86[29] and B3LYP[30] levels of theory using STO-3G,[31] 3-21G,[32] 6-31G, and 6-31G(d)[33,34] basis sets. The vertical electron affinity (VEA), and vertical ionization potential (VIP) were calculated at the BP86 level using 6-31G(d) basis set. The calculation of TD-DFT spectrum for $Li_{90}P_{90}$ was performed by BP86 functional (6-31G(d) basis set). The highest occupied molecular orbital lowest occupied molecular orbital (HOMO–LUMO) gap energy was obtained using HF/6-31G(d)//BP86/6-31G(d) level of theory. Chemical bonding analysis was performed using natural bond orbital (NBO)[21] and adaptive natural density partitioning (AdNDP)[22] methods. All quantum-chemical calculations were performed using the Gaussian 09 program.[35] Molecular visualization was performed utilizing the Chemcraft[36] and Molekel 4.3 programs.[37]

Cohesive energy was calculated using the following formula: $E_c(\mathrm{Li}n\mathrm{P}n)=E(\mathrm{Li})+\mathrm{E(P)}-E(\mathrm{Li}n\mathrm{P}n)$, where $E(\mathrm{Li}n\mathrm{P}n)$ is the total energy of Li*n*P*n*divided by number (n) of LiP units, E(Li) and E(P) are the total energies of isolated lithium and phosphorus atoms, respectively. Total energies for all structures were calculated using plane-wave DFT method within the Vienna ab initio simulations package (VASP, version 4.6)[38-41] with PAW pseudopotentials from the VASP

database[42,43] and the PBE density functional.[44,45] The default plane-wave cutoff energy of the associated pseudopotential was used. The Brillouin zone was sampled with a G-centered Monkhorst–Pack grid.[46]

References

[1] J. D. Watson, F. H. C. Crick, *Nature* **1953**, *171*, 737.

[2] W. Fiers, R. Contreras, G. Haegeman, R. Rogiers, A. Van de Voorde, H. Van Heuverswyn, J. Van Herreweghe, G. Volckaert, M. Ysebaert, *Nature* **1978**, *273*, 113.

[3] J. Cairns, *J. Mol. Biol*. **1963**, *6*, 208.

[4] J. Lederberg, *Physiol. Rev*. **1952,** *32*, 403.

[5] J. M. Lehn, A. Rigault, J. Siegel, J. Harrowfield, B. Chevrier, D. Moras, *Proc. Natl. Acad. Sci. USA* **1987**, *84*, 2565.

[6] V. Soghomonian, Q. Chen, R. C. Haushalter, J. Zubieta, C. J. O'Connor, *Science* **1993**, *259*, 1596.

[7] C.-S. Liu, G.-H. Sun, M. Li, L.-Q. Guo, L.-M. Zhou, S.-M. Fang, *Open Crystall. J*. **2008**, *1*, 24.

[8] S.-H. Yu, H. Cölfen, K. Tauer, M. Antonietti, *Nat. Mater*. **2005**, *4*, 51.

[9] M. Yang, N. A. Kotov, *J. Mater. Chem*. **2010**, *21*, 6775.

[10] H. Morito, H. Yamane, *Angew. Chem. Int. Ed*. **2010**, *49*, 3638.

[11] Q. Zhang, M.-Q. Zhao, D.-M. Tang, F. Li, J.-Q. Huang, B. Liu, W.-C. Zhu, Y.-H. Zhang, F. Wei, *Angew. Chem. Int. Ed*. **2010**, *49*, 3642.

[12] C. Song, M. G. Blaber, G. Zhao, P. Zhang, H. C. Fry, G. C. Schatz, N. L. Rosi, *Nano Lett*. **2013**, *13*, 3256.

[13] S.-Y. Lai, T.-W. Lin, Y.-H. Chen, C.-C. Wang, G.-H. Lee, M. Yang, M. Leung, S.-M. Peng, *J. Am. Chem. Soc.* **1999**, *121*, 250.

[14] D. T. Cromer, *Acta. Cryst*. **1959**, *12*, 36.

[15] D. T. Cromer, *Acta. Cryst*. **1959**, *12*, 41.

[16] A. S. Ivanov, A. J. Morris, K. V. Bozhenko, C. J. Pickard, A. I. Boldyrev, *Angew. Chem. Int. Ed*. **2012**, *51*, 8330.

[17] C. J. Pickard, R. J. Needs, *Phys. Rev. Lett.* **2006**, *97*, 045504.

[18] C. J. Pickard, R. J. Needs, *J. Phys. Condens. Matter* **2011**, *23*, 053201.

[19] A. K. Jissy, A. Datta, *Phys. Chem. Lett.* **2013**, *4*, 1018.

[20] B. A. Hess, L. J. Schaad, *J. Am. Chem. Soc*. **1971**, *93*, 2413.

[21] J. P. Foster, F. Weinhold, *J. Am. Chem. Soc*. **1980**, *102*, 7211.

[22] D. Yu. Zubarev, A. I. Boldyrev, *Phys. Chem. Chem. Phys*. **2008**, *10*, 5207.

[23] S. M. Kauzlarich, *Chemistry, Structure and Bonding of Zintl Phases and Ions*, VCH: New York, **1996**.

[24] W. Hönle, H. G. von Schnering, *Chem. Rev*. **1988**, *88*, 243.

[25] J. Fulmer, D. C. Kaseman, J.-A. Dolyniuk, K. Lee, S. Sen, K. Kovnir, *Inorg. Chem*. **2013**, *52*, 7061.

[26] H. Szatyłowicz, N. Sadlej-Sosnowska, *J. Chem. Inf. Model*. **2010**, *50*, 2151.

[27] C. X. Cui, M. Kertesz, *J. Am. Chem. Soc*. **1989**, *111*, 4216.

[28] B. Meyer, *Chem. Rev*. **1976**, *76*, 367.

[29] F. Weigend, R. Ahlrichs, *Phys. Chem. Chem. Phys*. **2005**, 7, 3297.

[30] C. Lee, W. Yang, R. G. Parr, *Phys. Rev. B* **1988**, *37*, 785.

[31] W. J. Hehre, R. F. Stewart, J. A. Pople, *J. Chem. Phys*. **1969**, *51*, 2657.

[32] J. S. Binkley, J. A. Pople, W. J. Hehre, *J. Am. Chem. Soc*. **1980**, *102*, 939.

[33] G. A. Petersson, M. A. Al-Laham, *J. Chem. Phys*. **1991**, *94*, 6081.

[34] G. A. Petersson, A. Bennett, T. G. Tensfeldt, M. A. Al-Laham, W. A. Shirley, J. Mantzaris, *J. Chem. Phys*. **1988**, *89*, 2193.

[35] M. J. Frisch, G. W. Trucks, H. B. Schlegel, G. E. Scuseria, M. A. Robb, J. R. Cheeseman, G. Scalmani, V. Barone, B. Mennucci, G. A. Petersson, H. Nakatsuji, M. Caricato, X. Li, H. P. Hratchian, A. F. Izmaylov, J. Bloino, G. Zheng, J. L. Sonnenberg, M. Hada, M. Ehara, K. Toyota, R. Fukuda, J. Hasegawa, M. Ishida, T. Nakajima, Y. Honda, O. Kitao, H. Nakai, T. Vreven, J. A. Montgomery, Jr., J. E. Peralta, F. Ogliaro, M. Bearpark, J. J. Heyd, E. Brothers, K. N. Kudin, V. N. Staroverov, R. Kobayashi, J. Normand, K. Raghavachari, A. Rendell, J. C. Burant, S. S. Iyengar, J. Tomasi, M. Cossi, N. Rega, J. M. Millam, M. Klen e, J. E. Knox, J. B. Cross, V. Bakken, C. Adamo, J. Jaramillo, R. Gomperts, R. E. Stratmann, O. Yazyev, A. J. Austin, R. Cammi, C. Pomelli, J. W. Ochterski, R. L. Martin, K. Morokuma, V. G. Zakrzewski, G. A. Voth, P. Salvador, J. Dannenberg, S. Dapprich, A. D. Daniels, Ö. Farkas, J. B. Foresman, J. V. Ortiz, J. Cioslowski, and D. J. Fox, *Gaussian, Inc.*, Wallingford, CT, **2009**.

[36] http://www.chemcraftprog.com

[37] U. Varetto, *Molekel 5.4.0.8*, Swiss National Supercomputing Centre: Manno, Switzerland, **2009**.

[38] G. Kresse, J. Hafner, *Phys. Rev. B: Condens. Matter Mater. Phys.* **1993**, *47*, 558.

[39] G. Kresse, J. Hafner, *Phys. Rev. B: Condens. Matter Mater. Phys.* **1994**, *49*, 14251.

[40] G. Kresse, J. Furthmuller, *Phys. Rev. B: Condens. Matter Mater. Phys.* **1996**, *54*, 11169.

[41] G. Kresse, J. Furthmuller, *Comput. Mater. Sci.* **1996**, *6*, 15.

[42] P. E. Blochl, *Phys. Rev. B: Condens. Matter Mater. Phys*. **1994**, *50*, 17953.

[43] G. Kresse, D. Joubert, *Phys. Rev. B: Condens. Matter Mater. Phys.* **1999**, *59*, 1758.

[44] J. P. Perdew, K. Burke, M. Ernzerhof, *Phys. Rev. Lett.* **1996**, *77*, 3865.

[45] J. P. Perdew, K. Burke, M. Ernzerhof, *Phys. Rev. Lett*. **1997**, *78*, 1396.

[46] H. J. Monkhorst, J. D. Pack, *Phys. Rev. B: Condens. Matter Mater. Phys*. **1976**, *13*, 5188.

Table 8-1. Structural parameters of Li_7P_7 (C_1, ^1A), Li_8P_8 (C_1, ^1A), Li_9P_9 (C_1, ^1A) double helices, and $Li_{90}P_{90}$ (C_2, ^1A) circular double helix at different levels of theory. Distances between corresponding atoms are given in Å.

Atoms	Helix	Distances (BP86/6-31G(d))	Distances (B3LYP/6-31G(d))
P-P	Li_7P_7	2.25-2.28	2.23-2.29
	Li_8P_8	2.23-2.30	2.22-2.32
	Li_9P_9	2.28-2.31	2.24-2.31
	$Li_{90}P_{90}$	2.22-2.38	2.21-2.38
Li-P	Li_7P_7	2.34-3.97	2.32-3.94
	Li_8P_8	2.34-3.94	2.32-3.93
	Li_9P_9	2.33-3.98	2.31-3.96
	$Li_{90}P_{90}$	2.39-4.18	2.52-4.25
Li-Li	Li_7P_7	2.78-3.49	2.75-3.44
	Li_8P_8	2.77-3.34	2.75-3.30
	Li_9P_9	2.84-3.31	2.80-3.23
	$Li_{90}P_{90}$	2.63-3.07	2.64-3.05

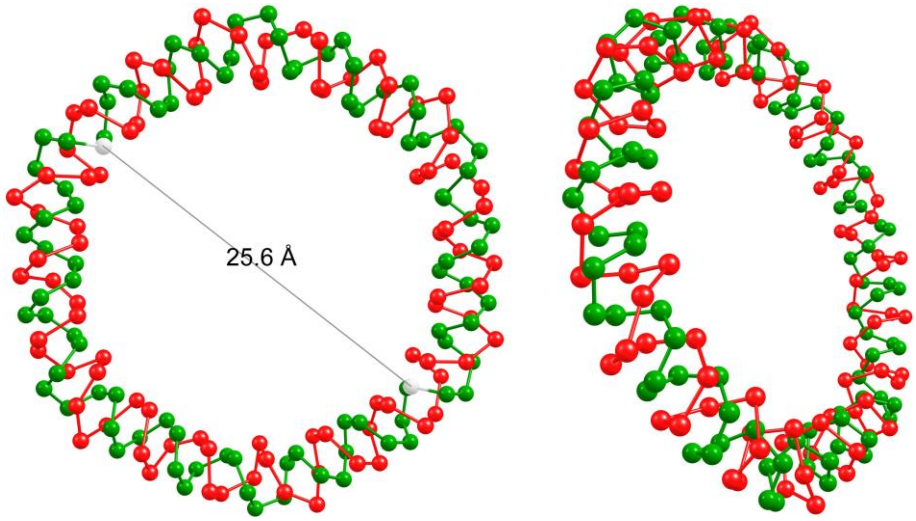

Figure 8-1. Optimized (BP86/6-31G(d)) $Li_{90}P_{90}$ (C_2, ^1A) double-helical toroid structure with internal diameter of 25.6 Å and its side view showing helical arrangement of lithium and phosphorus atoms. Colour scheme: green, phosphorus; red, lithium.

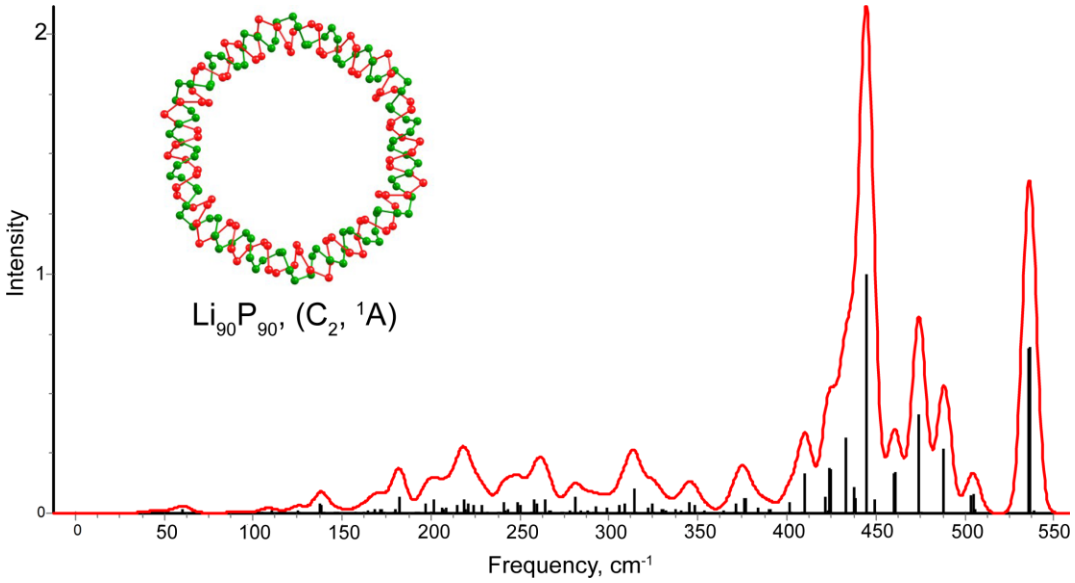

Figure 8-2. Simulated vibrational spectrum of $Li_{90}P_{90}$ cluster at the BP86/6-31G(d) level of theory.

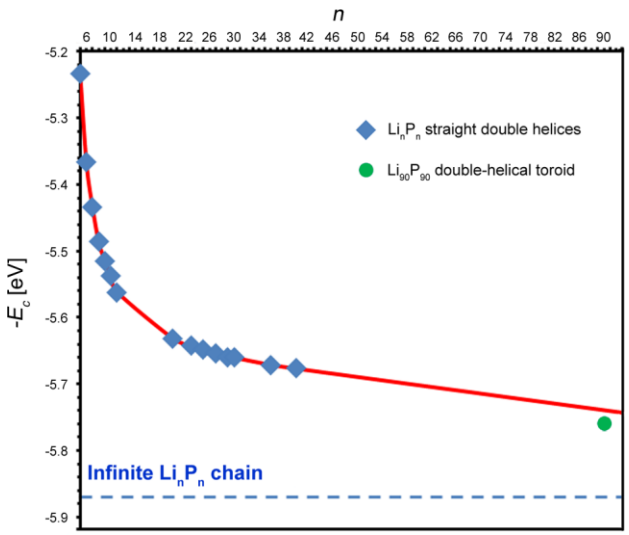

Figure 8-3. Cohesive energy per formula unit as a function of the number of units (n) in the Li_nP_n double helices. The blue rhombi correspond to straight double-helical clusters, whereas the green circle corresponds to the double-helical ring. The blue horizontal line corresponds to the cohesive energy of the infinite double-helical chain.

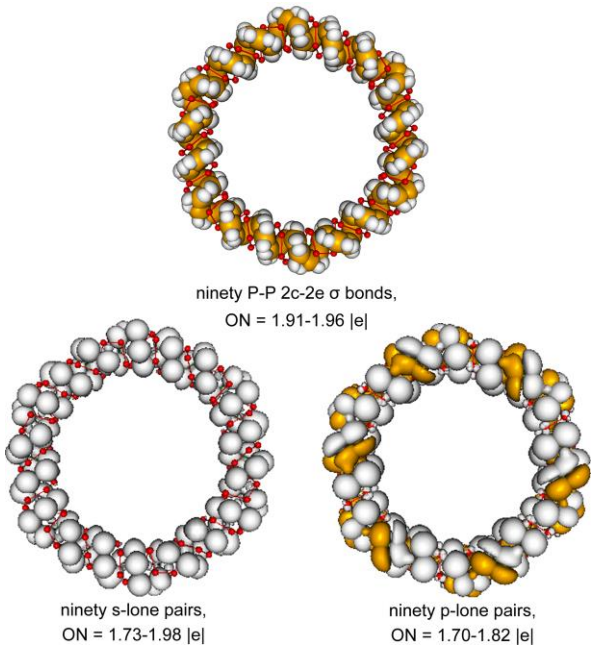

Figure 8-4. Chemical bonding pattern of $Li_{90}P_{90}$ shown by the AdNDP analysis. ON stands for occupation number.

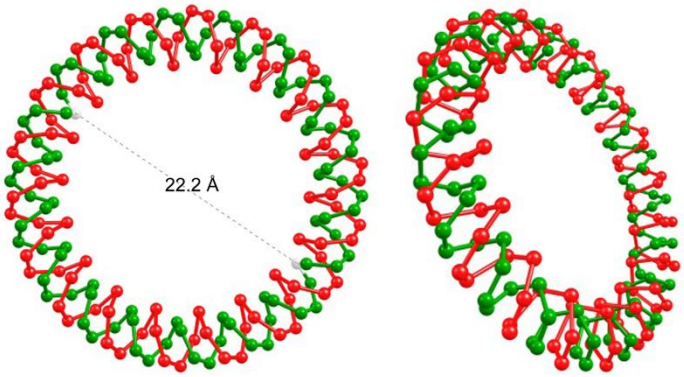

Figure 8-5. Optimized (BP86/STO-3G) $Li_{90}P_{90}$ (C_6, ^1A) double helical toroid structure with internal diameter of 22.2 Å.

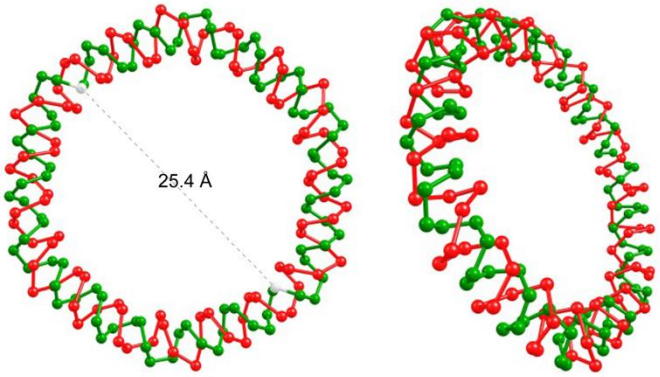

Figure 8-6. Optimized (B3LYP/6-31G(d)) $Li_{90}P_{90}$ (C_2, ^1A) double helical toroid structure with internal diameter of 25.4 Å.

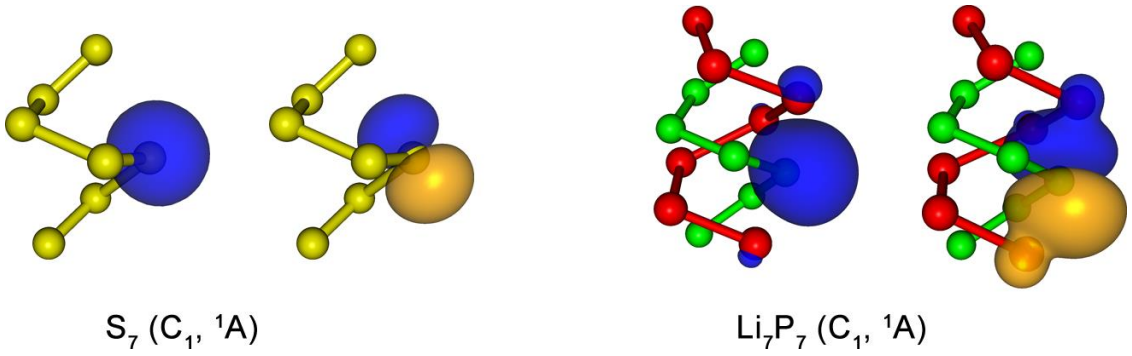

Figure 8-7. Lone pairs (s- and p-type) of S_7 (left) and Li_7P_7 (right) clusters showing the difference in the size of the corresponding orbitals.

CHAPTER 9

DECIPHERING AROMATICITY IN PORPHYRINOIDS VIA ADAPTIVE NATURAL DENSITY PARTITIONING[1]

Abstract

The adaptive natural density partitioning (AdNDP) method has been applied for the first time to porphyrinoids in order to describe their aromaticity. The analysis of π-electron system reveals that aromaticity of annulene originates from 6-π-electron delocalization, while aromaticity of porphyrin can be better described in terms of local aromaticities of the appended 6-π-electron pyrrolic heterocycles and 6-π-electron central fragment. The patterns of chemical bonding for porphyrinoids obtained by AdNDP are consistent with chemical intuition and lead to unique and compact graphic formulas.

9-1. Introduction

Porphyrins are macrocyclic compounds that have attracted much attention because of their unique structures and a wide spectrum of very useful physicochemical and biological properties, such as anion binding, stabilization of metal ions with unusual oxidation states, electron transfer, and construction of peculiar supramolecular assemblies. However, despite the successful syntheses of various porphyrinoids and their analogues, there is still the contentious debate between chemists about the generally accepted description of aromaticity in such complicated macrocyclic systems. The Hückel's rules[1] for aromaticity, stating that [4n + 2] π electrons result in an aromatic system, have played

1 Coauthored by Alexander S. Ivanov and Alexander I. Boldyrev. Reprinted with permission from *Org. Biomol. Chem.*, **2014**, 12, 6145-6150.

an important role in the development of diverse porphyrinoid chemistry since the early 1930s. Hence, the correct description of aromaticity and chemical bonding is vital for predicting new members of the porphyrin family and explaining their properties. In 1962 Sondheimer *et al.*[2] identified for the first time the resemblance between porphyrin and [18]annulene, proposing the interpretation of porphyrin structure as a multiple-bridged aromatic diaza[18]annulene system: „porphine and the derived porphyrins, as well as the phthalocyanines, are in fact the first known 18-electron systems related to [18]annulene." Later, Vogel *et al.*,[3] using annulen-like description of porphyrins, demonstrated the application of the Hückel [4n + 2] π aromaticity rule for various porphyrin homologues that has been quite helpful for the synthetic preparation of different porphyrinoids.[4] Lash *et al.*[5a] has recently synthesized dideazaporphyrin – the simplified component of a porphyrin, which lacks two of the pyrrole rings. It has also been proposed that this compound should act as a modified [18]annulene, and the prominent diatropic shifts in the ^{1}H NMR spectrum as well as the X-ray structure, which exhibits a nearly planar system, support that notion. The authors therefore concluded: "the aromatic characteristics of porphyrins clearly result from a number of features, but the essence of these properties appears to be encapsulated in the diaza[18]annulene substructure."[5a] However, despite the viability of the [18]annulene representation for porphyrinoid aromaticity, it has been increasingly questioned by theoretical chemists.

To date, there are a lot of computational models developed for the description of aromaticity in porphyrins, which are usually based on energetic, geometric, and magnetic criteria.[6-15] In 1998, Schleyer *et al.*,[6] using analysis of experimental bond lengths and computed nuclear independent chemical shifts (NICS) values, proposed that a more

appropriate description of the porphyrin moiety should be a 22 π-electron macrocycle with two C_2H_2 exocyclic bridges. According to this model, the NH groups are an integral part of the aromatic system and not just the inert bridging groups as suggested by the classic [18]annulene representation. However, Fowler *et al*.,[7] using ipsocentric current-density mapping techniques, suggested that the classic [18]annulene model of free base porphyrin is the most appropriate one. Aihara's studies based on the graph theory of aromaticity, have indicated that the aromatic characteristics of porphyrins are mainly due to the individual pyrrolic subunits.[8] The most recently published Schleyer's work[9] also shows that porphyrinoid aromaticity is not due primarily to the macrocyclic π conjugation of the corresponding annulene perimeters, and the appended 6π electron heterocycles of porphyrinoids confer aromaticity much more effectively than the macrocyclic [4n + 2] π electron conjugations.

As one may see, there is a disagreement between synthetic chemists and theoreticians, probably because there is no simple, intuitive, and at the same time physicaly precise explanation of aromaticity in porphyrinoids. In the recent highlight, Bröring, summarizing different views on the aromaticity in porphynoids, calls theoreticians for providing more clarification on the origin of aromaticity in porphyrins.[16] We now respond. In the current study we propose our model of π electron system and aromaticity in annulenes and porphyrinoids, using adaptive natural density partitioning (AdNDP) approach.[17] This approach leads to partitioning of the charge density of a molecule into elements with the highest-possible degree of localization of electron pairs such as the n-center two-electron (nc-2e) bonds, which include core electrons, lone pairs (LPs), 2c-2e bonds, etc. If some portion of the density cannot be localized in this manner,

it is represented using completely delocalized objects, which are associated with the concepts of aromaticity and antiaromaticity. From this point of view, AdNDP achieves seamless description of systems featuring both localized and delocalized bonding without invoking the concept of resonance. Additionally, our AdNDP approach has demonstrated effectiveness in the description of aromaticity in rather complicated chemical systems, such as graphene,[18] coronene,[19] isocoronene, circumcoronene,[20] and other organic molecules[19] as well as silabenzenes,[21] boron clusters[22], and triple-decker sandwich complexes.[23]

9-2. Results and discussion

In the present study, we use the AdNDP approach for the analysis of the molecular orbital wave function of the selected porphyrinoid macrocycles, including [18]annulene, dideazaporphyrin, [18]porphyrin, and dihydrodideazaporphyrin. According to our AdNDP analysis all σ bonds are well represented by classical two center – two electron (2c-2e) bonds and will not be discussed here.

Annulene $C_{18}H_{18}$ is an aromatic hydrocarbon with 18 π-electrons. According to the Hückel's [4n + 2] rule, its 18 π-electron system should be delocalized, resulting in a fully conjugated and planar structure with D_{6h} symmetry. Indeed, the X-ray diffraction analysis of $C_{18}H_{18}$ made by Hirshfeld et al.[24] yielded a roughly planar centrosymmetric molecule. The corresponding structures have also been proposed for [18]annulene[25] with the emphasis on the presence of 18 π-electron delocalized bonding in this molecule (Fig. 9-1, structures I and II). However, in spite of the fact that [18]annulene shows prominent aromatic features (large resonance energies and significant nuclear magnetic resonance ring currents), its reactivity more closely resembles a conjugated polyene rather than an

aromatic hydrocarbon.[2] The application of AdNDP for $C_{18}H_{18}$ leads to the π bonding pattern shown in Fig. 9-1. Surprisingly, AdNDP recovered six three center – two electron (3c-2e) π bonds with an occupation number (ON) of 1.92 |e| at the periphery of [18] annulene, and three 18c-2e π bonds with ON = 2.00 |e| delocalized over all the carbon atoms. Thus, according to our analysis we believe that only 6 π electrons (satisfying the [4n + 2] rule for aromaticity with n = 1) are responsible for the aromatic character of $C_{18}H_{18}$, whereas the remaining 12 π electrons form six conjugated 3c-2e π bonds, which might be in charge of the observed polyene-like chemical properties of [18]annulene.[2] The appropriate symbolic representation (Fig. 9-1, III) with conjugated 3c-2e π bonds is consistent with the appreciable C-C bond length alternation from 1.382 Å for 12 inner C-C bonds to 1.419 Å for 6 outer C-C bonds confirmed experimentally for this molecule.[24] However, Schleyer *et al.*,[26] using the ^{1}H NMR chemical shifts and energy computations with BHLYP[27] and KMLYP[28] methods, suggested that [18]annulene prefers C-C bond-length alternation and C_2 symmetry, rather than D_{6h} symmetry. The application of AdNDP to the less symmetric (C_2) bond-alternate [18]annulene yielded π-bonding picture (see Fig. 9-5) analogous to that of D_{6h} symmetric [18]annulene, which further proves the robustness of AdNDP method.

Dideazaporphyrin $C_{20}H_{16}N_2$ can be considered as structurally midway between [18]annulene and porphyrin. As it was discussed above, this molecule should behave similarly to [18]annulene.[5] Thus, our analysis revealed the bonding picture, which is almost identical to that of [18]annulene (Fig. 9-2), apart from the C=C bonds (ON = 1.86 |e|) of the corresponding heterocyclic rings. According to the AdNDP, the 18 π electron bonding framework of dideazaporphyrin consists of six peripheral 3c-2e π bonds (ON =

1.90-1.95 |e|), where two of them involve nitrogen atoms of the heterocyclic rings; and three completely delocalized 18c-2e π bonds with ON = 2.00 |e|. Hence, we may conclude that aromaticity of $C_{20}H_{16}N_2$ arises from 6 π electron core conjugations similar to what we observe for [18]annulene (Fig. 10-1). Interestingly, Schleyer's results, based on the block-localized wave function (BLW) calculations, show similar aromatic stabilization energies per carbon (ASE's) for dideazaporphyrin (+32.1 kcal/mol) and [18]annulene (+25.0 kcal/mol).[9] The corresponding symbolic representations of $C_{20}H_{16}N_2$ in the form of resonance and AdNDP structures are depicted in Fig. 9-2: structures I and II, respectively.

As the parent compound of the porphyrin series, [18]porphyrin $C_{20}H_{14}N_4$ occupies a unique position among other porphyrinoids. An X-ray crystallographic structure determination has been reported for the free base of porphine by Webb *et al*.[29] and the structure can be summarized briefly as the macrocyclic ring (Fig. 9-3) of four pyrroles alternately linked with four methine groups. Representative porphyrin structures illustrating two frequently used models for porphyrinoid aromaticity are shown in Fig. 9-3 (structures I and II). Structure I (Fig. 9-3, I), proposed by Vogel,[3] describes aromaticity in terms of the [18]annulene model with the involvement of the 18 π electrons in the main conjugation pathway, thus obeying the [4n + 2] rule with n = 4. In contrast, Schleyer's model[6] II (Fig. 9-3, II) indicates that all four pyrrole rings are incorporated into the aromatic system with the 22 π electrons, including the nitrogen electron lone pairs of the pyrrole subunits. The results of our AdNDP analysis and the corresponding symbolic representation of [18]porphyrin (structure III) are shown in Fig. 9-3. As expected, AdNDP revealed two localized C=C bonds (ON = 1.81 |e|) of the dehydropyrrolic rings

of $C_{20}H_{14}N_4$. Therefore, these bonds do not participate in aromaticity and can be viewed as exocyclic "ethylenic bridges" similarly to those of dideazaporphyrin (Fig. 9-2). However, instead of six 3c-2e peripheral π bonds present in [18]annulene and dideazaporphyrin, the AdNDP analysis established only two 3c-2e π bonds (ON = 1.96 |e|), which are reminiscent of the two C-N-C 3c-2e bonds in dideazaporphyrin. The delocalized π bonding pattern responsible for aromaticity in porphyrin was found to be quite interesting. According to our results, it comprises three aromatic systems, two of which represent pyrroles with three delocalized 5c-2e π bonds with ON = 2.00 |e| (satisfying the [4n + 2] rule for aromaticity with n = 1) and the third one is the larger heterocycle involving three 16c-2e π bonds with ON = 1.90 |e| (satisfying the [4n + 2] rule for aromaticity with n = 1) delocalized over the central fragment of a porphyrin molecule (Fig. 9-3). Hence, we can make a conclusion that aromaticity in porphyrin can be better described in terms of local aromaticities of two pyrrole rings and the central larger heterocyclic fragment. The picture of π chemical bonding (Fig. 9-3) shows that aromaticity in porphyrin has similar features with [18]annulene, i.e., the central porphyrin fragment involves three delocalized bonds as in [18]annulene, however, porphyrin aromaticity is different from [18]annulene aromaticity with respect to the presence of two appended 6 π electron pyrrolic subunits. Indeed, the total $NICS(0)_{\pi zz}$ values, computed at the heavy atom center, for porphyrin (-47.3 ppm), dideazaporphyrin (-43.5 ppm), and [18]annulene (-47.9 ppm) are approximately the same, while the calculated aromatic stabilization energy of porphyrin (+70.9 kcal/mol) has the highest value.[9] Thus, the description of aromaticity in porphyrin (model III) based on the results of the AdNDP analysis expresses the multifaceted nature of aromaticity similar to model II, however, at

the same time local aromaticity of the central 16 atom fragment of porphyrin closely resembles the 6-π- electron pathway found in [18]annulen (Fig. 9-1).

So far, our AdNDP approach worked well for the description of aromaticity and chemical bonding in aromatic [4n + 2] porphyrinoids. However, there are plenty of examples of stable and experimentally obtained antiaromatic macrocyclic [4n] annulenic π conjugated porphyrins, which show the opposite upfield/downfield ^{1}H NMR chemical shifts for the outer/inner protons.[30] Hence, in order to further confirm the validity of our approach, we performed AdNDP analysis for the representative antiaromatic porphyrinoid system – dihydrodideazaporphyrin[5] $C_{20}H_{18}N_2$, which adopts quasi-planar structure (Fig. 9-4). According to the AdNDP results, there are six polyene-like 2c-2e C-C π bonds (ON = 1.82-1.85 |e|, superimposed on the central molecular framework) and three delocalized 5c-2e π bonds with ON = 2.00 |e| on each pyrrolic subunits. The deviations of the occupation numbers of the 2c-2e C-C π bonds from the ideal value of 2.00 |e| are signatures of the conjugation between the recovered π bonds. This bonding picture shows that despite having 24 π electrons (satisfying the 4n rule for antiaromaticity), dihydrodideazaporphyrin (Fig. 9-4) is locally aromatic molecule with respect to two aromatic pyrrolic fragments. The central core of dihydrodideazaporphyrin does not contain any delocalized π bonds and can be better described in terms of peripheral localized 2c-2e π bonds. Thus, we believe that the presence of aromatic pyrrole rings and obscure antiaromaticity of the central molecular fragment (six π bonds in $C_{20}H_{18}N_2$ were found to have more localized, rather than delocalized character) can explain the peculiar viability of some successfully synthesized Hückel antiaromatic porphrinoids which are stable in spite of the fact that they have net 4n π electron counts.[30]

9-3. Experimental section

The detailed description of the AdNDP algorithm developed by Zubarev and Boldyrev can be found elsewhere.[17] From the computational point of view, AdNDP is a generalization of the NBO analysis by Weinhold.[31] AdNDP performs analysis of the first-order reduced density matrix with the purpose of obtaining its local block eigenfunctions with optimal convergence properties for describing the electron density. The local blocks of the first-order reduced density matrix correspond to the sets of n atoms (from one to all the atoms of the molecule) that are tested for the presence of a two-electron object (nc-2e bonds, including core electrons and lone pairs as a special case of n = 1) associated with this particular set of n atoms. The n atomic sets are formed and checked in an exhaustive manner, so that the recovered nc-2e bonding elements always correspond to the point group symmetry of the system after these bonding elements are superimposed onto the molecular frame. For the given n atomic block those eigenvectors are accepted whose occupation numbers (eigenvalues) exceed the established threshold value, usually close to 2.00 |e|. Thus, Lewis's idea of an electronic pair as the essential element of bonding is preserved. The AdNDP procedure is numerically efficient because it involves only a series of diagonalizations of density matrix blocks. It is unbiased in the sense that no preliminary ideas of the bonding pattern are required to perform analysis. The AdNDP code is a stand-alone program that uses output from Gaussian 09. The geometry optimization and normal-mode analysis for the studied systems were carried out using the hybrid density functional B3LYP[32] method with the 6-311++G** basis set[33] as implemented in the Gaussian 09 software package.[34] The density matrix used for the basis of the natural atomic orbitals as well as for the transformation between atomic

orbital and natural atomic orbital basis sets, which are used by the AdNDP program, was generated at the B3LYP/3-21G level of theory by means of the NBO code[35] incorporated into Gaussian 09. It is known that the results of NBO analysis do not generally depend on the quality of the basis set, so the choice of the level of theory for the AdNDP application is adequate. The visualization of the results of the calculations was performed by using MOLEKEL 5.4.0.8.[36]

9-4. Conclusions

In summary, we presented a new approach for the description of aromaticity in porphyrinoids. It was found that [18]annulene has only three completely delocalized π bonds associated with its aromaticity. Other 12π electrons are in fact responsible for the conjugated 3c-2e π bonds formation, which can be likely manifested by polyene-like properties of [18]annulene. The results of our AdNDP analysis for porphyrin demonstrate that the appended 6π aromatic sextets together with the 6π aromatic core molecular fragment of porphyrin confer aromaticity much more efficiently than the "bridged [18]annulene" model. The AdNDP representations of porphyrinoids are novel and consistent with geometrical parameters of the studied molecules. It is also worthy to note that the patterns of chemical bonding recovered by AdNDP comply with chemical intuition and lead to unique compact graphic formulas. The significant advancement made in the current study is that the bonding patterns and formulas are derived from the MO wave function *via* a unified and well-defined quantum chemical procedure. Although the proposed assessment of aromaticity in porphyrinoids is practically based on qualitative analysis, the obtained π bonding pictures are generally in agreement with the results of quantitative theoretical approaches, such as NICS,[6-9] BLW[9] and current-density

maps[7] techniques. Since the presented approach combines both simplicity and quantum-chemical background, we believe that our representation of aromaticity in porphyrinoids would be clear for both preparative organic chemists and theoreticians. Hence, the results of our work can provide a new look at the diverse chemistry of porphyrinoids and might be helpful in understanding and rational design of novel porphyrinoid compounds.

Notes and references

1 (*a*) E. Hückel, Z. Phys., 1931, **70**, 204; (*b*) E. Hückel, Z. Phys., 1932, **76**, 628; (*c*) E. Hückel, Z. Elektrochem., 1937, **43**, 752; (*d*) W. von E. Doering and F. L. Detert, J. Am. Chem. Soc., 1951, **73**, 876.

2 F. Sondheimer, R. Wolovsky and Y. Amiel, J. Am. Chem. Soc., 1962, **84**, 274.

3 E. Vogel, Pure Appl. Chem., 1993, **65**, 143.

4 (*a*) F.-P. Montforts, B. Gerlach and F. Höper, Chem. Rev., 1994, **94**, 327; (*b*) W. Flitsch, Adv. Heterocycl. Chem., 1988, **43**, 73; (*c*) Y. Inokuma, J. H. Kwon, T. K. Ahn, M.-C. Yoon, D. Kim and A. Osuka, Angew. Chem., 2006, **118**, 975; Angew. Chem. Int. Ed., 2006, **45**, 961; (*d*) H. Rexhausen and A. Gossauer, J. Chem. Soc. Chem. Commun., 1983, 275.

5 (*a*) T. D. Lash, S. A. Jones and G. M. Ferrence, J. Am. Chem. Soc., 2010, **132**, 12786; (*b*) T. D. Lash, J. Porphyrins Phthalocyanines, 2011, **15**, 1093; (*c*) T. D. Lash and M. J. Hayes, Angew. Chem., Int. Ed. 1997, **36**, 840; (*d*) T. D. Lash, J. L. Romanic and M. J. Hayes, Chem. Commun. 1999, 819; (*e*) D. I. AbuSalim and T. D. Lash, Org. Biomol. Chem., 2013, **11**, 8306.

6 M. K. Cyrański, T. M. Krygowski, M. Wisiorowski, N. J. R. van Eikema Hommes and P. von R. Schleyer, Angew. Chem. 1998, **110**, 187; Angew. Chem. Int. Ed., 1998, **37**, 177.

7 (*a*) E. Steiner and P. W. Fowler, Chem. Phys. Chem., 2002, **1**, 114; (*b*) E. Steiner, A. Soncini and P. W. Fowler, Org. Biomol. Chem., 2005, **3**, 4053.

8 (*a*) J.-i. Aihara, E. Kimura and T. M. Krygowski, Bull. Chem. Soc. Jpn., 2008, **81**, 826; (*b*) J.-i. Aihara, J. Phys. Chem. A 2008, **112**, 5305.

9 J. I. Wu, I. Fernández and P. von R. Schleyer, J. Am. Chem. Soc,. 2013, **135**, 315.

10 (*a*) M.-S. Liao and S. Scheiner, J. Chem. Phys., 2002, **117**, 205; (*b*) M.-S. Liao and S. Scheiner, Comput. Chem., 2002, **23**, 1391.

11 T. M. Krygowski, J. Chem. Inf. Comput. Sci., 1993, **33**, 70.

12 (*a*) P. von R. Schleyer, C. Maerker, A. Dransfeld, H. Jiao and N. J. R. v. E. Hommes, J. Am. Chem. Soc., 1964, **29**, 1923; (*b*) Z. Chen, C. S. Wannerere, C. Corminboeuf, R. T. Puchta and P. von R. Schleyer, Chem. Rev., 2005, **105**, 3842.

13 A. Osuka and S. Saito, Chem. Commun., 2011, **47**, 4330.

14 M. K. Cyrański, Chem. Rev. 2005, **105**, 3773.

15 (*a*) P. von R. Schleyer, P. K. Freeman, H. Jiao and B. Goldfuss, Angew. Chem., 1995, **107**, 332; Angew. Chem. Int. Ed., 1995, **34**, 337; (*b*) P. Von R. Schleyer and H. Jiao, Pure Appl. Chem., 1996, **28**, 209; (*c*) U. Fleischer, W. Kutzelnigg, P. Lazzeretti and V. Müllenkamp, J. Am. Chem. Soc., 1994, **116**, 5298; (*d*) H. Jiao, P. von R. Schleyer and M. N. Glukhovtsev, J. Phys. Chem., 1996, **110**, 12299.

16 M. Bröring, Angew. Chem. Int. Ed., 2011, **50**, 2436.

17 D. Yu. Zubarev and A. I. Boldyrev, Phys. Chem. Chem. Phys., 2008, **10**, 5207.

18 I. A. Popov, K. V. Bozhenko and A. I. Boldyrev, Nano Res., 2012, **5**, 117.

19 D. Yu. Zubarev and A. I. Boldyrev, J. Org. Chem., 2008, **73**, 9251.

20 I. A. Popov and A. I. Boldyrev, Eur. J. Org. Chem., 2012, 3485.

21 A. S. Ivanov and A. I. Boldyrev, J. Phys. Chem. A 2012, **116**, 9591.

22 (*a*) A. P. Sergeeva, D. Yu. Zubarev, H.-J. Zhai, A. I. Boldyrev and L. S. Wang, J. Am. Chem. Soc., 2008, **130**, 9248; (*b*) W. Huang, A. P. Sergeeva, H.-J. Zhai, B. B. Averkiev, L.-S. Wang and A. I. Boldyrev, Nature Chem., 2010, **2**, 202.

23 (*a*) A. S. Ivanov, K. V. Bozhenko and A. I. Boldyrev, Inorg. Chem., 2012, **51**, 8868; (*b*) A. P. Sergeeva and A. I. Boldyrev, Phys. Chem. Chem. Phys., 2010, **12**, 12050.

24 F. L. Hirshfeld and D. Rabinovich, Acta Cryst., 1965, **19**, 235.

25 S. Gorter, E. Rutten-Keulemans, M. Krever and C. Romers, Acta Cryst., 1995, **51**, 1036.

26 C. S. Wannere, K. W. Sattelmeyer, Henry F. Schaefer III and P. von R. Schleyer, Angew. Chem. Int. Ed., 2004, **43**, 4200.

27 A. D. Becke, J. Chem. Phys., 1993, **98**, 5648.

28 J. K. Kang and C. B. Musgrave, J. Chem. Phys., 2001, **115**, 11040.

29 L. E. Webb and E. B. Fleischer, J. Chem. Phys., 1965, **43**, 3100.

30 (*a*) J. L. Sessler, S. J. Weghorn, Y. Hiseada and V. Lynch, Chem.-Eur. J., 1995, **1**, 56; (*b*) C. Liu, D. M. Shen and Q. Y. Chen, J. Am. Chem. Soc., 2007, **129**, 5814; (*c*) T. Hayashi, Y. Nakashima, K. Ito, T. Ikegami, I. Aritome, A. Suzuki and Y. Hisaeda, Org. Lett., 2003, **5**, 2845; (*d*) T. Kakui, S. Sugawara, Y. Hirata, S. Kojima and Y. Yamamoto, Chem.-Eur. J., 2011, **17**, 7768; (*e*) J. A. Cissel and T.

P. Vaid, A. L. Rheingold, J. Am. Chem. Soc., 2005, **127**, 12212; (*f*) J. A. Cissel, T. P. Vaid and G. P. A. Yaps, Org. Lett., 2006, **8**, 2401.

31 F. Weinhold and C. R. Landis, Valency and Bonding: A Natural Bond Orbital Donor-Acceptor Perspective; Cambridge University Press: Cambridge, U.K., 2005.

32 (*a*) R. G. Parr and W. Yang, Density-Functional Theory of Atoms and Molecules; Oxford University Press: Oxford, 1989; (*b*) A. D. Becke, J. Chem. Phys., 1993, **98**, 5648; (*c*) J. P. Perdew, J. A. Chevary, S. H. Vosko, K. A. Jackson, M. R. Pederson, D. J. Singh and C. Fiolhais, Phys. Rev. B 1992, **46**, 6671.

33 (*a*) V. A. Rassolov, M. A. Ratner, J. A. Pople, P. C. Redfern and L. A. J. Curtiss, Comput. Chem., 2001, **22**, 976; (*b*) M. S. Gordon, J. S. Binkley, J. A. Pople, W. J. Pietro and W. J. Hehre, J. Am. Chem. Soc., 1982, **104**, 2797. (*c*) W. J. Pietro, M. M. Francl, W. J. Hehre, D. J. Defrees, J. A. Pople and J. S. Binkley, J. Am. Chem. Soc., 1982, **104**, 5039; (*d*) T. Clark, J. Chandrasekhar, G. W. Spitznagel and P. v. R. Schleyer, J. Comput. Chem., 1983, **4**, 294.

34 Gaussian 09, Revision B.0.1, M. J. Frisch, G. W. Trucks, H. B. Schlegel, G. E. Scuseria, M. A. Robb, J. R. Cheeseman, G. Scalmani, V. Barone, B. Mennucci, G. A. Petersson, H. Nakatsuji, M. Caricato, X. Li, H. P. Hratchian, A. F. Izmaylov, J. Bloino, G. Zheng, J. L. Sonnenberg, M. Hada, M. Ehara, K. Toyota, R. Fukuda, J. Hasegawa, M. Ishida, T. Nakajima, Y. Honda, O. Kitao, H. Nakai, T. Vreven, J. A. Montgomery, Jr., J. E. Peralta, F. Ogliaro, M. Bearpark, J. J. Heyd, E. Brothers, K. N. Kudin, V. N. Staroverov, R. Kobayashi, J. Normand, K. Raghavachari, A. Rendell, J. C. Burant, S. S. Iyengar, J. Tomasi, M. Cossi, N. Rega, J. M. Millam,

M. Klene, J. E. Knox, J. B. Cross, V. Bakken, C. Adamo, J. Jaramillo, R. Gomperts, R. E. Stratmann, O. Yazyev, A. J. Austin, R. Cammi, C. Pomelli, J. W. Ochterski, R. L. Martin, K. Morokuma, V. G. Zakrzewski, G. A. Voth, P. Salvador, J. Dannenberg, S. Dapprich, A. D. Daniels, Ö. Farkas, J. B. Foresman, J. V. Ortiz, J. Cioslowski, and D. J. Fox, Gaussian, Inc., Wallingford CT, 2009.

35 E. D. Glendening, A. E. Reed, J. E. Carpenter and F. Weinhold, NBO, version 3.1.

36 U. Varetto, Molekel 5.4.0.8, Swiss National Supercomputing Centre: Manno, Switzerland, 2009.

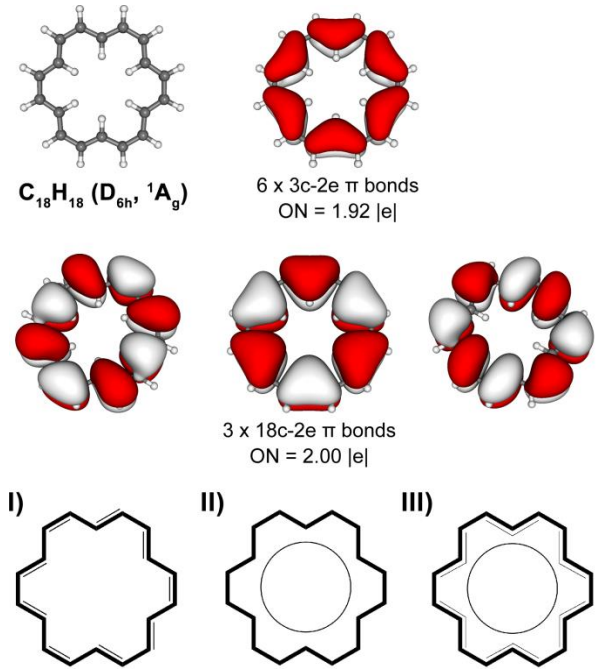

Fig. 9-1. AdNDP π bonding pattern for [18]annulene. The corresponding point group symmetry and spectroscopic state are given in parenthesis. I), II) possible bond structures proposed for [18]annulene; III) symbolic representation of [18]annulene according to AdNDP. Here and elsewhere three center – two electron (3c-2e) bonds and delocalized bonding in the AdNDP symbolic representation are depicted with bend lines and circles, respectively.

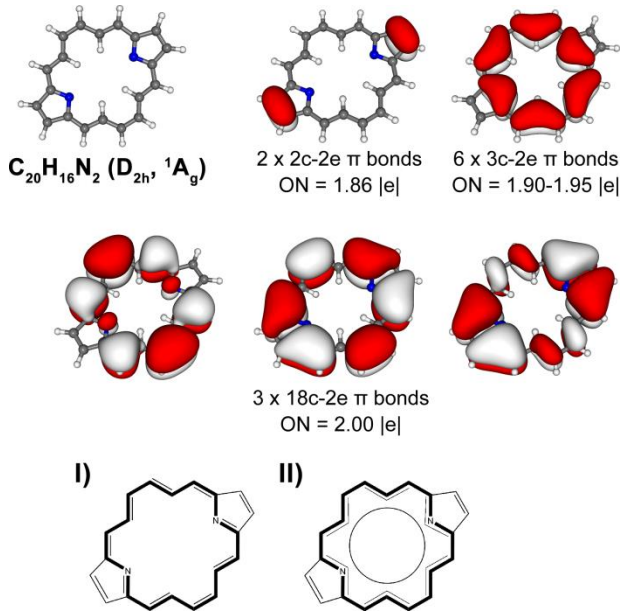

Fig. 9-2. AdNDP π bonding pattern for dideazaporphyrin. The corresponding point group symmetry and spectroscopic state are given in parenthesis. I) possible resonance structure proposed for dideazaporphyrin; II) symbolic representation of dideazaporphyrin according to AdNDP.

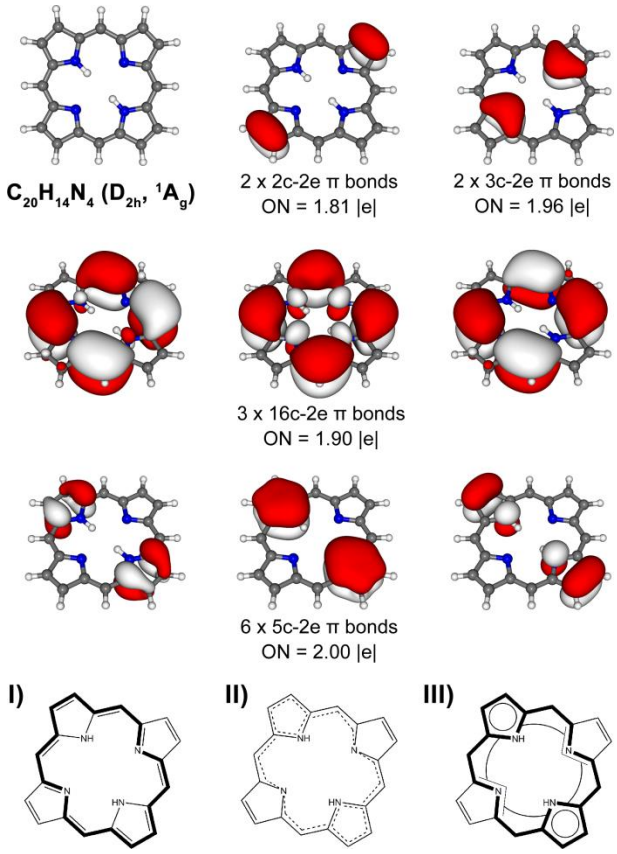

Fig. 9-3. AdNDP π bonding pattern for porphyrin. The corresponding point group symmetry and spectroscopic state are given in parenthesis. I), II), III) representative porphyrin structures illustrating three different models for porphyrinoid aromaticity, where I) shows the 18-π-electron delocalization, II) - the 22-π-electron delocalization, and III) - the three local 6-π-electron delocalizations recovered by AdNDP.

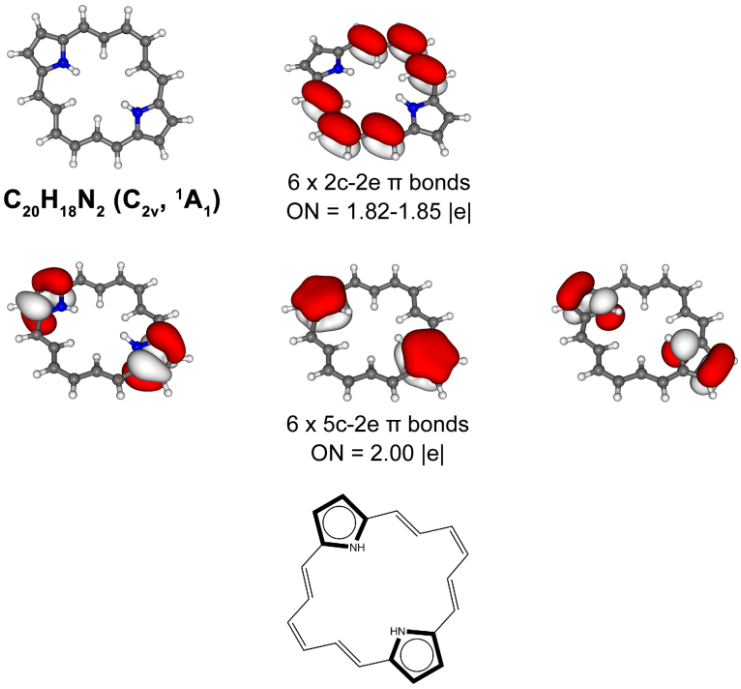

Fig. 9-4. AdNDP π bonding pattern and symbolic representation of antiaromatic dihydrodideazaporphyrin. The corresponding point group symmetry and spectroscopic state are given in parenthesis.

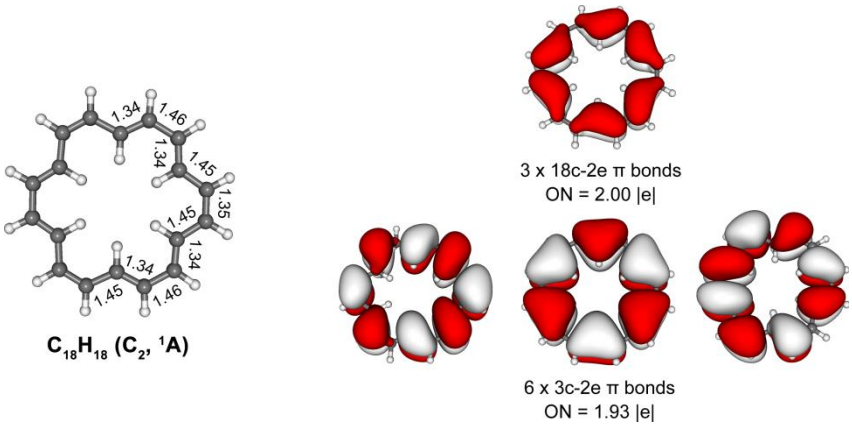

Fig. 9-5. AdNDP π bonding pattern for C_2 symmetric bond-alternate [18]annulene. The corresponding point group symmetry and spectroscopic state are given in parenthesis.

CHAPTER 10

THE I=X (X = O, N, C) DOUBLE BOND IN HYPERVALENT IODINE COMPOUNDS: IS IT REAL?[1]

Abstract

I-X (X = O, N, C) bonding was analyzed in the related hypervalent iodine compounds based on adaptive natural density partitioning (AdNDP) approach. The results confirm the presence of I→X σ dative bond, as opposed to the widely used I=X notation. A clear formulation of the electronic structure of these hypervalent iodine compounds would be useful in establishing reaction mechanisms and electronic structures in bioinorganic problems of general applicability.

10-1. Introduction

Organic derivatives of polyvalent iodine, commonly known as hypervalent iodine reagents, have found widespread application in organic synthesis as versatile, efficient, and environmentally sustainable reagents.[1] Despite extensive practical interest in these compounds, a relatively small number of computational studies on structure and reactivity of polyvalent iodine compounds have been published.[2] In particular, an important question about the existence of I=X (X=O, N, C) double bonds in organic derivatives of trivalent and pentavalent iodine has not been reliably answered. Structures of key hypervalent iodine reagents, such as iodosylarenes (**1**), iodonium imides (**2**), iodonium ylides (**3**), iodylarenes (**4**), 2-iodoxybenzoic acid (IBX, **5**), are commonly

[1] Coauthored by Alexander S. Ivanov, Ivan A. Popov, Alexander I. Boldyrev, and Viktor V. Zhdankin. Reprinted with permission from *Angew. Chem. Int. Ed*. **2014**, 53, 9617–962.

shown in the original research papers, books, and reviews in the form of compounds with a double bond at the iodine atom (Figure 10-1).[1,2]

X-ray structural studies of these compounds in the solid state are inconclusive because the real molecular structure of hypervalent iodine derivatives is masked by extensive networks of intermolecular secondary bonds resulting in a highly aggregated polymeric structure.[3] For example, X-ray powder diffraction and EXAFS studies of iodosylbenzene have indicated a zigzag polymeric chain structure (**6**) in which monomeric PhIO units are linked by intermolecular I···O secondary bonds.[3a] In spite of the numerous experimental structural studies of hypervalent iodine compounds,[1] the question about the real nature of the I=X bonding remains open. Bonding description in such molecules is very important for understanding the structural, physical, and chemical properties. In the current study we show the single dative [two-center two-electron (2c-2e) bond where two electrons derive from the same atom] character of chemical bonding between I and O, I and N, and I and C atoms in hypervalent iodine compounds, and it is controversial with respect to the common I=X double-bond representation.

10-2. Results and discussion

To establish a reliable picture of the chemical bonding we have probed various hypervalent iodine molecules, such as IO_4^-, PhIO, $PhIO_2$, $PhIO_3$, PhINR (R=SO_2Ph), and $PhICR_2$ (R=CO_2Me). The geometries of all the structures were optimized at the PBE0/I/Stuttgart/H, C, N, O, S/aug-cc-pVTZ[4-8] level of theory with follow-up frequency calculations. All the structures were checked to be true minima with no imaginary frequencies. Chemical bonding analysis was performed using the adaptive natural density partitioning (AdNDP) method, which achieves a seamless description of systems

featuring both localized and delocalized bonding without invoking the concept of resonance.[9] The AdNDP approach has demonstrated effectiveness in the description of chemical bonding in many organic,[10] inorganic systems,[11] and clusters.[12]

It is known that the metaperiodate anion is composed of one iodine and four oxygen atoms, and is generally represented by having three double bonds between I and O, and one single I—O σ bond with a negative charge on the oxygen atom (Figure 10-2a). Application of the AdNDP method for the metaperiodate anion leads to the chemical bonding pattern shown in Figure 10-2.

AdNDP recovered one s-type and two p-type electron lone pairs (1c-2e) on each oxygen atom with occupation numbers (ONs) in the range of 1.84-1.99 |e|. Four 2c-2e I—O σ bonds (ON=2.00|e|) originate from the donation of electron density directly from iodine, thus indicating the dative character of these bonds. In addition, NBO analysis was performed to determine a charge distribution in this species. According to it, every oxygen atom bears a negative charge of −1.14, while iodine is positively charged (+3.56). Thus, our analysis shows that single dative I:→O bonds should be used to describe chemical bonding in IO_4^-. The appropriate symbolic representation according to the AdNDP analysis is demonstrated in Figure 10-2b.

Iodosylbenzene was first synthesized by C. Willgerodt from iodobenzene in 1892 and it has the empirical formula PhIO.[13] Similar to the IO_4^- case, it has been described as having a I═O bond (structure **1**, Figure 10-1), a formulation which clearly breaks the octet rule at iodine. The results of the AdNDP analysis and the corresponding symbolic representation of PhIO are summarized in Figure 10-3. As expected, AdNDP revealed three lone pairs (ON=1.75–1.99|e|) on the oxygen atom, one dative 2c-2e I→O σ bond

with ON=2.00|e|. The bonding between iodine and the carbon atom of the Ph group derives from the sharing of an electron pair between these atoms and thus represents a common single covalent I—C σ bond (ON=1.97|e|). The remaining electrons of I form two lone pairs with ON=1.99 |e| as shown in Figure 10-3. Complete AdNDP analysis of PhIO is given in Figure 10-6. We obtained a similar bonding pattern for $PhIO_2$ (see Figure 10-7) and $PhIO_3$ (see Figure 10-8), where the bonding between the oidine and oxygen atoms represents a single dative 2c-2e I→O σ bond and confirms the absence of I═O bonds. The situation described here appears to be akin to other oxyanions, including the well-known sulfate, nitrate, and phosphate anions (all of which we do not represent with a double-bond symbol) with an oxygen atom accepting the dative bond.

More complicated cases where the nature of the I—X bonding remains contentious were investigated using an iodonium imide and iodonium ylide (structures **2** and **3**; Figure 10-1). Results of the AdNDP analyses on I—N and I—C fragments and nearby atoms are shown in Figure 10-4 and Figure 10-5, respectively.

As one can see, in the iodonium imide PhINR ($R=SO_2Ph$) there are two lone pairs on N with ON=1.84–1.97 |e| and two lone pairs on I with ON=1.97–1.99|e| (Figure 10-4). Covalent bonds at the studied fragments are represented by 2c-2e I—C and 2c-2e N—S σ bonds with ON=1.91|e| and ON=1.96|e|, respectively. Again, the bonding between I and N has a dative character and is represented by the single 2c-2e I→N σ bond according to our analysis. The chemical bonding picture of the iodonium ylide $PhICR_2$ ($R=CO_2Me$) shows one dative I→C σ bond (ON=1.96|e|), one 2c-2e bond between I and C of the Ph fragment with ON=1.97|e|, two lone pairs on I (ON=1.96–1.99|e|), two 2c-2e C—C σ

bonds (ON=1.98|e|), and one 3c-2e π bond (ON=1.80 |e|) delocalized over three carbon atoms (Figure 10-5).

The 3c-2e π bond is responsible for the bending of the C-C-C fragment and can actually be represented by a lone pair on the central carbon atom with a somewhat lower occupation number (ON=1.48|e|). This data is supported by the NBO analysis, thus showing a positive charge of +0.75 on two flanking carbon atoms and a negative charge of −0.58 on the central carbon atom. The need to form the 3c-2e π bond comes from the fact that the carbon atom is less electronegative than either N or O and needs some help from its neighboring carbon atoms, thus transforming a lone pair into the 3c-2e π bond. The presence of this 3c-2e π bond seems to explain the C—C bond length (1.44 Å) on this fragment which is something average between the single and double C—C bond lengths. Similar cases wherein a 3c-2e π bond originates from the lone pair on the central carbon atom and makes the corresponding C–C distances shorter than a typical C—C bond length, are exemplified by such molecules as $C_8B_2^-$, C_9B^-, and C_{10}^-.[10g]

The bonding picture developed for $PhIC(CO_2Me)_2$ through the AdNDP analysis shows that the single dative I→C σ bond can be formed only if electron-withdrawing groups like CO_2Me take some electron density from the carbon atom (its charge is not −1.0 but only −0.58) connected to the iodine atom because the carbon atom is not electronegative enough to acquire two electrons from the iodine atom alone.

Essentially, the studied iodine compounds can be described as Lewis bases bonded to Lewis acids [-O, $-NSO_2Ph$, and $-C(CO_2Me)_2$]. This description means that the Lewis acidity of the three latter species should be related to the strength of the bonding to the iodine-containing Lewis base. Hence, the strength of donor–acceptor interactions

would be defined by the Lewis basicity/acidity of the components. The computed interaction energies between donor (PhI-) and corresponding acceptors suggest that -O ($-211.4\ kcal\ mol^{-1}$) is a stronger Lewis acid than -NSO_2Ph ($-132.0\ kcal\ mol^{-1}$) and -$C(CO_2Me)_2$ ($-163.6\ kcal\ mol^{-1}$) and that the strength of the donor–acceptor bonds follows the trend for the acceptors: O>$C(CO_2Me)_2$>NSO_2Ph. Thus, we believe that the derived description of the presented hypervalent iodine compounds as donor–acceptor complexes might be a very useful model for classifying known iodine compounds as well as for the design and prediction of novel molecules where the Lewis base and/or the Lewis acid are changed. Furthermore, our results might also be relevant to a broader range of existing compounds such as the carbodiphosphorane $Ph_3P{=}C{=}PPh_3$,[14] the borylene complex $(BH)L_2$,[15] the silylones SiL_2,[16] as well as the germylones GeL_2[17] (with different N-heterocyclic carbenes as ligands L), where a single dative bond rather than the double-bond character was confirmed based on their electronic structures and chemical behavior.[18-21]

According to the obtained chemical bonding pictures of all the studied molecules, it is clearly seen that the octet rule is obeyed in each case. Although we have used the term hypervalent throughout our discussion, it is noteworthy that it was purposely used to describe molecules which contain elements in any of their oxidation states other than their lowest oxidation state, and is in concordance with Musher's definition of a hypervalent molecule.[22] However, we agree with Gillespie and Silvi[23] who concluded that hypervalence is not a useful concept as hypervalent molecules are not different in any significant way from Lewis octet molecules.

10-3. Conclusions

In conclusion, we performed chemical-bonding analyses on several hypervalent iodine compounds where the presence of I=O, I=N, and I=C bonds was questionable. The AdNDP approach for the analyses of the MO wave functions of the corresponding compounds revealed only single I→X dative-bond character. The significant advancement made in the current study is that the bonding patterns and formulas are derived from the MO wave function by a unified and well-defined quantum chemical procedure. In particular, we believe that our representation of the studied hypervalent compounds might clarify the question of I—X double/single bond notation used in student courses and in current textbooks. We also believe that our theoretical findings can serve as a general guideline for the synthesis of new molecules with unusual bonds and reactivities.

10-4. Computational and theoretical methods

The detailed description of the AdNDP algorithm developed by Zubarev and Boldyrev can be found elsewhere.[9] From the computational point of view, AdNDP is a generalization of the NBO analysis by Weinhold.[24] AdNDP performs analysis of the first-order reduced density matrix with the purpose of obtaining its local block eigenfunctions with optimal convergence properties for describing the electron density. The local blocks of the first-order reduced density matrix correspond to the sets of *n* atoms (from one to all the atoms of the molecule) which are tested for the presence of a two-electron object (*n*c-2e bonds, including core electrons and lone pairs as a special case of *n*=1) associated with this particular set of *n* atoms. The n atomic sets are formed and checked in an exhaustive manner, so that the recovered *n*c-2e bonding elements

always correspond to the point group symmetry of the system after these bonding elements are superimposed onto the molecular frame. For the given n atomic block those eigenvectors are accepted whose occupation numbers (eigenvalues) exceed the established threshold value, usually close to 2.00|e|. Thus, Lewis's idea of an electronic pair as the essential element of bonding is preserved. The AdNDP procedure is numerically efficient because it involves only a series of diagonalizations of density matrix blocks. It is unbiased in the sense that no preliminary ideas of the bonding pattern are required to perform analysis. The AdNDP code is a stand-alone program that uses output from Gaussian 09. The density matrix used for the basis of the natural atomic orbitals as well as for the transformation between atomic orbital and natural atomic orbital basis sets, which are used by the AdNDP program, was generated at the B3LYP/LANL2DZ[25,26] level of theory by means of the NBO code[27] incorporated into Gaussian 09.[28] It is known that the results of NBO analysis do not generally depend on the quality of the basis set, so the choice of the level of theory for the AdNDP application is adequate. The visualization of the results of the calculations was performed by using MOLEKEL 5.4.0.8.[29]

References

[1] For books and selected reviews on hypervalent iodine chemistry, see: a) A. Varvoglis, *Hypervalent Iodine in Organic Synthesis,* Academic Press, London, 1997; b) *Hypervalent Iodine Chemistry*; T. Wirth, Ed.; Springer-Verlag, Berlin, 2003; c) V. V. Zhdankin, *Hypervalent Iodine Chemistry: Preparation, Structure, and Synthetic Applications of Polyvalent Iodine Compounds*; Wiley, Chichester, 2013; d) P. Dauban, R. H. Dodd, *Synlett* **2003**, 1571; e) S. Quideau, T. Wirth,

Tetrahedron **2010**, *66*, 5737; f) E. A. Merritt, B. Olofsson, *Synthesis* **2011**, 517; g) J. P. Brand, D. F. Gonzalez, S. Nicolai, J. Waser, *Chem. Commun.* **2011**, *47*, 102; h) A. Duschek, S. F. Kirsch, *Angew. Chem.* **2011**, *123*, 1562; *Angew. Chem., Int. Ed.* **2011**, *50*, 1524; i) J. L. F. Silva, B. Olofsson, *Nat. Prod. Rep.* **2011**, *28*, 1722; j) M. S. Yusubov, V. V. Zhdankin, *Curr. Org. Synth.* **2012**, *9*, 247; k) M. Brown, U. Farid, T. Wirth, *Synlett* **2013**, *24*, 424.

[2] Key references to computational studies on hypervalent iodine: a) A. I. Boldyrev, V. V. Zhdankin, J. Simons, P. J. Stang, *J. Am. Chem. Soc.* **1992**, *114*, 10569; b) V. E. Mylonas, M. P. Sigalas, G. A. Katsoulos, C. A. Tsipis, A. G. Varvoglis, *J. Chem. Soc., Perkin Trans. 2* **1994**, 1691; c) M. Boucher, D. Macikenas, T. Ren, J. D. Protasiewicz, *J. Am. Chem. Soc.* **1997**, *119*, 9366; d) G. A. Landrum, N. Goldberg, R. Hoffmann, *J. Chem. Soc., Dalton Trans.* **1997**, 3605; e) G. A. Landrum, N. Goldberg, R. Hoffmann, R. M. Minyaev, *New J. Chem.* **1998**, *22*, 883; f) V. V. Zhdankin, R. M. Arbit, B. J. Lynch, P. Kiprof and V. G. Young, *J. Org. Chem.* **1998**, *63*, 6590; g) U. H. Hirt, M. F. H. Schuster, A. N. French, O. G. Wiest, T. Wirth, *Eur. J. Org. Chem.* **2001**, 1569; h) P. Kiprof, V. Zhdankin, *ARKIVOC* **2003**, *(vi)*, 170; i) G. Barea, F. Maseras, A. Lledos, *New J. Chem.* **2003**, *27*, 811; j) J. T. Su, W. A. Goddard, III, *J. Am. Chem. Soc.* **2005**, *127*, 14146; k) M. Ochiai, T. Sueda, K. Miyamoto, P. Kiprof, V. V. Zhdankin, *Angew. Chem.* **2006**, *118*, 8383; *Angew. Chem., Int. Ed.* **2006**, *45*, 8203; l) P. K. Sajith, C. H. Suresh, *Inorg. Chem.* **2012**, *51*, 967; m) P. K. Sajith, C. H. Suresh, *Inorg. Chem.* **2013**, *52*, 6046.

[3] a) C. J. Carmalt, J. G. Crossley, J. G. Knight, P. Lightfoot, A. Martin, M. P. Muldowney, N. C. Norman, A. G. Orpen, *J. Chem. Soc., Chem. Commun.* **1994**, 2367; b) D. Macikenas, E. Skrzypczak-Jankun, J. D. Protasiewicz, *Angew. Chem.* **2000**, *112*, 2063; *Angew. Chem., Int. Ed.* **2000**, *39*, 2007; c) D. Macikenas, E. Skrzypczak-Jankun, J. D. Protasiewicz, *J. Am. Chem. Soc.* **1999**, *121*, 7164.

[4] R. A. Kendall, T. H. Dunning, R. J. Harrison, *J. Chem. Phys.* **1992**, *96*, 6796.

[5] T. H. Dunning, *J. Chem. Phys.* **1989**, *90*, 1007.

[6] A. Bergner, M. Dolg, W. Kuchle, H. Stoll, H. Preuss, *Mol. Phys.* **1993**, *80*, 1431.

[7] M. Kaupp, P. v. R. Schleyer, H. Stoll, H. Preuss, *J. Chem. Phys.* **1991**, *94*, 1360.

[8] M. Dolg, H. Stoll, H. Preuss, R. M. Pitzer, *J. Phys. Chem.* **1993**, *97*, 5852.

[9] D. Yu. Zubarev, A. I. Boldyrev, *Phys. Chem. Chem. Phys*. **2008**, *10*, 5207.

[10] a) D. Yu. Zubarev, A. I. Boldyrev, *J. Org. Chem*. **2008**, *73*, 9251; b) I. A. Popov, A. I. Boldyrev, *Eur. J. Org. Chem.* **2012**, 3485; c) A. Popov, K. V. Bozhenko, A. I. Boldyrev, *Nano Res.* **2012**, *5*, 117; d) I. A. Popov, Y. Li, Z. Chen, A. I. Boldyrev, *Phys. Chem. Chem. Phys*. **2013**, 15, 6842; e) A. S. Ivanov, A. I. Boldyrev, *J. Phys. Chem. A* **2012**, *116*, 9591; f) I. A. Popov, A. I. Boldyrev, *J. Phys. Chem. C* **2012**, *116*, 3147; g) I. A. Popov, V. F. Popov, K. V. Bozhenko, I. Cernusak, A. I. Boldyrev, *J. Chem. Phys.* **2013**, *139*, 114307.

[11] a) L. Cheng, Y. Yuan, X. Zhang, J. Yang, *Angew. Chem. Int. Ed.* **2013**, *52*, 9035; b) A. S. Ivanov, K. V. Bozhenko, A. I. Boldyrev, *Inorg. Chem*. **2012**, *51*, 8868; c) A. P. Sergeeva, A. I. Boldyrev, *Phys. Chem. Chem. Phys*. **2010**, *12*, 12050; d) T. R. Galeev, A. S. Ivanov, C. Romanescu, W.-L. Li, K. V. Bozhenko, L.-S. Wang, A. I. Boldyrev, *Phys. Chem. Chem. Phys*. **2011**, *13*, 8805; e) A. S. Ivanov, K. V.

Bozhenko, A. I. Boldyrev, *J. Chem. Theory and Comput*. **2011**, *8*, 135; f) W.-L. Li, A. S. Ivanov, J. Federic, C. Romanescu, I. Cernusak, A. I. Boldyrev, L.-S. Wang, *J. Chem. Phys.* **2013**, *139*, 104312; g) A. S. Ivanov, A. I. Boldyrev, G. Frenking, *Chem. Eur. J.* **2014**, *20*, 2431; h) J. K. Olson, A. S. Ivanov, A. I. Boldyrev, *Chem. Eur. J.* **2014**, *DOI: 10.1002/chem.201402572*; i) I. A. Popov, A. I. Boldyrev, *Comp. Theor. Chem.* **2013**, *1004*, 5; j) I. A. Popov, W.-L. Li, Z. A. Piazza, A. I. Boldyrev, L.-S. Wang, *J. Phys. Chem. A* **2014**, *DOI:10.1021/jp411867q*; k) A. P. Sergeeva, I. A. Popov, Z. A. Piazza, W.-L. Li, C. Romanescu, L.-S. Wang, A. I. Boldyrev, *Acc. Chem. Res*. **2014**, *47*, 1349; l) M. Perić, L. Andjelković, M. Zlatar, C. Daul, M. Gruden-Pavlović, *Polyhedron* **2014**, DOI: 10.1016/j.poly.2014.02.005; m) A. C. Castro, E. Osorio, J. L. Cabellos, E. Cerpa, E. Matito, M. Solà, M. Swart, G. Merino, *Chem. Eur. J.* **2014**, *20*, 4583; n) S. Blanchard, L. Fensterbank, G. Gontard, E. Lacôte, G. Maestri, M. Malacria, *Angew. Chem. Int. Ed.* **2014**, *53*, 1987; o) A. Wagner, E. Kaifer, H.-J. Himmel, *Chem. Eur. J.* **2013**, *19*, 7395.

[12] a) L. Cheng, *J. Chem. Phys.* **2012**, *136*, 104301; b) Y.-B. Wu, Y.-Q. Li, H. Bai, H.-G. Lu, S.-D. Li, H.-J. Zhai, Z.-X. Wang *J. Chem. Phys.* **2014**, *140*, 104302; c) W.-L. Li, L. Xie, T. Jian, C. Romanescu, X. Huang, L.-S. Wang, *Angew. Chem.* **2014**, *126*, 1312; d) Y. Pei, S. Lin, J. Su, C. Liu, *J. Am. Chem. Soc.* **2013**, *135*, 19060; e) Q. Chen, H. Bai, J.-C. Guo, C.-Q. Miaoab, S.-D. Li, *Phys. Chem. Chem. Phys.* **2011**, *13*, 20620.

[13] C. Willgerodt *Ber. Dtsch. Chem. Ges.* **1892**, *25*, 3494.

[14] F. Ramirez, N. B. Desai, B. Hansen, N. McKelvie, *J. Am. Chem. Soc.* **1961**, *83*, 3539.

[15] R. Kinjo, B. Donnadieu, M. A. Celik, G. Frenking, G. Bertrand, *Science* **2011**, *333*, 610.

[16] a) K. C. Mondal, H. W. Roesky, F. Klinke, M. C. Schwarzer, G. Frenking, B. Niepçtter, H. Wolf, R. Herbst-Irmer, D. Stalke, *Angew. Chem.* **2013**, *125*, 3036; *Angew. Chem. Int. Ed.* **2013**, *52*, 2963; b) Y. Xiong, S. Yao, S. Inoue, J. D. Epping, M. Driess, *Angew. Chem.* **2013**, *125*, 7287; *Angew. Chem. Int. Ed.* **2013**, *52*, 7147.

[17] a) Y. Xiong, S. Yao, G. Tan, S. Inoue, M. Driess, *J. Am. Chem. Soc.* **2013**, *135*, 5004; b) Y. Li, K. C. Mondal, H. W. Roesky, H. Zhu, P. Stollberg, R. Herbst-Irmer, D. Stalke, D. M. Andrade, *J. Am. Chem. Soc.* **2013**, *135*, 12422.

[18] R. Tonner, F. Öxler, B. Neumüller, W. Petz, G. Frenking, *Angew. Chem.* **2006**, *118*, 8206; *Angew. Chem. Int. Ed.* **2006**, *45*, 8038.

[19] M. A. Celik, R. Sure, S. Klein, R. Kinjo, G. Bertrand, G. Frenking, *Chem. Eur. J.* **2012**, *18*, 5676.

[20] a) N. Takagi, T. Shimizu, G. Frenking, *Chem. Eur. J.* **2009**, *15*, 3448; b) N. Takagi, T. Shimizu, G. Frenking, *Chem. Eur. J.* **2009**, *15*, 8593; c) N. Takagi, G. Frenking, *Theor. Chem. Acc.* **2011**, *129*, 615.

[21] G. Frenking, *Angew. Chem. Int. Ed.* **2014**, DOI: 10.1002/anie.201311022

[22] J. L. Musher, *Angew. Chem. Int. Ed. Engl.* **1969**, *8*, 54.

[23] R. J. Gillespie, B. Silvi, *Coord. Chem. Rev.* **2002**, *233-234*, 53.

[24] F. Weinhold, C. R. Landis, *Valency and Bonding: A Natural Bond Orbital Donor-Acceptor Perspective*, Cambridge University Press: Cambridge, **2005**.

[25] a) R. G. Parr, W. Yang, *Density-Functional Theory of Atoms and Molecules*, Oxford University Press: Oxford, **1989**; b) A. D. Becke, *J. Chem. Phys.* **1993**, *98*, 5648; c) J. P. Perdew, J. A. Chevary, S. H. Vosko, K. A. Jackson, M. R. Pederson, D. J. Singh, C. Fiolhais, *Phys. Rev. B* **1992**, *46*, 6671.

[26] P. J. Hay, W. R. Wadt, *J. Chem. Phys.* **1985**, *82*, 299.

[27] E. D. Glendening, A. E. Reed, J. E. Carpenter, F. Weinhold, NBO, version 3.1.

[28] Gaussian 09, Revision B.0.1, M. J. Frisch, G. W. Trucks, H. B. Schlegel, G. E. Scuseria, M. A. Robb, J. R. Cheeseman, G. Scalmani, V. Barone, B. Mennucci, G. A. Petersson, H. Nakatsuji, M. Caricato, X. Li, H. P. Hratchian, A. F. Izmaylov, J. Bloino, G. Zheng, J. L. Sonnenberg, M. Hada, M. Ehara, K. Toyota, R. Fukuda, J. Hasegawa, M. Ishida, T. Nakajima, Y. Honda, O. Kitao, H. Nakai, T. Vreven, J. A. Montgomery, Jr., J. E. Peralta, F. Ogliaro, M. Bearpark, J. J. Heyd, E. Brothers, K. N. Kudin, V. N. Staroverov, R. Kobayashi, J. Normand, K. Raghavachari, A. Rendell, J. C. Burant, S. S. Iyengar, J. Tomasi, M. Cossi, N. Rega, J. M. Millam, M. Klene, J. E. Knox, J. B. Cross, V. Bakken, C. Adamo, J. Jaramillo, R. Gomperts, R. E. Stratmann, O. Yazyev, A. J. Austin, R. Cammi, C. Pomelli, J. W. Ochterski, R. L. Martin, K. Morokuma, V. G. Zakrzewski, G. A. Voth, P. Salvador, J. Dannenberg, S. Dapprich, A. D. Daniels, Ö. Farkas, J. B. Foresman, J. V. Ortiz, J. Cioslowski, and D. J. Fox, Gaussian, Inc, Wallingford, CT, **2009**.

[29] U. Varetto, Molekel 5.4.0.8, Swiss National Supercomputing Centre, Manno, Switzerland, **2009**.

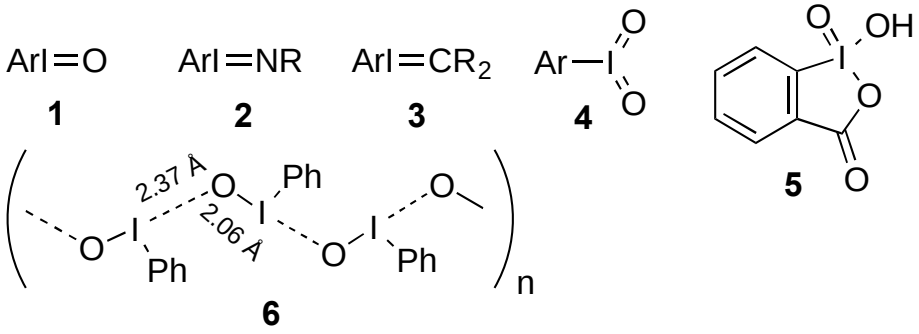

Figure 10-1. Common representation of hypervalent iodine compounds with I=X (X= O, N, C) double bonds (structures **1**-**5**) adopted in research literature and the polymeric structure of iodosylbenzene **6**.

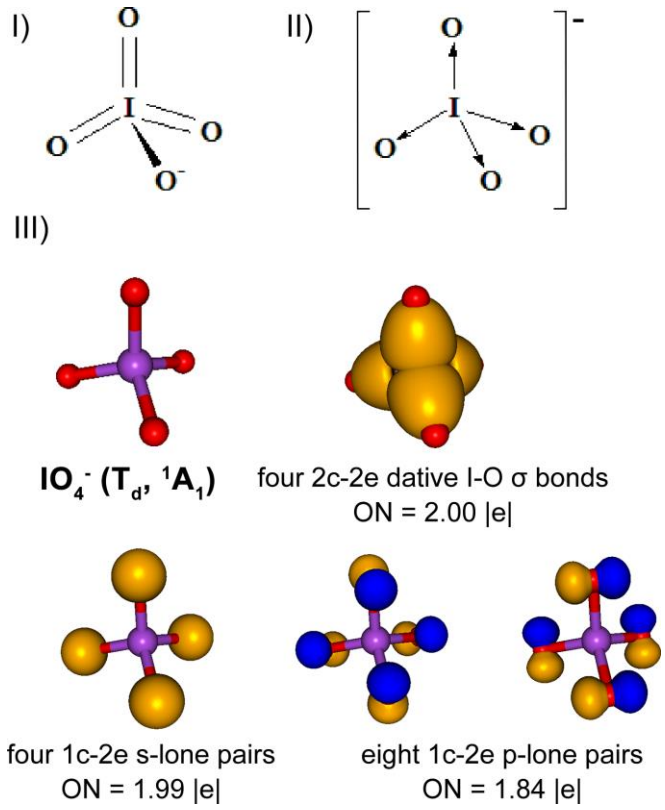

Figure 10-2. I) General representation of the IO4- structure; II) Symbolic representation of IO4- according to AdNDP; III) AdNDP bonding pattern of IO4-. The corresponding point group symmetry and spectroscopic state of IO4- are given in parenthesis. ON stands for the occupation number here and elsewhere.

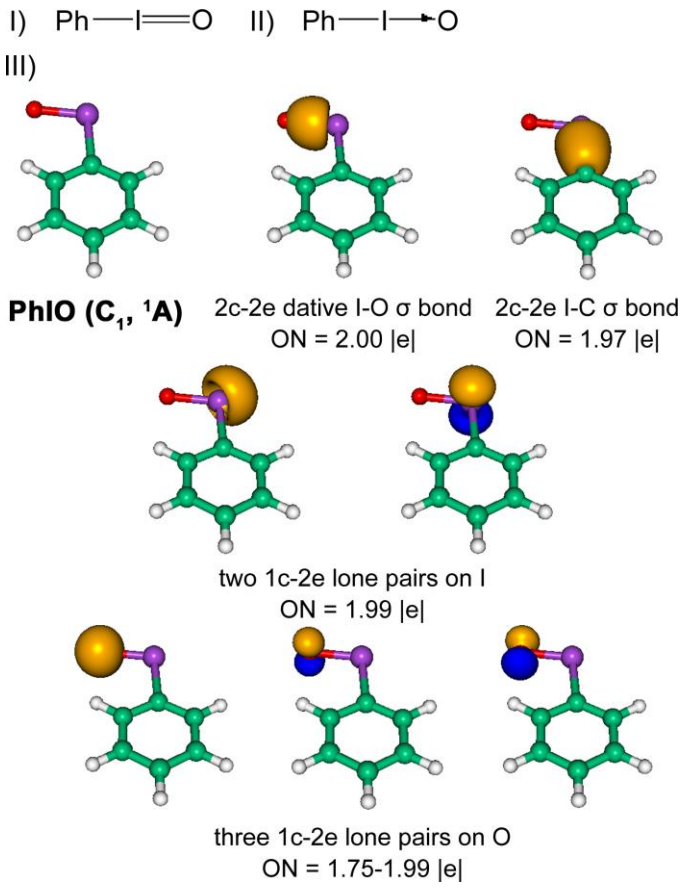

Figure 10-3. I) General representation of the PhIO structure; II) Symbolic representation of PhIO according to AdNDP. III) AdNDP bonding pattern for PhIO). The corresponding point group symmetry and spectroscopic state of PhIO are given in parenthesis.

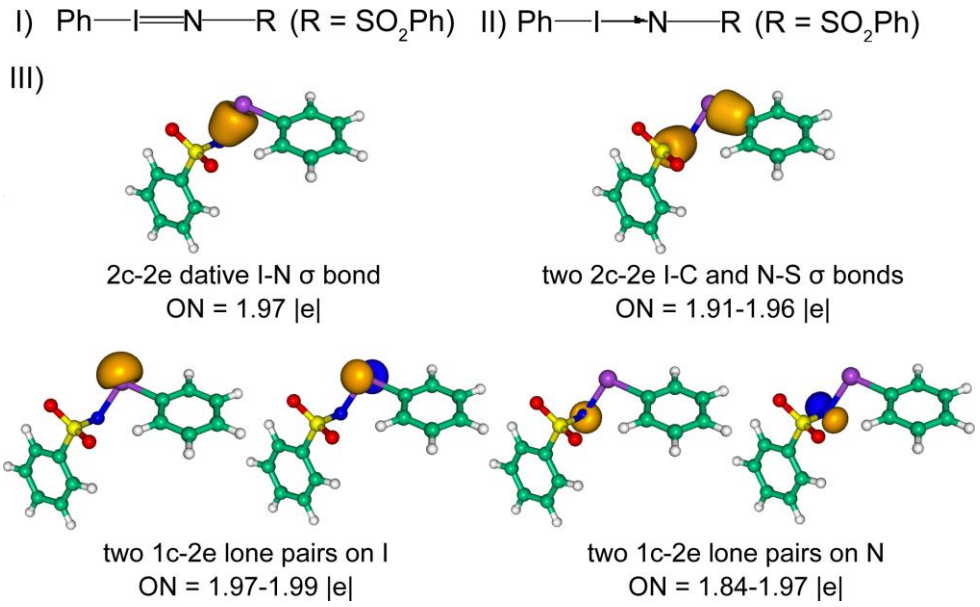

Figure 10-4. I) General representation of the $PhINSO_2Ar$ structure; II) Symbolic representation of $PhINSO_2Ar$ according to AdNDP; III) AdNDP bonding pattern of the $PhINSO_2Ph$ molecule on the I-N, S-N, and I-C fragments.

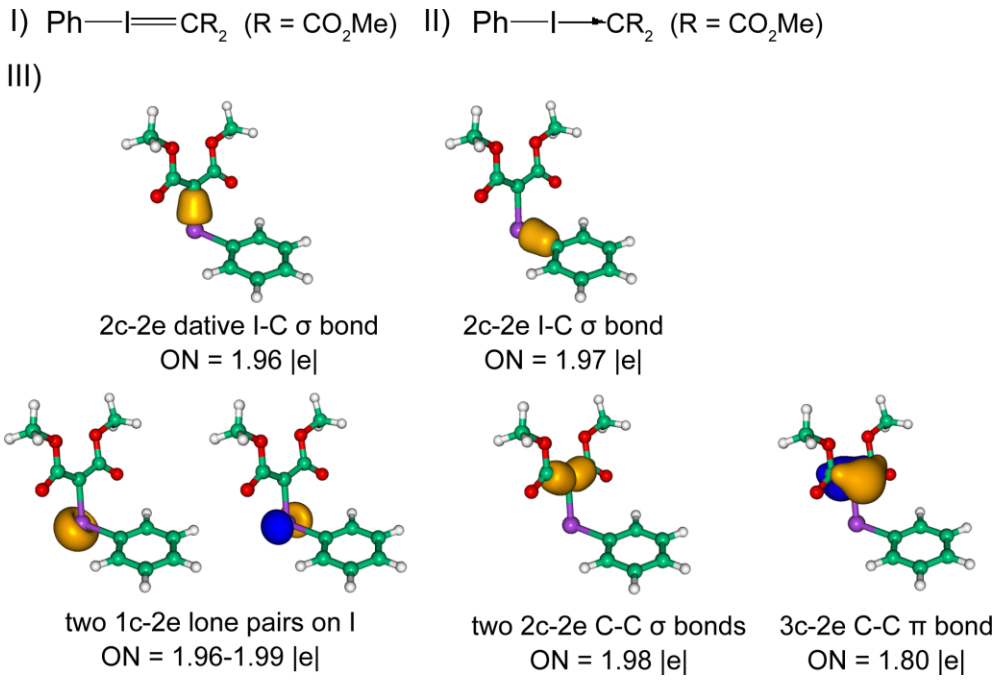

Figure 10-5. I) General representation of the $PhIC(CO_2Me)_2$ structure; II) Symbolic representation of $PhIC(CO_2Me)_2$ according to AdNDP; III) AdNDP bonding pattern of the $PhIC(CO_2Me)_2$ molecule on the I-C, C-C fragments.

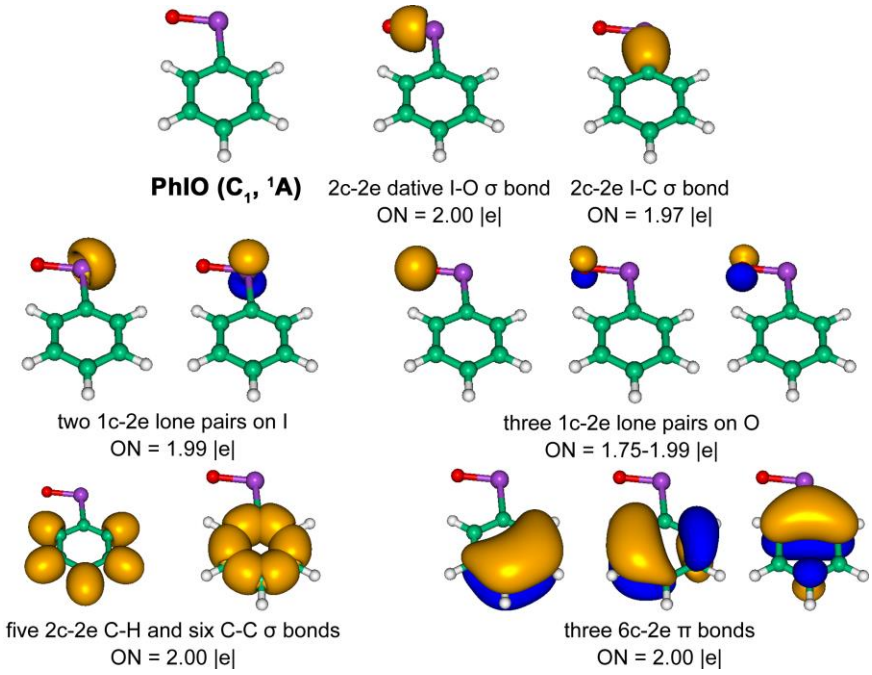

Figure 10-6. Complete AdNDP analysis of chemical bonding in PhIO molecule. ON stands for the occupation number here and elsewhere.

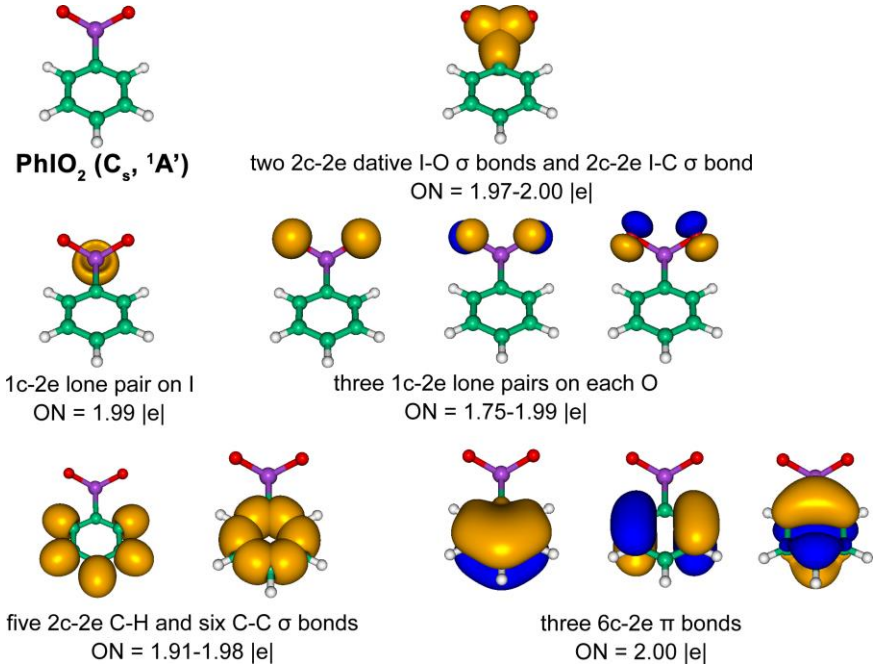

Figure 10-7. Complete AdNDP analysis of chemical bonding in $PhIO_2$ molecule.

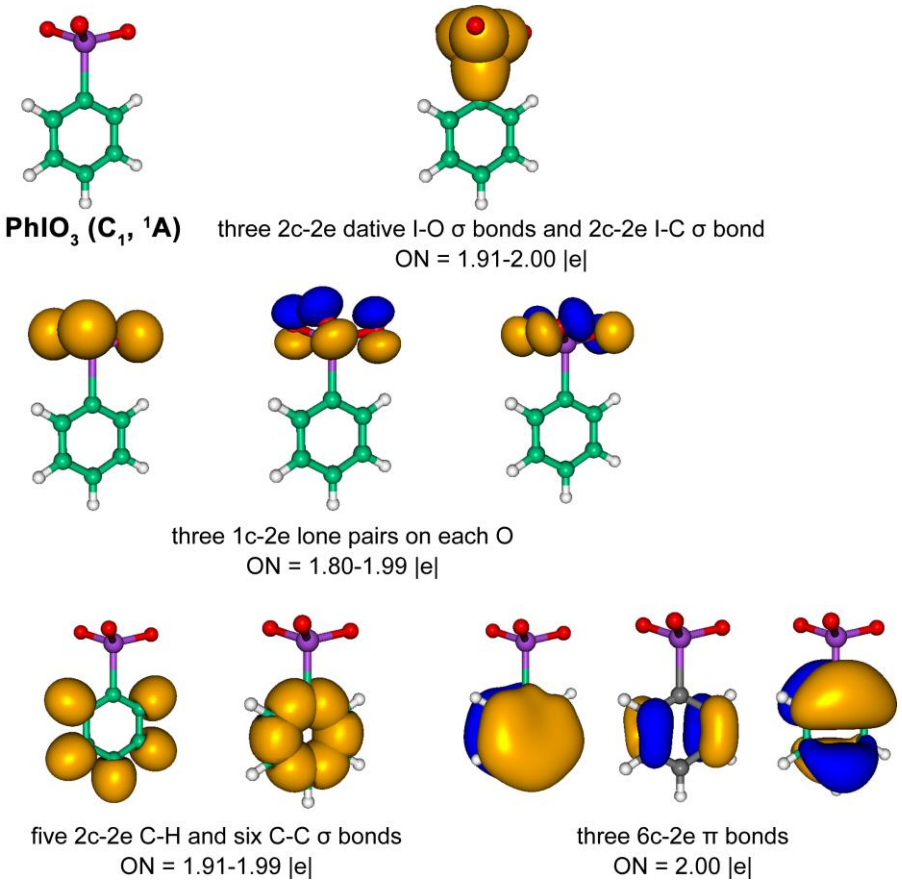

Figure 10-8. Complete AdNDP analysis of chemical bonding in $PhIO_3$ molecule.

CHAPTER 11

$Si_{6-n}C_nH_6$ (n = 0–6) SERIES: WHEN DO SILABENZENES BECOME PLANAR AND GLOBAL MINIMA?[1]

Abstract

In the current work we studied a structural transition from non-planar three-dimensional structures to planar benzene-like structures in the $Si_{6-n}C_nH_6$ (n = 0–6) series. We performed unbiased Coalescence-Kick global minimum and low-lying isomers search for the Si_6H_6, Si_5CH_6, $Si_4C_2H_6$, $Si_3C_3H_6$, $Si_2C_4H_6$ and SiC_5H_6 stoichiometries at the B3LYP/6-31G** level of theory. The lowest isomers were recalculated at the CCSD(T)/CBS//B3LYP/6-311++G** level of theory. It was shown that the pseudo Jahn-Teller effect, which is responsible for the deformation of planar Si_6H_6, Si_5CH_6 and $Si_4C_2H_6$ structures, is suppressed at n = 3 (the planar structure of 1,3,5-trisilabenzene). We also showed that the 3D-2D transition, which occurs only at n = 5, is due to the aromaticity of monosilabenzene (SiC_5H_6) along with other factors, such as stronger C–C σ bonds compared to weaker C–Si and Si–Si σ bonds.

11-1. Introduction

Silicon and carbon are both in the fourth column of the Periodic Table, however, structures and properties of their compounds are very different. As for hydrocarbons with C_6H_6 stoichiometry, the aromatic benzene molecule is by far the lowest-energy structure, with benzvalene and prismane being more than 70 kcal/mol higher.[1] Silicon hydrides Si_xH_y, contrary to hydrocarbons, are usually characterized by electron-poor bonds,[2-5]

[1] Coauthored by Alexander S. Ivanov and Alexander I. Boldyrev. Reprinted with permission from *J. Phys. Chem. A* **2012**, 116, 9591−9598.

weaker π-π interaction,[6,7] and even the hydrocarbon analogs satisfying the octet rule are not the most stable isomers on the potential energy surface (PES) of Si_xH_y.[8-12] In spite of that the question regarding the possibility of planar benzene-like silicon analogs has been addressed long ago[13,14] and it continues to be the subject of research nowadays.[15,16] Hexasilabenzene (structure I.33, Figure 11-1) has been studied considerably[14,17] as a molecule analogous to benzene, and its aromaticity has also been discussed.[18] It is turned out that the D_{6h} hexasilabenzene structure I.33 is not even a local minimum, but a first-order saddle point. Geometry optimization along the imaginary mode leads to the distorted nonplanar chairlike structure I.32 (D_{3d}, $^1A_{1g}$).[14] According to the present calculations at CCSD(T)/CBS//B3LYP/6-311++G**, chairlike structure I.32 (Figure 11-1) is 51.4 kcal/mol higher than the global minimum structure I.1 and 20.7 kcal/mol higher than prismane I.18 (Figure 11-1), which has been considered as the global minimum structure of Si_6H_6 for almost thirty years.[13,17,19] It was recently shown that prismane is just a local minimum on the Si_6H_6 PES and structure I.1 is the global minimum for Si_6H_6 stoichiometry.[20] Structure I.1 was isolated and characterized in the form of aryl-substituted Si_6H_6 according to the latest experimental reports.[21]

A structural transition from the three-dimensional non-planar structures to the two-dimensional planar benzene-like structures is expected to occur in the $Si_{6-n}C_nH_6$ (n = 0–6) series upon sequential substitution of the Si atoms by C atoms. In this work we present a systematic study of $Si_{6-n}C_nH_6$ (n = 0–6) series and demonstrate that benzene-like structures become the lowest energy isomers only at n = 5 (SiC_5H_6). The above mentioned distortion of the D_{6h} hexasilabenzene Si_6H_6 was traced in the series also. We showed that the pseudo Jahn-Teller (PJT) effect, which is responsible for such a

distortion, is completely suppressed at n = 3 (the planar structure of 1,3,5-trisilabenzene $Si_3C_3H_6$).

11-2. Computational and theoretical methods

A computational search for the global minima structures of Si_6H_6, Si_5CH_6, $Si_4C_2H_6$, $Si_3C_3H_6$, $Si_2C_4H_6$ and SiC_5H_6 stoichiometries was performed using the Coalescence Kick (CK) program written by Averkiev.[22] In the CK method, a random structure is first checked for connectivity: if all atoms in the structure belong to one fragment, then the structure is considered as connected, and the Berny algorithm[23] for geometry optimization procedure is applied to it. However, in most cases, a randomly generated structure is fragmented; that is, the structure contains several fragments nonbonded with each other including cases with just one atom not being connected. In these cases, the coalescence procedure is applied to the fragmented structure - all of the fragments are pushed to the center of mass simultaneously. The magnitude of shift should be small enough so that atoms do not approach each other too closely but large enough so that the procedure converges in a reasonable amount of time. In the current version of the CK program, a 0.2 Å shift is used. The obtained structure is checked for connectivity again, and the procedure repeats. When two fragments approach each other close enough, they "coalesce" to form a new fragment, which will be pushed as a whole in the following steps. Obviously, at some point, all fragments are coalesced. This method does not deal with cases when, in a randomly generated structure, two atoms are too close to each other. To avoid this problem, the initial structures are generated in a very large box with all three linear dimensions being 4* (the sum of atomic covalent radii). Hence, usually an initially generated random structure consists of separated atoms as initial

fragments. The current version of the program is designed for the global minimum searches of both single molecules of desired composition and complexes of molecules like solvated anions (e.g., $SO_4^{2-}•4H_2O$),[24,25] where the initial geometry of each molecular unit is specified in the input file. In the latter case, the two molecular units of the complex are considered as connected in a fragment if the distances between two of their atoms are less than the sum of the corresponding van der Waals radii.

The CK calculations were performed at the B3LYP level of theory[26-28] using the 6-31G** split-valence basis set.[29] Low-lying isomers, within 50 kcal/mol with respect to the lowest energy isomer, were reoptimized with follow up frequency calculations at the B3LYP level of theory using the 6-311++G** basis set.[30-33] The final relative energies of the found low-lying isomers were calculated at the CCSD(T)/CBS level by extrapolating CCSD(T)/cc-pvDZ and CCSD(T)/cc-pvTZ[34-38] to the infinite basis set using the Truhlar formula.[39,40] Though the CCSD(T)/CBS results may sometimes be less accurate than CCSD(T)/cc-pvTZ results, here we present the results of the CCSD(T)/CBS level of theory for evaluating relative energies of isomers in the $Si_{6-n}C_nH_6$ (n = 0–6) series. The relative energies at B3LYP/6-311++G**, CCSD(T)/cc-pvDZ, CCSD(T)/cc-pvTZ, and CCSD(T)/CBS for all studied isomers can be found in the Figures 11-5 – 11-10.

A chemical bonding analysis was performed using Adaptive Natural Density Partitioning (AdNDP) recently proposed by Zubarev and Boldyrev[41,42] and Natural Bond Orbital (NBO) analysis developed by Weinhold.[43,44] The AdNDP approach leads to partitioning of the charge density into elements with the lowest possible number of atomic centers per electron pair: n-center, two-electron (nc–2e) bonds, including core electrons, lone pairs, 2c–2e bonds, etc. If some part of the density cannot be localized in

this manner, it is represented using completely delocalized objects, similar to canonical MOs, naturally incorporating the idea of the completely delocalized bonding. Thus, AdNDP achieves a seamless description of different types of chemical bonds. The density matrix in the basis of the natural atomic orbitals as well as the transformation between atomic orbital and natural atomic orbital basis sets was generated at the B3LYP/6-31G** level of theory by means of the NBO 3.1 code[45] incorporated into Gaussian 09. It is known that the results of the NBO and AdNDP analysis do not generally depend on the quality of the basis set, so the choice of the level of theory for the AdNDP analysis is adequate. All ab initio calculations were done using the Gaussian 09 program.[46] AdNDP calculations were performed using the program written by Zubarev. Molecular structure visualization was performed with the Chemcraft[47] and Molekel 5.4.0.8[48] programs.

11-3. Results and discussion

In the current article we investigated two transitions in the $Si_{6-n}C_nH_6$ (n = 0–6) series upon replacing silicon atoms by carbon atoms. Our first goal was to track where the pseudo Jahn-Teller effect, responsible for the distortion of planar silabenzene structures is completely suppressed, and the silabenzenes become local minima. Then, we moved on to determination at what n the planar silabenzene isomers become global minimum structures.

11-3.1. Si_6H_6 Isomers

In spite of the fact that five isomers for C_6H_6 stoichiometry: benzene, benzvalene, Dewar-benzene, prismane, and bicyclopropenyl have been isolated and well known,[49-52]

only the hexasilaprismane (structure I.18 (D_{3h},$^1A_1$'), Figure 11-2) derivative with six tetracoordinate sp^3 Si atoms was synthesized until recently. In 2010 K. Abersfelder et al.[53] experimentally obtained the tricyclic hexasilabenzene isomer (Si_6R_6 with R = 2,4,6-*i*$Pr_3C_6H_2$). This compound was reported as stable and according to X-ray crystallography it has a chairlike tricyclic silicon frame. One year later, the same authors isolated and characterized an aryl-substituted version of the global minimum (structure I.1 (C_{2v}, $^1A_1$), Figure 11-2) on the Si_6H_6 potential energy surface.[21] Hence, three isomers of Si_6H_6 were synthesized to present day.

In our search for the global minimum structure of Si_6H_6, all low-lying isomers revealed by the CK program (at B3LYP/6-31G*) were reoptimized at B3LYP/6-311++G** and obtained geometries were used for single point energy calculations at CCSD(T)/cc-vDZ, CCSD(T)/cc-pvTZ, CCSD(T)/CBS (see Figure 11-5). Our results for Si_6H_6 are in accordance with calculations reported by M. Moteki et al.[20] The most stable isomer on the Si_6H_6 PES is structure I.1, with the third lowest isomer (structure I.3, Figure 11-2) lying 17.7 kcal/mol above the global minimum. The D_{6h} benzene-like planar structure I.33 (Figure 11-1) is not a minimum, but is a first-order saddle point. Geometry optimization along the imaginary frequency mode leads to distorted chairlike isomer I.32. Planar hexasilabenzene is 51.5 kcal/mol higher in energy than the global minimum I.1 according to our calculations.

The deviation from planarity in hexasilabenzene is caused by the only source of instability of high-symmetry configurations of polyatomic systems, namely, the Jahn-Teller vibronic coupling,[54,55] the pseudo-Jahn-Teller (PJT) effect to be exact in this case. The distortion of the structure I.33 into the structure I.32 along the b_{2g} mode occurs due

to vibronic coupling of HOMO (e_{1g}) and LUMO+2 (e_{2g}). The product of their symmetries contains the symmetry of the imaginary mode (b_{2g}):

$$e_{1g} \otimes e_{2g} = b_{1g} \oplus b_{2g} \oplus e_{1g} \qquad (1)$$

Hence, the symmetry rule[56] for the PJT effect is satisfied as is the second condition[56]: the symmetry of the imaginary mode (b_{2g}) of the D_{6h} structure corresponds to the symmetric (a_{1g}) mode in the distorted D_{3d} isomer. The HOMO and LUMO+2 gap is 9.78 eV (HF/cc-pvTZ//B3LYP/6-311++G**). The other two closest in energy OMO-UMO pairs [HOMO-1 (a_{2u}) – LUMO+3 (b_{1u}) and HOMO-4 (e_{1u}) – LUMO (e_{2u})] corresponding the symmetry rule, have significantly larger energy gaps: 12.69 and 13.30 eV, respectively. Evidently, the 9.78 eV OMO – UMO gap is small enough to cause the PJT effect. The chairlike structure I.32 is only 2.0 kcal/mol lower (B3LYP/6-311++G**) than planar structure I.33 after zero-point energy correction. It is worthy to notice that hexasilabenzene is aromatic[18], but aromaticity itself is not sufficient to make the planar geometry stable and deformation occurs due to the PJT effect.

11-3.2. Si_5CH_6 Isomers

Our CK global minimum search for Si_5CH_6 stoichiometry revealed that structure II.1 (Figure 11-2) is the global minimum. Structure II.1 is very similar to the global minimum structure of Si_6H_6. The only difference is that one Si is substituted by C atom. The second lowest isomer of Si_5CH_6, structure II.2 (Figure 11-6), lying 4.9 kcal/mol higher, is a permutational isomer of the global minimum, with one carbon atom located on the opposite side. Four representative isomers of Si_5CH_6 are shown in Figure 11-2. The benzene-like structure II.20 (Figure 11-6) is 43.9 kcal/mol higher in energy. Again,

as it was in the case of hexasilabenzene, monosubstituted Si_6H_6 is a saddle point, but with two imaginary frequency modes [$\omega_1(b_1) = 140.4i$ cm^{-1} and $\omega_2(a_2) = 43.2i$ cm^{-1}]. The PJT effect is responsible for the two imaginary frequency modes (b_1 and a_2) in the planar C_{2v} structure. Optimization of Si_5CH_6 along the b_1 and a_2 imaginary vibrational modes leads to the C_s structure. Two OMO-UMO pairs giving the b_1 symmetry as a direct product of their symmetries (equations (2) and (3)) are HOMO-1 (b_1) – LUMO+1 (a_1) and HOMO (a_2) – LUMO+3 (b_2) with the energy gaps of 10.08 and 9.67 eV (HF/cc-pvTZ//B3LYP/6-311++G**), respectively.

$$b_1 \otimes a_1 = b_1 \qquad (2)$$

$$a_2 \otimes b_2 = b_1 \qquad (3)$$

The direct products of the symmetries of HOMO (a_2) – LUMO+2 (a_1) as well as HOMO-2 (b_2) – LUMO (b_1) (energy gaps are 9.01 and 10.57 eV, respectively) are a_2:

$$a_2 \otimes a_1 = a_2 \qquad (4)$$

$$b_2 \otimes b_1 = a_2 \qquad (5)$$

The symmetries of two imaginary modes in the C_{2v} structure (b_1 and a_2) correspond to the totally symmetric mode a’ in the distorted structure II.19 (C_s, ^{1}A’) (Figure 11-2). Thus, both PJT conditions are met. Substitution of one Si atom in hexasilabenzene leads to higher OMO-UMO gaps in Si_5CH_6, but the increased gaps are not large enough to prevent orbital coupling and kill the PJT effect.

11-3.3. $Si_4C_2H_6$ Isomers

The CK search of the $Si_4C_2H_6$ species revealed that the potential energy surface has more low-lying structures than that of Si_6H_6 and Si_5CH_6. We found many structures that are similar to Si_6H_6 and Si_5CH_6 isomers, but with two carbons in the skeleton. The global minimum is the C_{2v} structure III.1 (Figure 11-1). Prismane structure III.49 is now higher than the benzene-like structure III.43 (Figure 11-7) on 2.8 kcal/mol (CCSD(T)/CBS//B3LYP/6-311++G**). Of the three benzene-like isomers, only the 1,2,4,5-isomer (structure III.52 (D_{2h},^1A_g), Figure 11-7) has a planar ground state, but it is the highest among all benzene-like isomers of $Si_4C_2H_6$. The 1,2,3,5-isomer III.43 is 8.9 kcal/mol lower than the 1,2,3,4-isomer III.51 (C_{2v}, $^1A_1$) (Figure 11-7), however, both of them are just first-order saddle points with imaginary frequency modes of $\omega(b_1)=151.2i$ cm^{-1} and $\omega(a_2)=184.2i$ cm^{-1}, respectively. The b_1 imaginary frequency mode in the C_{2v} structure III.43 is again a consequence of the PJT effect, but the a_2 mode is now real. Optimization of the structure along b_1 imaginary mode lead to the C_s structure III.42 (Figure 11-2). The direct product of HOMO (b_1) and LUMO+2 (a_1) yields b_1, which is the symmetry of the imaginary mode:

$$b_1 \otimes a_1 = b_1 \qquad (6)$$

The HOMO and LUMO+2 gap is 9.77 eV (HF/cc-pvTZ//B3LYP/6-311++G**). The closest in energy OMO-UMO pairs, giving a_2 as a direct product of symmetries, HOMO (b_1) – LUMO+3 (b_2) and HOMO-1 (a_2) – LUMO+2 (a_1) have the energy gaps of 10.46 and 11.32 eV, respectively. Interestingly, this small increase in the UMO-OMO gap is enough to suppress the PJT effect along the a_2 mode.

Structure III.51 (the 1,2,3,4-isomer of $Si_4C_2H_6$) undergoes the PJT distortion along a_2 imaginary frequency mode into twisted C_2 structure III.50 because of interaction of HOMO (a_2) with LUMO+2 (a_1) (the HOMO – LUMO+2 gap, computed at HF/cc-pvTZ//B3LYP-6-311++G**, is 9.24 eV).

Finally, for the D_{2h} structure III.52 (the 1,2,4,5-isomer of $Si_4C_2H_6$) two lowest vibrational frequencies ($\omega_1(b_{2g})$ = 73.5 cm^{-1} and $\omega_2(a_u)$ = 73.9 cm^{-1}) have a small but real values for both frequencies. The gap between the closest OMO-UMO pair [HOMO (b_{1g}) – LUMO+3 (b_{3g})] leading to b_{2g} symmetry is 9.93 eV and the OMO-UMO pair [HOMO (b_{1g}) – LUMO+4 (b_{1u})] leading to a_u symmetry is 10.15 eV. Obviously, the OMO-UMO gap is now higher than in the two other cases and that is enough to kill the PJT effect in this case.

11-3.4. $Si_3C_3H_6$ Isomers

From our CK search for the global minimum structure of $Si_3C_3H_6$ stoichiometry, we found that again structure IV.1 (Figure 11-2) similar to the global minimum structures of Si_6H_6 - $Si_4C_2H_6$ is the lowest energy isomer on the $Si_3C_3H_6$ PES. The prismane isomer IV.16, lying 36.6 kcal/mol above the global minimum, is now the least stable of the considered structures shown in Figure 11-2. Of the three planar isomers, 1,3,5-trisilabenzene (structure IV.3, Figure 11-2) is the lowest one, and it has been thoroughly studied theoretically.[57-60] Moreover, in 2003 it was synthesized as a ligand according to the experimental reports.[61] The 1,3,5-trisilabenzene is the global minimum (at B3LYP/6-311++G**//B3LYP/6-311++G**, Figure 11-8), however, our most accurate single-point calculations at CCSD(T)/CBS//B3LYP/6-311++G** showed that planar structure IV.3 is the third lowest isomer, following the isomers IV.2 and IV.1, respectively (Figure 11-2).

We can see that in our $Si_{6-n}C_nH_6$ series at n = 3, the energy difference between three-dimensional and planar structures is not large anymore (6.5 kcal/mol).

The lowest frequency [ω(e'') = 211.7 cm^{-1}] for the planar D_{3h} structure IV.3 is real. The gap (HF/cc-pvTZ//B3LYP/6-311++G**) between the closest OMO-UMO pair [HOMO (e'') – LUMO+1 (a_1')] leading to e'' symmetry is now as large as 11.91 eV. Hence, a substantial increase in the OMO-UMO gap is responsible for quenching the PJT effect. The experimental observation of planarity of 1,3,5-trisilabenzene also proves the point that the PJT is completely suppressed at n = 3.

However, the other two planar isomers: 1,2,3-trisilabenzene IV.9 and 1,3,5-trisilabenzene IV.14 (Figure 11-8), lying 19.8 and 23.5 kcal/mol higher than the global minimum, are first-order saddle points with small out-of-plane imaginary frequencies of 84.5*i* cm^{-1} and 66.0*i* cm^{-1}, respectively. Geometry optimization along b_1 (structure IV.9) and a'' (structure IV.14) imaginary frequency modes would give the C_s structure IV.11 and the C_1 structure IV.15 (Figure 11-8), accordingly. The difference in total energies between the saddle-point planar structures and the corresponding C_s and C_1 structures is smaller than the difference in zero-point energy corrections for these structures, with the zero-point energy for the C_s and C_1 isomers being slightly larger. Thus, after zero-point energy corrections the planar structures of 1,2,3-trisilabenzene IV.9 and 1,3,5-trisilabenzene IV.14 are of lower energy than the corresponding C_s IV.11 and C_1 IV.15 structures.

11-3.5. $Si_2C_4H_6$ Isomers

According to the results of our CK search, structure V.1 is the global minimum and it is analogous to structures I.3, II.4, III.7, and IV.2 in the $Si_{6-n}C_nH_6$ series. Structure

V.10, analogs of which have been global minima until n = 4 in the series, is 24.5 kcal/mol above the global minimum. Prismane isomer V.22 is now 58.5 kcal/mol higher than the global minimum structure. Of the three planar isomers, structure V.2 is the most stable, with the C_{2v} structure V.3 and D_{2h} structure V.7 (Figure 11-9) being second and third planar lowest-lying structures, respectively. Again, planar structure V.2 of disilabenzene is the global minimum at B3LYP/6-311++G**//B3LYP/6-311++G**, but is only the second lowest isomer according to the CCSD(T)/CBS//B3LYP/6-311++G** level of theory.

A lot of theoretical works were devoted to the investigation of disilabenzenes.[60,62,63] Our values of the relative energies are in agreement with those obtained by U. Deva Priyakumar et al.[63] First experimental isolation of disilabenzenes derivative was reported in 1987, when hexamethyl-substituted 1,4-disilabenzene has been synthesized.[64] In 2001 J. Dysard et al.[65] experimentally proved the existence of silabenzene and 1,4-disilabenzene as ruthenium complexes.

11-3.6. SiC_5H_6 Isomers

For the SiC_5H_6 stoichiometry we found that monosilabenzene VI.1 is the global minimum with the second isomer VI.2 lying significantly higher (the difference in energy is 18.0 kcal/mol at CCSD(T)/CBS//B3LYP/6-311++G**). The prismane struc-ture VI.17 is higher in energy than the global minimum by 77.0 kcal/mol. The selected lowest isomers are presented in Figure 11-2. A more extensive set of alternative structures is given in Figure 11-10.

According to our systematic computational study, the 3D-2D transition occurs only at n = 5, where planar monosilabenzene structure becomes much more stable than the three-dimensional structures.

A large number of theoretical studies were done on monosi-labenzene before its spectral data and matrix isolation.[66-69] The derivative of monosilabenzene (2,6-bis(trimethylsilyl)-1,4,-di(terbutyl)monosilabenzene) is known to be stable in solution.[70]

Our results regarding Si_6H_6, Si_5CH_6, $Si_4C_2H_6$, $Si_3C_3H_6$, $Si_2C_4H_6$, and SiC_5H_6 silabenzenes are generally in agreement with calculations made by K. Baldridge et al.[60], however, we were not able to find any theoretical or experimental data concerning Si_5CH_6, $Si_4C_2H_6$, and $Si_3C_3H_6$ isomers in the literature.

11-3.7. C_6H_6 Isomers

The aforementioned systematic computational study[1] of the C_6H_6 isomers revealed 215 minimum energy structures, with 84 structures being within 100 kcal/mol in energy relative to the benzene global minimum structure. Benzene is the most stable isomer. In this article, we present four isomers of C_6H_6 in Figure 11-2. According to our calculations, prismane VII.4 is higher in energy than the third isomer (VII.3) and the second isomer (VII.2), respectively. The relative energies of the presented structures are given at the CCSD(T)/CBS//B3LYP/6-311++G** level of theory.

11-3.8. Chemical Bonding Pictures Revealed by the AdNDP

In order to interpret our results from the chemical bonding point of view, we performed the AdNDP analysis for the global minimum structures. The results of our analysis for these structures are shown in Figure 11-3 and Figure 11-4.

There are two interpretations of chemical bonding for the Si_6H_6 global minimum structure (I.1) (Figure 11-3). According to the first picture (Figure 11-3, I.1.a)), the AdNDP analysis revealed six two-center, two-electron (2c-2e) Si–H σ bonds, six 2c-2e Si–Si σ bonds, all with occupation numbers (ON) ranging from 1.82 |e| to 1.99 |e|; two lone pairs with ON = 1.62 |e| on two silicon atoms, and one three-center, two electron (3c-2e) σ bond (ON = 1.99 |e|).

In order to improve this zero-order chemical bonding model, we need to accept all bonding elements which have ON close to 2.00 |e| and allow the bonding elements with low occupation numbers to be delocalized over larger number of atoms. In other words, in our new AdNDP search we accepted bonding patterns with ON higher than 1.80 |e|. Therefore, the AdNDP revealed six 2c-2e Si–H σ bonds, eight 2c-2e Si–Si σ bonds (all with ON = 1.86-1.99 |e|), and one δ bond between two silicon atoms (Figure 11-3, I.2.b)). Hence, we offer two chemical bonding pictures that can describe chemical bonding in the Si_6H_6 global minimum structure.

We also performed the AdNDP analysis for the Si_5CH_6 (II.1), $Si_4C_2H_6$ (III.1), $Si_3C_3H_6$ (IV.1), $Si_2C_4H_6$ (V.1) and SiC_5H_6 (VI.1) global minimum structures. Results of these analyses are presented in Figure 11-4 (for Si_5CH_6, $Si_4C_2H_6$, and $Si_3C_3H_6$ global minimum structures, accepted bonding patterns with ON higher than 1.80|e| were chosen).

For the Si_5CH_6 global minimum structure II.1, we found six 2c-2e Si–H σ bonds with ON = 1.98 – 1.99 |e| (not shown in Figure 11-4), eight 2c-2e Si–Si σ bonds (ON = 1.89 – 1.99 |e|), and one 3c-3e Si–Si δ bond (ON = 1.98 |e|). The $Si_4C_2H_6$ global minimum structure III.1 has six 2c-2e Si–H σ bonds with ON = 1.98 – 1.99 |e| (not shown

in Figure 11-4), eight 2c-2e Si–Si σ bonds (ON = 1.85 – 1.99 |e|), and one 2c-2e Si–Si δ bond (ON = 1.99 |e|). The $Si_3C_3H_6$ global minimum structure IV.1 has the chemical bonding picture similar to that of III.1: six 2c-2e Si–H σ bonds with ON = 1.98 – 1.99 |e| (not shown in Figure 11-4), eight 2c-2e Si–Si σ bonds (ON = 1.86 – 1.98 |e|), and one 2c-2e Si-Si δ bond (ON = 1.98 |e|). For the $Si_2C_4H_6$ global minimum structure V.1, the AdNDP revealed six 2c-2e Si–H σ bonds with ON = 1.98 – 1.99 |e| (not shown in Figure 11-4), seven 2c-2e Si–Si σ bonds (ON = 1.77 – 1.99 |e|), one lone pair on silicon atom with ON = 1.99 |e| and one 3c-2e Si–Si σ bond (ON = 1.97 |e|). The planar monosilabenzene global minimum structure VI.1 has six 2c-2e Si–H σ bonds with ON = 1.98 – 2.00 |e| (not shown in Figure 11-4), six 2c-2e Si–Si σ bonds with occupation numbers being close to ideal values of 2.00 |e|; and three six-center two electron (6c-2e) Si–Si π bonds (ON = 2.00 |e|) confirming the presence of π-aromaticity in this molecule.

11-4. Conclusions

We presented a systematic study of the $Si_{6-n}C_nH_6$ (n = 0–6) series. We performed unbiased CK global minimum and low-lying isomers search for the Si_6H_6, Si_5CH_6, $Si_4C_2H_6$, $Si_3C_3H_6$, $Si_2C_4H_6$ and SiC_5H_6 species at the B3LYP/6-31G** level of theory. The lowest isomers were recalculated at the CCSD(T)/CBS//B3LYP/6-311++G** level of theory. We found that the OMO-UMO gap between MOs involved in the PJT effect is increasing with substitution of the Si atoms by the C atoms, which gradually leads to the suppression of the PJT effect in 1,3,5-trisilabenzene. Recently, it was shown in the $C_xH_xP_{6-x}$ (x = 0–6)[71] and $C_xH_xP_{4-x}$ (x = 0–4)[72] series that isolobal substitution of an atom or a group by a more electronegative atom or group can be considered as a new mechanism for the suppression of the PJT effect.

As we can see from our chemical bonding analysis, the most stable structure VI.1 for SiC_5H_6 is aromatic. The NICS values, obtained by K. Baldridge et al.[60] show that aromaticity increases with decreasing number of silicon atoms along the silabenzenes series. However, the transition from three-dimensional structures to planar structures occurs only at n = 5 in the $Si_{6-n}C_nH_6$ (n = 0–6) series. Thus, relating stability with aromaticity in silicon-carbon compounds could be risky. According to our results there are also other reasons for the switch in the relative stabilities in the considered series upon the substitution of silicon atoms by carbon atoms. The environment in which the Si atoms are located and the strain energy in the skeleton of silicon structures are some factors in explaining the observed stabilities. The isomer, in which all silicon atoms are tetracoordinated was found to be more stable among other isomers of the Si_6H_6, Si_5CH_6, $Si_4C_2H_6$ and $Si_3C_3H_6$ stoichiometries. Hence, the silicon atoms would prefer to be tetracoordinated and form three-dimensional structures that can be explained by the weak π-bonding of silicon atoms with carbon atoms or with another Si. Our theoretical study may be useful for understanding geometry, properties and nature of the Si-C compounds and may become a guiding tool for experimental research in this area.

References

(1) Dinadayalane, T. C.; Priyakumar, U. D.; Sastry, G. N. *J. Phys. Chem. A* **2004**, *108*, 11433.

(2) Malrieu, J. P.; Trinquier, G. *J. Am. Chem. Soc.* **1989**, *111*, 5916.

(3) Jacobsen, H.; Ziegler, T. *J. Am. Chem. Soc.* **1994**, *116*, 3667.

(4) Scherer, O. J.; Sitzmann, H.; Wolmershauser, G. *Angew. Chem. Int. Ed.* **1985**, *24*, 351.

(5) Nagase, S.; Kobayashi, K.; Takagi, N. *J. Organomet. Chem.* **2000**, *611*, 264.

(6) Frenking, G.; Krapp, A.; Nagase, S.; Takagi, N.; Sekiguchi, A. *ChemPhysChem*. **2006**, *7*, 799.

(7) Power, P. P. *Chem. ReV.* **1999**, *99*, 3463.

(8) Sari, L.; McCarthy, M. C.; Schaefer, H. F., III.; Thaddeus, P. *J. Am. Chem. Soc.* **2003**, *125*, 11409.

(9) Binkley, J. S. *J. Am. Chem. Soc.* **1984**, *106*, 603.

(10) Nagase, S.; Nakano, M. *Angew. Chem., Int. Ed. Engl.* **1988**, *27*, 1081.

(11) Yates, B. F.; Schaefer, H. F., III. *Chem. Phys. Lett.* **1989**, *155*, 563.

(12) Kosa, M.; Karni, M.; Apeloig, Y. *J. Chem. Theory Comput.* **2006**, *2*, 956.

(13) Sax, A.; Janoschek, R. *Angew. Chem., Int. Ed. Engl.* **1986**, *25*, 651.

(14) Nagase, S.; Teramae, H.; Kudo, T. *J. Chem. Phys.* **1987**, *86*, 4513.

(15) Zdetsis, A. D. *J. Chem. Phys.* **2007**, 214306.

(16) Santos, J. C.; Contreras, M.; Merino, G. *Chem. Phys. Letters*, **2010**, *496*, 172.

(17) Nagase, S.; Kudo, T.; Aoki, M. *J. Chem. Soc., Chem. Commun*. **1985**, 1121.

(18) Schleyer, P. v. R.; Jiao, H.; Hommes, N. J. R. v. E.; Malkin, V. G.; Malkina, O. N. *J. Am. Chem. Soc.* **1997**, *119*, 12669.

(19) Zhao, M.; Gimarc, B. M. *Inorg. Chem.* **1996**, *35*, 5378.

(20) Moteki, M.; Maeda, S.; Ohno, K. *Organometallics* **2009**, *28*, 2218.

(21) Abersfelder, K.; White, A. J. P; Berger, R. J. F; Rzepa, H. S; Scheschkewitz, D. *Angew. Chem. Int. Ed*. **2011**, *50*, 7936.

(22) Sergeeva, A. P.; Averkiev, B. B.; Zhai, H. J.; Boldyrev, A. I.; Wang, L. S. *J. Chem. Phys.* **2011**, *134*, 224304.

(23) Schlegel, H. B. *J. Comput. Chem.* **1982**, *3*, 214.

(24) Wang, X. B.; Nicholas, J. B.; Wang, L. S. *J. Chem. Phys.* **2000**, *113*, 10837.

(25) Wang, X. B.; Sergeeva, A. P.; Yang, J.; Xing, X. P.; Boldyrev, A. I.; Wang, L. S. *J. Phys. Chem. A* **2009**, *113*, 5567.

(26) Becke, A. D. *J. Chem. Phys.* **1993**, *98*, 5648.

(27) Vosko, S. H.; Wilk, L.; Nusair, M. *Can. J. Phys.* **1980**, *58*, 1200.

(28) Lee, C.; Yang, W.; Parr, R. G. *Phys. Rev. B: Condens. Matter* **1988**, *37*, 785.

(29) Binkley, J. S.; Pople, J. A.; Hehre, W. J. *J. Am. Chem. Soc.* **1980**, *102*, 939.

(30) Rassolov, V. A.; Ratner, M. A.; Pople, J. A.; Redfern, P. C.; Curtiss, L. A. *J. Comput. Chem.* **2001**, *22*, 976.

(31) Gordon, M. S.; Binkley, J. S.; Pople, J. A.; Pietro, W. J.; Hehre, W. J. *J. Am. Chem. Soc.* **1982**, *104*, 2797.

(32) Pietro, W. J.; Francl, M. M.; Hehre, W. J.; Defrees, D. J.; Pople, J. A.; Binkley, J. S. *J. Am. Chem. Soc.* **1982**, *104*, 5039.

(33) Clark, T.; Chandrasekhar, J.; Spitznagel, G. W.; Schleyer, P. v. R. *J. Comput. Chem.* **1983**, *4*, 294

(34) Woon, D. E.; Dunning, T. H., Jr. *J. Chem. Phys.* **1993**, *98*, 1358.

(35) Kendall, R. A.; Dunning, T. H.; Harrison, R. J. *J. Chem. Phys.* **1992**, *96*, 6796.

(36) Dunning, T. H.; *J. Chem. Phys.* **1989**, *90*, 1007.

(37) Peterson, K. A.; Woon, D. E.; Dunning, T. H. *J. Chem. Phys*. **1994**, *100*, 7410.

(38) Wilson, A.; van Mourik, T.; Dunning, T. H. *THEOCHEM* **1997**, *388*, 339.

(39) Truhlar, D. G. *Chem. Phys. Lett.* **1998**, *294*, 45.

(40) Fast, P. L.; Sanchez, M. L.; Truhlar, D. G. *J. Chem. Phys.* **1999**, *111*, 2921.

(41) Zubarev, D. Yu.; Boldyrev, A. I. *Phys. Chem. Chem. Phys.* **2008**, *10*, 5207.

(42) Zubarev, D. Yu.; Robertson, N.; Domin, D.; McClean, J.; Wang, J. H.; Lester, W. A.; Whitesides, R.; You, X. Q.; Frenklach, M. J. *Phys. Chem. C* **2010**, *114*, 5429.

(43) Foster, J. P.; Weinhold, F. *J. Am. Chem. Soc.* **1980**, *102*, 7211.

(44) Reed, A. E.; Curtiss, L. A.; Weinhold, F. *Chem. Rev.* **1988**, *88*, 899.

(45) Glendening, E. D.; Reed, A. E.; Carpenter, J. E.; Weinhold, F. *NBO*, version 3.1.

(46) Frisch, M. J.; Trucks, G. W.; Schlegel, H. B.; Scuseria, G. E.; Robb, M. A.; Cheeseman, J. R.; Scalmani, G.; Barone, V.; Men-nucci, B.; Petersson, G. A.; Nakatsuji, H.; Caricato, M.; Li, X.; Hratchian, H. P.; Izmaylov, A. F.; Bloino, J.; Zheng, G.; Sonnenberg, J. L.; Hada, M.; Ehara, M.; Toyota, K.; Fukuda, R.; Hasega-wa, J.; Ishida, M.; Nakajima, T.; Honda, Y.; Kitao, O.; Nakai, H.; Vreven, T.; Montgomery, J. A., Jr.; Peralta, J. E.; Ogliaro, F.; Bearpark, M.; Heyd, J. J.; Brothers, E.; Kudin, K. N.; Staroverov, V. N.; Kobayashi, R.; Normand, J.; Raghavachari, K.; Rendell, A.; Burant, J. C.; Iyengar, S. S.; Tomasi, J.; Cossi, M.; Rega, N.; Millam, N. J.; Klene, M.; Knox, J. E.; Cross, J. B.; Bakken, V.; Adamo, C.; Jaramillo, J.; Gomperts, R.; Stratmann, R. E.; Yazyev, O.; Austin, A. J.; Cammi, R.; Pomelli, C.; Ochterski, J. W.; Martin, R. L.; Morokuma, K.; Zakrzewski, V. G.; Voth, G. A.; Salvador, P.; Dannenberg, J. J.; Dapprich, S.; Daniels, A. D.; Farkas, O.;Foresman, J. B.; Ortiz, J. V.; Cioslowski, J.; Fox, D. J. *Gaussian 09*, Revision B.01; Gaussian, Inc.: Wallingford, CT, **2010**.

(47) http://www.chemcraftprog.com

(48) Varetto, U. *Molekel*, version 5.4.0.8; Swiss National Super-computing Centre: Manno, Switzerland, **2009**.

(49) Foote, J. K.; Mallon, M. H.; Pitts, J. N. *J. Am. Chem. Soc.* **1966**, *88*, 3698.

(50) van Tamelen, E. E.; Pappas, S. P. *J. Am. Chem. Soc.* **1963**, *85*, 3297.

(51) Katz, T. J.; Acton, N. *J. Am. Chem. Soc.* **1973**, *95*, 2738.

(52) Billups, W. E.; Haley, M. M. *Angew. Chem., Int. Ed. Engl*. **1989**, *28*, 1711.

(53) Abersfelder, K.; White, A.; Rzepa, H.; Scheschkewitz, D. **2010**, *Science*, 327, 564.

(54) Bersuker, I. B. *Chem. Rev.* **2001**, *101*, 1067.

(55) Bersuker, I. B. In *The Jahn-Teller Effect*; Cambridge University Press: Cambridge, U.K., **2006**.

(56) Pearson, R. G. *Proc. Natl. Acad. Sci. U. S. A.*, **1975**, *72*, 2104.

(57) Matsunaga, N.; Gordon, M. S. *J. Am. Chem. Soc.* **1994**, *116*, 11407.

(58) Matsunaga, T. R.; Cundari, T. R.; Schmidt, M. W.; Gordon, M. S. *Theor. Chim. Acta* **1992**, *83*, 57.

(59) Pipek, J.; Mezey, P. G. *J. Chem. Phys*. **1989**, *90*, 4916.

(60) Baldridge, K. K.; Uzan, O.; Martin, J. M. L. *Organometallics* **2000**, *19*, 1477.

(61) Bjarnason, A.; Arnason, I. *Angew. Chem., Int. Ed. Engl.* **1992**, *31*, 1633.

(62) Baldridge, K. K.; Gordon, M. S. *J. Am. Chem. Soc.* **1984**, *106*, 369.

(63) Deva Priyakumar U.; Saravanan, D.; Narahari Sastry, G. *Organometallics* **2002**, *21*, 4823.

(64) Welsh, K. M.; Rich, J. D.; West, R. *J. Organomet. Chem*. **1987**, *325*, 105.

(65) Dysard, J. M.; Tilley, T. D.; Woo, T. K. *Organometallics* **2001**, *20*, 1195.

(66) Barton, T. J.; Burns, G. T. *J. Am. Chem. Soc.* **1978**, *100*, 5246.

(67) Maier, G.; Mihm, G.; Reisenauer, H. P. *Angew. Chem., Int. Engl. Ed.* **1980**, *19*, 52.

(68) Maier, G.; Mihm, G.; Reisenauer, H. P. *Chem. Ber.* **1982**, *115*, 801.

(69) Solouki, B.; Rosmus, P.; Bock, H.; Maier, G. *Angew. Chem., Int.Ed. Engl.* **1980**, *19*, 51.

(70) Markl, G.; Hofmeister, P. *Angew. Chem., Int. Ed. Engl.* **1979**, *18*,789.

(71) Galeev, T. R.; Boldyrev, A. I. *Phys. Chem. Chem. Phys.* **2011**, *13*, 20549.

(72) Ivanov, A. S.; Bozhenko, K. V.; Boldyrev, A. I. *J. Chem. Theory Comput.* **2012**, *8*, 135.

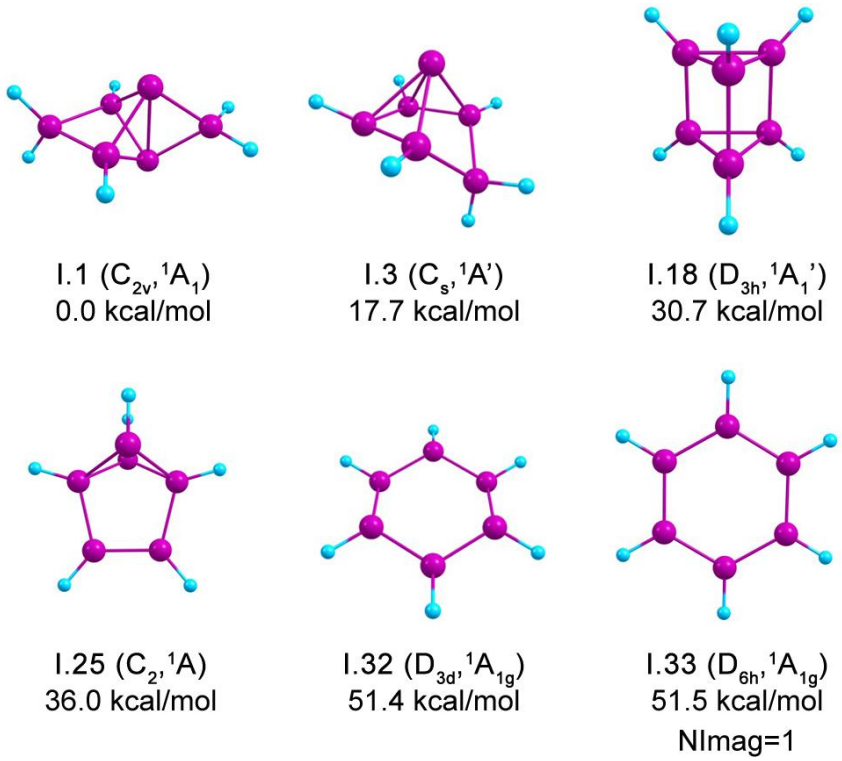

Figure 11-1. Selected lowest-energy structures of Si_6H_6, their point group symmetries, spectroscopic states and ZPE (B3LYP/6-311++G**) corrected relative energies (CCSD(T)/CBS//B3LYP/6-311++G**). The structures are labeled in accordance with Figure 11-5.

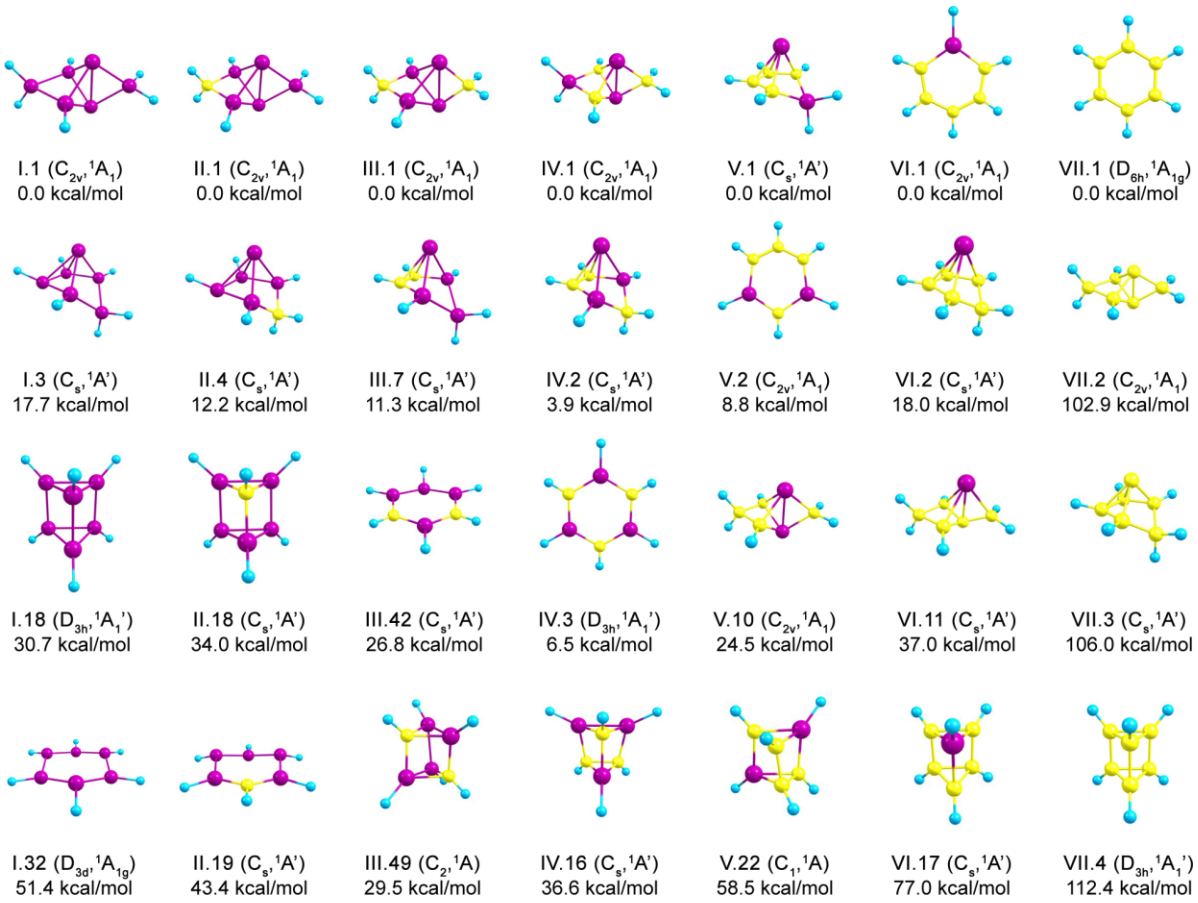

Figure 11-2. Representative optimized isomers of each species in the $Si_{6-n}C_nH_6$ (n = 0–6) series, their point group symmetries, spectroscopic states and ZPE (B3LYP/6-311++G**) corrected relative energies (CCSD(T)/CBS//B3LYP/6-311++G**). Here and elsewhere the yellow, violet and blue spheres represent carbon, silicon and hydrogen atoms, respectively.

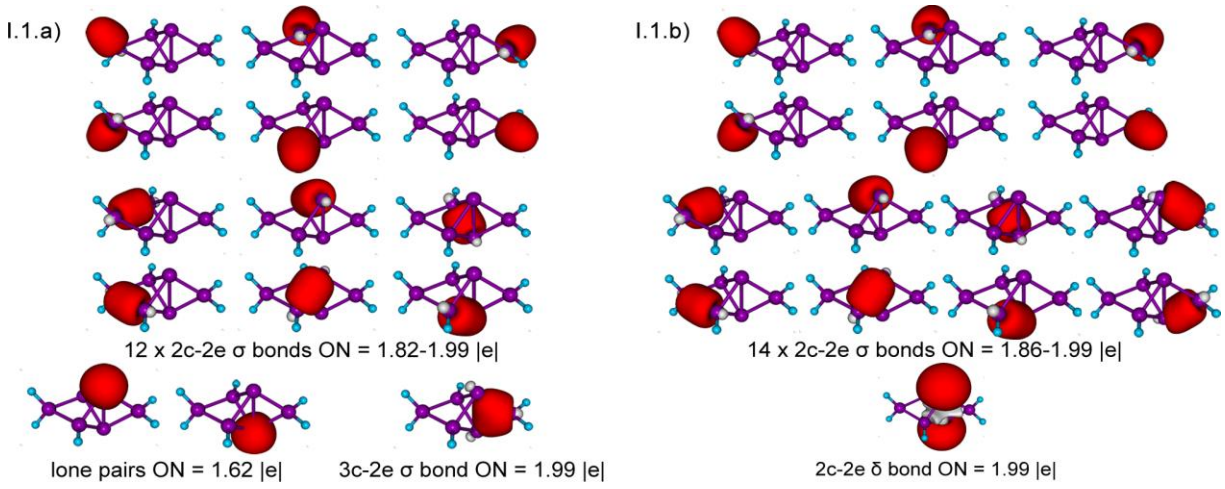

Figure 11-3. Two representations of chemical bonding patterns of the I.1 global minimum structure revealed by the AdNDP.

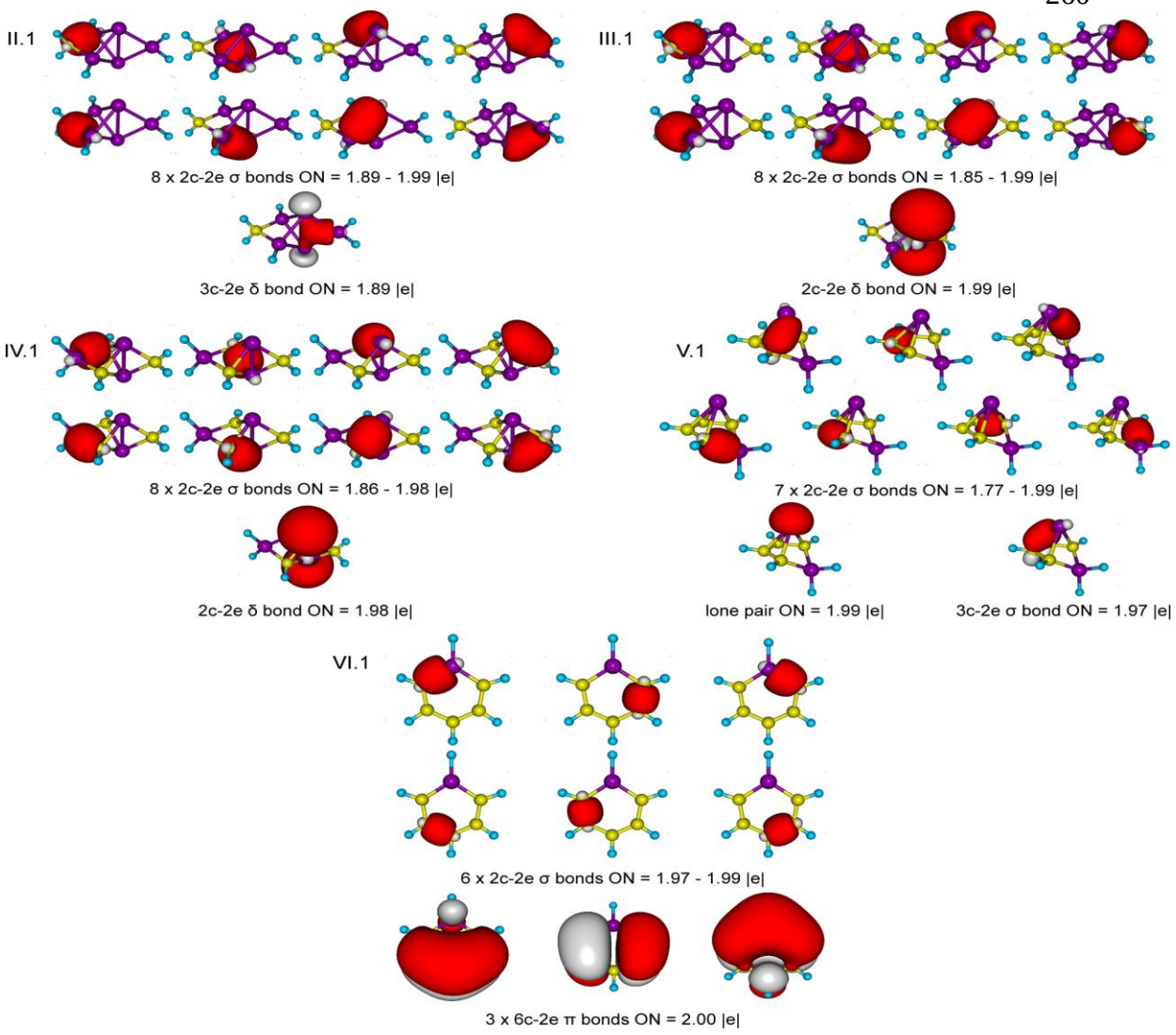

Figure 11-4. Chemical bonding patterns of the II.1, II.1, IV.1, V.1 and VI.1 global minimum structures revealed by the AdNDP.

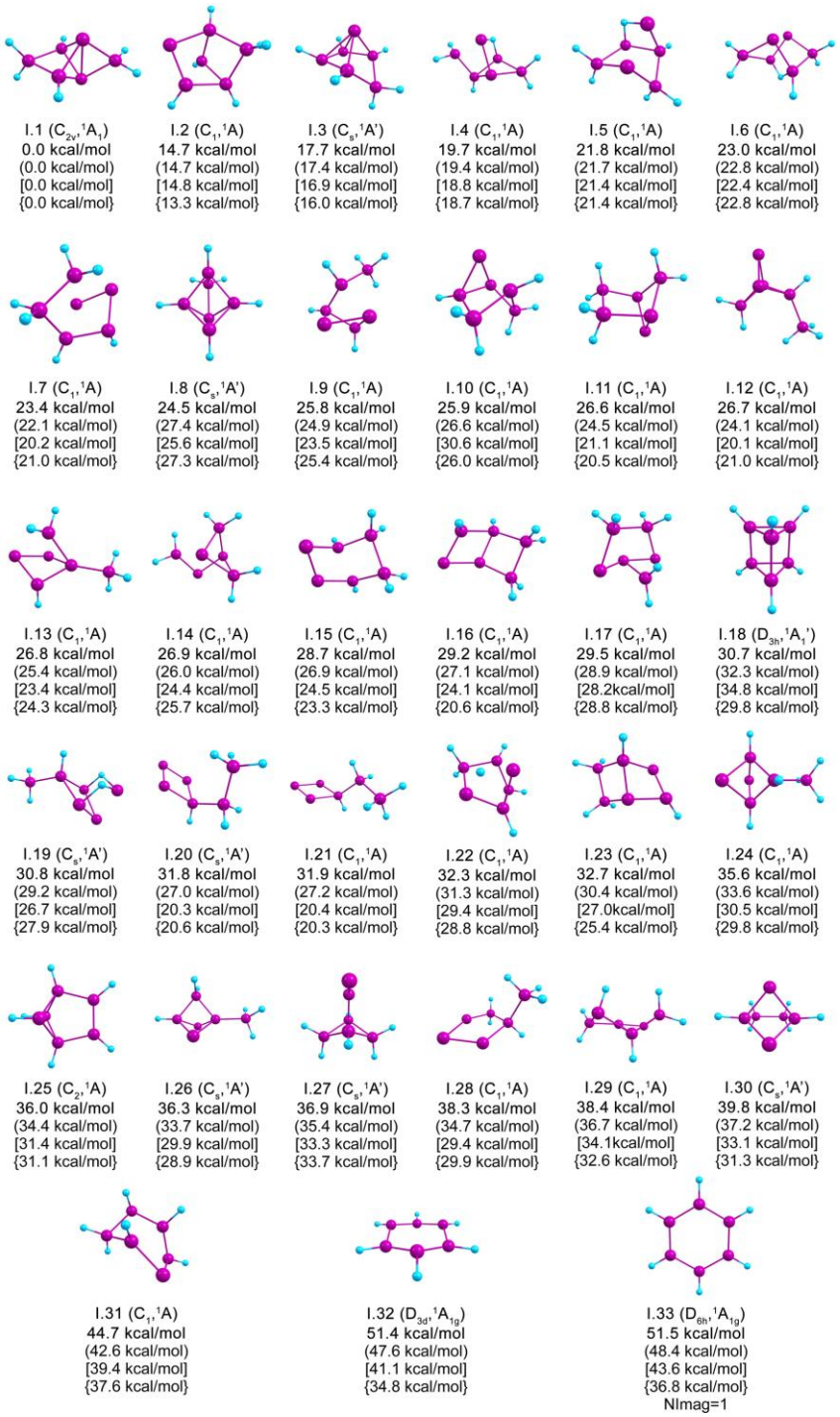

Figure 11-5. Lowest-lying structures of Si_6H_6, their point group symmetries, spectroscopic states and ZPE corrected relative energies. The energies are given at: CCSD(T)/CBS (bold), CCSD(T)/cc-pvTZ (in brackets), CCSD(T)/cc-pvDZ (square brackets), and B3LYP/6-311++G** (curly brackets), all at B3LYP/6-311+G* optimized geometries.

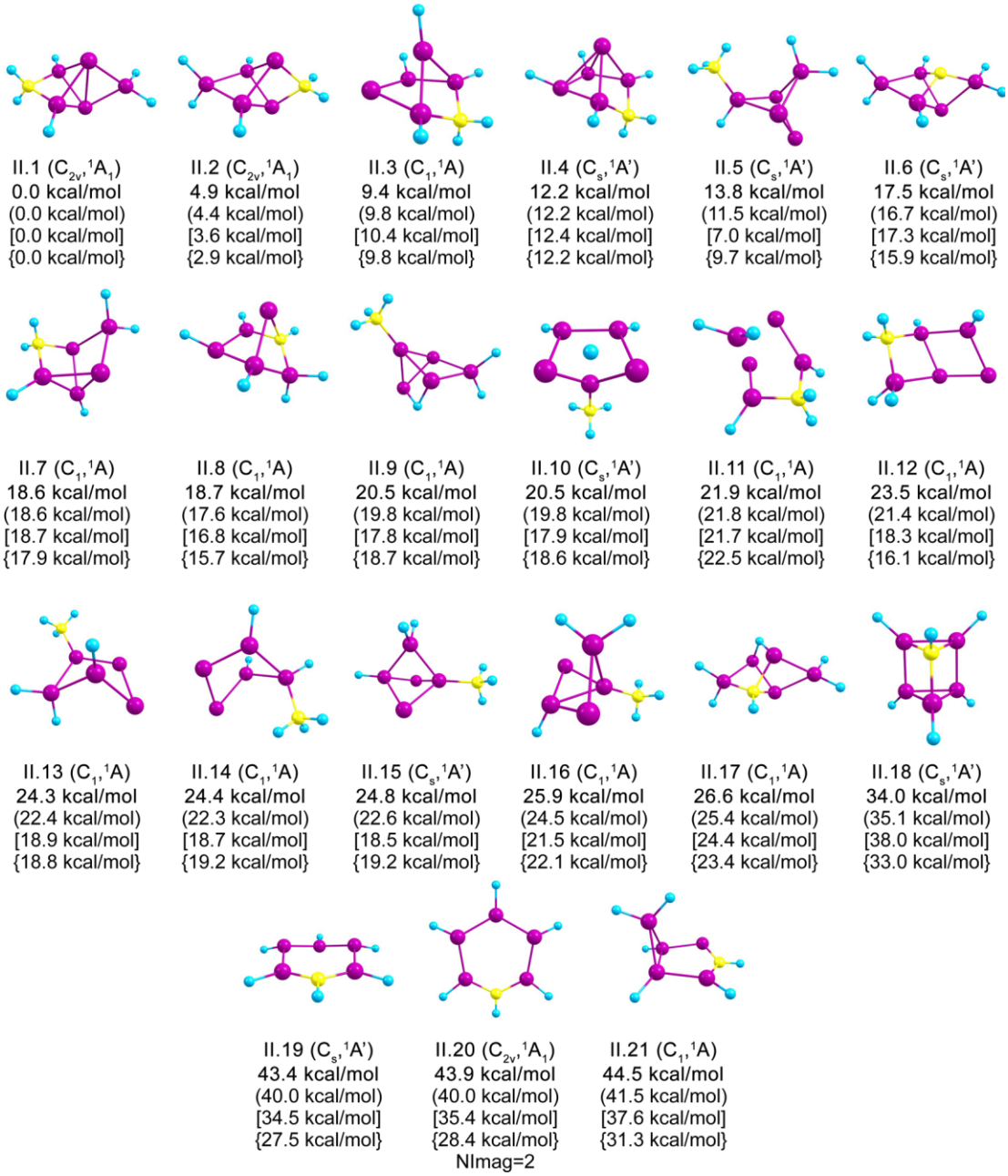

Figure 11-6. Lowest-lying structures of Si_5CH_6, their point group symmetries, spectroscopic states and ZPE corrected relative energies. The energies are given at: CCSD(T)/CBS (bold), CCSD(T)/cc-pvTZ (in brackets), CCSD(T)/cc-pvDZ (square brackets), and B3LYP/6-311++G** (curly brackets), all at B3LYP/6-311++G** optimized geometries.

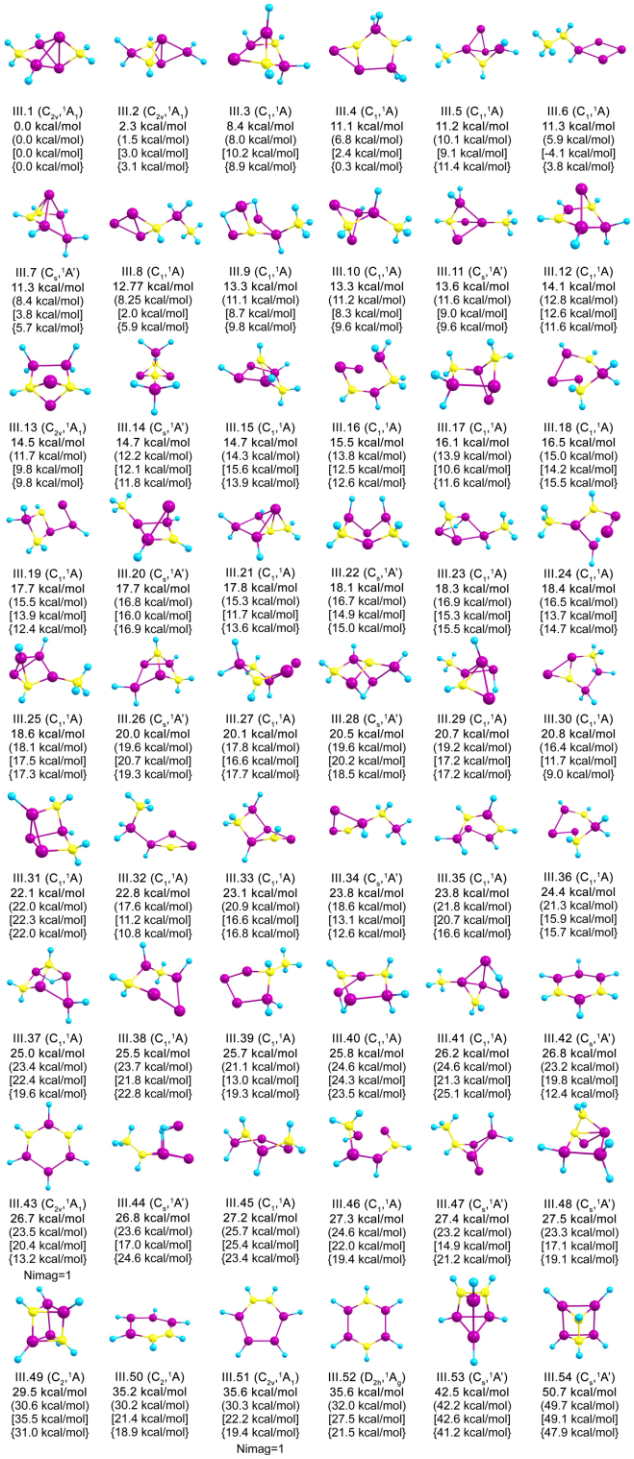

Figure 11-7. Lowest-lying structures of $Si_4C_2H_6$, their point group symmetries, spectroscopic states and ZPE corrected relative energies. The energies are given at: CCSD(T)/CBS (bold), CCSD(T)/cc-pvTZ (in brackets), CCSD(T)/cc-pvDZ (square brackets), and B3LYP/6-311++G** (curly brackets), all at B3LYP/6-311++G** optimized geometries.

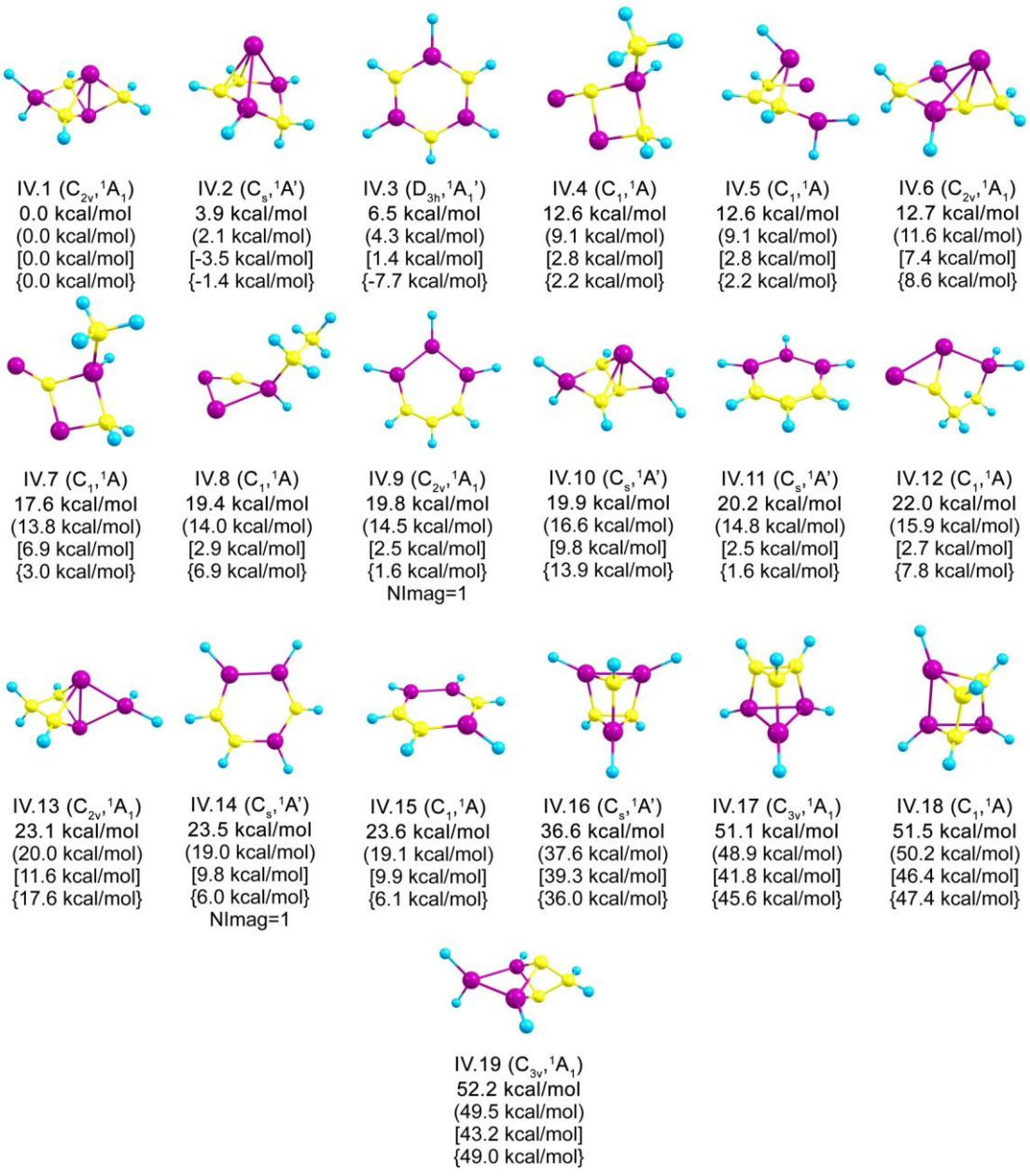

Figure 11-8. Lowest-lying structures of $Si_3C_3H_6$, their point group symmetries, spectroscopic states and ZPE corrected relative energies. The energies are given at: CCSD(T)/CBS (bold), CCSD(T)/cc-pvTZ (in brackets), CCSD(T)/cc-pvDZ (square brackets), and B3LYP/6-311++G** (curly brackets), all at B3LYP/6-311++G** optimized geometries.

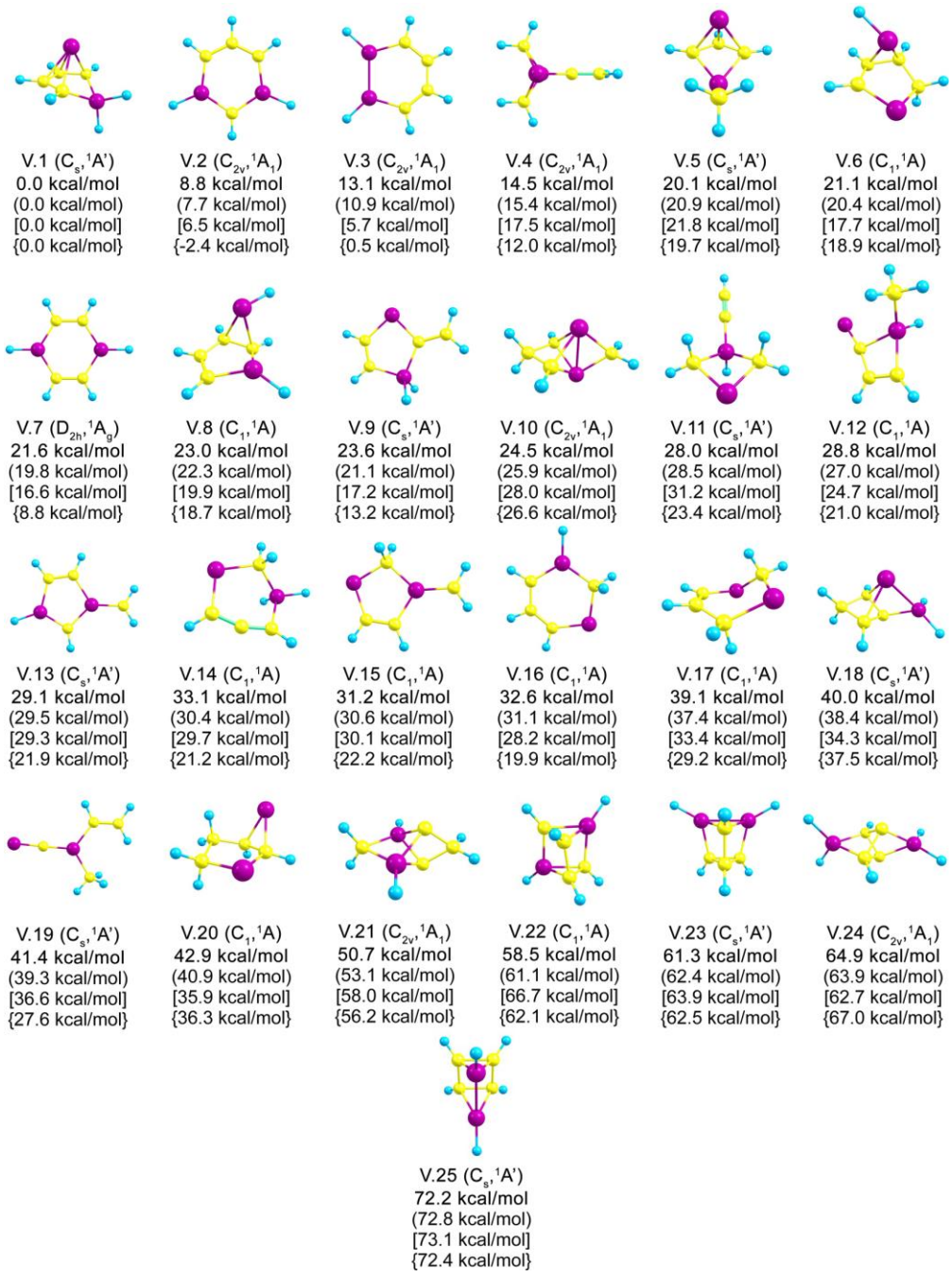

Figure 11-9. Lowest-lying structures of $Si_2C_4H_6$, their point group symmetries, spectroscopic states and ZPE corrected relative energies. The energies are given at: CCSD(T)/CBS (bold), CCSD(T)/cc-pvTZ (in brackets), CCSD(T)/cc-pvDZ (square brackets), and B3LYP/6-311++G** (curly brackets), all at B3LYP/6-311++G** optimized geometries.

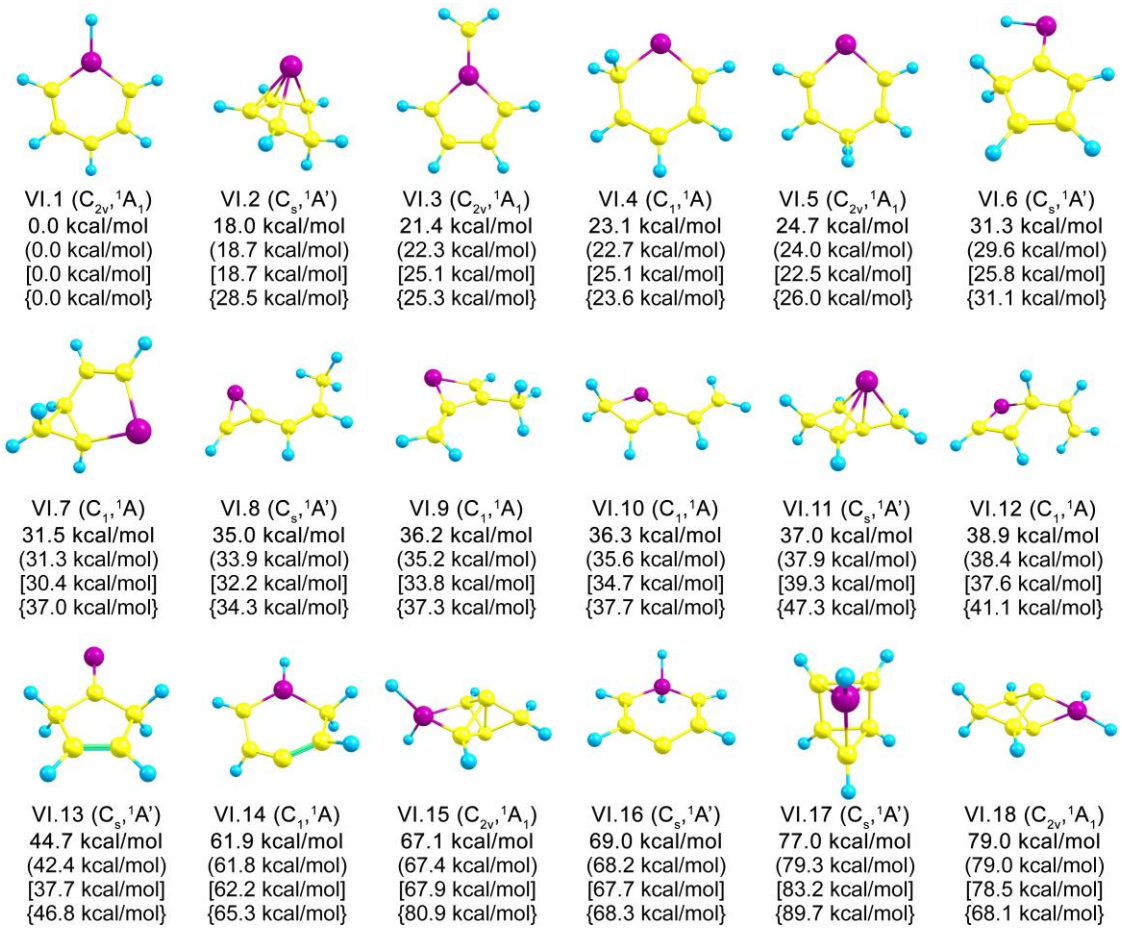

Figure 11-10. Lowest-lying structures of SiC_5H_6, their point group symmetries, spectroscopic states and ZPE corrected relative energies. The energies are given at: CCSD(T)/CBS (bold), CCSD(T)/cc-pvTZ (in brackets), CCSD(T)/cc-pvDZ (square brackets), and B3LYP/6-311++G** (curly brackets), all at B3LYP/6-311++G** optimized geometries.

CHAPTER 12

ON THE SUPPRESSION MECHANISM OF THE PSEUDO-JAHN−TELLER EFFECT IN MIDDLE E_6 (E = P, As, Sb) RINGS OF TRIPLE-DECKER SANDWICH COMPLEXES[1]

Abstract

Quantum chemical calculations of the $CpMoE_6MoCp$ (E = P, As, Sb) triple-decker sandwich complexes showed that E_6 fragments in the central decks of the complexes are planar. Analysis of molecular orbitals involved in vibrational coupling demonstrated that filling the unoccupied molecular orbitals involved in vibronic coupling with electron pairs of Mo atoms suppresses the PJT effect in the $CpMoE_6MoCp$ (E = P, As, Sb) sandwich, with the E_6 ring becoming planar (D_{6h}) upon complex formation. The AdNDP analysis revealed that bonding between $C_5H_5^-$ units and Mo atoms has a significant ionic contribution, while bonding between Mo atoms and E_6 fragment becomes appreciably covalent through the δ type M→L back-donation mechanism.

12-1. Introduction

A planar aromatic structure of benzene is by far the most stable isomer for C_6H_6 stoicheometry.[1-3] One can think that the molecule *cyclo*-P_6 (hexaphosphabenzene) being a valence isoelectronic analogue of benzene may have a planar hexagonal structure. In 1985 Scherer et. al.[4] synthesized and characterized the $\{(\eta^5\text{-}Me_5C_5)Mo\}_2(\mu,\eta^6\text{-}P_6)$ triple-decker sandwich complex, containing a planar P_6 ring with almost equal P-P

[1] Coauthored by Alexander S. Ivanov, Konstantin V. Bozhenko, and Alexander I. Boldyrev. Reprinted with permission from *Inorg. Chem.*, **2012**, *51* (16), pp 8868–8872. Copyright © 2012 American Chemical Society.

bonds.[5] The experimental P-P bond lengths, (2.167 Å and 2.175 Å) are in a good agreement with the theoretical P-P bond (2.125 Å), which is intermediate between typical values for the single P-P bond of 2.233 Å in P_2H_4 and the double 2.044 Å in P_2H_2 (all at MP2/6-31G*).[6] Therefore, the planarity of the P_6 cluster in the triple-decker complex indicates that indeed, it is aromatic and analogous to benzene. The *cyclo*-As_6 planar molecule was also first coordinatively stabilized by Scherer et. al.[7] in 1989, as the central deck of the sandwich complex similar to $\{(\eta^5\text{-}Me_5C_5)Mo\}_2(\mu, \eta^6\text{-}P_6)$. The chemical bonding and electronic structure of the metallocenes with P_6 and other aromatic molecules have been thoroughly discussed by Jemmis et. al.[8-10] However, despite the observation of hexagonal aromatic hexaphosphabenzene in the triple-decker complex, theoretical calculations revealed[6,11-20] that there are at least seven non-planar P_6 isomers lower in energy than the benzene-like D_{6h} structure I.7 (Figure 12-1).

Moreover, the planar structure I.7 is not a minimum, but a second-order saddle point. Geometry optimization following the first imaginary frequency mode of the D_{6h} structure leads to the D_2 distorted structure I.6, which is 2.7 kcal/mol lower in energy. According to the most accurate calculations,[6,20] the global minimum structure of P_6 is the benzvalene-like structure I.1 with the prismane-like isomer I.2 being the second lowest and the other isomers lying significantly higher in energy.

Galeev and Boldyrev showed[20] that the out-of-plane distortion in the P_6 (D_{6h}) is due to the pseudo Jahn-Teller (PJT) effect.[21,22] Jahn-Teller vibronic effects were shown by Bersuker[23-25] to be the only source of instability of high-symmetry configurations of polyatomic systems. The distortion of the structure I.7 into the structure I.6 occurred due to vibronic coupling of HOMO-1 (e_{2g}) and LUMO (e_{2u}) in P_6 (Figure 12-2).

The direct product of their symmetries contains e_{2u}, which is the symmetry of the imaginary mode:

$$e_{2g} \otimes e_{2u} = a_{1u} \oplus a_{2u} \oplus e_{2u} \quad (1)$$

The symmetry of the imaginary mode (e_{2u}) of the D_{6h} structure corresponds to the totally symmetric (a) mode in the distorted D_2 isomer. Thus, both conditions of the PJT effect (PJTE) are met.[20] The HOMO-1 and LUMO gap is 8.29 eV (HF/cc-pvTZ//B3LYP/6-311+G*).[17] The planarization of the P_6 ring in the {(η^5-Me_5C_5)Mo}$_2$(μ, η^6-P_6) complex is due to the suppression of the PJT effect. It was shown that the PJTE may be suppressed by increasing the energy gap to the active excited state in the porphyrin ring of hemoglobin via oxygenation and by substitution that populates the excited state upon small ligand coordination to hemoproteins.[26] Most recently, two more mechanisms for the suppression of the PJT effect have been proposed: by the gap increase between the interacting OMO-UMO pair in the external electrostatic field of cations[27] and by occupying the interacting UMO with an electron pair upon complexation.[28] In this article, we demonstrate that the suppression of the PJT effect in P_6 cluster being the middle deck of the {(η^5-Me_5C_5)Mo}$_2$(μ, η^6-P_6) sandwich complex is due to the second mechanism.

12-2. Theoretical section

We selected the following neutral complexes $CpMoE_6MoCp$ (E = P, As, Sb) as models for our computational analysis of chemical bonding in the experimentally observed triple-decker complex. Geometry optimization and follow-up frequency calculations for the isolated planar E_6 and our model were performed at the hybrid

Hartree-Fock/DFT (B3LYP) level of theory.[29-31] A double-ζ basis set (LanL2DZ)[32] for Mo and Sb and standard 6-31G* basis set for other atoms (P, As, C, H) were used.

A chemical bonding analysis of the vibronic coupling was performed at the RHF level of theory using LanL2DZ basis set for Mo and Sb and 6-31G* basis set for other atoms. Additionally, in order to gain more insight into the structure and chemical bonding of the triple-decker sandwich complexes we performed the Adaptive Natural Density Partitioning method developed in our lab by Zubarev and Boldyrev, which has been successfully applied for the analysis of chemical bonding in boron clusters,[33] prototypical aromatic organic molecules,[34] gold clusters,[35] and the triple-decker sandwich complex $[Pd_4(\mu_4\text{-}C_9H_9)(\mu_4\text{-}C_8H_8)][BAr^f{}_4]$ ($BAr^f{}_4$ = $B\{3,5\text{-}(CF_3)_2(C_6H_3)\}_4$).[36] The AdNDP method performs analysis of the first-order reduced density matrix with the purpose of obtaining its local block eigenfunctions with optimal convergence properties for describing the electron density. The local blocks of the first- order reduced density matrix correspond to the sets of n atoms (from one to all the atoms of the molecule) that are tested for the presence of a two-electron object (n-center two electron (nc-2e) bonds, including core electrons and lone pairs as a special case of n = 1) associated with this particular set of n atoms. The AdNDP search starts with core electron pairs and lone pairs (1c-2e), then 2c-2e, 3c-2e, . . . and finally nc-2e bonds. On each step the density matrix is depleted for the density corresponding to the appropriate bonding elements. The AdNDP procedure can also be applied to specified molecular fragments. This user-directed form of the AdNDP analysis is analogous to the directed search option of the standard NBO code. The recovered nc-2e bonding elements always correspond to the point-group symmetry of the system after these bonding elements are superimposed onto the

molecular frame. For the given n-atomic block those eigenvectors are accepted whose occupation numbers (eigenvalues) exceed the established threshold value, and which usually are chosen to be close to 2.00 |e|. Thus, Lewis's idea of an electronic pair as the essential element of bonding is preserved. We consider a molecule as being aromatic if a delocalized bonding is encountered in a planar cyclic system by means of the AdNDP analysis and the number of electrons occupying the delocalized bonds satisfies the 4n + 2 rule. The AdNDP calculations were performed at the B3LYP level of theory using LanL2DZ (Mo, Sb) and 6-31G* (P, As, C, H) basis sets. All the calculations were done using Gaussian 09 software package.[37] Pictures of molecular structures, molecular orbitals and chemical bonds were made using MOLEKEL 5.4.0.8.[38]

12-3. Results and discussion

Our geometry optimization and follow-up frequency calculations of the model $CpMoE_6MoCp$ (E = P, As, Sb) complexes confirm that the C_i structure (shown in Figure 12-3) is an energy minimum and E_6 fragments are planar for all practical purposes.

The calculated phosphorus-phosphorus bond length R(P-P) in the P_6 fragment of the $CpMoP_6MoCp$ complex: R(P-P) = 2.22 Å is very close to the experimentally measured R(P-P) = 2.17 Å, but it is a little bit longer than an optimized R(P-P) = 2.13 Å of the isolated D_{6h} structure P_6. Similarly, the calculated R(As-As) = 2.40 Å in the As_6 fragment is somewhat longer than R(As-As) = 2.33 Å in the isolated D_{6h} As_6 structure. Surprisingly, the optimized R(Sb-Sb) = 2.73 Å in the Sb_6 fragment of the $CpMoSb_6MoCp$ complex was found to be shorter than R(Sb-Sb) = 2.79 Å in the corresponding isolated D_{6h} structure.

As mentioned above, the canonical LUMO of P_6 ring is responsible for the PJT distortion in this structure due to mixing with the HOMO-1 (Figure 12-2).

From our molecular orbital analysis (Figure 12-4) one can see that upon complex formation, the molecular orbital (LUMO) corresponding to the empty one in the isolated P_6 structure is now occupied in the triple-decker complex (HOMO-5). Therefore, to suppress the PJT effect, all unoccupied orbitals connected with its occurrence in the planar P_6 must be occupied in the resultant $CpMoP_6MoCp$ sandwich complex. Using similar analysis for $CpMoAs_6MoCp$ and $CpMoSb_6MoCp$, it was found that the same mechanism is responsible for killing the PJT effect in both com complexes, though we do not exclude some influence from the first mechanism.

In order to analyze chemical bonding in the studied triple-decker complexes we initially performed the general AdNDP search for lone pairs and two-center two-electron (2c-2e) bonds in the whole $CpMoP_6MoCp$ complex. After depleting the overall density for the lone pairs and 2c-2e bonds, we then performed user-directed search of chemical bonding on each of the fragments ($C_5H_5^-$, P_6, MoP_6Mo) of the sandwich complex separately. The results of this analysis are shown in Figure 12-5.

As expected, the AdNDP analysis revealed the presence of five 2c-2e C-C σ-bonds with the occupation numbers (ON) equal to 1.97 |e| and five 2c-2e C-H σ-bonds (ON = 1.98 |e|) for every $C_5H_5^-$ units, six lone pairs on every phosphorus atom (not shown in Figure 12-5) and one direct 2c-2e σ-bond (ON = 2.00 |e|) between two Mo atoms.

The direct AdNDP search on each $C_5H_5^-$ units recovered three 5c-2e π-bonds (ON = 1.97 – 1.99 |e|), which are responsible for π-aromaticity of these fragments.

Because of high occupation numbers of π-bonds in our direct search on $C_5H_5^-$, it is clear that they do not participate in the π type back-donation to Mo atoms. Thus, bonding between two $C_5H_5^-$ units and two Mo atoms in the analyzed complex has a significant ionic contribution. The AdNDP search revealed six 2c-2e P-P σ-bonds (ON = 1.73 |e|) for the planar P_6 unit. Such deviation from an absolute ON = 2.00 |e| implies that these 2c-2e P-P σ-bonds are delocalized over larger number of atoms. However, occupation numbers of 1.73 |e| are large enough and are therefore acceptable for the picture of our qualitative analysis. There are also seven bonds of different types on the fragment which comprises the P_6 unit and two Mo atoms (MoP_6Mo). Three bonds shown in Figure 12-5h are primarily 6c-2e (excluding negligible anti-bonding interactions between P_6 and Mo atoms) π-bonds (with occupation numbers lying within the 1.90 – 2.00 |e| range) and they are in charge of π-aromaticity in the P_6 fragment.

Another four bonds with ON = 1.94 |e| (shown in Figure 12-5i) are responsible for the covalent bonding between Mo and P_6 through the δ type M→L back-donation mechanism. These bonds are formed by interactions of occupied $d_{x^2-y^2}$ and d_{xy} atomic orbitals of Mo atom with partially antibonding π-molecular orbitals of P_6. An occupation of partially antibonding π-orbitals is responsible for the elongation of P-P bond lengths upon complexation. The AdNDP analysis of chemical bonding in the $CpMoAs_6MoCp$ and $CpMoSb_6MoCp$ complexes revealed similar chemical bonding patterns as in the $CpMoP_6MoCp$. The δ type M→L back-donation mechanism was previously described by Rayon and Frenking for bis(benzene)chromium[39] as well as Diaconescu et al. for an inverted $(m\text{-}C_6H_6)[U(NH_2)_2]_2$ sandwich complex.[40]

12-4. Conclusions

Quantum chemical calculations of the $CpMoE_6MoCp$ (E = P, As, Sb) triple-decker sandwich complexes showed that E_6 fragments in the central decks of the complexes are planar. These results agreed with the experimentally observed $\{(\eta^5\text{-}Me_5C_5)Mo\}_2(\mu,\eta^6\text{-}P_6)$,[4] $\{(\eta^5\text{-}Me_5C_5)W\}_2(\mu,\eta^6\text{-}P_6)$, $\{(\eta^5\text{-}Me_4EtC_5)V\}_2(\mu,\eta^6\text{-}P_6)$[41] and $\{(\eta^5\text{-}Me_4EtC_5)Mo\}_2(\mu,\eta^6\text{-}As_6)$[7] triple-decker sandwich complexes. We are not aware of any experimental data on the decker complexes with Sb_6 fragment.

Thus, we only made a theoretical prediction of the existence of the planar *cyclo*-Sb_6 as the central deck.

The analysis of molecular orbitals involved in vibrational coupling showed that filling the intervenient molecular orbitals with electron pairs of Mo atoms suppresses the PJT effect in the $CpMoE_6MoCp$ (E = P, As, Sb), with the E_6 ring becoming planar (D_{6h}). Thus, the complexation may be considered as the second example of the suppression of the PJT effect after the reaction between Si_6Cl_{12} and a Lewis base (e.g., Cl^-) to give planar $[Si_6Cl_{14}]^{2-}$ dianionic complexes.[28]

Our AdNDP analysis revealed that bonding between $C_5H_5^-$ units and Mo atoms in the examined triple-decker sandwich complexes is primarily ionic while bonding between Mo atoms and E_6 fragment is appreciably covalent through the δ type M→L back-donation mechanism.

We believe that suppressing the PJT effect due to the filling unoccupied molecular orbitals during the complex formation is not limited to our examples, but is much more common phenomenon in chemistry. We hope that the current work will

attract attention to this suppression mechanism which can become a good tool for constructing new materials with desired planar highly-symmetric species.

References

(1) Gutman, I.; Potgieter, J. H. *J. Chem. Ed*. **1994**, 71, 222.

(2) Nagendrappa. G. *Resonance (India)* **2001**, May, 74.

(3) Dinadayalane, T. C.; Priyakumar, U. D.; Sastry, G. N. *J. Phys. Chem. A* **2004**, 108, 11433.

(4) Scherer, O. J.; Sitzmann, H.; Wolmershauser, G. *Angew. Chem. Int. Ed*. **1985**, 24, 351.

(5) Scherer, O. J. *Angew. Chem. Int. Ed*. **2000**, 39, 1029.

(6) Hiberty, P. C.; Volatron, F. *Heteroatom Chem*. **2007**, 18, 129.

(7) Scherer, O. J.; Sitzmann, H.; Wolmershauser, G. *Angew. Chem. Int. Ed*. **1989**, 28, 212.

(8) Jemmis, E. D.; Reddy, A. C. *Organometallics* **1988**, 7, 1561-1564.

(9) Reddy, A. C.; Jemmis, E. D. *Organometallics* **1992**, 11, 3894-3900.

(10) Rani, D. U.; Prasad, D. L. V. K.; Nixon, J. F.; Jemmis, E. D. *J. Comput. Chem.* **2007**, 28, 310.

(11) Nguyen, M. T.; Hegarty, A. F. *J. Chem. Soc. Chem. Comm*. **1986**, 383.

(12) Jones, R. O.; Hohl, D. J. *J. Chem. Phys*. **1990**, 92, 6710.

(13) Jones, R. O.; Seiferd, G. *J. Chem. Phys*. **1992**, 96, 7564.

(14) Warren, D. S.; Gimarc, B. M. *J. Am. Chem. Soc*. **1992**, 114, 5378.

(15) Kobayashi, K.; Miura, H.; Nagase. S. *J. Mol. Struct.: THEOCHEM*. **1994**, 69, 311.

(16) Gimarc, B. M.; Zhao, M. *Coord. Chem. Rev*. **1997**, 158, 385.

(17) Haeser, M.; Schneider, U.; Alhrichs, R. *J. Am. Chem. Soc*. **1992**, 114, 9551.

(18) Ballone, P.; Jones, R. O. *J. Chem. Phys*. **1994**, 100, 4941.

(19) Haser, M.; Treutler, O. *J. Chem. Phys*. **1995**, 102, 3703.

(20) Galeev, T. R.; Boldyrev, A. I. *Phys. Chem. Chem. Phys*. **2011**, 13, 20549.

(21) Opik, U.; Pryce, M. H. L. *Proc. R. Soc. London A* **1957**, 238, 425.

(22) Bersuker, I. B. *Phys. Lett. A* **1966**, 20, 589.

(23) Bersuker, I. B. *Chem. Rev*. **2001**, 101, 1067.

(24) Bersuker, I. B. In *The Jahn-Teller Effect*; Cambridge University Press: Cambridge, U.K., **2006**.

(25) Boggs, J. E.; Polinger, V. Z. In *The Jahn-Teller Effect and Beyond: Selected Works of Isaac Bersuker with Commentaries*, The Academy of Sciences of Moldova: Chisnau, Moldova, **2008**.

(26) Bersuker, I. B.; Stavrov S. S. *Coord. Chem. Rev.* **1988**, 88, 1-68.

(27) Sergeeva, A. P.; Boldyrev, A. I. *Organometallics* **2010**, 29, 3951.

(28) Pokhodnya, K.; Olson, C.; Dai, X.; Schulz, D. L.; Boudjouk, P.; Sergeeva, A. P.; Boldyrev, A. I. *J. Chem. Phys*. **2011**, 134, 014105.

(29) Becke, A. D. *J. Chem. Phys*. **1993**, 98, 5648.

(30) Vosko, S. H.; Wilk, L.; Nusair, M. *Can. J. Phys*. **1980**, 58, 1200.

(31) Lee, C.; Yang, W.; Parr, R. G. *Phys. Rev. B: Condens. Matter* **1988**, 37, 785.

(32) Hay, P. J.; Wadt, W. R. *J. Chem. Phys*., **1985**, 82, 299.

(33) Zubarev, D. Yu.; Boldyrev, A. I. *Phys. Chem. Chem. Phys*. **2008**, 10, 5207.

(34) (*a*) Zubarev, D. Yu.; Boldyrev, A. I. *J. Org. Chem*. **2008**, 73, 9251. (*b*) Popov, I. A.; Boldyrev, A. I. *Eur. J. Org. Chem*. **2012**, 3485.

(35) Zubarev, D. Yu.; Boldyrev, A. I. *J. Phys. Chem*. **2009**, 13, 866.

(36) Sergeeva, A. P.; Boldyrev, A. I. *Phys.Chem.Chem.Phys.* **2010**, 12, 12050-12054.

(37) Frisch, M. J.; Trucks, G. W.; Schlegel, H. B.; Scuseria, G. E.; Robb, M. A.; Cheeseman, J. R.; Scalmani, G.; Barone, V.; Mennucci, B.; Petersson, G. A.; Nakatsuji, H.; Caricato, M.; Li, X.; Hratchian, H. P.; Izmaylov, A. F.; Bloino, J.; Zheng, G.; Sonnenberg, J. L.; Hada, M.; Ehara, M.; Toyota, K.; Fukuda, R.; Hasegawa, J.; Ishida, M.; Nakajima, T.; Honda, Y.; Kitao, O.; Nakai, H.; Vreven, T.; Montgomery, J. A., Jr.; Peralta, J. E.; Ogliaro, F.; Bearpark, M.; Heyd, J. J.; Brothers, E.; Kudin, K. N.; Staroverov, V. N.; Kobayashi, R.; Normand, J.; Raghavachari, K.; Rendell, A.; Burant, J.

C.; Iyengar, S. S.; Tomasi, J.; Cossi, M.; Rega, N.; Millam, N. J.; Klene, M.; Knox, J. E.; Cross, J. B.; Bakken, V.; Adamo, C.; Jaramillo, J.; Gomperts, R.; Stratmann, R. E.; Yazyev, O.; Austin, A. J.; Cammi, R.; Pomelli, C.; Ochterski, J. W.; Martin, R. L.; Morokuma, K.; Zakrzewski, V. G.; Voth, G. A.; Salvador, P.; Dannenberg, J. J.; Dapprich, S.; Daniels, A. D.; Farkas, O.; Foresman, J. B.; Ortiz, J. V.; Cioslowski, J.; Fox, D. J. *Gaussian 09*, Revision B.01; Gaussian, Inc.: Wallingford, CT, **2010**.

(38) Varetto, U. *Molekel*, version 5.4.0.8; Swiss National Super-computing Centre: Manno, Switzerland, *2009*.

(39) Rayon, V. M.; Frenking, G. *Organometallics* **2003**, 22, 3304.

(40) Diaconescu, P. L.; Arnold, P. L.; Baker, T. A.; Mindiola D. J.; Cummins, C. C. *J. Am. Chem. Soc.* **2000**, 122, 6108.

(41) Scherer, O. J.; Schwalb, J.; Swarowsky, H.; Wolmershauser, G.; Kaim, W.; Gross, R. *Chem. Ber*. **1988**, 121, 443-449.

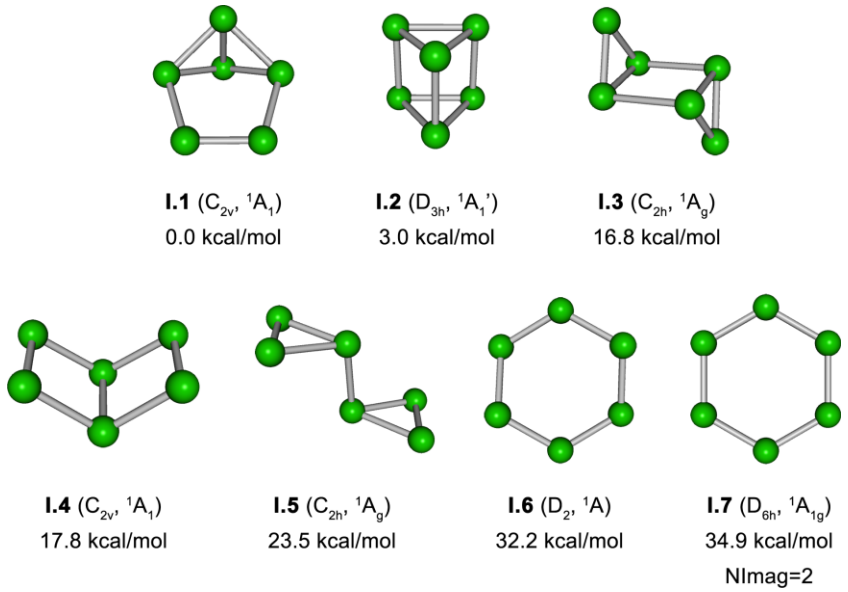

Figure 12-1. Selected lowest-energy structures of P_6, their point group symmetries, spectroscopic states and ZPE (B3LYP/6-311+G*) corrected relative energies (CCSD(T)/CBS//B3LYP/6-311+G*).

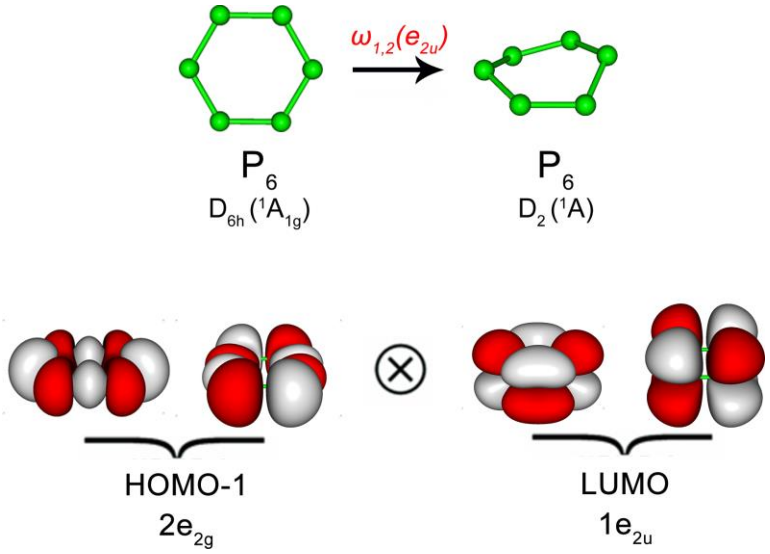

Figure 12-2. Interaction of the pairs of occupied and unoccupied molecular orbitals of the D_{6h} ($^1A_{1g}$) structure of P_6 responsible for the PJT effect: interactions cause distortion toward the D_2 (^1A) structure upon following the doubly degenerate $\omega_{1,2}(e_{2u})$ imaginary frequency mode.

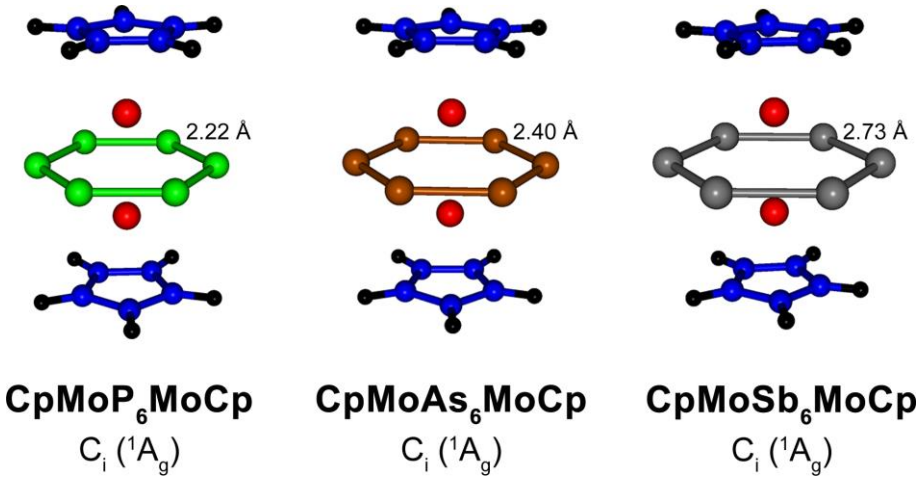

Figure 12-3. Optimized structures, point group symmetry, spectroscopic states and bond lengths of the middle-deck fragments in the triple-decker sandwich complexes.

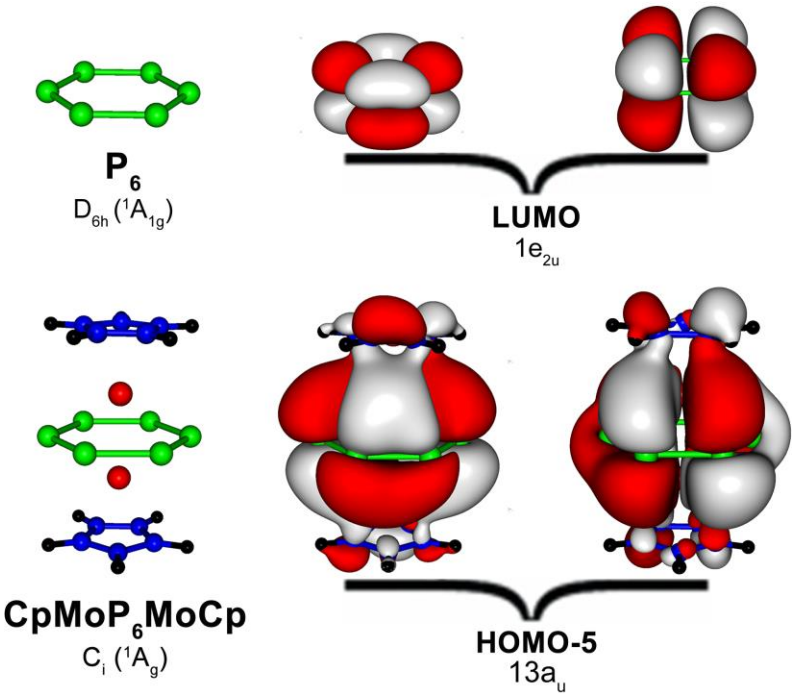

Figure 12-4. One-to-one correspondence of unoccupied canonical molecular orbitals of P_6 (D_{6h}, $^1A_{1g}$) to those of $CpMoP_6MoCp$ (C_i, ^1A_g), where occupation in the latter results in the suppression of the PJT effect.

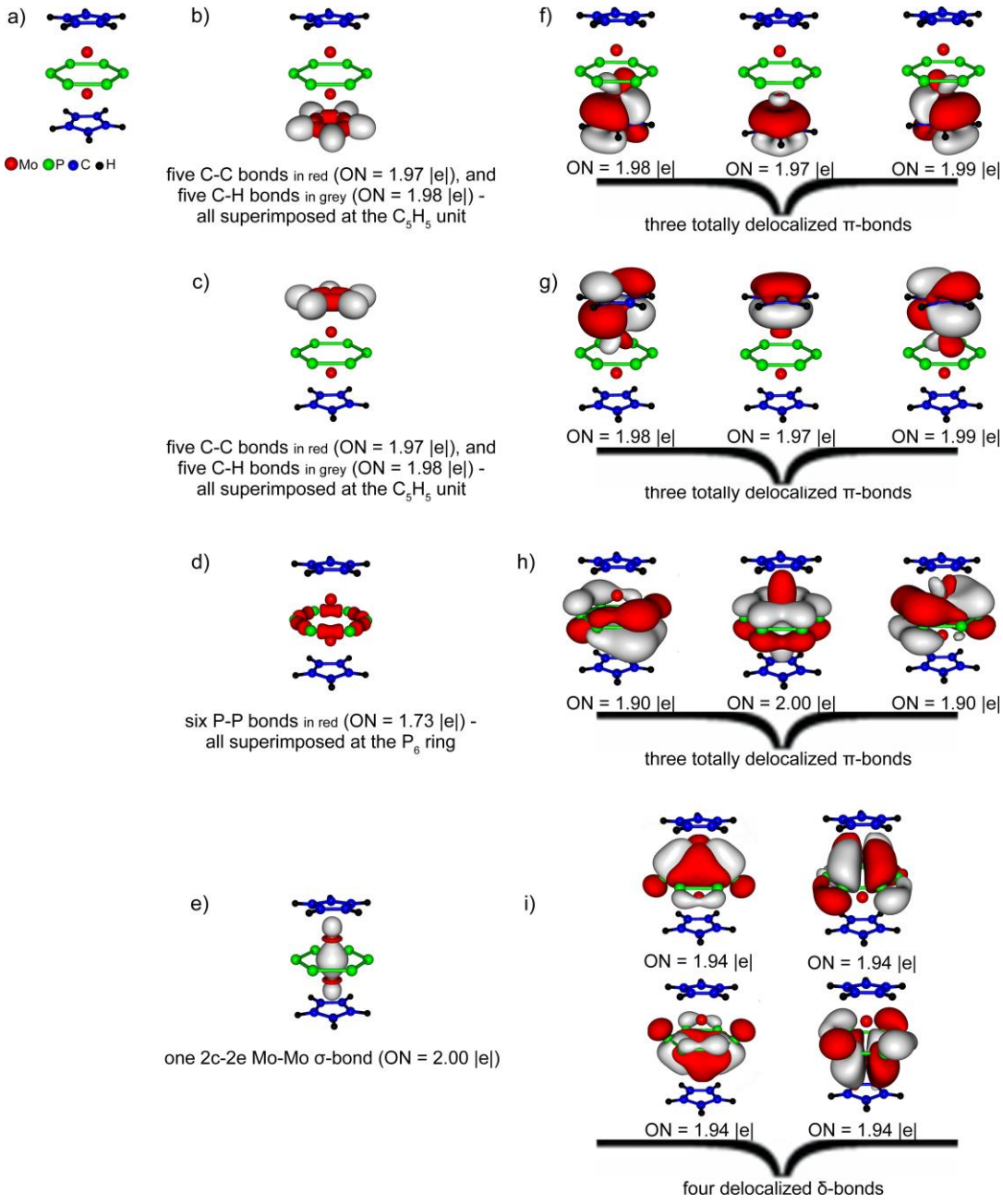

Figure 12-5. The chemical bonding picture of the $CpMoP_6MoCp$ triple-decker sandwich complex a) obtained by the AdNDP method: b), c) σ-bonds recovered on the $C_5H_5^-$ units; d) σ-bonds recovered on the P_6 unit; e) direct Mo-Mo σ-bond; f), g) π-bonds recovered on the $C_5H_5^-$ units; h) π-bonds recovered on the MoP_6Mo fragment; i) δ-bonds recovered on the MoP_6Mo fragment.

CHAPTER 13

PSEUDO JAHN-TELLER ORIGIN OF BUCKLING DISTORTIONS IN TWO-DIMENSIONAL TRIAZINE-BASED GRAPHITIC CARBON NITRIDE (g-C_3N_4) SHEETS[1]

Abstract

Due to its direct band gap and light mass, the recently synthesized triazine-based, graphitic carbon nitride (*TGCN*) is considered as a promising material for future microelectronics. However, despite the structural similarity with completely planar carbon-only graphene, *TGCN* sheets are different because of the presence of buckling distortions making the *TGCN* sheets non-planar. In this article we show that the sufficiently strong coupling between the unoccupied molecular orbitals (UMOs) with occupied molecular orbitals (OMOs) leads to pseudo Jahn−Teller distortions (PJT) and consequent buckling of *TGCN* layers. Doping the *TGCN* with doubly charged cations such as Be^{2+} can suppress the PJT distortions resulting in a completely planar structure. A proper understanding of the mechanism of the PJT effect in *TGCN* is crucial for tailoring properties that are relevant for practical applications.

13-1. Introduction

Two-dimensional (2D) materials have attracted a lot of attention owing not only their unique electronic structures, but useful physical and chemical properties including specific optical activity, high carrier mobility, and high electrical and thermal

[1] Coauthored by Alexander S. Ivanov, Evan Miller, Alexander I. Boldyrev, Yuichiro Kameoka, Tohru Sato, and Kazuyoshi Tanaka. Reprinted with permission from *J. Phys. Chem. C,* **2015**, *119* (21), pp 12008-12015.

conductivity.[1,2] Since successful exfoliation of single layers of graphite, graphene[3] has been considered by researches as the most promising candidate material for nanoelectronics, even suggested to replace silicon based materials in future microelectronic devices. However, graphene is missing the typical electronic band gap that would make it a semiconductor. Recently, G. Algara-Siller et al.[4] prepared crystals of triazine-based graphitic carbon nitride (*TGCN*), a layered material that is similar to graphite, but which contains nitrogen. The material was synthesized using an ionothermal, interfacial reaction starting with the inexpensive substance dicyandiamide. The density functional theory (DFT) calculations showed that *TGCN* material has a direct band gap of 1.6 - 2.0 eV.[4] Thus, graphitic carbon nitride is of immense interest for electronic devices including field-effect transistors and light-emitting diodes. Moreover, g-C_3N_4 graphitic carbon nitride can be used as a valuable photocatalyst with high thermal and chemical stability, making it potentially suitable for solar energy conversion and environmental regeneration.[5-10] However, despite these useful applications in the field of catalysis and electronics, the structure of g-C_3N_4 graphitic carbon nitride seems to be still poorly understood. Recent combined experimental and theoretical studies support a corrugated structure rather than a planar one.[4] Therefore, g-C_3N_4 graphitic carbon nitride layers are not atomically thin and thus not strictly two-dimensional. An interesting question arises here: what is the source of instability of g-C_3N_4 planar sheets toward puckering distortions?

Previous periodic DFT calculations showed that 2D C_3N_4 (g-C_3N_4) graphene sheets spontaneously distort along a direction perpendicular to the layers leading to buckled structures.[11] The authors also demonstrated that the instability of the planar

configuration stems from the repulsion between the lone pairs on the two-coordinated nitrogen atoms, and buckling causes these lone pairs to reorient, thus reducing their steric repulsion. However, D. Vodak et al.[12] concluded that although the nitrogen–nitrogen repulsive forces are important, they are not absolute in determining the stability of the triazine-based C_3N_4 networks. Hence, this explanation clarifies only the origin of some particular structural properties, contributing partially to the solution of problem. As pointed out by I. Bersuker et al.,[13] the best approach to investigate molecular geometries should be based on how electrons control molecular configurations. The vibronic coupling theory,[14,15] which considers how electronic states and their changes influence nuclear configurations, has proven to be the best approach for the description of molecular shapes since it is based on the first principles. A manifestation of vibronic coupling or electron-vibration coupling is the pseudo Jahn-Teller effect (PJTE) – the only source of instability and distortions of high-symmetry configurations of any polyatomic system in nondegenerate states.[16-19] In this article, we prove on the basis of orbital vibronic coupling density analysis[20-22] that the instability of planar triazine-based graphitic carbon nitride sheets is due to the strong coupling between the unoccupied molecular orbitals (UMOs) with occupied molecular orbitals (OMOs) resulting in the pseudo Jahn-Teller distortions of *TGCN* sheets.

13-2. Methods and computational details

To elucidate the nature of instability of *TGCN* sheets toward puckering distortions by using orbital vibronic coupling density analysis, calculations on a cluster model $C_9N_{12}H_6$ with three aromatic 1,3,5-triazine rings (T3G) extracted from the periodic structure and capped with hydrogen atoms at optimized positions, were undertaken. The

T3G structure was also extended to triangular cuts of a graphitic structure containing 6, 10, and 15 triazine units (T6G, T10G, and T15G, respectively). Both planar and buckled clusters were optimized using the hybrid DFT functionals M05-2X and B3PW91, as implemented in Gaussian 09 software.[23] The M05-2X functional is the Truhlar's hybrid meta exchange-correlation functional, which is known to describe dispersion interactions better than traditional DFT functionals.[24,25] B3PW91, gradient corrected correlation functional, has shown very accurate results for assessing band-gaps in semiconductors.[26,27] The 6-31+G(d,p)[28] basis set was employed for the calculations. Additional frequency calculations were performed for ensuring real vibrational modes for the minimum ground state structures. Metal ions doped complexes (T3G ⋯ 2M, M = Li^+, Be^{2+}) were also reoptimized with follow-up frequency calculations at the M05-2X/aug-cc-pvDZ and M05-2X/aug-cc-pvTZ[29,30] levels of theory to insure the vibrational stability of these species. The binding energy (Bind. En.) between doped metal ions T3G cluster (T3G ⋯ 2M) and the stand-alone T3G cluster was defined as: Bind. En. = E(T3G) + 2E(M) - E(T3G ⋯ 2M).

The periodic calculations were done using the Vienna ab initio simulation package (VASP) DFT code[31] using the projector-augmented-wave (PAW) method. The energy cutoff for the plane waves was set to 400 eV. The atom positions are relaxed within the general-gradient approximation (GGA), using Perdew-Burke-Ernzerhof (PBE) functional.[32,33] 9 × 9 × 1 k-point sampling with Monkhorst–Pack scheme[34] was employed for integration over the first Brillouin zone. Beryllium ions doped *TGCN* sheet was also capped on both sides by oxygen atoms to balance the ions charges. The criteria for

convergence in energy and force are 10^{-4} eV and 0.01 eV/Å, respectively. A vacuum space of 20 Å was introduced between adjacent layers.

Chemical bonding analysis of the buckled T3G cluster ($C_9N_{12}H_6$) was performed at the M05-2X/6-31+G(d,p) level of theory using the adaptive natural density partitioning (AdNDP) method,[35] which has been used successfully to analyze the chemical bonding of porphyrins,[36] silabenzenes,[37] mixed carbon-phosphorus,[38] and carbon-boron clusters.[39] Chemical bonding analysis of the corrugated *TGCN* sheet was performed using a recently developed solid state adaptive natural density partitioning (SSAdNDP) method (Galeev et al.).[40] Both methods are extensions of the natural bonding orbital (NBO) method developed for molecules by Foster and Weinhold[41,42] and for extended systems by Dunnington and Schmidt.[43] The AdNDP method analyzes the first-order reduced density matrix in order to obtain its local block eigenfunctions with optimal convergence properties for an electron density description. The obtained local blocks correspond to the sets of n atoms (n ranging from one to the total number of atoms in the molecule) that are tested for the presence of two-electron objects (n-center two electron (nc-2e) bonds, including core electrons and lone pairs as a special case of n = 1) associated with this particular set of n atoms. AdNDP initially searches for core electron pairs and lone pairs (1c-2e), then 2c-2e, 3c-2e, …, and finally nc-2e bonds. At every step the density matrix is depleted of the density corresponding to the appropriate bonding elements. AdNDP accepts only those bonding elements whose occupation numbers (ONs) exceed the specified threshold values, which are usually chosen to be close to 2.00 |e|. However, the criterion for ONs might be adjustable for a particular case in the AdNDP procedure. When all the recovered nc-2e bonding elements are superimposed onto the molecular

frame the overall pattern always corresponds to the point group symmetry of the system. Thus, the AdNDP method recovers both Lewis bonding elements (1c-2e and 2c-2e objects, corresponding to the core electrons and lone pairs, and two-center two-electron bonds) and delocalized bonding elements, which are associated with the concepts of aromaticity and antiaromaticity. From this point of view, AdNDP achieves seamless description of systems featuring both localized and delocalized bonding without invoking the concept of resonance. In SSAdNDP a projection algorithm is used to obtain a representation of the delocalized PW DFT results in a localized AO basis. As long as an appropriate AO basis set is chosen (it is usually trimmed of any functions with angular momentum $l \geq 4$ as well as diffuse functions with exponents <0.1), projection is found to result in an accurate density matrix.[43] In this study cc-pvDZ basis set was used to represent the projected PW density using a 9 × 9 × 1 k-point grid. This basis set was selected so that on average less than 1% of the density of each occupied plane wave band was lost in projecting into the AO basis to guarantee that the density matrix used in the SSAdNDP procedure accurately represents the original plane wave results. The Visualization for Electronic and Structural Analysis software (VESTA, series 3)[44] and Molekel 5.4.0.8[45] were used for visualizations of the considered structures.

The PJT instability $E_{PJT}(Q)$ in potential energy surface is described by the following expression[20-22]:

$$E_{PJT}(Q_{e''}) = -\sum_{i\in occ,\, j\in unocc} k_{e''}^{(i,j)} Q_{e''}^2 = -\sum_{i\in occ,\, j\in unocc} \left(\frac{|\, f_{e''}^{(i,j)} \,|^2}{\varepsilon_j - \varepsilon_i} \right) Q_{e''}^2 , \qquad (1)$$

where $f_{e''}^{(i,j)} = \int \psi_i^*(\mathbf{r}) \left(\frac{\partial u(\mathbf{r})}{\partial Q_{e''}} \right)_0 \psi_j(\mathbf{r}) d^3\mathbf{r}$ is orbital vibronic coupling constant (OVCC). OVCC $f_{e''}^{(i,j)}$ can be expressed in terms of orbital vibronic coupling density (OVCD) $\eta_{e''}^{(i,j)}(\mathbf{r})$:

$$f_{e''}^{(i,j)} = \int \eta_{e''}^{(i,j)}(\mathbf{r}) d^3\mathbf{r}, \text{ where } \eta_{e''}^{(i,j)}(\mathbf{r}) = \psi_i^*(\mathbf{r}) \left(\frac{\partial u(\mathbf{r})}{\partial Q_{e''}} \right)_0 \psi_j(\mathbf{r}).$$

The degenerate e" vibrational vectors with an imaginary frequency were symmetrized. Mass-weighted normal modes were used for the calculations of OVCC and OVCD. All the OVCD analyses were performed by using our in-house codes.

13-3. Results and discussion

Our geometry optimization and follow-up frequency calculations of $C_9N_{12}H_6$ cluster model (T3G) confirm that the D_{3h} symmetric planar structure is indeed not stable and was found to be only a third order saddle point on the potential energy surface. The D_{3h} T3G structure has three modes with imaginary frequencies: degenerate e" and a_2" modes. The imaginary frequencies e" indicate that the planar T3G structure is unstable for the displacement along the e" modes in plane, and the symmetry lowers into the C_s distorted structure with non-zero dihedral angles between the neighboring triazine units. It means that e" modes give rise to a distortion leading to the C_s minimum structure. On the other hand, the a_2" vibrational mode with the imaginary frequency gives rise to the out of plane deformation into a structure with C_3 symmetry. According to our calculations, C_s structure is 4.3 kcal/mol (M05-2X/6-31+G(d,p)) more stable than C_3

structure. Thus, e" modes have a bigger impact on the distortion of D_{3h} planar T3G cluster. To clarify the origin of the driving force of the PJT instability, we performed the orbital vibronic coupling density (OVCD) analyses for the e" mode.

Table 13-1 summarizes the calculated energy gaps between interacting OMO-UMO orbitals and orbital vibronic coupling constants (OVCCs). The degenerate HOMOs are the 71st and 72nd MOs, while the LUMO is the 73rd MO. It can be clearly seen from $k_{e"}^{(i,j)}$ values that the largest contribution to the PJT instability comes not from the HOMO-LUMO pair, but from the orbital pair of occupied 55th MO and the next LUMO (74th). Although the small orbital energy gap value between HOMO (71st) and LUMO (73rd) is essential in the PJT instability, according to eq 1 there is another parameter $f_{e"}^{(i,j)}$, the orbital vibronic coupling constant that can compensate for large OMO-UMO gap values. Such dependence of the PJT effect on different parameters was first shown on the example of NH_3 molecule, where the instability of the planar D_{3h} symmetric configuration toward trigonal pyramidal shape is caused by the vibronic coupling of the OMO-UMO pair with the orbital energy gap (Δ) of ~ 14 eV, while the contribution to the instability of a lower excited state at Δ ~ 5 eV was found to be very small.[46] Our calculations for T3G cluster show that the vibronic coupling between the 55th MO and the next LUMO (74th), which has the largest OVCC value, is the main source of the PJT instability. We can elucidate the reason why this orbital pair yields the large OVCC on the basis of the orbital vibronic coupling density (OVCD) analysis.

The vibrational vectors of the imaginary (PJT) $e_{\varepsilon}"$ mode have large displacements of the nitrogen atoms as shown in Figure 13-1, (a). Accordingly, the

derivative of the potential $u(\mathbf{r})$ with respect to the normal coordinate $Q_{e''}$ has the large distribution around the nitrogen atoms (Figure 13-1, (e)). Since both MO(55) and MO(74) have large MO coefficients on the nitrogen atoms (Figure 13-1, (b) and (c)), the orbital overlap between MO(55) and MO(74) becomes large around the nitrogen atoms (Figure 13-1, (d)). Therefore, the OVCD around the nitrogen atoms are large (Figure 13-1, (f)). On the other hand, the orbital overlap between the HOMO and LUMO has small distribution around the nitrogen atoms, since the LUMO has no coefficients on the nitrogen atoms. Therefore, if the orbital overlap around the nitrogen atoms can be reduced, the PJT instability would be suppressed.

13-4. Triazine-based graphitic carbon nitride clusters

In order to trace the growth of *TGCN* sheet and get a more thorough characterization of the distortions in *TGCN* layers, we investigated structural and electronic properties of bigger triazine-based clusters, starting from T3G cluster to T15G cluster, which contains up to 15 aromatic triazine units (Figure 13-2). A common feature for all the ground state structures of the triazine-based graphitic carbon nitride clusters is the puckering distortions in the open-hollow site. In T6G, T10G, and T15G structures the formed ripples are always localized within the open-hollow site and fresh ripples appear in the adjoining rings. A deviation (R) from planarity in T3G cluster model is 0.72 Å. Interestingly, this value remains almost the same for the bigger triazine-based graphitic carbon nitride clusters (Table 13-2) and for the periodic corrugated structure of *TGCN* sheet (R = 0.91 Å). As one may see from Table 13-2, the corrugated structures become more stable than the planar ones upon addition of more triazine units. The buckled structure is more stable than the planar one by about 114 kcal/mol for T15G cluster. The

HOMO-LUMO energy separation of a system often serves as a simple measure of chemical stability and conductivity.[47] The HOMO-LUMO gaps for T3G-T15G clusters are given in Table 13-2. It is well known that the DFT calculated HOMO–LUMO gaps only represent an approximation to the fundamental gap, which is defined as the difference between the ionization potential and electron affinity.[48] Our results (Table 13-2, HOMO-LUMO gap) for T3G-T15G show different values of the energy gaps depending on the choice of a DFT method (the nature of the exchange-correlation functional and the amount of Hartree-Fock exchange it includes). C. Musgrave and coworkers[49] compared various DFT methods for molecular orbital eigenvalue calculations and came to a conclusion that time-dependent (TD) calculations are required to describe accurately the HOMO-LUMO gaps. They demonstrated that TD-DFT calculations reliably predict the HOMO-LUMO gaps for all tested DFT methods, thus confirming that the excitation energy of the first singlet excited state is probably the most reasonable approximation to the HOMO-LUMO gap in molecules.[49] As one may see from Table 13-2, our TD-B3PW91/6-31+G(d,p) results suggest that a subsequent addition of triazine rings gradually decreases the HOMO-LUMO gap in the clusters, leading to a band gap (which is, at the materials level, equivalent to the molecular fundamental gap) of 1.62 eV in the periodic *TGCN* structure. The analogous trend in the dependence of HOMO-LUMO gaps on the cluster size was observed for polycyclic aromatic hydrocarbons[50] and silicene clusters.[51] It is also worthy to note that the band gap in the *TGCN* sheet is considerably smaller than the fundamental gap in the triazine-based clusters, because in the solid state π-conjugated triazines adjacent to the unit that carries a charge significantly polarize thus stabilizing the anionic and cationic states.[48]

13-5. Chemical bonding

To gain more insight into the structure and chemical bonding in the *TGCN* sheet, we performed the adaptive natural density partitioning (AdNDP)[35,40] analysis. The results of our analysis for the periodic structure of a corrugated *TGCN* layer are shown in Figure 13-3, (a). The general SSAdNDP search revealed that all σ C-N bonds are well represented by classical two center-two electron (2c-2e) bonds (not shown in Figure 13-3). In addition, the SSAdNDP identified one s-type lone pair on each of the N atoms of a triazine fragment with the occupation number (ON) equals to 1.9 |e|, and one p-type lone pair, ON = 1.7 |e|, on the 3-coordinate nitrogen atom, which is linking three triazine units. Three 6c-2e delocalized π bonds on each of the C_3N_3 triazine moieties were found by directed search with ON = 2.0 |e|, highlighting each triazine ring's aromaticity. Therefore, a corrugated *TGCN* sheet can be viewed as a network consisting of aromatic triazine rings joined by 3-coordinate nitrogen atoms. The resulting picture of our AdNDP analysis for T3G cluster model is shown in Figure 13-3, (b). Similar to the results derived for the periodic *TGCN* structure, the use of AdNDP enabled direct classical 2c-2e σ C-N bonds to be found with ON value of 1.9 |e| (not shown in Figure 13-3), one s-type lone pair on each N atom in triazine units (ON = 1.9 |e|) and one p-type lone pair on the nitrogen atom connecting two triazine rings (ON = 1.7 |e|). Such similarity between chemical bonding pattern for the periodic *TGCN* structure and finite T3G structure further supports our choice of a cluster model for investigations of the pseudo Jahn-Teller effect in triazine-based graphitic carbon nitride sheet.

13-6. Suppression of the PJT effect

The knowledge of the mechanism of the PJT allows for manipulation of this effect by means of external perturbations that either populate the active excited states with electrons, making them inactive, or increase the energy gap Δ between vibronically coupled orbitals. These factors can diminish the PJT effect and may result in its full suppression. The first example of such quenching of the PJT effect was observed in metalloporphyrins and hemoproteins: the metal (iron) atom is driven out-of-plane by the PJT, but it returns back in plane by oxygenation (O_2 molecule coordination), which quenches the PJT effect by increasing the energy gap to the active excited state.[52] Recently, we proposed two more mechanisms for suppression of the PJT effect: by the gap increase between the interacting OMO–UMO pair in the external electrostatic field of cations[53,54] and by occupying the interacting UMO with an electron pair upon complexation.[55] D. Jose et al.[56] also reported that puckering distortions in silicene, the all Si analogue of graphene, are due to the PJT effect in the individual six membered Si_6 rings, and the coordination of Li^+ cations to the rings can suppress the PJT distortions resulting in a planar structure.

We performed DFT calculations to investigate whether the binding of metal ions can suppress PJT effect and flatten out the structure of triazine-based graphitic carbon nitride cluster T3G. G. Zhu et al.[57] showed that lithium-doped triazine-based graphitic C_3N_4 sheets can be good materials for hydrogen storage, however, the stable configuration of the lithium doped structures was found to be not strictly planar. The results of our initial calculations showed that in the presence of two Li^+ cations, the puckered T3G structure becomes planar to form D_{3h} symmetric complex. The lithium

doped T3G structure (T3G ⋯ $2Li^+$) was found to be stable at the M05-2x/3-21G level of theory, however, at higher levels of theory (M05-2X/6-31+G (d,p) and M05-2X/aug-cc-pvTZ) it is not even a minimum, being only a third order saddle point on the potential energy surface. The optimization of T3G ⋯ $2Li^+$ complex along imaginary frequency modes yields a buckled C_s symmetric structure, but the deviation from the planarity (R = 0.52 Å) is now less pronounced than in pure T3G cluster. Interestingly, a crystallographically characterized poly(bis(triazine) triimide) lithium chloride (PTI/LiCl) compound[58] - the closest structural analog of *TGCN* has less pronounced buckling than the corrugation of the *TGCN* layer.[4] Therefore, the electrostatic field of lithium cations is unable to completely suppress the PJT effect in the T3G cluster. However, we found that doping T3G with beryllium ions Be^{2+} seems to be sufficient for quenching the PJT effect and obtaining a completely planar beryllium doped D_{3h} symmetric T3G ⋯ $2Be^{2+}$ complex, which remains stable at the high level of theory – M05-2X/aug-cc-pvTZ (Figure 13-4, (a)). Imaginary vibrational frequencies have not been observed, verifying that T3G ⋯ $2Be^{2+}$ structure is indeed a local minimum on the potential energy surface. The lowest frequency is observed at 83 cm^{-1}. We also searched for the favorable binding site of Be ions by placing them at different possible positions of T3G cluster: the center of triazine (C_3N_3) ring, the open-hollow site, the top sites of atoms, and the bridge sites over the C-N bonds. We found that the open-hollow site with a binding energy of 11.14 eV (M05-2X/6-31+G(d,p)) is the most favorable Be ions binding site of T3G cluster. It is also interesting to note that the distances between adjacent nitrogen atoms (2.42 Å) in the open-hollow site of the optimized T3G ⋯ $2Be^{2+}$ complex are almost the same as the distances (2.44 Å) between the nitrogens in the unstable planar T3G configuration. The

distance between the metal ion and the T3G is 1.69 Å. In addition, a natural population analysis (NPA) was performed to determine a charge distribution on Be. According to it, Be ions bear a substantial positive charge of +1.51 (M05-2X/aug-cc-pvDZ). Remarkably, doping T3G cluster with the two Be^{2+} ions decreases the HOMO-LUMO energy gap to 2.88 eV (TD-B3PW91/6-31+G(d,p)) restoring the planarity of T3G structure (Figure 13-4, (a)). We also performed additional calculations to figure out how the position and concentration of Be ions affect the structure of T3G cluster. According to our results, doping T3G with one Be^{2+} ion is not sufficient for achieving a planar configuration of T3G. Geometry optimization of T3G ⋯ Be^{2+} complex leads to the C_3 symmetric local minimum structure with the Be ion located above the open-hollow site of T3G cluster. However, the T3G ⋯ Be^{2+} structure flattens out upon addition of another Be ion on the opposite side of T3G. The D_{3h} symmetric T3G ⋯ $2Be^{2+}$ complex with a completely planar T3G fragment (Figure 13-4, (a)) was also found to be the most energetically favorable molecular configuration among all the considered $2Be^{2+}$ doped structures. Increasing the concentration of Be ions leads to the tremendous electrostatic repulsion between adjacent Be, and we were not able to achieve any local minima.

In order to extend our results obtained for the T3G molecular fragment to a periodic triazine-based graphitic carbon nitride structure, we performed solid-sate VASP calculations for the extended system. In agreement with the results on the T3G cluster model, the *TGCN* sheet is now planar in the presence of Be^{2+} ions (Figure 13-4, (b)). The computed binding energy is 7.38 eV and Be is positively charged (+1.2) according to the periodic NBO analysis. It is also worthy to note that the presence of Be^{2+} ions sufficiently lowers band gap of *TGCN* sheet by approximately 0.8 eV, making it a narrow-band gap

semiconductor (Figure 13-4, (c)). Hence, the induced planarity in *TGCN* sheet leads to a closure of the band gap and doping *TGCN* sheet with metal cations can be used to tune the band gap in this material. It should be noted that the Be^{2+} decorated *TGCN* sheet represents only a crude theoretical model of interactions between Be ions and *TGCN*, however, we believe that a 2D *TGCN* sheet might become synthesized at rather specific experimental conditions. For instance, as it was mentioned above, one of the closet structural analogs of *TGCN* - poly(bis(triazine) triimide) lithium chloride (PTI/LiCl) compound - has already been synthesized and thoroughly characterized.[58] In this structure the voids between almost planar triazine layers are filled with Li^+ and Cl^- ions. Thus, we hope that Be ions doped *TGCN* with a completely planar configuration might be synthesized as well using the appropriate beryllium containing salt instead of LiCl. Another possible way of the experimental realization of a planar *TGCN* structure is to deposit the *TGCN* on a suitable substrate.

To clarify the suppression mechanism of the PJT effect in the Be^{2+} doped triazine-based graphitic carbon nitride, we performed the OVCD analysis for the e_g'' mode (100 cm^{-1}) of T3G ⋯ $2Be^{2+}$ cluster, which corresponds to the PJT mode of the pristine T3G with the imaginary frequency (Figure 13-5). Figures 13-5 (a) and (b) show 67th and 76th MOs which correspond to the MOs shown in Figure 13-1 for bare T3G cluster. The MO coefficients of the nitrogen atoms close to the Be ions are decreased. The potential derivative (Figure 13-5, (d)) is also decreased in the same region. As the result, the OVCD (Figure 13-5, (e)) has a small distribution. Therefore the PJT effect in this system is completely suppressed. Interestingly, the PJT effect in T3G ⋯ $2Be^{2+}$ complex is essentially quenched by lowering $|f_{e''}^{(i,j)}|^2$ term in equation 1, though the energy gap

between the 67^{th} OMO and 76^{th} UMO pair is small. Hence, according to our results, the application of the external electrostatic field of cations may sometimes decrease the energy gap between the interacting orbitals, but at the same time this may result in a small value of orbital vibronic coupling constant leading to the vanishing of the PJT instability.

13-7. Conclusions

In conclusion, we have analyzed the microscopic origin of instability of planar 2D sheets of triazine-based graphitic carbon nitride (*TGCN*) toward puckering distortions. On the basis of the OVCD analysis for the pseudo Jahn-Teller effect, it was shown that the instability stems from the orbital vibronic couplings between the unoccupied molecular orbitals and occupied molecular orbitals of the *TGCN* sheet. A proper understanding of the mechanism of buckling distortions in *TGCN* is crucial for tailoring properties that are relevant for practical applications. It was also found that the puckering in the *TGCN* sheet can be suppressed to re-induce planarity using Be^{2+} ions and such doping lowers the band gap in this material by 0.8 eV. Hence, we expect that our studies will provide a new method for engineers to tailor the puckering distortions in the *TGCN* sheets and also to tune the band gap in this material by using an external electric field without any chemical modification.

References

(1) Miro, P.; Audiffred, M.; Heine, T. An Atlas of Two-Dimensional Materials. *Chem. Soc. Rev.* **2014**, *43*, 6537–6554.

(2) Fiori, G.; Bonaccorso, F.; Iannaccone, G.; Palacios, T.; Neumaier, D.; Seabaugh, A.; Banerjee, S. K.; Colombo, L. Electronics Based on Two-Dimensional Materials. *Nature Nanotech*. **2014**, *9*, 768–779.

(3) Novoselov, K. S.; Jiang, D.; Schedin, F.; Booth, T. J.; Khotkevich, V. V.; Morozov, S. V.; Geim, A. K. Two-Dimensional Atomic Crystals. *Proc. Natl. Acad. Sci. USA* **2005**, *102*, 10451–10453.

(4) Algara-Siller, G.; Severin, N.; Chong, S. Y.; Björkman, T.; Palgrave, R. G.; Laybourn, A.; Antonietti, M.; Khimyak, Y. Z.; Krasheninnikov, A. V.; Rabe, J. P.; et al. Triazine-Based Graphitic Carbon Nitride: a Two-Dimensional Semiconductor. *Angew. Chem. Int. Ed.* **2014**, *53*, 7450–7455.

(5) Ong, W.-J.; Tan, L.-L.; Chai, S. P.; Yong, S. T. Heterojunction Engineering of Graphitic Carbon Nitride (g-C_3N_4) via Pt Loading With Improved Daylight-Induced Photocatalytic Reduction of Carbon Dioxide to Methane. *Dalton Trans*. **2015**, *44*, 1249–1257.

(6) Wang, X.; Maeda, K.; Thomas, A.; Takanabe, K.; Xin, G.; Carlsson, J. M.; Domen, K.; Antonietti, M. A Metal-Free Polymeric Photocatalyst for Hydrogen Production from Water under Visible Light. *Nat. Mater*. **2009**, *8*, 76–80.

(7) Cao, S.-W.; Liu, X.-F.; Yuan, Y.-P.; Zhang, Z.-Y.; Liao, Y.-S.; Fang, J.; Loo, S. C. J.; Sum, T. C.; Xue, C. Solar-to-Fuels Conversion Over In_2O_3/g-C_3N_4 Hybrid Photocatalysts. *Appl. Catal. B* **2014**, *147*, 940–946.

(8) Liu, G.; Niu, P.; Sun, C.; Smith, S. C.; Chen, Z.; Lu, G. Q.; Cheng, H.-M. Unique Electronic Structure Induced High Photoreactivity of Sulfur-Doped Graphitic C_3N_4. *J. Am. Chem. Soc.* **2010**, *132*, 11642–11648.

(9) Du, A.; Sanvito, S.; Li, Z.; Wang, D.; Jiao, Y.; Liao, T.; Sun, Q.; Ng, Y. H.; Zhu, Z.; Amal, R.; et al. Hybrid Graphene and Graphitic Carbon Nitride Nanocomposite: Gap Opening, Electron–Hole Puddle, Interfacial Charge Transfer, and Enhanced Visible Light Response. *J. Am. Chem. Soc*. **2012**, *134*, 4393–4397.

(10) Butchosa, C.; Guiglion, P.; Zwijnenburg, M. A. Carbon Nitride Photocatalysts for Water Splitting: A Computational Perspective. *J. Phys. Chem. C* **2014**, *118*, 24833–24842.

(11) Deifallah, M.; McMillan, P.F.; Corá, F. *J. Phys. Chem. C* **2008**, *112*, 5447–5453.

(12) Vodak, D. T.; Kim, K.; Iordanidis, L.; Rasmussen, P. G.; Matzger, A. J.; Yaghi, O. M. Computation of Aromatic C_3N_4 Networks and Synthesis of the Molecular Precursor $N(C_3N_3)_3Cl_6$. *Chem. Eur. J*. **2003**, *9*, 4197–4201.

(13) Bersuker, I. B. Pseudo-Jahn−Teller Effect−A Two-State Paradigm in Formation, Deformation, and Transformation of Molecular Systems and Solids. *Chem. Rev*. **2013**, *113*, 1351–1390.

(14) Yarkony, D. R. Nonadiabatic Derivative Couplings. In *Encyclopedia of Computational Chemistry*, 2002, 3.

(15) Azumi, T.; Matsuzak, K. What Does The Term “Vibronic Coupling” Mean? *Photochem. and Photobiol*. **1977**, *25*, 315–326.

(16) Bersuker, I. B. *The Jahn-Teller Effect*. Cambridge University Press: Cambridge, U.K., 2006.

(17) Bersuker, I. B.; Polinger, V. Z. *Vibronic Interactions in Molecules and Crystals*. Springer: New York, 1989.

(18) Bersuker, I. B.; Gorinchoi, N. N.; Polinger, V. Z. On the Origin of Dynamic Instability of Molecular Systems. *Theor. Chim. Acta* **1984**, *66*, 161–172.

(19) Bersuker, I. B. Symmetry, Instability, Stereochemistry and Phase Transitions in Coordination Compounds. *Pure Appl. Chem*. **1988**, *60*, 1167–1174.

(20) Muya, J. T.; Sato, T.; Nguyen, M. T.; Ceulemans, A. Pseudo Jahn-Teller Origin of Icosahedral Instability in Boron Buckyball. *Chem. Phys. Lett*. **2012**, *543*, 111–116.

(21) Sato, T.; Uejima, M.; Iwahara, N.; Haruta, N.; Shizu, K.; Tanaka, K. Vibronic Coupling Density and Related Concepts. *J. Phys. Conf. Ser.* **2013**, *428*, 012010 1–19.

(22) Kameoka, Y.; Sato, T.; Kouyama, T.; Tanaka, K.; Kato, T. Pseudo Jahn-Teller Origin of Distortion in [6]Cycloparaphenylene. *Chem. Phys. Lett*. **2014**, *598*, 69–74.

(23) Frisch, M. J.; Trucks, G. W.; Schlegel, H. B.; Scuseria, G. E.; Robb, M. A.; Cheeseman, J. R.; Scalmani, G.; Barone, V.; Mennucci, B.; Petersson, G. A. *Gaussian 09*, Revision B.01; Gaussian, Inc.: Wallingford, CT, **2009**.

(24) Zhao, Y.; Schultz, N. E.; Truhlar, D. G. J. Design of Density Functionals by Combining the Method of Constraint Satisfaction with Parametrization for Thermochemistry, Thermochemical Kinetics, and Noncovalent Interactions. *Chem. Theory Comput*. **2006**, *2*, 364–382.

(25) Zhao, Y.; Truhlar, D. G. Density Functionals with Broad Applicability in Chemistry. *Acc. Chem. Res*. **2008**, *41*, 157–167.

(26) Becke, A. D. Density-Functional Thermochemistry. III. The Role of Exact Exchange. *J. Chem. Phys*. **1993**, *98*, 5648–5652.

(27) Xiao, H.; Tahir-Kheli, J.; Goddard III, W. A. Accurate Band Gaps for Semiconductors from Density Functional Theory. *J. Phys. Chem. Lett*. **2011**, *2*, 212–217.

(28) Hariharan, P. C.; Pople, J. A. Influence of Polarization Functions on MO Hydrogenation Energies. *Theor. Chim. Acta* **1973**, *28*, 213–222.

(29) Dunning, T. H. Gaussian Basis Sets for Use in Correlated Molecular Calculations. I. The Atoms Boron through Neon and Hydrogen. *J. Chem. Phys*. **1989**, *90*, 1007–1023.

(30) Balabanov, N. B.; Peterson, K. A. Systematically Convergent Basis Sets for Transition Metals. I. All-Electron Correlation Consistent Basis Sets for the 3d Elements Sc-Zn. *J. Chem. Phys.* **2005**, *123*, 064107 1–15.

(31) Kresse, G.; Furthmuller, J. Efficient Iterative Schemes for Ab Initio Total-Energy Calculations Using a Plane-Wave Basis Set. *Phys. Rev. B* **1996**, *54*, 11169–11186.

(32) Perdew, J. P.; Burke, K.; Ernzerhof, M. Generalized Gradient Approximation Made Simple. *Phys. Rev. Lett*. **1996**, *77*, 3865–3868.

(33) Heyd, J.; Scuseria, G. E.; Ernzerhof, M. J. Hybrid Functionals Based on a Screened Coulomb Potential. *Chem. Phys*. **2003**, *118*, 8207–8215.

(34) Monkhorst, H. J.; Pack, J. D. Special Points for Brillouin-Zone Integrations. *Phys. Rev. B* **1976**, *13*, 5188–5192.

(35) Zubarev, D. Y.; Boldyrev, A. I. Developing Paradigms of Chemical Bonding: Adaptive Natural Density Partitioning. *Phys. Chem. Chem. Phys*. **2008**, *10*, 5207–5217.

(36) Ivanov, A. S.; Boldyrev, A. I. Deciphering Aromaticity in Porphyrinoids via Adaptive Natural Density Partitioning. *Org. Biomol. Chem*. **2014**, *12*, 6145–6150.

(37) Ivanov, A. S.; Boldyrev, A. I. $Si_{6-n}C_nH_6$ (n = 0-6) Series: When Do Silabenzenes Become Planar and Global Minima? *J. Phys. Chem. A* **2012**, *116*, 9591–9598.

(38) Ivanov, A. S.; Bozhenko, K. V.; Boldyrev, A. I. Peculiar Transformations in the $C_xH_xP_{4-x}$ (x = 0-4) Series. *J. Chem. Theory and Comput*. **2011**, *8*, 135–140.

(39) Galeev, T. R.; Ivanov, A. S.; Romanescu, C.; Li, W.-L.; Bozhenko, K. V.; Wang, L.-S.; Boldyrev, A. I. Molecular Wheel to Monocyclic Ring Transition in Boron-Carbon Mixed Clusters $C_2B_6^-$ and $C_3B_5^-$. *Phys. Chem. Chem. Phys*. **2011**, *13*, 8805–8810.

(40) Galeev, T. R.; Dunnington, B. D.; Schmidt, J. R.; Boldyrev, A. I. Solid State Adaptive Natural Density Partitioning: A Tool for Deciphering Multi-Center Bonding in Periodic Systems. *Phys. Chem. Chem. Phys*. **2013**, *15*, 5022–5029.

(41) Foster, J. P.; Weinhold, F. Natural Hybrid Orbitals. *J. Am. Chem. Soc.* **1980**, *102*, 7211–7218.

(42) Weinhold, F.; Landis, C. R. *Valency and Bonding, a Natural Bond Orbital Donor–Acceptor Perspective*. Cambridge University Press: Cambridge, 2005.

(43) Dunnington, B. D.; Schmidt, J. R. Generalization of Natural Bond Orbital Analysis to Periodic Systems: Applications to Solids and Surfaces via Plane-Wave Density Functional Theory. *J. Chem. Theory Comput*. **2012**, *8*, 1902–1911.

(44) Momma, K.; Izumi, F. VESTA 3 for Three-Dimensional Visualization of Crystal, Volumetric and Morphology Data. *J. Appl. Crystal*. **2011**, *44*, 1272–1276.

(45) Varetto, U. Molekel 5.4.0.8, Swiss National Supercomputing Centre, Manno (Switzerland).

(46) Bersuker, I. B.; Gorinchoi, N. N.; Polinger, V. Z. On the Origin of Dynamic Instability of Molecular Systems. *Theor. Chim. Acta*. **1984**, *66*, 161–172.

(47) Hess, B. A. Jr.; Schaad, L. J. Hueckel Molecular Orbital π Resonance Energies. Benzenoid Hydrocarbons. *J. Am. Chem. Soc*. **1971**, *93*, 2413–2416.

(48) Bredas, J.-L. Mind the gap! *Mater. Horiz*., **2014**, *1*, 17–19.

(49) Zhang, G.; Musgrave, C. B. Comparison of DFT Methods for Molecular Orbital Eigenvalue Calculations. *J. Phys. Chem. A* **2007**, *111*, 1554–1561.

(50) Gao, X.; Zhou, Z.; Zhao, Y.; Nagase, S.; Zhang, S. B.; Chen, Z. Comparative Study of Carbon and BN Nanographenes: Ground Electronic States and Energy Gap Engineering. *J. Phys. Chem. C* **2008**, *112*, 12677–12682.

(51) Jose, D.; Datta, A. Structures and Electronic Properties of Silicene Clusters: A Promising Material for FET and Hydrogen Storage. *Phys. Chem. Chem. Phys*. **2011**, *13*, 7304–7311.

(52) Bersuker, I. B.; Stavrov, S. S. Structure and Properties of Metalloporphyrins and Hemoproteins: The Vibronic Approach. *Coord. Chem. Rev*. **1988**, *8*, 1–68.

(53) Sergeeva, A. P.; Boldyrev, A. I. Flattering a Puckered Pentasilacyclopentadienide Ring by Suppression of the Psudo Jahn-Teller Effect. *Organometallics* **2010**, *29*, 3951–3954.

(54) Pokhodnya, K.; Olson, C.; Dai, X.; Schulz, D. L.; Boudjouk, P.; Sergeeva, A. P.; Boldyrev, A. I. Flattening a Puckered Cyclohexasilane Ring by Suppression of the Pseudo-Jahn-Teller Effect. *J. Chem. Phys*. **2011**, *134*, 014105 1–5.

(55) Ivanov, A. S.; Bozhenko, K. V.; Boldyrev, A. I. On the Suppression Mechanism of the Pseudo Jahn-Teller Effect in Middle E_6 (E=P, As, Sb) Rings of Triple-Decker Sandwich Complexes. *Inorg. Chem*. **2012**, *8*, 8868–8874.

(56) Jose, D.; Datta, A. Understanding of the Buckling Distortions in Silicene. *J. Phys. Chem. C* **2012**, *116*, 24639–24648.

(57) Zhu, G.; Lü, K.; Sun, Q.; Kawazoe, Y.; Jena P. Lithium-Doped Triazine-Based Graphitic C_3N_4 Sheet for Hydrogen Storage at Ambient Temperature. *Comput. Mat. Scie*. **2014**, *81*, 275–279.

(58) Wirnhier, E.; Döblinger, M.; Gunzelmann, D.; Senker, J.; Lotsch, B. V.; Schnick, W. Poly(triazine imide) with Intercalation of Lithium and Chloride Ions $[(C_3N_3)_2(NH_xLi_{1-x})_3 \cdot LiCl]$: A Crystalline 2D Carbon Nitride Network. *Chem. Eur. J*. **2011**, *17*, 3213–3221.

Table 13-1. The calculated orbital energy gap $\varepsilon_j - \varepsilon_i$, orbital vibronic coupling constants (OVCCs) of the e" mode $f_{e"}^{(i,j)}$, and OVCC over orbital energy gap $k_{e"}^{(i,j)}$ between occupied valence orbital *i* and unoccupied orbital *j*. Only the orbital pairs with large $k_{e"}^{(i,j)}$ are tabulated.

i (irrep.)	*j* (irrep.)	$\varepsilon_j - \varepsilon_i$ (a.u.)	$f_{e"}^{(i,j)}$ ($\times 10^{-3}$ a.u.)	$k_{e"}^{(i,j)}$ ($\times 10^{-5}$ a.u.)
55 (a_1')	74 (e'')	0.5046	-2.2131	0.9707
58 (e')	76 (a_2'')	0.4782	-2.1448	0.9620
72 (e')	81 (a_2'')	0.4906	1.9285	0.7581
⋮	⋮	⋮	⋮	⋮
71 (e')	73 (a_1'')	0.2692	-0.1181	0.0052

Table 13-2. The energy difference (ΔE) between planar and corrugated structures, HOMO-LUMO gaps, largest frequency of buckling, and root-mean square displacement of atomic coordinates (R), necessary to achieve a planar configuration. All the values are given at M05-2X/6-31+G(d,p), B3PW91/6-31+G(d,p) (in brackets), and TD-B3PW91/6-31+G(d,p) (in curly brackets).

Clusters	$\Delta E = E_{planar} - E_{corrugated}$ (kcal/mol)	HOMO-LUMO gap (eV)	Frequency of buckling (cm^{-1})	R values (Å)
T3G ($C_9N_{12}H_6$)	7.41 [6.86]	7.83 [4.93] {3.95}	-148.38 [-147.65]	0.72 [0.69]
T6G ($C_{18}N_{25}H_9$)	34.53 [33.34]	7.42 [4.64] {3.86}	-256.36 [-253.79]	0.86 [0.82]
T10G ($C_{30}N_{42}H_{12}$)	67.73 [69.28]	7.27 [4.54] {3.74}	-213.76 [214.53]	0.85 [0.82]
T15G ($C_{45}N_{63}H_{15}$)	114.64 [111.22]	7.19 [4.47] {3.70}	-217.64 [-224.27]	0.91 [0.89]

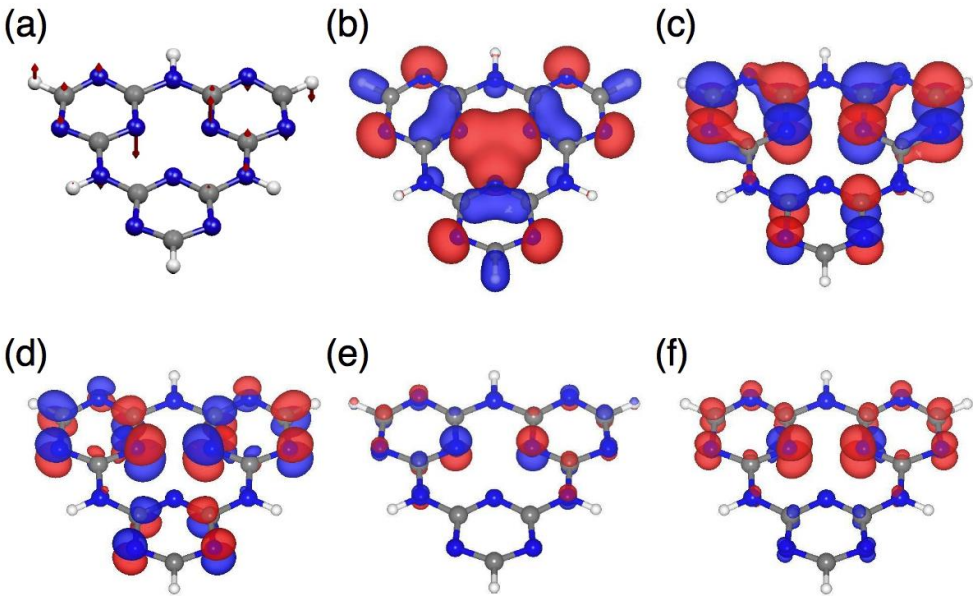

Figure 13-1. (a) Vibrational vector for the PJT e_g'' mode of planar T3G cluster, (b) 55th MO, (c) next LUMO (74th), (d) overlap between MO(55) and MO(74), (e) potential derivative for the PJT e_g'' mode, and (f) orbital vibronic coupling density (OVCD). The isovalues are 3×10^{-2} a.u. for (b) and (c), 1×10^{-3} a.u. for (d), 1×10^{-2} a.u. for (e), and 1×10^{-5} a.u. for (f).

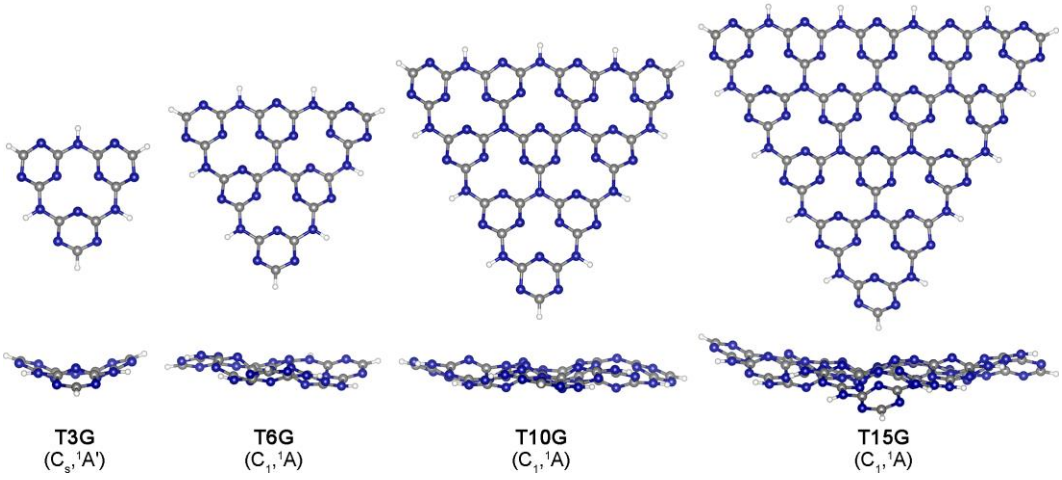

Figure 13-2. Structures of graphitic triazine-based clusters, their point group symmetries, and spectroscopic states. Here and elsewhere the gray, blue, and white spheres represent carbon, nitrogen, and hydrogen atoms, respectively.

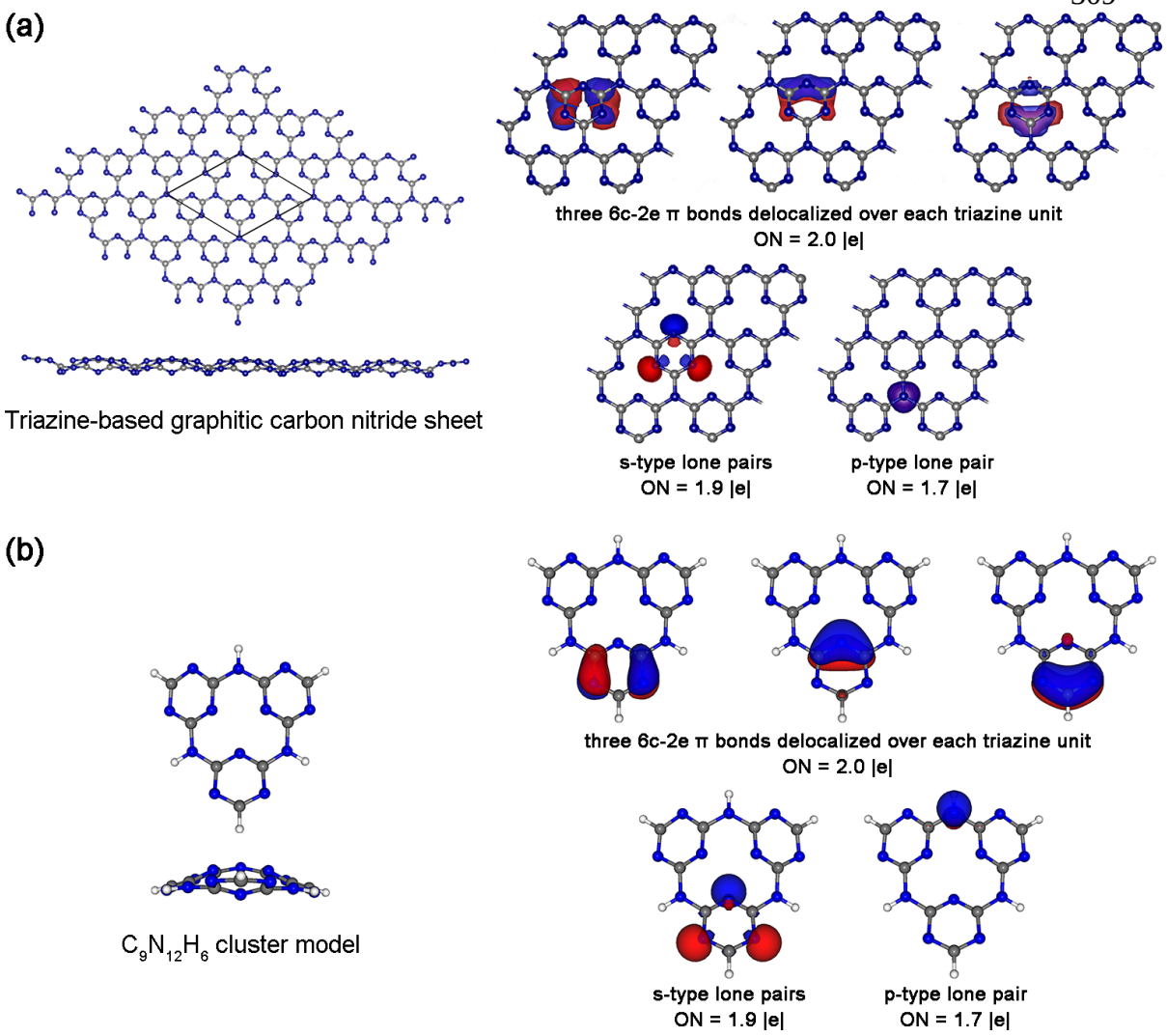

Figure 13-3. (a) Structure and SSAdNDP chemical bonding pattern for *TGCN* sheet, (b) structure and AdNDP chemical bonding pattern for T3G cluster model. ON stands for occupation numbers. The isovalues are 8×10^{-3} a.u.

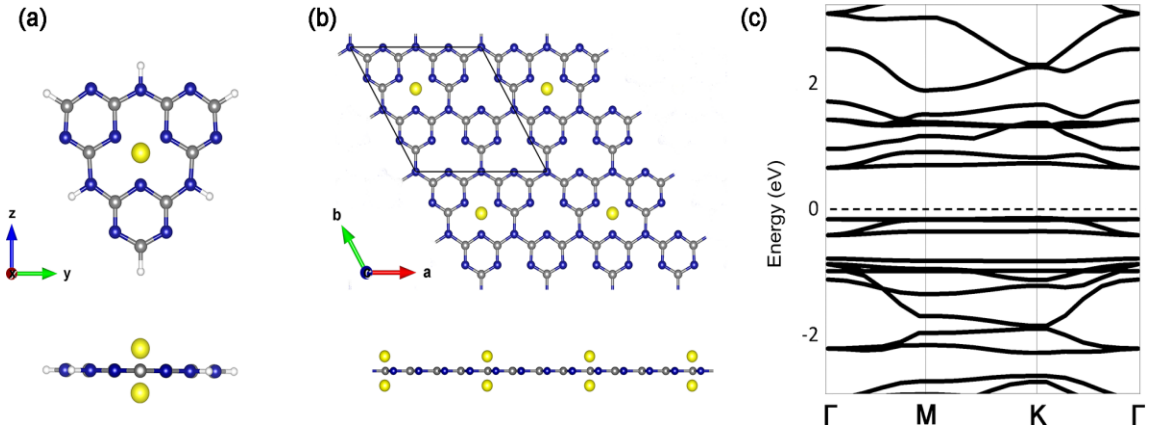

Figure 13-4. (a) Top and side views of optimized T3G ⋯ $2Be^{2+}$ complex, (b) top and side views of optimized Be^{2+} decorated *TGCN* sheet, (c) its band structure.

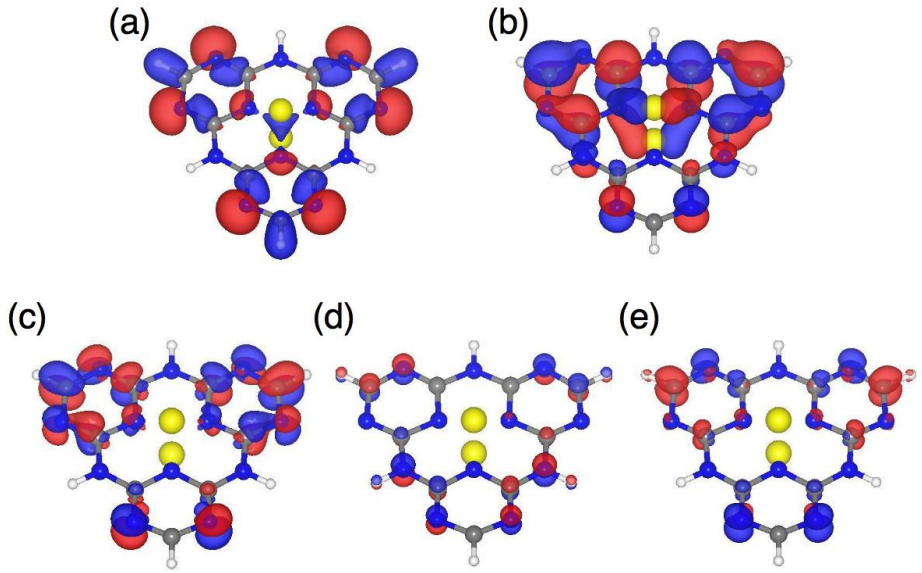

Figure 13-5. (a) 67th MO, (b) next LUMO (76th), (c) overlap between MO(67) and MO(76), (d) potential derivative for the e_g'' mode, and (e) orbital vibronic coupling density (OVCD). The isovalues are 3×10^{-2} a.u. for (a) and (b), 1×10^{-3} a.u. for (c), 1×10^{-2} a.u. for (d), and 1×10^{-5} a.u. for (e).

CHAPTER 14

SUMMARY

Design and prediction of novel unusual molecules and materials have always been a dream for chemists. Nowadays, this dream came true. The great progress in computer technology – together with the advancements of the quantum chemical theory and the corresponding software – provided for the first time in history an opportunity to predict new molecules, clusters, and solids before experimentalists can observe or synthesize them. For now reliable predictions can be made primarily for relatively small (up to 20–30 atoms) molecular systems. However, recent advances in the solid-state quantum chemistry opened the door into the design of new solid-state materials, showing the applicability of quantum chemical theory in modern nanotechnology.[1]

Initially, experimentalists were rather skeptical about the usefulness of theoretical calculations in chemistry. For instance, theoretical predictions[2,3] of famous buckyball molecules[4] in the late 1960s went completely unnoticed and ignored by the scientific community. Another example is that there was a time when experimental spectroscopy chemists were dealing only with the development of methods for obtaining the spectra of molecular systems without any interpretation of their spectral features. But today the vast majority of papers report joint experimental and theoretical results. It is well established that using electronic structure calculations, one can obtain a full picture of the properties of a polyatomic system and even predict the existence and stability of yet unknown chemical systems. Therefore, theoretical chemistry is now firmly moving from being just an instrument for explaining experimental results towards being a reliable tool for exploring new, yet unknown molecules, clusters, nanostructures and materials.

This dissertation presented the results on the successfully predicted and already produced (in some cases) unusual molecules, clusters, nanoparticles, and solids. A common thread through all of the research projects included in the thesis has been an attempt to rationalize size- and composition-dependent properties of the species based on understanding of their electronic structure and chemical bonding. The detailed achievements from this dissertation are summarized as the followings.

As it was stated in the introduction, clusters are very exotic species being generated in a molecular beam for a short period of time. However, such systems possess unique electronic structure and chemical bonding. Additionally, they were found exceptionally promising catalysts due to many electronic and structural characteristics.[5] The joint experimental and theoretical investigations of two anionic boron-carbon mixed $C_2B_6^-$ and $C_3B_5^-$ clusters has led to the conclusion that a novel type of structural transition occurs in the series of $C_xB_{8-x}^-$ (x = 1–8) species upon increase of the carbon content from x = 2 to x = 3.[6] A thorough analysis of chemical bonding in this type of clusters identified that strong covalent 2c-2e σ bonds between C and B atoms play a crucial role in the carbon atoms' preference for peripheral positions in the cyclic structures. The established wheel to ring structural transition can be explained by the fact that carbon atoms tend to increase stabilizing electrostatic field at the center of the cluster, which makes the presence of the central boron atom unnecessary.

Another joint experimental and theoretical study[7] elucidated the growth of small tantalum doped boron clusters leading to the formation of the highest coordination $Ta©B_{10}^-$ molecular wheel,[8] which has attracted considerable public attention[9] owing to its high symmetry and the record high coordination number in planar species. It was

shown that TaB_3^-, TaB_4^-, and TaB_5^- clusters adopt peculiar fan-like global minimum structures. However, boron atoms do not nucleate smoothly around a Ta atom on the way to the decacoordinated $Ta©B_{10}^-$ molecular wheel, since TaB_6^- global minimum represents a hexagonal structure with a boron atom in the center and the Ta atom being on the periphery. The chemical bonding analysis confirmed that the competition between B–B interactions and Ta–B interactions play an important role in determination of the most energetically stable isomers of the TaB_n^- (n = 3–8) clusters.

Collaboration with photoelectron spectroscopy experimentalists requires a good theoretical description of their spectra. Although the calculations of vertical electron detachment energies (VDE) of clusters were performed in the Prof. Boldyrev group, there were no theoretical tools capable of assessing the intensities of peaks in photoelectron spectra. According to the results of our experimental collaborators,[10-12] the produced spectra usually contain vibrational progression with different intensities of spectral lines. The developed program is able to calculate the so-called Franck-Condon factors to make the appropriate assessment of intensities in the vibrational progression of the spectra. It is expected that this tool would aid in the spectral assignments and also can be used as a second test (after VDE) for the accuracy in establishing the global minimum structures of clusters produced in a molecular beam.

The rest of the research projects in this dissertation were purely theoretical. However, the results of such theoretical investigations can serve as a guide for further experimental studies of the predicted species.

The dichloride $Cl^–Cl^-$ - water species were first molecular clusters studied in this dissertation. Despite the confirmation of $Cl^–Cl^-$ association in aqueous solution and

crystalline state,[13] the existence of stable dichloride anion pair in the gas phase was questioned. This dissertation described *ab initio* study of microsolvation of dichloride anion pair in the gas phase. It was shown that stabilization of the Cl^{-}–Cl^{-} pair by waters leads to the formation of cyclic H_2O structures that bridge the Cl^{-} ions.[14] It has also been predicted that the complete stabilization of gaseous Cl^{-}–Cl^{-} may likely be achieved at 36 water molecules, and the large clusters of $[Cl_2(H_2O)_{36}]^{2-}$ and $[Cl_2(H_2O)_{40}]^{2-}$ are expected to exhibit properties analogous to bulk aqueous solutions. Overall, this work could help chemical engineers and geochemists to understand processes of Cl^{-}–Cl^{-} solvation in the bulk.[15]

The "electronic transmutation principle" postulated in the Prof. Boldyrev group[16] can be a powerful tool for predicting new clusters and molecules. This principle assumes that elements, by acquiring an extra electron, begin to have the chemical bonding and geometric structure properties of compounds composed of neighboring elements.[16] In this dissertation the electronic transmutation was applied to find species analogous to ozone molecule. The predicted Li_3N_3 cluster with a novel N_3^{3-} molecular motif, which is structurally similar to O_3 molecule, represents a viable species and thus might be experimentally produced.[17] However, any attempts to find crown-like Li_5P_5, Li_6P_6, Li_7P_7, Li_8P_8, and Li_9P_9 species analogous to small sulfur clusters[18] have failed. Instead, the double helix structures were surprisingly confirmed to be the global minima for Li_7P_7-Li_9P_9 stoichiometries.[19] A detailed analysis of chemical bonding in these clusters revealed that the more ionic the bond between lithium and phosphorous, the more likely are the helical structures to form. It was found that the double helical nanoparticles can exist as an infinite double helical chain composed of Li and P ions and also can be packed

together in two crystals, one having adjacent helices with the same orientation and another with helices in opposite orientation. Another interesting discovery is that LiP species may form $Li_{90}P_{90}$ nanotoroid with internal diameter of 2.56 nanometers.[20] The findings of such simplest inorganic double helices can expand our knowledge of these compounds and have implications for future nanotechnology applications.[21]

Thorough analysis of chemical bonding can be useful in the rational design of new compounds. Adaptive Natural Density Partitioning (AdNDP) method[22,23] was applied to porphyrinoids to describe their aromaticity.[24] The analysis revealed that the appended 6π aromatic sextets together with the 6π aromatic core molecular fragment of porphyrin confer aromaticity much more efficiently than the well-known "bridged [18]annulene" model[25] It was also shown that annulene, dideazaporphyrin, porphyrin, and dihydrodideazaporphyrin molecules can be represented using novel and unique compact graphic formulas, which comply with chemical intuition and provide a new look at the diverse chemistry of porphyrinoids. Another study was devoted to the analysis of chemical bonding in hypervalent iodine compounds.[26] The AdNDP approach for the analyses of the molecular orbital wave functions of the compounds containing I–X (X = O,N,C) bonds revealed only single I–⟶X dative-bond character, as opposed to the widely used I=X double bond notion. This discovery may be useful when it comes to understanding reaction mechanisms, and suggests the textbooks may need correcting.[27]

Jahn-Teller (JT) and pseudo Jahn-Teller (PJT) effects[28] are the main sources of instability of highly symmetric and planar ring structures. A systematic computational study of $Si_{6-n}C_nH_6$ (n = 0–6) molecules showed the pseudo Jahn-Teller effect, which is responsible for the deformation of planar Si_6H_6, Si_5CH_6, and $Si_4C_2H_6$ structures, is

suppressed at n = 3 (the planar structure of 1,3,5-trisilabenzene).[29] However, the planar cyclic global minimum structure can only be achieved at n = 5 owing to aromaticity and strong C–C σ bonds at the periphery of monosilabenzene SiC_5H_6 molecule. Occupied and unoccupied molecular orbitals responsible for the distortions from planarity were identified for each species according to their symmetry requirements. It was also found that the isolobal substitution of the Si atoms by the C atoms increases the energy gaps between the interacting orbitals leading to complete suppression of the PJT effect. The second way to quench the PJT effect was shown on an example of $\{(\eta^5\text{-}Me_5C_5)Mo\}_2(\mu,\eta^6\text{-}P_6)$ triple-decker sandwich complex.[30] The P_6 ring which is not planar in the gas phase due to the PJT effect becomes planar upon complexation. It was proposed that the PJT effect in P_6 is suppressed by filling the intervenient molecular orbitals with electron pairs of Mo atoms. The observation and subsequent manipulation of the PJT effect is not limited to isolated molecules and clusters. It was demonstrated that the PJT effect is also responsible for buckling distortions in the recently synthesized triazine-based graphitic carbon nitride (TGCN) material.[31] Occupied and unoccupied molecular orbital pair, which has the largest impact on the instability of TGCN planar configuration, was determined based on the orbital vibronic coupling density analysis.[32] The PJT effect can be completely suppressed by doping TGCN with Be^{2+} ions. It was found that the PJT effect in this case is essentially quenched by lowering orbital vibronic coupling constant values, though the energy gap between the interacting orbitals pair is small. Hence, lowering values of orbital vibronic coupling constant can be viewed as a novel mechanism for the vanishing of the PJT instability. In summary, this work demonstrated that understanding the PJT effect can be a general and powerful tool for

rationalizing the origin of molecular and solid state structures which is a first step to more specific prediction of new materials with tailored properties.

References

(1) Ivanov, A. S.; Boldyrev, A. I. *Phys. Chem. Chem. Phys*. **2012**, *14*, 15943–15952.

(2) Bochvar, D. A.; Gal'pern, E. G. *Dokl. Akad. Nauk SSSR* **1973**, *209*, 610.

(3) Osawa, E. *Kagaku (Kyoto)* **1970**, *25*, 854.

(4) Kroto, H. W.; Heath, J. R.; Obrien, S. C.; Curl, R. F.; Smalley, R. E. *Nature* **1985**, *318*, 162–163.

(5) Gates, B. C. *Chem. Rev*. **1995**, *95*, 511–522.

(6) Galeev, T. R.; Ivanov, A. S.; Romanescu, C.; Li, W.-L.; Bozhenko, K. V.; Wang, L.-S.; Boldyrev, A. I. *Phys. Chem. Chem. Phys*. **2011**, *13*, 8805–8810.

(7) Li, W.-L.; Ivanov, A. S.; Federic, J.; Romanescu, C.; Cernusak, I.; Boldyrev, A. I.; Wang, L.-S. *J. Chem. Phys*. **2013**, *139*, 104312.

(8) Galeev, T. R.; Romanescu, C.; Li, W.-L.; Wang, L.-S.; Boldyrev, A. I. *Angew. Chem. Int. Ed.* **2012**, *51*, 2101–2105.

(9) a) Heine, T.; Merino, G. *Angew. Chem. Int. Ed.* **2012**, *51*, 4275–4276; b) Ritter, S. K. C&EN, 2012, 90, 38; c) Bradley, D. Chemistry World, Feb. 6, 2012.

(10) Zhai, H.-J.; Wang, L.-S.; Alexandrova, A. N.; Boldyrev, A. I.; Zakrzewski, V. G. *J. Phys. Chem. A* **2003**, *107*, 9319.

(11) Zhai, H.-J.; Wang, L.-S.; Alexandrova, A. N.; Boldyrev, A. I. *J. Chem. Phys. A*, **2002**, *117*, 7917.

(12) Alexandrova, A. N.; Boldyrev, A. I.; Zhai, H.-J.; Wang, L.-S.; Steiner, E.; Fowler, P. W. *J. Phys. Chem. A* **2003**, *107*, 1359.

(13) Gao, J.; Boudon, S.; Wipff, G. *J. Am. Chem. Soc.* **1991**, *113*, 9610–9614.

(14) Ivanov, A. S.; Frenking, G.; Boldyrev, A. I. *J. Phys. Chem. A* **2014**, *118*, 7375–7384.

(15) Bradley, D. Chemistry Views, March 4, 2014, DOI: 10.1002/chemv.201400016.

(16) Olson, J. K.; Boldyrev, A. I. *Chem. Phys. Lett.* **2012**, *523*, 83–86.

(17) Olson, J. K.; Ivanov, A. S.; Boldyrev, A. I. *Chem. Eur. J.* **2014** , *20*, 6636–6640.

(18) Meyer, B. *Chem. Rev*. **1976**, *76*, 367−388.

(19) Ivanov, A. S.; Morris, A. J.; Bozhenko, K. V.; Pickard, C. J.; Boldyrev, A. I. *Angew. Chem. Int. Ed.* **2012**, *51*, 8330−8333.

(20) Ivanov, A. S.; Boldyrev, A. I.; Frenking, G. *Chem. Eur. J.* **2014**, *20*, 2431−2435.

(21) a) Ritter, S. K. C&EN, 2012, 90, 33; b) Torrisi, A. Thomas Young Center, Aug. 15, 2012.

(22) Zubarev, D. Yu. Analysis of Chemical Bonding in Clusters by Means of the Adaptive Natural Density Partitioning. PhD Dissertation, Utah State University: Logan, UT, 2008.

(23) Zubarev, D. Y.; Boldyrev, A. I. *Phys. Chem. Chem. Phys*. **2008**, *10*, 5207–5217.

(24) Ivanov, A. S.; Boldyrev, A. I. *Org. Biomol. Chem*. **2014**, *12*, 6145–6150.

(25) Sondheimer, F.; Wolovsky, R.; Amiel, Y. *J. Am. Chem. Soc.* **1962**, *84*, 274.

(26) Ivanov, A. S.; Popov, I. A.; Boldyrev, A. I.; Zhdankin, V. V. *Angew. Chem. Int. Ed*. **2014**, *53*, 9617–9621.

(27) Stoye, E. Chemistry World, July 11, 2014

(28) Bersuker, I. B. *Chem. Rev*. **2013**, *113*, 1351–1390.

(29) Ivanov, A. S.; Boldyrev, A. I. *J. Phys. Chem. A* **2012**, *116*, 9591–9598.

(30) Ivanov, A. S.; Bozhenko, K. V.; Boldyrev, A. I. *Inorg. Chem*. **2012**, *8*, 8868–8872.

(31) Algara-Siller, G.; Severin, N.; Chong, S. Y.; Björkman, T.; Palgrave, R. G.; Laybourn, A.; Antonietti, M.; Khimyak, Y. Z.; Krasheninnikov, A. V.; Rabe, J. P.; et al. *Angew. Chem. Int. Ed.* **2014**, *53*, 7450–7455.

(32) Ivanov, A. S.; Miller, E. D.; Boldyrev, A. I.; Kameoka, Y.; Sato, T.; Tanaka, K. *J. Phys. Chem. C* **2015**

APPENDIX

COPYRIGHT PERMISSIONS

Molecular wheel to monocyclic ring transition in boron–carbon mixed clusters $C_2B_6^-$ and $C_3B_5^-$

T. R. Galeev, A. S. Ivanov, C. Romanescu, W. Li, K. V. Bozhenko, L. Wang and A. I. Boldyrev, *Phys. Chem. Chem. Phys.*, 2011, **13**, 8805
DOI: 10.1039/C1CP20359B

RSC

- For reproduction of material from all other RSC journals:
  [Original citation] - Reproduced by permission of The Royal Society of Chemistry

If you are the author of this article you still need to obtain permission to reproduce the whole article in a third party publication with the exception of reproduction of the whole article in a thesis or dissertation.

Information about reproducing material from RSC articles with different licences is available on our Permission Requests page.

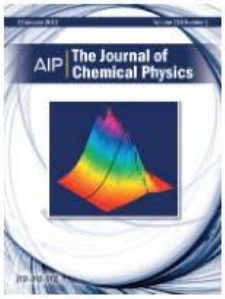

Title: On the way to the highest coordination number in the planar metal-centred aromatic Ta©B10− cluster: Evolution of the structures of TaBn− (n = 3–8)

Author: Wei-Li Li,Alexander S. Ivanov,Jozef Federič, et al.

Publication: Journal of Chemical Physics

Volume/Issue 139/10

Publisher: AIP Publishing LLC

Date: Sep 12, 2013

Page Count: 13

Order Completed

Thank you very much for your order.

Click here for Payment Terms and Conditions.

Get a printable version for your records.

License Number	3611120655338
Order Date	Apr 16, 2015
Publisher	AIP Publishing LLC
Publication	Journal of Chemical Physics
Article Title	On the way to the highest coordination number in the planar metal-centred aromatic Ta©B10− cluster: Evolution of the structures of TaBn− (n = 3–8)
Author	Wei-Li Li,Alexander S. Ivanov,Jozef Federič, et al.
Online Publication Date	Sep 12, 2013
Volume number	139
Issue number	10
Type of Use	Thesis/Dissertation
Requestor type	Author (original article)
Format	Print and electronic
Portion	Excerpt (> 800 words)
Will you be translating?	No
Title of your thesis / dissertation	COMPUTATIONAL PREDICTION AND RATIONAL DESIGN OF NOVEL MOLECULES, CLUSTERS, AND SOLID STATE MATERIALS FOR ENERGY RELATED APPLICATIONS
Expected completion date	Jun 2015
Estimated size (number of pages)	300
Total	0.00 USD

ORDER MORE... CLOSE WINDOW

RightsLink®

Home | Account Info | Help | Live Chat

Title:	Stabilization of a Cl−−Cl− Anion Pair in the Gas Phase: Ab Initio Microsolvation Study	Logged in as: Alexander Ivanov
Author:	Alexander S. Ivanov, Gernot Frenking, Alexander I. Boldyrev	LOGOUT
Publication:	The Journal of Physical Chemistry A	
Publisher:	American Chemical Society	
Date:	Sep 1, 2014	

PERMISSION/LICENSE IS GRANTED FOR YOUR ORDER AT NO CHARGE

This type of permission/license, instead of the standard Terms & Conditions, is sent to you because no fee is being charged for your order. Please note the following:

- Permission is granted for your request in both print and electronic formats, and translations.
- If figures and/or tables were requested, they may be adapted or used in part.
- Please print this page for your records and send a copy of it to your publisher/graduate school.
- Appropriate credit for the requested material should be given as follows: "Reprinted (adapted) with permission from (COMPLETE REFERENCE CITATION). Copyright (YEAR) American Chemical Society." Insert appropriate information in place of the capitalized words.
- One-time permission is granted only for the use specified in your request. No additional uses are granted (such as derivative works or other editions). For any other uses, please submit a new request.

BACK | CLOSE WINDOW

Title:	Inorganic Double-Helix Structures of Unusually Simple Lithium–Phosphorus Species
Author:	Alexander S. Ivanov,Andrew J. Morris,Konstantin V. Bozhenko,Chris J. Pickard,Alexander I. Boldyrev
Publication:	Angewandte Chemie International Edition
Publisher:	John Wiley and Sons
Date:	Jul 23, 2012

Order Completed

Thank you for your order.

This Agreement between Alexander S. Ivanov ("You") and John Wiley and Sons ("John Wiley and Sons") consists of your license details and the terms and conditions provided by John Wiley and Sons and Copyright Clearance Center.

Your confirmation email will contain your order number for future reference.

Get the printable license.

License Number	3611120904072
License date	Apr 16, 2015
Licensed Content Publisher	John Wiley and Sons
Licensed Content Publication	Angewandte Chemie International Edition
Licensed Content Title	Inorganic Double-Helix Structures of Unusually Simple Lithium–Phosphorus Species
Licensed Content Author	Alexander S. Ivanov,Andrew J. Morris,Konstantin V. Bozhenko,Chris J. Pickard,Alexander I. Boldyrev
Licensed Content Date	Jul 23, 2012
Licensed Content Pages	4
Type of use	Dissertation/Thesis
Requestor type	Author of this Wiley article
Format	Print and electronic
Portion	Full article
Will you be translating?	No
Title of your thesis / dissertation	COMPUTATIONAL PREDICTION AND RATIONAL DESIGN OF NOVEL MOLECULES, CLUSTERS, AND SOLID STATE MATERIALS FOR ENERGY RELATED APPLICATIONS
Expected completion date	Jun 2015
Expected size (number of pages)	300
Requestor Location	Alexander S. Ivanov 50 North Sarah Street PROVIDENCE, UT 84332 United States Attn: Alexander S. Ivanov
Billing Type	Invoice

JOHN WILEY AND SONS LICENSE TERMS AND CONDITIONS

Ap

This Agreement between Alexander S. Ivanov ("You") and John Wiley and Sons (Wiley and Sons") consists of your license details and the terms and conditions pro John Wiley and Sons and Copyright Clearance Center.

License Number	3611120904072
License date	Apr 16, 2015
Licensed Content Publisher	John Wiley and Sons
Licensed Content Publication	Angewandte Chemie International Edition
Licensed Content Title	Inorganic Double-Helix Structures of Unusually Simple Lit Phosphorus Species
Licensed Content Author	Alexander S. Ivanov,Andrew J. Morris,Konstantin V. Bozh J. Pickard,Alexander I. Boldyrev
Licensed Content Date	Jul 23, 2012
Pages	4
Type of use	Dissertation/Thesis
Requestor type	Author of this Wiley article
Format	Print and electronic
Portion	Full article
Will you be translating?	No
Title of your thesis / dissertation	COMPUTATIONAL PREDICTION AND RATIONAL DESIGN C MOLECULES, CLUSTERS, AND SOLID STATE MATERIALS I ENERGY RELATED APPLICATIONS
Expected completion date	Jun 2015
Expected size (number of pages)	300
Requestor Location	Alexander S. Ivanov 50 North Sarah Street PROVIDENCE, UT 84332 United States Attn: Alexander S. Ivanov
Billing Type	Invoice
Billing Address	Alexander S. Ivanov 50 North Sarah Street

Print This Page

Title:	Inorganic Double-Helix Nanotoroid of Simple Lithium □Phosphorus Species
Author:	Alexander S. Ivanov,Alexander I. Boldyrev,Gernot Frenking
Publication:	Chemistry - A European Journal
Publisher:	John Wiley and Sons
Date:	Feb 2, 2014

Order Completed

Thank you for your order.

This Agreement between Alexander S. Ivanov ("You") and John Wiley and Sons ("John Wiley and Sons") consists of your license details and the terms and conditions provided by John Wiley and Sons and Copyright Clearance Center.

Your confirmation email will contain your order number for future reference.

Get the printable license.

License Number	3611121041668
License date	Apr 16, 2015
Licensed Content Publisher	John Wiley and Sons
Licensed Content Publication	Chemistry - A European Journal
Licensed Content Title	Inorganic Double-Helix Nanotoroid of Simple Lithium□Phosphorus Species
Licensed Content Author	Alexander S. Ivanov,Alexander I. Boldyrev,Gernot Frenking
Licensed Content Date	Feb 2, 2014
Licensed Content Pages	5
Type of use	Dissertation/Thesis
Requestor type	Author of this Wiley article
Format	Print and electronic
Portion	Full article
Will you be translating?	No
Title of your thesis / dissertation	COMPUTATIONAL PREDICTION AND RATIONAL DESIGN OF NOVEL MOLECULES, CLUSTERS, AND SOLID STATE MATERIALS FOR ENERGY RELATED APPLICATIONS
Expected completion date	Jun 2015
Expected size (number of pages)	300
Requestor Location	Alexander S. Ivanov 50 North Sarah Street PROVIDENCE, UT 84332 United States Attn: Alexander S. Ivanov
Billing Type	Invoice
Billing address	Alexander S. Ivanov 50 North Sarah Street PROVIDENCE, UT 84332

JOHN WILEY AND SONS LICENSE TERMS AND CONDITIONS

Ap

This Agreement between Alexander S. Ivanov ("You") and John Wiley and Sons (Wiley and Sons") consists of your license details and the terms and conditions pro John Wiley and Sons and Copyright Clearance Center.

License Number	3611121041668
License date	Apr 16, 2015
Licensed Content Publisher	John Wiley and Sons
Licensed Content Publication	Chemistry - A European Journal
Licensed Content Title	Inorganic Double-Helix Nanotoroid of Simple Lithium□Ph Species
Licensed Content Author	Alexander S. Ivanov,Alexander I. Boldyrev,Gernot Frenki
Licensed Content Date	Feb 2, 2014
Pages	5
Type of use	Dissertation/Thesis
Requestor type	Author of this Wiley article
Format	Print and electronic
Portion	Full article
Will you be translating?	No
Title of your thesis / dissertation	COMPUTATIONAL PREDICTION AND RATIONAL DESIGN C MOLECULES, CLUSTERS, AND SOLID STATE MATERIALS I ENERGY RELATED APPLICATIONS
Expected completion date	Jun 2015
Expected size (number of pages)	300
Requestor Location	Alexander S. Ivanov 50 North Sarah Street PROVIDENCE, UT 84332 United States Attn: Alexander S. Ivanov
Billing Type	Invoice
Billing Address	Alexander S. Ivanov 50 North Sarah Street PROVIDENCE, UT 84332

Print This Page

Deciphering aromaticity in porphyrinoids *via* adaptive natural density partitioning

A. S. Ivanov and A. I. Boldyrev, *Org. Biomol. Chem.*, 2014, **12**, 6145
DOI: 10.1039/C4OB01018C

- For reproduction of material from all other RSC journals:
  [Original citation] - Reproduced by permission of The Royal Society of Chemistry

If you are the author of this article you still need to obtain permission to reproduce the whole article in a third party publication with the exception of reproduction of the whole article in a thesis or dissertation.

Information about reproducing material from RSC articles with different licences is available on our Permission Requests page.

Title: The I□X (X=O,N,C) Double Bond in Hypervalent Iodine Compounds: Is it Real?

Author: Alexander S. Ivanov,Ivan A. Popov,Alexander I. Boldyrev,Viktor V. Zhdankin

Publication: Angewandte Chemie International Edition

Publisher: John Wiley and Sons

Date: Jul 9, 2014

Order Completed

Thank you for your order.

This Agreement between Alexander S. Ivanov ("You") and John Wiley and Sons ("John Wiley and Sons") consists of your license details and the terms and conditions provided by John Wiley and Sons and Copyright Clearance Center.

Your confirmation email will contain your order number for future reference.

Get the printable license.

License Number	3611130013116
License date	Apr 16, 2015
Licensed Content Publisher	John Wiley and Sons
Licensed Content Publication	Angewandte Chemie International Edition
Licensed Content Title	The I□X (X=O,N,C) Double Bond in Hypervalent Iodine Compounds: Is it Real?
Licensed Content Author	Alexander S. Ivanov,Ivan A. Popov,Alexander I. Boldyrev,Viktor V. Zhdankin
Licensed Content Date	Jul 9, 2014
Licensed Content Pages	5
Type of use	Dissertation/Thesis
Requestor type	Author of this Wiley article
Format	Print and electronic
Portion	Full article
Will you be translating?	No
Title of your thesis / dissertation	COMPUTATIONAL PREDICTION AND RATIONAL DESIGN OF NOVEL MOLECULES, CLUSTERS, AND SOLID STATE MATERIALS FOR ENERGY RELATED APPLICATIONS
Expected completion date	Jun 2015
Expected size (number of pages)	300
Requestor Location	Alexander S. Ivanov 50 North Sarah Street PROVIDENCE, UT 84332 United States Attn: Alexander S. Ivanov
Billing Type	Invoice
Billing address	Alexander S. Ivanov 50 North Sarah Street

JOHN WILEY AND SONS LICENSE TERMS AND CONDITIONS

A

This Agreement between Alexander S. Ivanov ("You") and John Wiley and Sons (Wiley and Sons") consists of your license details and the terms and conditions pro John Wiley and Sons and Copyright Clearance Center.

License Number	3611130013116
License date	Apr 16, 2015
Licensed Content Publisher	John Wiley and Sons
Licensed Content Publication	Angewandte Chemie International Edition
Licensed Content Title	The I□X (X=O,N,C) Double Bond in Hypervalent Iodine Compounds: Is it Real?
Licensed Content Author	Alexander S. Ivanov,Ivan A. Popov,Alexander I. Boldyrev Zhdankin
Licensed Content Date	Jul 9, 2014
Pages	5
Type of use	Dissertation/Thesis
Requestor type	Author of this Wiley article
Format	Print and electronic
Portion	Full article
Will you be translating?	No
Title of your thesis / dissertation	COMPUTATIONAL PREDICTION AND RATIONAL DESIGN C MOLECULES, CLUSTERS, AND SOLID STATE MATERIALS I ENERGY RELATED APPLICATIONS
Expected completion date	Jun 2015
Expected size (number of pages)	300
Requestor Location	Alexander S. Ivanov 50 North Sarah Street PROVIDENCE, UT 84332 United States Attn: Alexander S. Ivanov
Billing Type	Invoice
Billing Address	Alexander S. Ivanov 50 North Sarah Street

Print This Page

RightsLink®

Home | Account Info | Help | Live Chat

Title: On the Suppression Mechanism of the Pseudo-Jahn–Teller Effect in Middle E6 (E = P, As, Sb) Rings of Triple-Decker Sandwich Complexes

Logged in as: Alexander Ivanov

LOGOUT

Author: Alexander S. Ivanov, Konstantin V. Bozhenko, Alexander I. Boldyrev

Publication: Inorganic Chemistry

Publisher: American Chemical Society

Date: Aug 1, 2012

PERMISSION/LICENSE IS GRANTED FOR YOUR ORDER AT NO CHARGE

This type of permission/license, instead of the standard Terms & Conditions, is sent to you because no fee is being charged for your order. Please note the following:

- Permission is granted for your request in both print and electronic formats, and translations.
- If figures and/or tables were requested, they may be adapted or used in part.
- Please print this page for your records and send a copy of it to your publisher/graduate school.
- Appropriate credit for the requested material should be given as follows: "Reprinted (adapted) with permission from (COMPLETE REFERENCE CITATION). Copyright (YEAR) American Chemical Society." Insert appropriate information in place of the capitalized words.
- One-time permission is granted only for the use specified in your request. No additional uses are granted (such as derivative works or other editions). For any other uses, please submit a new request.

BACK | CLOSE WINDOW

Title:	All-Nitrogen Analogue of Ozone: Li3N3 Species
Author:	Jared K. Olson,Alexander S. Ivanov,Alexander I. Boldyrev
Publication:	Chemistry - A European Journal
Publisher:	John Wiley and Sons
Date:	Apr 17, 2014

Order Completed

Thank you for your order.

This Agreement between Alexander S. Ivanov ("You") and John Wiley and Sons ("John Wiley and Sons") consists of your license details and the terms and conditions provided by John Wiley and Sons and Copyright Clearance Center.

Your confirmation email will contain your order number for future reference.

Get the printable license.

License Number	3611121215567
License date	Apr 16, 2015
Licensed Content Publisher	John Wiley and Sons
Licensed Content Publication	Chemistry - A European Journal
Licensed Content Title	All-Nitrogen Analogue of Ozone: Li3N3 Species
Licensed Content Author	Jared K. Olson,Alexander S. Ivanov,Alexander I. Boldyrev
Licensed Content Date	Apr 17, 2014
Licensed Content Pages	5
Type of use	Dissertation/Thesis
Requestor type	Author of this Wiley article
Format	Print and electronic
Portion	Full article
Will you be translating?	No
Title of your thesis / dissertation	COMPUTATIONAL PREDICTION AND RATIONAL DESIGN OF NOVEL MOLECULES, CLUSTERS, AND SOLID STATE MATERIALS FOR ENERGY RELATED APPLICATIONS
Expected completion date	Jun 2015
Expected size (number of pages)	300
Requestor Location	Alexander S. Ivanov 50 North Sarah Street PROVIDENCE, UT 84332 United States Attn: Alexander S. Ivanov
Billing Type	Invoice
Billing address	Alexander S. Ivanov 50 North Sarah Street PROVIDENCE, UT 84332 United States

JOHN WILEY AND SONS LICENSE TERMS AND CONDITIONS

Ap

This Agreement between Alexander S. Ivanov ("You") and John Wiley and Sons (Wiley and Sons") consists of your license details and the terms and conditions pro John Wiley and Sons and Copyright Clearance Center.

License Number	3611121215567
License date	Apr 16, 2015
Licensed Content Publisher	John Wiley and Sons
Licensed Content Publication	Chemistry - A European Journal
Licensed Content Title	All-Nitrogen Analogue of Ozone: Li3N3 Species
Licensed Content Author	Jared K. Olson,Alexander S. Ivanov,Alexander I. Boldyrev
Licensed Content Date	Apr 17, 2014
Pages	5
Type of use	Dissertation/Thesis
Requestor type	Author of this Wiley article
Format	Print and electronic
Portion	Full article
Will you be translating?	No
Title of your thesis / dissertation	COMPUTATIONAL PREDICTION AND RATIONAL DESIGN C MOLECULES, CLUSTERS, AND SOLID STATE MATERIALS I ENERGY RELATED APPLICATIONS
Expected completion date	Jun 2015
Expected size (number of pages)	300
Requestor Location	Alexander S. Ivanov 50 North Sarah Street PROVIDENCE, UT 84332 United States Attn: Alexander S. Ivanov
Billing Type	Invoice
Billing Address	Alexander S. Ivanov 50 North Sarah Street PROVIDENCE, UT 84332 United States

Print This Page

RightsLink®

Home | Account Info | Help | Live Chat

Title: Si6–nCnH6 (n = 0–6) Series: When Do Silabenzenes Become Planar and Global Minima?

Author: Alexander S. Ivanov, Alexander I. Boldyrev

Publication: The Journal of Physical Chemistry A

Publisher: American Chemical Society

Date: Sep 1, 2012

Logged in as: Alexander Ivanov

LOGOUT

PERMISSION/LICENSE IS GRANTED FOR YOUR ORDER AT NO CHARGE

This type of permission/license, instead of the standard Terms & Conditions, is sent to you because no fee is being charged for your order. Please note the following:

- Permission is granted for your request in both print and electronic formats, and translations.
- If figures and/or tables were requested, they may be adapted or used in part.
- Please print this page for your records and send a copy of it to your publisher/graduate school.
- Appropriate credit for the requested material should be given as follows: "Reprinted (adapted) with permission from (COMPLETE REFERENCE CITATION). Copyright (YEAR) American Chemical Society." Insert appropriate information in place of the capitalized words.
- One-time permission is granted only for the use specified in your request. No additional uses are granted (such as derivative works or other editions). For any other uses, please submit a new request.

BACK | CLOSE WINDOW

RightsLink®

Home | Account Info | Help | Live Chat

Title:	Pseudo Jahn-Teller Origin of Buckling Distortions in Two-Dimensional Triazine-Based Graphitic Carbon Nitride (g-C3N4) Sheets
Author:	Alexander S. Ivanov, Evan D. Miller, Alexander I. Boldyrev, et al
Publication:	The Journal of Physical Chemistry C
Publisher:	American Chemical Society
Date:	May 1, 2015

Logged in as:
Alexander Ivanov
Account #:
3000910079

LOGOUT

PERMISSION/LICENSE IS GRANTED FOR YOUR ORDER AT NO CHARGE

This type of permission/license, instead of the standard Terms & Conditions, is sent to you because no fee is being charged for your order. Please note the following:

- Permission is granted for your request in both print and electronic formats, and translations.
- If figures and/or tables were requested, they may be adapted or used in part.
- Please print this page for your records and send a copy of it to your publisher/graduate school.
- Appropriate credit for the requested material should be given as follows: "Reprinted (adapted) with permission from (COMPLETE REFERENCE CITATION). Copyright (YEAR) American Chemical Society." Insert appropriate information in place of the capitalized words.
- One-time permission is granted only for the use specified in your request. No additional uses are granted (such as derivative works or other editions). For any other uses, please submit a new request.

BACK | CLOSE WINDOW

Brown University
Department of Chemistry
324 Brook Street, Box H
Providence, Rhode Island 02912
Tel: (401) 863-3389 Fax: (401) 863-2594
E-mail: Lai-Sheng_Wang@brown.edu
http://casey.brown.edu/chemistry/research/LSWang/

Lai-Sheng Wang
Professor

March 13, 2015

Mr. Alexander S. Ivanov
Utah State University
0300 Old Main Hill
Logan, UT 84322-0300

Dear Mr. Ivanov,

This letter is to confirm that you have my permission to use the following papers in part or in full for preparation or presentation of your dissertation.

- "On the Way to the Highest Coordination Number in the Planar Metal-Centred Aromatic Ta©B_{10}^- Cluster: Evolution of the Structures of TaB_n^- (n = 3-8)" Wei-Li Li, Alexander S. Ivanov, Jozef Federic, Constantin Romanescu, Ivan Cernusak, Alexander I. Boldyrev, Lai-Sheng Wang, J. Chem. Phys, 2013, 139, 104312

- "Molecular Wheel to Monocyclic Ring Transition in Boron-Carbon Mixed Clusters $C_2B_6^-$ and $C_3B_5^-$" Timur R. Galeev, Alexander S. Ivanov, Constantin Romanescu, Wei-Li Li, Konstantin V. Bozhenko, Lai-Sheng Wang and Alexander I. Boldyrev, Phys. Chem. Chem. Phys., 2011, 13, 8805-8810

Sincerely,

Lai-Sheng Wang

Alexander S. Ivanov
Utah State University
0300 Old Main Hill
Logan, UT 84322-0300

NAME DATE
ORGANIZATION
ADDRESS
CITY, STATE, ZIP CODE

Dear Alexander S. Ivanov,

This letter is to confirm that you have my permission to use the following papers in part or in full for preparation or presentation of your dissertation.

-"Molecular Wheel to Monocyclic Ring Transition in Boron-Carbon Mixed Clusters $C_2B_6^-$ and $C_3B_5^-$" Timur R. Galeev, Alexander S. Ivanov, Constantin Romanescu, Wei-Li Li, Konstantin V. Bozhenko, Lai-Sheng Wang and Alexander I. Boldyrev, Phys. Chem. Chem. Phys., 2011, 13, 8805-8810

-"Peculiar Transformations in the $C_xH_xP_{4-x}$ (x = 0-4) Series" Alexander S. Ivanov, Konstantin V. Bozhenko, and Alexander I. Boldyrev, J. Chem. Theory and Comput., 2011, 8(1), 135-140

-"Inorganic Double-Helix Structures of Unusually Simple Li-P Species" Alexander S. Ivanov, Andrew J. Morris, Konstantin V. Bozhenko, Chris J. Pickard, Alexander I. Boldyrev, Angew. Chem. Int. Ed., 2012, 51, 33, 8330-8333

-"On the Suppression Mechanism of the Pseudo-Jahn-Teller Effect in Middle E_6 (E=P, As, Sb) Rings of Triple-Decker Sandwich Complexes" Alexander S. Ivanov, Konstantin V. Bozhenko and Alexander I. Boldyrev, Inorganic Chemistry, 2012, 8(1), 8868-8872

Sincerely,

Prof. Konstantin V. Bozhenko K Bozhenko

Constantin Romanescu
217-11 Dervock Cres.
Toronto, ON M2K 1A6
Canada

March 29, 2015

Dear Mr. Alexander Ivanov,

This letter is to confirm that you have my permission to use the following papers in part or in full for preparation or presentation of your dissertation.

- "On the Way to the Highest Coordination Number in the Planar Metal-Centred Aromatic Ta©B_{10}^- Cluster: Evolution of the Structures of TaB_n^- (n = 3-8)" Wei-Li Li, Alexander S. Ivanov, Jozef Federic, Constantin Romanescu, Ivan Cernusak, Alexander I. Boldyrev, Lai-Sheng Wang, J. Chem. Phys, 2013, 139, 104312

- "Molecular Wheel to Monocyclic Ring Transition in Boron-Carbon Mixed Clusters $C_2B_6^-$ and $C_3B_5^-$" Timur R. Galeev, Alexander S. Ivanov, Constantin Romanescu, Wei-Li Li, Konstantin V. Bozhenko, Lai-Sheng Wang and Alexander I. Boldyrev, Phys. Chem. Chem. Phys., 2011, 13, 8805-8810

Sincerely,

Constantin Romanescu

COMENIUS UNIVERSITY IN BRATISLAVA
FACULTY OF NATURAL SCIENCES
DEPARTMENT OF PHYSICAL AND THEORETICAL CHEMISTRY
Head: Prof. RNDr. Ivan Černušák, DrSc.
Mlynská dolina CH1 - 340, 842 15 Bratislava 4

Alexander S. Ivanov
Utah State University
0300 Old Main Hill
Logan, UT 84322-0300

Bratislava, March 13, 2015

Re.: Confirmation

Dear Alexander S. Ivanov,

This letter is to confirm that you have my permission to use the following paper in part or in full for preparation or presentation of your dissertation.

"On the Way to the Highest Coordination Number in the Planar Metal-Centred Aromatic $Ta©B_{10}^-$ Cluster: Evolution of the Structures of TaB_n^- (n = 3-8)" Wei-Li Li, Alexander S. Ivanov, Jozef Federic, Constantin Romanescu, Ivan Černušák, Alexander I. Boldyrev, Lai-Sheng Wang, J. Chem. Phys, 2013, 139, 104312.

Sincerely Yours,

I. Černušák

Prof. Ivan Černušák

☎ + 421 2 602 96 429
IČO: 00397865 06

Fax: + 421 2 602 96 231
IČ DPH: SK2020845332

✉ cernusak@fns.uniba.sk
Internet: http://www.fns.uniba.sk

Alexander S. Ivanov
Utah State University
0300 Old Main Hill
Logan, UT 84322-0300

Jozef Federic
Computing Centre of Slovak Academy of Sciences
Dubravska cesta 9
Bratislava 845 35
SLOVAKIA

March 18, 2015

Dear Alexander S. Ivanov,

This letter is to confirm that you have my permission to use the following paper in part or in full for preparation or presentation of your dissertation.

> "On the Way to the Highest Coordination Number in the Planar Metal-Centred Aromatic $Ta©B_{10}^-$ Cluster: Evolution of the Structures of TaB_n^- (n = 3-8)" Wei-Li Li, Alexander S. Ivanov, Jozef Federic, Constantin Romanescu, Ivan Cernusak, Alexander I. Boldyrev, Lai-Sheng Wang, J. Chem. Phys, 2013, 139, 104312

Sincerely,

Jozef Federic

Alexander S. Ivanov
Utah State University
0300 Old Main Hill
Logan, UT 84322-0300

Prof. Gernot Frenking
Fachbereich Chemie
Philipps Universität Marburg
Hans-Meerwein-Str. 4
D-35043 Marburg
Germany

Marburg, March 13, 2015

Dear Alexander S. Ivanov,

This letter is to confirm that you have my permission to use the following papers in part or in full for preparation or presentation of your dissertation.

-"Stabilization of Cl^-Cl^- Anion Pair in the Gas Phase: Ab Initio Microsolvation Study" Alexander S. Ivanov, Gernot Frenking, Alexander I. Boldyrev, J. Phys. Chem. A, 2014, 118, 7375-7384

-"Inorganic Double-Helix Nanotoroid of Simple Lithium-Phosphorus Species" Alexander S. Ivanov, Alexander I. Boldyrev, Gernot Frenking, Chem. Eur. J., 2014, 20, 2431-2435

Sincerely,

Timur R. Galeev
Yale University
266 Whitney Ave
New Haven, CT 06520

Alexander S. Ivanov
Utah State University
0300 Old Main Hill
Logan, UT 84322-0300

March 10, 2015

Dear Alexander S. Ivanov:

This letter is to confirm that you have my permission to use the following paper in part or in full for preparation or presentation of your dissertation.

> "Molecular Wheel to Monocyclic Ring Transition in Boron-Carbon Mixed Clusters $C_2B_6^-$ and $C_3B_5^-$" Timur R. Galeev, Alexander S. Ivanov, Constantin Romanescu, Wei-Li Li, Konstantin V. Bozhenko, Lai-Sheng Wang and Alexander I. Boldyrev, Phys. Chem. Chem. Phys., 2011, 13, 8805-8810

Sincerely,

Timur Galeev

Alexander S. Ivanov
Utah State University
0300 Old Main Hill
Logan, UT 84322-0300

NAME DATE
ORGANIZATION
ADDRESS
CITY, STATE, ZIP CODE

Dear Alexander S. Ivanov,

This letter is to confirm that you have my permission to use the following papers in part or in full for preparation or presentation of your dissertation.

- "On the Way to the Highest Coordination Number in the Planar Metal-Centred Aromatic $Ta©B_{10}^-$ Cluster: Evolution of the Structures of TaB_n^- (n = 3-8)" Wei-Li Li, Alexander S. Ivanov, Jozef Federic, Constantin Romanescu, Ivan Cernusak, Alexander I. Boldyrev, Lai-Sheng Wang, J. Chem. Phys, 2013, 139, 104312

- "Molecular Wheel to Monocyclic Ring Transition in Boron-Carbon Mixed Clusters $C_2B_6^-$ and $C_3B_5^-$" Timur R. Galeev, Alexander S. Ivanov, Constantin Romanescu, Wei-Li Li, Konstantin V. Bozhenko, Lai-Sheng Wang and Alexander I. Boldyrev, Phys. Chem. Chem. Phys., 2011, 13, 8805-8810

Sincerely,

Dr. Wei-Li Li

Alexander S. Ivanov
Utah State University
0300 Old Main Hill
Logan, UT 84322-0300

Andrew Morris
TCM Group
Cavendish Laboratory
University of Cambridge
CB3 0HE

13th March 2015

Dear Alexander S. Ivanov,

This letter is to confirm that you have my permission to use the following paper in part or in full for preparation or presentation of your dissertation.

> "Inorganic Double-Helix Structures of Unusually Simple Li-P Species" Alexander S. Ivanov, Andrew J. Morris, Konstantin V. Bozhenko, Chris J. Pickard, Alexander I. Boldyrev, Angew. Chem. Int. Ed., 2012, 51, 33, 8330-8333

Sincerely,

Dr. Andrew J. Morris

Alexander S. Ivanov
Utah State University
0300 Old Main Hill
Logan, UT 84322-0300

Jared K. Olson
Utah State University
0300 Old Main Hill
Logan, UT 84322-0300

18 Mar 2015

Dear Alexander S. Ivanov,

This letter is to confirm that you have my permission to use the following paper in part or in full for preparation or presentation of your dissertation.

> "All-Nitrogen Analogue of Ozone: Li_3N_3 Species" Jared K. Olson, Alexander S. Ivanov, Alexander I. Boldyrev, Chem. Eur. J., 2014, 20, 6636-6640

Sincerely,

Dr. Jared K. Olson

Alexander S. Ivanov
Utah State University
0300 Old Main Hill
Logan, UT 84322-0300

Chris Pickard 13/3/2015
UCL
Gower Street
London, UK, WC1E 6BT

Dear Alexander S. Ivanov,

This letter is to confirm that you have my permission to use the following paper in part or in full for preparation or presentation of your dissertation.

> "Inorganic Double-Helix Structures of Unusually Simple Li-P Species" Alexander S. Ivanov, Andrew J. Morris, Konstantin V. Bozhenko, Chris J. Pickard, Alexander I. Boldyrev, Angew. Chem. Int. Ed., 2012, 51, 33, 8330-8333

Sincerely,

Prof. Chris J. Pickard

Alexander S. Ivanov
Utah State University
0300 Old Main Hill
Logan, UT 84322-0300

03/11/2015

Dear Alexander S. Ivanov,

This letter is to confirm that you have my permission to use the following paper in part or in full for preparation or presentation of your dissertation.

> "The I=X (X = O, N, C) Double Bond in Hypervalent Iodine Compounds: Is it Real?" Alexander S. Ivanov, Ivan A. Popov, Alexander I. Boldyrev, Viktor V. Zhdankin, Angew. Chem. Int. Ed., 2014, 53, 9617-9621

Sincerely,

Ivan A. Popov

Alexander S. Ivanov
Utah State University
0300 Old Main Hill
Logan, UT 84322-0300

Prof. Viktor V. Zhdankin 3/13/2015

University of Minnesota Duluth
1039 University Drive
Duluth, MN 55812

Dear Alexander S. Ivanov,

This letter is to confirm that you have my permission to use the following paper in part or in full for preparation or presentation of your dissertation.

> "The I=X (X = O, N, C) Double Bond in Hypervalent Iodine Compounds: Is it Real?" Alexander S. Ivanov, Ivan A. Popov, Alexander I. Boldyrev, Viktor V. Zhdankin, Angew. Chem. Int. Ed., 2014, 53, 9617-9621

Sincerely,

Viktor Zhdankin

Prof. Viktor V. Zhdankin

Alexander S. Ivanov
Utah State University
0300 Old Main Hill
Logan, UT 84322-0300

NAME: Evan Miller
DATE: 6/1/2015
ORGANIZATION: Utah State University
ADDRESS: 1055 E 70 N
CITY, STATE, ZIP CODE: American Fork, Utah 84003

Dear Alexander S. Ivanov,

This letter is to confirm that you have my permission to use the following paper in part or in full for preparation or presentation of your dissertation.

> "Pseudo Jahn–Teller Origin of Buckling Distortions in Two-Dimensional Triazine-Based Graphitic Carbon Nitride (g-C_3N_4) Sheets" A. S. Ivanov, E. Miller, A. I. Boldyrev, Y. Kameoka, T. Sato, K. Tanaka, 2015, 119, 12008–12015

Sincerely,

Evan Miller

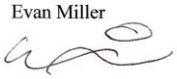

Alexander S. Ivanov
Utah State University
0300 Old Main Hill
Logan, UT 84322-0300

Yuichiro Kameoka
60 Tanabedojo
Kyotanabe, Kyoto, Japan 610-0331

23 May 2015

Dear Alexander S. Ivanov,

This letter is to confirm that you have my permission to use the following paper in part or in full for preparation or presentation of your dissertation.

> "Pseudo Jahn–Teller Origin of Buckling Distortions in Two-Dimensional Triazine-Based Graphitic Carbon Nitride (g-C_3N_4) Sheets" A. S. Ivanov, E. Miller, A. I. Boldyrev, Y. Kameoka, T. Sato, K. Tanaka, DOI: 10.1021/acs.jpcc.5b02299

Sincerely,

亀岡優一郎
Yuichiro Kameoka

Alexander S. Ivanov
Utah State University
0300 Old Main Hill
Logan, UT 84322-0300

Tohru Sato
Department of Molecular Engineering,
Graduate School of Engineering,
Kyoto University
Nishikyo-ku,
Kyoto, 615-8510, Japan

May 25, 2015

Dear Alexander S. Ivanov,

This letter is to confirm that you have my permission to use the following paper in part or in full for preparation or presentation of your dissertation.

> "Pseudo Jahn–Teller Origin of Buckling Distortions in Two-Dimensional Triazine-Based Graphitic Carbon Nitride (g-C_3N_4) Sheets" A. S. Ivanov, E. Miller, A. I. Boldyrev, Y. Kameoka, T. Sato, K. Tanaka, DOI: 10.1021/acs.jpcc.5b02299

Sincerely,

Professor Tohru Sato

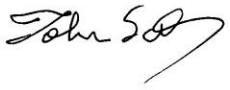

Alexander S. Ivanov
Utah State University
0300 Old Main Hill
Logan, UT 84322-0300

May 23, 2015

Kazuyoshi Tanaka
Fukui Institute for Fundamental Chemistry, Kyoto University
34-4 Nishihiraki-cho, Takano, Sakyo-ku
Kyoto, 606-8103 Japan

Dear Alexander S. Ivanov,

This letter is to confirm that you have my permission to use the following paper in part or in full for preparation or presentation of your dissertation.

> "Pseudo Jahn–Teller Origin of Buckling Distortions in Two-Dimensional Triazine-Based Graphitic Carbon Nitride (g-C_3N_4) Sheets" A. S. Ivanov, E. Miller, A. I. Boldyrev, Y. Kameoka, T. Sato, K. Tanaka, DOI: 10.1021/acs.jpcc.5b02299

Sincerely,

Professor Kazuyoshi Tanaka

CURRICULUM VITAE

Alexander S. Ivanov

(May, 2015)

Department of Chemistry and Biochemistry

Utah State University

0300 Old Main Hill, Logan, UT 84322

E-mail: alexander.ivanov88@gmail.com

Webpage: http://ion.chem.usu.edu/~boldyrev/aleksandr.php

ACADEMIC DEGREES

Ph. D. Chemistry *2011-2015*

Department of Chemistry and Biochemistry, Utah State University

Graduate Advisor: Dr. Alex I. Boldyrev

M. Sc. Physical Chemistry. *Summa cum laude.* *2010-2012*

Peoples' Friendship University of Russia, Moscow

Graduate Advisor: Dr. Konstantin V. Bogenko

B. Sc. Chemistry. *Summa cum laude.* *2005-2010*

Peoples' Friendship University of Russia, Moscow

Undergraduate Advisor: Dr. Konstantin V. Bogenko

AWARDS AND HONORS

Marjorie H. Gardner Teaching Award *2015*

Utah State University

Outstanding Graduate Student in Chemistry Award *2014*

Utah State University

Award for Early Research Progress in Chemistry *2013*

Utah State University

USU Graduate Division Research Travel Grant *2013*

Utah State University

M. Sc. Honor Diploma (*Summa cum laude*) *2012*

Peoples' Friendship University of Russia, Moscow

Dr. Gryaznov Memorial Award for Excellence in Science *2010*

Peoples' Friendship University of Russia, Moscow

Best Graduate Student in Science – 2010 Award *2010*

Peoples' Friendship University of Russia, Moscow

B. Sc. Honor Diploma (*Summa cum laude*) *2010*

Peoples' Friendship University of Russia, Moscow

Scholarship for Outstanding Academic Achievements *2005 – 2012*

TEACHING EXPERIENCE

CHEM 1225. Principles of Chemistry II. Utah State University *Spring 2015*

CHEM 2325. Organic Chemistry II. Utah State University *Spring 2014*

CHEM 1215. Principles of Chemistry I. Utah State University *Spring 2013*

CHEM 1215. Principles of Chemistry I. Utah State University *Spring 2012*

College Level Chemistry Teaching. PFUR, Moscow *Fall 2010*

PROFESSIONAL ACTIVITIES

Internships: Agilent Technologies, Inc., Russian Office (Moscow) *Summer 2010*

Memberships: American Chemical Society (ACS) *2011-present*

Reviewer for: Journal of the American Chemical Society (ACS Publications), Journal of Chemical Theory and Computation (ACS Publications), Journal of Chemical Physics (AIP), Molecular Physics

CONFERENCE PROCEEDINGS AND SEMINARS

03/2015 249th National ACS Meeting & Exposition. Division of Physical Chem. "*Stabilization of a $Cl^{-}Cl^{-}$ Anion Pair in the Gas Phase: Ab initio Microsolvation Study*", Denver, CO, USA; (Poster)

10/2014 19th International Conference on Commercializing Micro- and Nanotechnology. "*Inorganic Double-Helix Nanocoils for Future Microelectronic Devices*", Salt Lake City, UT, USA; (Poster)

09/2014 Chemistry and Biochemistry Departmental Seminar, "*Reliable Predictions of New Molecules, Clusters, and Materials Using Computational Methods*", Logan, UT, USA; (Talk)

07/2014 2nd International Conference on Chemical Bonding, Kauai, HI, USA (administrative support)

11/2013 Physical and Analytical Chemistry Seminar, "*Quantum Chemical Studies of Novel LiP Clusters and LiP Nanowires*", Logan, UT, USA; (Talk)

04/2013 245th National ACS Meeting & Exposition. Division of Inorganic Chem. "*Simplest inorganic double-helix structures*", New Orleans, LA, USA; (Poster)

PUBLICATIONS

(May, 2015)

Sum of the times cited: **97**; h-index: **7** (Google Scholar)

[1] **A. S. Ivanov**, E. Miller, Y. Kameoka, K. Tanaka, A. I. Boldyrev, T. Sato, "Pseudo Jahn-Teller Origin of Buckling Distortions in Two-Dimensional Triazine-Based Graphitic Carbon Nitride (g-C_3N_4) Sheets" *J. Phys. Chem. C*, 119,

12008-12015, 2015 [impact factor = 4.8]

[2] **A. S. Ivanov**, I. A. Popov, A. I. Boldyrev, V. V. Zhdankin, "The I=X (X = O, N, C) Double Bond in Hypervalent Iodine Compounds: Is it Real?" *Angew. Chem. Int. Ed.,* 53, 9617-9621, 2014 [impact factor = 13.7]

Highlighted in ***Chemistry World****, 2014, July 11*

[3] **A. S. Ivanov** and A. I. Boldyrev, "Deciphering Aromaticity in Porphyrinoids via Adaptive Natural Density Partitioning" *Org. Biomol. Chem.,* 12, 6145-6150, 2014 [impact factor = 3.5]

[4] J. K. Olson, **A. S. Ivanov**, A. I. Boldyrev, "All-Nitrogen Analogue of Ozone: Li_3N_3 Species" *Chem. Eur. J.,* 20, 6636-6640, 2014 [impact factor = 5.7]

[5] **A. S. Ivanov**, A. I. Boldyrev, G. Frenking, "Inorganic Double-Helix Nanotoroid of Simple Lithium-Phosphorus Species" *Chem. Eur. J.*, 20, 2431-2435, 2014 [impact factor = 5.7]

Featured on the cover of the ***Chemical & Engineering News****, 2014, Vol. 92*

[6] **A. S. Ivanov**, G. Frenking, A. I. Boldyrev, "Stabilization of Cl^-Cl^- Anion Pair in the Gas Phase: Ab Initio Microsolvation Study" *J. Phys. Chem. A,* 118, 7375-7384, 2014 (K. D. Jordan Festschrift) [impact factor = 2.8]

Highlighted in ***Chemistry Views****, 2014, March 04*

[7] W. L. Li, **A. S. Ivanov**, J. Federic, C. Romanescu, I. Cernusak, A. I. Boldyrev, L.-S. Wang, "On the way to the highest coordination number in the planar metal-

centred aromatic Ta©B_{10} cluster: Evolution of the Structures of TaB_n^- (n = 3-8)" *J. Chem. Phys*., 139, 104312, 2013 [impact factor = 3.1]

[8] **A. S. Ivanov** and A. I. Boldyrev, "Reliable Predictions of Unusual Molecules" *Phys. Chem. Chem. Phys*., 14, 15943-15952, 2012 (review article) [impact factor = 4.2]

*Designated a "**Hot Article**" by Phys. Chem. Chem. Phys. Journal, 2012, Nov. 09*

[9] **A. S. Ivanov** and A. I. Boldyrev, "$Si_{6-n}C_nH_6$ (n = 0-6) Series: When Do Silabenzenes Become Planar and Global Minima?" *J. Phys. Chem. A*, 116, 9591-9598, 2012 [impact factor = 2.8]

[10] **A. S. Ivanov**, K. V. Bozhenko, A. I. Boldyrev, "On the Suppression Mechanism of the Pseudo-Jahn-Teller Effect in Middle E_6 (E = P, As, Sb) Rings of Triple-Decker Sandwich Complexes" *Inorganic Chemistry*, 8, 8868-8872, 2012 [impact factor = 4.8]

[11] **A. S. Ivanov**, A. J. Morris, K. V. Bozhenko, C. J. Pickard, A. I. Boldyrev, "Inorganic Double-Helix Structures of Unusually Simple Li-P Species" *Angew. Chem. Int. Ed.*, 33, 8330-8333, 2012 [impact factor = 13.7]

Highlighted in:

***Chemical & Engineering News**, 2012, Vol. 90, Issue 33;*

***The London Centre for Theory and Simulation of Materials** (UK), 2012, Aug. 15;*

***Utah State Today**, 2012, August 16; and other media*

[12] **A. S. Ivanov**, K. V. Bozhenko, A. I. Boldyrev, "Peculiar Transformations in the $C_xH_xP_{4-x}$ (x = 0-4) Series" *J. Chem. Theor. Comput.*, 8, 135-140, 2011 [impact factor = 5.3]

[13] T. R. Galeev, **A. S. Ivanov**, C. Romanescu, W.-L. Li, K. V Bozhenko, L.-S. Wang, A. I. Boldyrev, "Molecular Wheel to Monocyclic Ring Transition in Boron-Carbon Mixed Clusters $C_2B_6^-$ - $C_3B_5^-$" *Phys. Chem. Chem. Phys.*, 13, 8805-8810, 2011 [impact factor = 4.2]